Advances in Geologic Disposal Safety Assessment and an Unsaturated Alluvium Reference Case

Spent Fuel and Waste Disposition

Prepared for
U.S. Department of Energy
Spent Fuel and Waste Science Technology

P.E. Mariner, E.R. Stein, S.D. Sevougian,
L.J. Cunningham, J.M. Frederick,
G.E. Hammond, T.S. Lowry,
S. Jordan, and E. Basurto
Sandia National Laboratories

September 17, 2018
SFWD-SFWST-2018-000509
SAND2018-11858 R

Sandia National Laboratories

ACKNOWLEDGEMENTS

EXECUTIVE SUMMARY

The Spent Fuel and Waste Science and Technology (SFWST) Campaign of the U.S. Department of Energy (DOE) Office of Nuclear Energy (NE), Office of Fuel Cycle Technology (OFCT) is conducting research and development (R&D) on geologic disposal of spent nuclear fuel (SNF) and high level nuclear waste (HLW). Two high priorities for SFWST disposal R&D are design concept development and disposal system modeling (DOE 2011, Table 6). These priorities are directly addressed in the SFWST Geologic Disposal Safety Assessment (GDSA) work package, which is charged with developing a disposal system modeling and analysis capability for evaluating disposal system performance for nuclear waste in geologic media.

This report describes specific GDSA activities in fiscal year 2018 (FY 2018) toward the development of *GDSA Framework*, an enhanced disposal system modeling and analysis capability for geologic disposal of nuclear waste. *GDSA Framework* employs the PFLOTRAN thermal-hydrologic-chemical multi-physics code (Hammond et al. 2011a; Lichtner and Hammond 2012) and the Dakota uncertainty sampling and propagation code (Adams et al. 2012; Adams et al. 2013). Each code is designed for massively-parallel processing in a high-performance computing (HPC) environment. Multi-physics representations in PFLOTRAN are used to simulate various coupled processes including heat flow, fluid flow, waste dissolution, radionuclide release, radionuclide decay and ingrowth, precipitation and dissolution of secondary phases, and radionuclide transport through engineered barriers and natural geologic barriers to the biosphere. Dakota is used to generate sets of representative realizations and to analyze parameter sensitivity.

In FY 2018, major advances in the capabilities and testing of *GDSA Framework* included:

- A new stepwise linear regression capability for identifying and evaluating the most significant uncertain inputs in a simulation;

- Automation for mapping boundary and initial conditions to grid cells in regions where multi-phase thermodynamic states may occur, as in the case of unsaturated formations;

- Development of a model framework for integrating and simultaneously tracking multiple coupled degradation models for each waste package; and

- Demonstration and documentation of numerous new quality assurance test cases that compare PFLOTRAN results to analytical solutions.

As these advances progressed within the GDSA group, integration with other SFWST work accelerated. The agenda of the SFWST Annual Working Group Meeting this year was driven by the GDSA group to enhance integration across the campaign. At this meeting, "evaluation" sessions were held that were aimed at assessing the current state-of-the-art of various ongoing R&D activities, the remaining R&D effort appropriate for those activities, and the current priority of those activities for each of the major generic repository host-rock environments. Results of these sessions are documented in this report. These sessions were in preparation for the FY 2019 SFWST Roadmap Update Workshop scheduled for January 2019.

As part of the GDSA Uncertainty and Sensitivity Analysis Methods work package (SF-18SN01030405), initial steps were taken in FY 2018 to ensure that *GDSA Framework* has a comprehensive sensitivity analysis capability that has the potential to benefit repository performance assessment (PA). This report addresses both traditional repository PA methods (stepwise linear regression, simple and partial correlation coefficients) and more computationally expensive variance-based methods recently made feasible by advances in theory and in computer hardware and software. The former work well when the system can be approximated with a linear (or monotonic), additive model, but may fail to adequately

capture nonlinearities and parameter interactions. The latter can be applied to highly coupled nonlinear models to capture nonlinear (nonmonotonic) dependencies and parameter interactions. The shale reference case developed in FY 2017 was used to exercise new capabilities, including stepwise linear regression and main and total sensitivity indices calculated via polynomial chaos expansion and Gaussian process metamodels.

In addition, as part of the GDSA Repository Systems Analysis work package (SF-18SN01030407), a new unsaturated alluvium reference case was conceptualized this year. This reference case considers the thick alluvial valleys of the Great Basin in the western United States and the low-permeability playa/lacustrine sediments situated therein. Several features of this type of host rock are favorable to waste isolation, including low groundwater fluxes, low permeability, and low water saturation. This type of environment is favorable to the disposal of dual purpose canisters because low water saturation greatly reduces the possibility of criticality events. This report focuses on the natural barrier system, movement of water through these sediments, and the physical and chemical characteristics of the host rock. A reference case repository layout is under development and has been meshed for *GDSA Framework* simulation in FY 2019.

Each year, *GDSA Framework* and its underlying codes improve as additional modelers and programmers from around the world use, apply, and contribute to it. *GDSA Framework* is accessible to anyone because the primary codes, PFLOTRAN and Dakota, are open source, available for free download, and have supporting documentation online. This year the GDSA group worked to increase the number of users and participants by

- Conducting two PFLOTRAN short courses, one in New Mexico and one in Taiwan;

- Expanding online documentation of verification testing, generic reference cases, and code features;

- Maintaining a collaborative website for *GDSA Framework* (pa.sandia.gov); and

- Presenting multiple papers and posters on *GDSA Framework* capabilities at international conferences and meetings.

Simulation of increasingly complicated problems continues to affirm that HPC-capable codes can be used to simulate important multi-physics couplings directly in a total system performance assessment of a geologic repository. The generic repository applications modeled to date indicate that *GDSA Framework* can simulate complex coupled processes in a multi-kilometer domain while simultaneously simulating sub-meter-scale coupled behavior in the repository.

This report fulfills the GDSA Framework Development work package (SF-18SN01030406) level 2 milestone – *Advances in Geologic Disposal Safety Assessment and an Unsaturated Alluvium Reference Case* (M2SF-18SN010304062).

CONTENTS

Page

FIGURES

TABLES

NOMENCLATURE

1D, 2D, 3D	one-, two-, and three-dimensional
ANL	Argonne National Laboratory
CSNF	commercial SNF
d	day
DGR	deep geologic repository
DOE	U.S. Department of Energy
DPC	dual-purpose canister
DR	disposal research
DRZ	disturbed rock zone
DSNF	DOE SNF
EBS	engineered barrier system
EDZ	excavation disturbed zone
Eq.	equation
FEP	feature, event, and process
FMD	Fuel Matrix Degradation
ft	feet
FTE	full-time employee
FY	fiscal year
g	gram
GDSA Framework	Geologic Disposal Safety Assessment Framework
HDF5	hierarchical data format, version 5
HF	higher fidelity
HLW	high-level radioactive waste
HPC	high-performance computing
ISC	importance to safety case
J	Joule
K	Kelvin
L	liter
LANL	Los Alamos National Laboratory
LBNL	Lawrence Berkeley National Laboratory
LF	lower fidelity
LHS	latin hypercube sampling
LOE	level of effort
MIC	microbially-influenced corrosion

NOMENCLATURE (CONT.)

NaN	not a number
NA	not applicable
NBS	natural barrier system
NE	Office of Nuclear Energy
NEA	Nuclear Energy Agency
NNSS	Nevada National Security Site
NUMO	Nuclear Waste Management Organization of Japan
NV	Nevada
OFCT	Office of Fuel Cycle Technology
ORNL	Oak Ridge National Laboratory
PA	performance assessment
PCC	partial correlation coefficient
PCE	polynomial chaos expansion
PDE	partial differential equation
Pe	Peclet number
PETSc	Portable Extensible Toolkit for Scientific Computation
pH	negative logarithm of hydrogen ion activity
PNNL	Pacific Northwest National Laboratory
PRCC	partial rank correlation coefficient
PRESS	predicted error sum of squares
PWR	pressurized water reactor
QA	quality assurance
R&D	research and development
RBSN	Rigid-Body-Spring-Network
SA	sensitivity analysis
SAL	state-of-the-art level
SCC	simple correlation coefficient
SFWST	Spent Fuel and Waste Science and Technology
SIAM	Society for Industrial and Applied Mathematics
SNF	spent nuclear fuel
SNL	Sandia National Laboratories
SRC	standardized regression coefficient
SRCC	simple rank correlation coefficient
T	time unit
TBD	to be determined
TH	thermal-hydrologic
THC	thermal-hydrologic-chemical
THM	thermal-hydrologic-mechanical
THMC	thermal-hydrologic-mechanical-chemical
TRU	transuranic

NOMENCLATURE (CONT.)

UFD	Used Fuel Disposition
UFDC	UFD Campaign
UFDDPM	UFD decay process model
URL	underground research laboratory
V&V	verification and validation
W	watt
WF	waste form
WFPM	Waste Form Process Model
WIPP	Waste Isolation Pilot Plant
WP	waste package
yr	year

1.   INTRODUCTION

The Spent Fuel and Waste Science and Technology (SFWST) Campaign of the U.S. Department of Energy (DOE) Office of Nuclear Energy (NE), Office of Fuel Cycle Technology (OFCT) is conducting research and development (R&D) on geologic disposal of spent nuclear fuel (SNF) and high level nuclear waste (HLW). Two of the highest priorities for SFWST disposal R&D are design concept development and disposal system modeling (DOE 2011, Table 6). These priorities are directly addressed in the SFWST Geologic Disposal Safety Assessment (GDSA) Framework Development work package, which is charged with developing a disposal system modeling and analysis capability for evaluating disposal system performance for nuclear waste in geologic media. Disposal options for SNF and HLW include mined repository concepts in salt, shale, and crystalline rock and deep borehole disposal in crystalline rock (Arnold et al. 2011; Hardin et al. 2012). An additional option examined this year is disposal in unsaturated alluvial sediments.

In 2013, GDSA transitioned to a framework based on PFLOTRAN and Dakota, a framework that GDSA continues to develop today. PFLOTRAN is a multiphase flow and reactive transport model for describing surface and subsurface processes (Hammond et al. 2011a; Lichtner and Hammond 2012), and Dakota is an uncertainty quantification and sensitivity analysis code (Adams et al. 2012; Adams et al. 2013). These codes were chosen to provide the primary modeling framework because they are open source, massively parallel, and together have the potential to simulate a total integrated geologic repository system and its surroundings probabilistically and in three dimensions. The developing modeling capability is called *GDSA Framework*, which stands for Geologic Disposal Safety Assessment Framework.

This report describes GDSA accomplishments for fiscal year 2018 (FY 2018). Prior development and accomplishments are documented in Mariner et al. (2015); Mariner et al. (2016); Mariner et al. (2017); Sevougian et al. (2013); Sevougian et al. (2014); Freeze et al. (2013b); Clayton et al. (2011); Freeze and Vaughn (2012); and Vaughn et al. (2013).

The overall objective of the GDSA Framework Development work package is to develop a disposal system modeling and analysis capability that supports the prioritization of Disposal Research (DR) R&D and the evaluation of disposal system performance, including uncertainty, for a range of disposal options and host rocks. The purpose is to develop a GDSA capability that:

- Integrates updated conceptual models of subsystem processes and couplings developed under this and other DR work packages,

- Is used to evaluate DR R&D priorities,

- Leverages existing computational capabilities (e.g., meshing, visualization, high-performance computing (HPC)) where appropriate, and

- Is developed and distributed in an open-source environment.

Six major tasks were identified for FY 2018:

- Identify additional capabilities needed to advance *GDSA Framework* to a robust PA model (e.g., multiphase processes, temperature dependencies, colloids, EBS degradation processes, control variate method, code efficiency, convergence, grid refinement). The GDSA work package works closely with other work packages in identifying these needs, determining what is required to sufficiently address them, and working to fulfill them.

- Integrate subsystem models developed under this and other work packages into the GDSA-PA system model architecture (e.g., waste form degradation, waste package degradation, colloid stability and transport, EBS chemistry, EBS flow and transport, fracture

representation, thermal-hydrological-mechanical processes, natural system flow and transport).

- Develop, perform, and document verification and validation analyses of relevant GDSA model processes and expand regression testing to demonstrate and assure continued quality.

- Demonstrate the freely-available PFLOTRAN *GDSA Framework* and modeling capability at national and international forums and conduct one or more workshops to promote accelerated use of the capability worldwide. Expanding the user base is expected to provide additional testing of the code and opportunities for additional development by outside contributors.

- Plan FY 2019 R&D integration and prioritization workshops to evaluate and summarize the status of SFWST R&D conducted since 2010 on generic deep geologic repositories (DGRs), and to prioritize R&D still desirable to enhance confidence in the generic safety case for DGRs in various host rocks. These workshops will be conducted jointly with the Crystalline, Argillite, and Salt work packages.

- Analyze how members of the public understand safety assessment and develop alternatives for providing and explaining the content of safety assessments to the lay public and other stakeholders. This work will be completed in FY 2019.

This report fulfills the GDSA Framework Development work package (SF-18SN01030406) level 2 milestone – *Advances in Geologic Disposal Safety Assessment and an Unsaturated Alluvium Reference Case* (M2SF-18SN010304062). In addition to reporting FY 2018 work package accomplishments, it reports in Sections 4 and 5 FY 2018 progress on two other work packages, the GDSA Uncertainty and Sensitivity Analysis Methods work package (SF-18SN01030405) and the GDSA Repository Systems Analysis (SF-18SN01030407) work package. This report builds on developments reported in previous *GDSA Framework* milestones: M3SF-17SN010304011 (Mariner et al. 2017); M3FT-16SN080304011 (Mariner et al. 2016); M2FT-15SN0808011 (Mariner et al. 2015); M3FT-14SN0808032 (Sevougian et al. 2014); and M3FT-13SN0808062 (Freeze et al. 2013a).

Section 2 discusses the GDSA PA vision and summarizes the conceptual model framework and the PFLOTRAN-based computational framework of *GDSA Framework*. Section 3 reports progress on *GDSA Framework* development activities and specific integration activities undertaken. Section 4 describes and applies new uncertainty quantification and sensitivity analysis capabilities and applies them to a generic commercial repository in shale. Section 5 develops a technical basis and conceptual model for a reference case repository located in unsaturated alluvial sediments. Conclusions are summarized in Section 6.

2.   GDSA PERFORMANCE ASSESSMENT

A performance assessment (PA) for underground disposal of nuclear waste requires a comprehensive analysis of features, events, and processes (FEPs) potentially affecting the release and transport of radionuclides to the biosphere. The foundation of a PA is the computational framework. Section 2.1 provides the GDSA long-term vision for *GDSA Framework*. The present computational framework and conceptual model framework are summarized in Section 2.2.

2.1   PA Vision

The long-term vision for the GDSA effort is to ensure that the GDSA modeling capability can adapt to, and take advantage of, future advances in computational software and hardware and future advances in process modeling. In line with this vision, the near-term mission is to develop a robust suite of fully functional generic repository reference case applications (1) for application to candidate sites by the time they are selected and (2) for evaluation of the effects of FEPs and input parameters on repository performance to inform R&D planning.

In consideration of the long-term vision, two open-source, HPC codes serve as the core of *GDSA Framework*: PFLOTRAN and Dakota. PFLOTRAN is a massively-parallel thermal-hydrologic-chemical (THC) flow and transport code, and Dakota is a versatile probabilistic code (Section 2.2.2). The PFLOTRAN code is being developed by the GDSA group to accommodate new geologic disposal process models and capabilities through additional code development and coupling with external process models. The HPC capabilities of PFLOTRAN and Dakota allow for ever higher fidelity in total system performance assessment modeling as more powerful HPC resources become available.

As the GDSA modeling capability evolves, the GDSA group will continue to generate and refine three-dimensional models of disposal repository concepts complete with surrounding geospheres and connected biospheres. Sensitivity analyses will be performed on these models to distinguish the importance of features, processes, and parameters on model results. These analyses are expected to assist prioritization of future disposal R&D.

2.2   PA Framework

A PA model is an important component of a comprehensive PA for a nuclear waste repository. In a comprehensive PA all plausible scenarios and processes that may affect repository performance are addressed. FEPs and scenarios are evaluated and screened. Potentially pertinent FEPs are identified for simulation in the PA model. Probabilistic simulations are performed, and results are evaluated against performance metrics. Uncertainty and sensitivity analyses may also be performed to inform prioritization of additional research and model development.

The PA framework consists of a conceptual model framework (Section 2.2.1) and a computational framework (Section 2.2.2). An overview of PA methodology and terminology is presented in Sevougian et al. (2014, Section 2.2) and Meacham et al. (2011, Section 1) and elsewhere (Rechard 2002).

2.2.1   Conceptual Model Framework

A conceptual model framework requires a coherent representation of pertinent FEPs. Figure 2-1 schematically illustrates the conceptual model framework for a repository system. To calculate a dose to a receptor in the biosphere, radionuclides released from the waste form must pass through the repository engineered barrier system (EBS) and the surrounding natural barrier system (NBS).

A FEPs database like the one developed and described in Freeze et al. (2011) can be used to help identify a full set of potentially important FEPs for a specific conceptual repository model. Many of the FEPs in a

FEPs database may be directly simulated in the PA model. In a comprehensive PA, excluded FEPs (i.e., FEPs not simulated in the PA model) must be addressed in separate analyses and arguments.

Important processes and events in the conceptual model are those that could significantly affect the movement of radionuclides in the EBS and NBS. Such processes and events include waste package corrosion, waste form dissolution, radionuclide release, radioactive decay, heat transfer, aqueous transport, advection, diffusion, sorption, aqueous chemical reactions, precipitation, buffer chemical reactions, gas generation, colloidal transport, earthquakes, and inadvertent human intrusion of the repository.
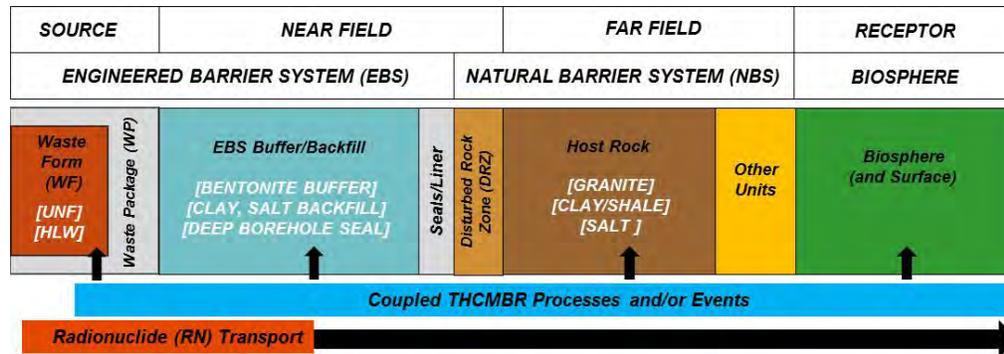
Figure 2-1   Schematic diagram of the conceptual model framework of a generic geologic disposal system

2.2.2   Computational Framework

Performance assessment requires simulation of a large set of realizations. For this reason, *GDSA Framework* is designed for massively-parallel processing in a HPC environment. *GDSA Framework* consists of the following components:

- Input parameter database

- Software for sampling, sensitivity analysis, and uncertainty quantification (Dakota)

- Petascale multiphase flow and reactive transport code (PFLOTRAN), working in concert with coupled process model codes (e.g., Fuel Matrix Degradation (FMD) Model)

- Computational support software and scripts for meshing, processing, and visualizing results (e.g., CUBIT, Python, ParaView, VisIt).

The flow of data and calculations through these components is illustrated in Figure 2-2. In a probabilistic simulation, Dakota generates stochastic input for each PA realization based on parameter uncertainty distributions and input parameter correlations. The sampled inputs are used by PFLOTRAN and its coupled process models to simulate source term release, EBS evolution, flow and transport through the EBS and NBS, and uptake in the biosphere. After the simulation, various software may be used to reduce and illustrate the output calculations of parameters and performance metrics. Dakota may also be used to evaluate the effects of parameter uncertainty on specific outputs.

Dakota and PFLOTRAN are the core simulation codes of *GDSA Framework*, the computational framework. These codes are described in more detail in Sections 2.2.2.1 and 2.2.2.2.
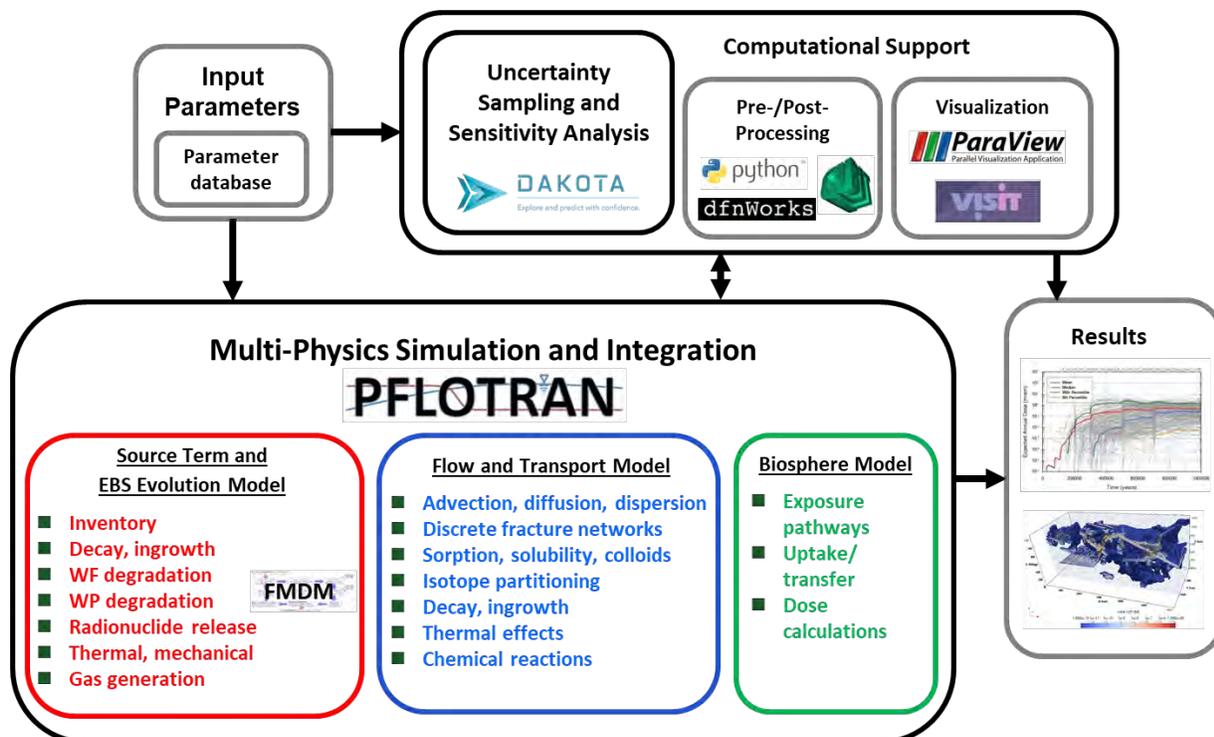
Figure 2-2 *GDSA Framework* **structure**

2.2.2.1   *Dakota*

The Dakota software toolkit is open source software developed and supported at Sandia National Laboratories (Adams et al. 2012; Adams et al. 2013). *GDSA Framework* uses Dakota's sampling schemes, principally Latin Hypercube Sampling (LHS), to propagate input value uncertainty into probabilistic PFLOTRAN simulations. Dakota is also used in sensitivity analyses to analyze the effects of input value uncertainty on probabilistic *GDSA Framework* results.

Dakota can be used to manage uncertainty quantification, sensitivity analyses, optimization, and calibration. Specific Dakota capabilities important to GDSA include (dakota.sandia.gov):

- Generic interface to simulations

- Mixed deterministic/probabilistic analysis

- Uncertainty quantification with sampling methods

- Scalable parallel computation on clusters.

2.2.2.2   *PFLOTRAN*

PFLOTRAN (Hammond et al. 2011a; Lichtner and Hammond 2012) is an open source, reactive multi-phase flow and transport simulator designed to leverage massively-parallel high-performance computing to simulate subsurface earth system processes. PFLOTRAN has been employed on petascale leadership-class DOE computing resources (e.g., Jaguar [at Oak Ridge National Laboratory (ORNL)] and Franklin/Hopper [at Lawrence Berkeley National Laboratory (LBNL)]) to simulate THC processes at the Nevada Test Site (Mills et al. 2007), multi-phase CO_2-H_2O for carbon sequestration (Lu and Lichtner 2007), CO_2 leakage within shallow aquifers (Navarre-Sitchler et al. 2013), and uranium fate and transport at the Hanford 300 Area (Hammond et al. 2007; Hammond et al. 2008; Hammond and Lichtner 2010;

Hammond et al. 2011b; Chen et al. 2012; Chen et al. 2013). PFLOTRAN is also under development for use in PA at the Waste Isolation Pilot Plant (WIPP).

PFLOTRAN solves the non-linear partial differential equations describing non-isothermal multi-phase flow, reactive transport, and geomechanics in porous media. Parallelization is achieved through domain decomposition using the Portable Extensible Toolkit for Scientific Computation (PETSc) (Balay et al. 2013). PETSc provides a flexible interface to data structures and solvers that facilitate the use of parallel computing. PFLOTRAN is written in Fortran 2003/2008 and leverages state of the art Fortran programming (i.e. Fortran classes, pointers to procedures, etc.) to support its object-oriented design. The code provides "factories" within which the developer can integrate a custom set of process models and time integrators for simulating surface and subsurface multi-physics processes. PFLOTRAN employs a single, unified framework for simulating multi-physics processes on both structured and unstructured grid discretizations (i.e. there is no duplication of the code that calculates multi-physics process model functions in support of structured and unstructured discretizations). The code requires a small, select set of third-party libraries (e.g., MPI, PETSc, BLAS/LAPACK, HDF5, Metis/Parmetis). Both the unified structured/unstructured framework and the limited number of third-party libraries greatly facilitate usability for the end user.

Specific PFLOTRAN capabilities for the simulation of generic disposal systems include:

- Multi-physics
    - Multi-phase flow
    - Multi-component transport
    - Biogeochemical processes
    - Thermal and heat transfer processes
- High-Performance Computing (HPC)
    - Built on PETSc – parallel solver library
    - Massively parallel
    - Structured and unstructured grids
    - Scalable from laptop to supercomputer
- Modular design based on object-oriented Fortran 2003/2008 for easy integration of new capabilities

3. *GDSA Framework* Development

Incorporating process models into *GDSA Framework* greatly facilitates evaluation of the importance of FEPs in PA applications. The approach of using detailed models directly in a PA is a continuation of the successful modeling approach adopted for the Waste Isolation Pilot Plant (WIPP) PAs (Rechard 1995; Rechard 2002; Rechard and Tierney 2005) and differs from the modeling approach adopted for past PAs for disposal of SNF and HLW in volcanic tuff (Rechard and Stockman 2014).

Section 3.1 describes the integration activities GDSA performed this year to identify and prioritize process models for incorporation in *GDSA Framework*. Section 3.2 discusses code development for FY 2018. Section 3.3 addresses the outreach work performed to promote collaboration and wider use of *GDSA Framework*.

3.1 Process Model Integration

In FY 2018 the model integration effort, i.e., integration of *GDSA Framework* with various process models, was part of a broader R&D integration effort across the SFWST Disposal Research (DR) Campaign, initiated to ensure that current generic-repository R&D priorities are still aligned with the R&D prioritization in the 2012 UFD Roadmap (DOE 2012), and to make appropriate re-alignments if necessary. For example, one priority that has increased significantly since 2012 is the present R&D focus on potential direct disposal of DPC waste packages, given the now large inventory of spent fuel stored in DPCs at U.S. nuclear reactor sites relative to the DPC inventory at the time of the Yucca Mountain license application (DOE 2008).

The FY 2018 broader R&D integration effort was initiated in preparation for the May 2018 SFWST Annual Working Group Meeting (http://energyworkshops.sandia.gov/nuclear/2018-sfwst-rd-team-meeting/), which incorporated several "evaluation" sessions aimed at assessing the current state-of-the-art of various ongoing R&D activities, the remaining R&D effort appropriate for those activities, and the current priority of those activities for each of the major generic repository host-rock environments: salt, argillite, and crystalline. These evaluation sessions—see Appendix A—resulted in modifications of the long-standing R&D Activities Table (see Table 3-1), which will serve as a key input to the FY 2019 SFWST Roadmap Update Workshop, to be held over 2½ days in January 2019 to confirm and/or re-align the generic R&D priorities established in 2012 (DOE 2012). The results of the January 2019 Roadmap Update Workshop will be documented in a level 2 milestone, due on April 30, 2019 (M2SF-18SN010304065), entitled *GDSA Framework Development and Process Model Integration*.

The evaluation methodology used in preparation for and during the May 2018 Annual Working Group Meeting is similar to what will be employed at the January 2019 Roadmap Update Workshop and is a form of decision analysis comparable to, but more straightforward than, the method used in DOE (2012). It consists of assigning a qualitative score to at least two key criteria formulated to prioritize various R&D activities. The score (e.g., "high," "medium," or "low") is based on expert evaluation of a qualitative metric scale for each criterion, as described later in this section (Table 3-2 and Table 3-3).

Table 3-1   SFWST R&D activities considered for potential integration into *GDSA Framework* and to support a safety case.

Task #	Task Name/ (and Work Package number -- if needed or helpful for more specificity)	Brief Task Description including Relevance (and/or input) to PA/GDSA (nPA = not direct input to PA)	Personnel/Lab	Type of Activity L = Literature review M = Modeling T = Testing or Experimental	Code (if applicable)	Importance to Safety Case (ISC) (H, M, or L -- see ISC table definitions) (Identify applicable Safety Case element from the provided figure)	Current "State of the Art" Level (SAL = 1, 2, 3, 4, or 5 -- see SAL table definitions) (Give brief update to applicable state-of-the-art "discussion(s)" shown in UFD Roadmap App. A, i.e., those discussion(s) for the highest scoring related FEPs)	Short-term (1 yr) R&D Priority Scores & Brief FY19 Work Scope Proposal (Priority Score = H, M, or L, based on combined ISC and SAL -- see PS table definitions) (Also give Roadmap Score for related FEP)	Long-term (2-5 yrs) R&D Priority Scores & Brief FY20-23 Work Scope Proposal (Priority Score = H, M, or L, based on combined ISC and SAL) ("Long-term" is most applicable to SAL = 5 issues) (Also give Roadmap Score for related FEP)	Related UFD Roadmap Issue(s)/FEP(s), and associated UFD Roadmap priority scores* (Find highest scoring related FEP in App. B of UFD Roadmap)	Other Notes/Comments (e.g., type of linkage to PA-GDSA; inputs required and/or linkages to other models and experiments)
	Ongoing Argillite/Crystalline/Salt/DPC/EBS Activities (WBS#s 1.08.01.03.01, 1.08.01.03.02, 1.08.01.03.03, 1.08.01.03.05, 1.08.01.03.08)										
1	CSNF repository argillite reference case	• Revise properties, EBS/repository design, conceptual models, etc., as necessary • Include multiphase flow (e.g., buffer resaturation) • Assess need for M and THM coupled processes in PA • Assess need for C and THC coupled processes in PA (e.g., for buffer and DRZ)	SNL et al.	L, M, T (mainly L, M)	GDSA	ISC=H	For subset (coupled processes) not done SAL=5 For properties, etc., SAL=3	PS Matrix Score = H; Roadmap Score = H For FY19 continue work on THMC coupled process model development Cross-reference with EBS/Int'n	PS Matrix Score = H; Roadmap Score = H For FY20-21 continue work on THMC coupled process model development Cross-reference with EBS/Int'n	• FEP not explicitly scored, but "disposal system modeling" rated as "high" priority as a "cross-cutting" issue.	•
2	CSNF repository crystalline reference case	• Develop a modeling capability to capture main stages of repository evolution. • Revise properties, EBS/repository design, conceptual models, etc., as necessary • Refine spatial heterogeneity by including deformation zone and more realistic fracture sets (and associated connectivity • Include multiphase flow (e.g., buffer resaturation) • Dual/multi-continuum for transport in granite	SNL et al.	L, M, T (mainly L, M)	GDSA					• FEP not explicitly scored, but "disposal system modeling" rated as "high" priority as a "cross-cutting" issue.	•
3	CSNF repository bedded salt reference case	• Revise properties, EBS/repository design, conceptual models, etc., as necessary • Include multiphase flow, if needed (e.g., heat pipes) • Assess need for M and THM coupled processes in PA • Assess need for Pitzer model for C	SNL et al.	L, M, T (mainly L, M)	GDSA					• FEP not explicitly scored, but "disposal system modeling" rated as "high" priority as a "cross-cutting" issue.	•
4	SNF Degradation	• Implmentation mixed potential model of spent fuel matrix degradation (including possible effect of Fe corrosion) • Radiolysis • Thermodynamics & stability of UO2 degradation phases (dehyd. schoepite, studtite, metastudtite) • Alternate electrochemical modeling for UO2 degradation	Frederick, Hammond, Weck, Jove Colon SNL; Jerden, ANL; Zuzax/Cantera Caporuscio LANL	M	PFLOTRAN/FMDM VASP (DFT calcs) Zuzax/Cantera	ISC = Medium ISC = High in Crystalline session SC element 3.3.1b	SAL = 3 SAL = 5 in Crystalline session From Roadmap: U.S. program evaluated the long-term behavior of LWR UOX in oxidizing environments. Other programs have evaluated and are modeling the degradation of UOX and MOX in reducing environments. Little information is available regarding the degradation/alteration of other UNF types.	PS Matrix Score = M; Roadmap Score = H PS Matrix Score = H in Crystalline Session For FY19 continue work on FMDM model development and code optimization EBS/Int'n	PS Matrix Score =M; Roadmap Score = H PS Matrix Score = H in Crystalline Session For FY20-21 continue work on FMDM model development and code optimization	• Primary FEP is 2.1.02.01; score = 4.01 • Other related FEPs have lower scores	• Direct implementation in PFLOTRAN already complete and now at the testing stage. • Additional development and more efficient coding suggested
4a	SNF Degradation testing activities	• Degradation testing and integration of testing results into mixed potential model of spent fuel matrix degradation	Caporuscio, LANL Jerden, ANL Jove-Colon, SNL	M, T	PFLOTRAN et al.	ISC = High SAL = 5 SC element 3.3.1b	SAL = 5 Little information is available regarding the degradation/alteration of other UNF types.	PS Matrix Score = H; Roadmap Score = H For FY19 continue work on FMDM model development and code optimization	PS Matrix Score = H; Roadmap Score = H For FY20-21 continue work on FMDM model development and code optimization	• Primary FEP is 2.1.02.01; score = 4.01 • Other related FEPs (2.1.02.06, 2.1.07.06, 2.1.11.02) have lower scores	• Further testing needed on other UNF types
5	(Pseudo) Colloid-Facilitated Transport Model	• Formation, stability, and transport of pseudocolloids in the near field and far field	Hammond SNL Reimus LANL Zavarin LLNL	M	PFLOTRAN	ISC = High SC element 3.3.2b	SAL = 5 From Roadmap: Significant work has been done. But the puzzle is yet to be put together. Evidence suggests that Pu travels further than Kd models would predict. Need improved models that can reproduce this observed behavior. Need improved techniques for insitu characterization and quantification of colloids. Leverage info from NAGRA working group on colloids. Colloid formation - Better understand formation from clay materials, sorption/desorption (attachment/detachment). Colloid instability in high ionic strength environments. Colloid transport - Need to reduce uncertainty in infiltration. Need to better represent heterogeneous behavior of colloids. Need better understanding of colloid transport behavior in unsaturated environments to reduce conservatisms in current models. Muliple rate kinetics and irreversibility of radionuclide sorption onto colloids - better understand size dependence.	PS Matrix Score = H; Roadmap Score = M For FY19 begin coupling LANL colloid model to GDSA Framework	PS Matrix Score = H; Roadmap Score = M For FY20 finish coupling LANL colloid model to GDSA Framework	• FEP 2.2.09.59 and 2.2.09.60; scores = 3.29	• Direct implementation in PFLOTRAN suggested, with perhaps some simplification of the conceptual model.
6	Intrinsic Colloids	• Intrinsic Pu colloid formation, stability, and transport in the near and the far fields, as a function of T	Hammond SNL Reimus LANL Zavarin LLNL	M	PFLOTRAN					• FEP 2.2.09.59 and 2.2.09.60; scores = 3.29	• Direct implementation in PFLOTRAN, with perhaps some simplification of the conceptual model.

Table 3-1 (cont.) SFWST R&D activities considered for potential integration into *GDSA Framework* and to support a safety case.

Task #	Task Name/ (and Work Package number -- if needed or helpful for more specificity)	Brief Task Description including Relevance (and/or input) to PA/GDSA (nPA = not direct input to PA)	Personnel/Lab	Type of Activity L = Literature review M = Modeling T = Testing or Experimental	Code (if applicable)	Importance to Safety Case (ISC) (H, M, or L -- see ISC table definitions) (Identify applicable Safety Case element from the provided figure)	Current "State of the Art" Level (SAL = 1, 2, 3, 4, or 5 -- see SAL table definitions) (Give brief update to applicable state-of-the-art "discussion(s)" shown in UFD Roadmap App. A, i.e., those discussion(s) for the highest scoring related FEPs)	Short-term (1 yr) R&D Priority Scores & Brief FY19 Work Scope Proposal (Priority Score = H, M, or L, based on combined ISC and SAL -- see PS table definitions) (Also give Roadmap Score for related FEP)	Long-term (2-5 yrs) R&D Priority Scores & Brief FY20-23 Work Scope Proposal (Priority Score = H, M, or L, based on combined ISC and SAL) ("Long-term" is most applicable to SAL = 5 issues) (Also give Roadmap Score for related FEP)	Related UFD Roadmap Issue(s)/FEP(s), and associated UFD Roadmap priority scores" (Find highest scoring related FEP in App. B of UFD Roadmap)	Other Notes/Comments (e.g., type of linkage to PA-GDSA; inputs required and/or linkages to other models and experiments)
Ongoing Argillite/Crystalline/Salt/DPC/EBS Activities (WBS#s 1.08.01.03.01, 1.08.01.03.02, 1.08.01.03.03, 1.08.01.03.05, 1.08.01.03.08)										
7	Discrete Fracture Network (DFN) Model	• Generation and representation of realistic fracture networks • Fluid flow& transport in fracture networks • Mapping tools (dfnWorks to PFLOTRAN) • Dual continuum; matrix diffusion	Stein, Hammond, Hadgu, Kalinina SNL; Hyman, Makedonska LANL	M	DFNWorks, PFLOTRAN, mapDFN.py, FracMan	ISC = High SC element 4.2e	SAL = 4 From Roadmap: The effects of geologic formation heterogeneity and their scale dependence is not fully understood. Need to consider/characterize scale dependence of properties for all physical transport processes. Effect of saturation on physical transport properties has additional uncertainty that could be reduced. Need to better understand bentonite/host rock interface (bentonite saturation) Advection follows flow, see FEP 2.2.08.01. Need to better understand the effect of channeling and advective flow-wetted surfaces on diffusion and sorption. Dispersion - Evaluate alternative advection/dispersion conceptual models. Diffusion - Need better characterizion / conceptualization of diffusion in small pores (e.g., clays) - membrane effect (EDL overlap). Need generic experimental work (e.g., enginieered materials). Dilution - Well understood.	PS Matrix Score = M; Roadmap Score = H FY19 Workscope…..		• Primary FEP is 2.2.09.51 (crystalline); score = 3.74 • Other related FEPs also have relatively high scores: 2.2.08.01,2.2.02.01,2.2.05.01, 2.2.08.02	potential FY17 enhancements: heat transport; fracture intersects borehole • Dual continuum/matrix diffusion ready now
8	HLW WF degradation (process model)	• Glass waste degradation • Radiolysis • Transition state theory	Rieke, PNNL Ebert, ANL	M	PFLOTRAN et al.					• Primary FEP is 2.1.02.02; score = 0.00 (because not considered part of UFD)	• Integration with Waste Form Campaign
9	Waste Package Degradation Model (mechanistic)	• Degradation of waste packages and canisters • Carbon steel; stainless steel; copper waste packages • Include various degradation processes (SCC, GC, LC, MIC, early failure)	Jove Colon SNL Caporuscio, LANL	M	PFLOTRAN et al.	ISC = Medium (for clay/shale) SC element 3.3.1b	SAL = 5	PS Matrix Score = M; Roadmap Score = H FY19 workscope: ….	PS Matrix Score = M; Roadmap Score = H FY20-21 workscope: …	• FEPs 2.1.03.02, 2.1.03.03, 2.1.03.04, 2.1.03.05; scores = 4.34	• Direct implementation in PFLOTRAN suggested (1D model), similar to SNF degradation • Currently evaluating development of thermodynamic relations for high T 316 SS corrosion phase assemblage (e.g., chromite, magnetite)
9a	Waste Package Degradation Testing	• Testing and experimental data for corrosion of carbon steel, stainless steel, and other potential waste package materials	Jove Colon SNL Caporuscio, LANL	T	N/A	ISC = Medium (for clay/shale) SC element 3.3.1b	SAL=5 Some knowledge gaps exist regarding degradation modes for various alloys under various conditions. Little/no information available regarding new/novel materials. Uncertainty in extrapolating short-term aboratory tests to long-time periods. Interest in gas generation resulting from corrosion in some programs (Europe) Little information known about novel alloys with increased resistance to corrosion.	PS Matrix Score = M; Roadmap Score = H	PS Matrix Score = M; Roadmap Score = H	• FEPs 1.03.02, 2.1.03.03, 2.1.03.04, 2.1.03.05; scores = 4.34	• Support for modeling efforts
9b	Waste Package Degradation Salt environment	• Testing and experimental data for corrosion of carbon steel, stainless steel, and other potential waste package materials in a salt repository	Kuhlman, Stauffer, Rutqvist, et al.	T	N/A	ISC = Medium (for salt) SC element 3.3.1b	SAL=5 Some knowledge gaps exist regarding degradation modes for various alloys under various conditions. Little/no information available regarding new/novel materials. Uncertainty in extrapolating short-term aboratory tests to long-time periods. Interest in gas generation resulting from corrosion in some programs (Europe) Little information known about novel alloys with increased resistance to corrosion.	PS Matrix Score = M; Roadmap Score = H	PS Matrix Score = M; Roadmap Score = H	• FEPs 2.1.03.02, 2.1.03.03, 2.1.03.04, 2.1.03.05; scores = 4.34	No credit is typically taken (e.g., at WIPP) for waste packages. Mechanical integrity of waste packages may be relevant to criticality for certain waste types (e.g., Pu). May be most relevant in early post-closure time frame (before room closese in first few hundred years). In a dry salt repository (i.e., very hot), the waste packages may survive better. Canisters may have a rind of dry salt deposited on them during dry-out. Run-of-mine salt backfill can be used for shielding of waste packages during emplacement and operational phases.
10	Salt Coupled THM processes	• Coupled thermal-hydrological-mechanical processes in salt EBS and EDZ	Rutqvist. Hu, Blanco-Martin LBNL	M	TOUGH-FLAC	ISC = High SC elements 3.3 & 4.2	SAL = 5 From Roadmap (for FEP 2.2.01.01): Need to know the evolution of the characteristics of the EDZ under the thermal-mechanical and wetting changes (clay and salt). Need to understand the coupled evolution of near-field host rock (EDZ) and backfill.	PS Matrix Score = H; Roadmap Score = H workscope:Coupled model development and validation along with phased field tests, including EBS with crushed backfill and host rock. Critical for critical for better parametrization (parameters for creep and permeability evolution, back-fill compaction). Prioritize work for intergration with PA (PFLOTRAN) including calculation of reponse surfaces for defined GDSA cases. J15. Will discuss in Nov 2018 meeting	PS Matrix Score = H; Roadmap Score = H	• Primary FEP is 2.2.08.06 (salt) • Other related FEPs include 2.1.08.03 and 2.2.01.01	• Response surface suggested (permeability and porosity fields/surfaces for EDZ and backfill)
11	Coupled THC processes in Salt	• Coupled thermal-hydrologic-chemical processes in a salt repository	Stauffer LANL Hammond SNL	M	FEHM, PFLOTRAN	ISC = High SC elements 3.3 & 4.2	SAL = 5 From Roadmap (for FEP 2.2.08.01): Need to develop improved modeling tools to represent fractures/fracture sets as discrete features in crystalline. Need information to characterize/model connectivity, channelization (e.g., tracer tests). Need to understand fracturation and healing in clays and salt. Water migration in salt is a unique process that needs to be better understtod. Need to understand thermal and pressure gradients and gas generation and migration. Need to capture and validate uncertainty.	FY18-19: Models continue to be tested against all available laboratory/field data as described in the LANL PICS task. Limited work was done in FY18 on integrating the new salt algorithms into PFOTRAN. This should become a priority moving forward. Will discuss in Nov 2018 meeting	FY19-23. Prioritize salt algorithms necessary to include in PFLOTRAN and get the necessary staff inloved to make the code changes. Recommend hiring a devoted postdoc for this work who could work jointly with Glenn Hammond and the LANL team.	• Primary FEP is 2.2.08.06 (salt); score = 7.73 • Another high-score FEP is 2.2.08.04; score = 7.10	• Hammond indicates that chemical components can be added to gas phase in PFLOTRAN formulation. • Important constitutive relationships still needed in PFLOTRAN include (Kuhlman): - Crushed salt thermal conductivity dependence on porosity and temperature, - Salt solubility in brine as a function of temperature, - Changes in salt porosity including precipitation and dissolution of salt, - Water vapor diffusion coefficient as a function of pressure, temperature, and porosity, - Power-law permeability-porosity relationship, - Water vapor pressure as a function of brine strength and temperature, and
12	Two-Part Hooke's Model (saturated)	• Clay deformation, constitutive model development for EDZ evolution in Argillite and Chrystalline rock.	Rutqvist, Zheng LBNL	M	TPHM-FLAC3D	ISC = Low SC elements 3.3 & 4.2	SAL = 5 it is modeling concept that had been proposed and tested in limited case. This concept has not been the meanstream concept for modeling the clay deformation. It's necessity has to be further examined. The Two-Parts Hooke's model should be viewed as a constitutive model that has been implemented into FLAC3D (and TOUGH-FLAC). The application can be, among others, EDZ evolution (how permeability and poroosity and stiffness varies). However, it has already been developed and should therefore be included as part of Argillite THM Coupled Processes models.	PS Matrix Score = L; Roadmap Score = M Work on this continues as part of Argillite Coupled THM Model Development. Two-parts Hooke's model is a constitutive model that can be and have been applied to model EDZ under mine-by experiments in Argillite		• Primary FEP is 2.2.01.01 (granite); score = 2.58	• Used to calculate the permeability/porosity evolution of EBS in clay formation using a continuum approach • Abstraction suggested (permeability, porosity, stress).

Table 3-1 (cont.) SFWST R&D activities considered for potential integration into *GDSA Framework* and to support a safety case.

Task #	Task Name/ (and Work Package number – if needed or helpful for more specificity)	Brief Task Description including Relevance (and/or input) to PA/GDSA (nPA = not direct input to PA)	Personnel/Lab	Type of Activity L = Literature review M = Modeling T = Testing or Experimental	Code (if applicable)	Importance to Safety Case (ISC) (H, M, or L -- see ISC table definitions) (Identify applicable Safety Case element from the provided figure)	Current "State of the Art" Level (SAL = 1, 2, 3, 4, or 5 -- see SAL table definitions) (Give brief update to applicable state-of-the-art "discussion(s)" shown in UFD Roadmap App. A, i.e., those discussion(s) for the highest scoring related FEPs)	Short-term (1 yr) R&D Priority Scores & Brief FY19 Work Scope Proposal (Priority Score = H, M, or L, based on combined ISC and SAL -- see PS table definitions) (Also give Roadmap Score for related FEP)	Long-term (2-5 yrs) R&D Priority Scores & Brief FY20-23 Work Scope Proposal (Priority Score = H, M, or L, based on combined ISC and SAL) ("Long-term" is most applicable to SAL = 5 issues) (Also give Roadmap Score for related FEP)	Related UFD Roadmap Issue(s)/FEP(s), and associated UFD Roadmap priority scores" (Find highest scoring related FEP in App. B of UFD Roadmap)	Other Notes/Comments (e.g., type of linkage to PA-GDSA; inputs required and/or linkages to other models and experiments)
Ongoing Argillite/Crystalline/Salt/DPC/EBS Activities (WBS#s 1.08.01.03.01, 1.08.01.03.02, 1.08.01.03.03, 1.08.01.03.05, 1.08.01.03.08)											
13	Simplified Representation of THMC processes in EBS (clay illitization)	• THMC (includes clay illitization)	Rutqvist, Zheng, LBNL Caporuscio, LANL	M	TOUGH REACT/FLAC3D	ISC = High SC elements 3.3 & 4.2	SAL = 4 Coupled THMC model that has been tested with in situ data was developed. Illitization is relatively well understood despite more testing is needed. Extracting a simplied representation takes great effort	PS Matrix Score = M; Roadmap Score = H EBS/ Int'l		• Primary FEP is 2.1.04.01; score = 3.50	• Response surface suggested (permeability, porosity, cation exchange capacity, swelling stress). • Chemical processes still under development
13a	Clay illitization experimental data re: Simplified Representation of THMC processes in EBS	• Input from high temperature experimental data, including lack of illitisation - dependent on bulk chemistry • Full chemistry reactive transport (RT) representation without mechanics	Caporuscio, LANL Jove Colon, SNL Rutqvist, Zheng, LBNL	M, T	Experimental data to inform TOUGH REACT/FLAC3D PFLOTRAN	ISC = High (for clay/shale) SC element 3.3.1c	SAL=5 • Chemical processes still under development, particularly at elevated temperature conditions	PS Matrix Score = M; Roadmap Score = H FY19 workscope: …	PS Matrix Score = M; Roadmap Score = H FY20-21 workscope: …	• Primary FEP is 2.1.04.01; score = 3.50	• Clay phase transformation in response to temperature could cause inhomogeneous swelling through the clay barrier • Response surface suggested (permeability, porosity, cation exchange capacity, swelling stress).
14	Argilllite Coupled THM processes modeling including host rock, EBS and EDZ (TOUGH-FLAC)	• Coupled thermal-hydrological-mechanical processes in Argillite host rock repository, including EBS (bentonite and backfill), and excavaton disturbed zone	Rutqvist, Xu LBNL	M	TOUGH-FLAC	ISC = High SC elements 3.3 & 4.2	SAL = 5 From Roadmap (for FEP 2.2.01.01): Need to know the evolution of the characteristics of the EDZ under the thermal-mechanical and wetting changes (clay and salt). Need to understand the coupled evolution of near-field host rock (EDZ) and backfill.	FY19 workscope: R&D for (1) confident modeling bentonite dual-structure behavior on permeability and resaturation, (2) confident modeling of EDZ evolution, including long-term sealing and healing and (3) model development for gas migration in bentonite and clay host rocks. Continued model validation agaions large scale field experiments related to international activities (Mont Terri Project and DECOVALEX 2019). Expand for modeling of fault activation fluid migration along faults. Linking of new TOUGH3 code with new FLAC3D V6 for more efficient simulations.	PS Matrix Score = H; Roadmap Score = H FY20-21 workscope: Continued model development and validation related to DECOVALEX-2023, incllduding (1) Fault actviation and fluid migration along faults, (2) field experiments on gas migration, and potential other tasks in DECOALEX-2023. Prioritize model for intergration with PA (PFLOTRAN) including calculation of reponse surfaces for defined GDSA cases.	• Primary FEP is 2.2.01.01 Evolution of EDZ (clay/shale); score = 8.00, Other FEPS include 2.1.04.01: Evolution and degradation of backfill/buffer, 2.2.11.06: Thermal mechanical effects of geophere, 2.1.12.03: Gas transport in EBS	• Response surface suggested (permeability and porosity fields/surfaces for EDZ and backfill.
15	THM discrete Fracture Modeling using Rigid-Body-Spring-Network (RBSN)	• Discrete Fracture Network (DFN) with THM (argillite/clay)	Kim, Rutqvist LBNL	M	TOUGH2-RBSN	ISC = High SC elements 3.3 & 4.2	SAL = 5 From Roadmap (for FEP 2.2.01.01): Need to know the evolution of the characteristics of the EDZ under the thermal-mechanical and wetting changes (clay and salt). Need to understand the coupled evolution of near-field host rock (EDZ) and backfill.	PS Matrix Score = H; Roadmap Score = H FY19 workscope: Continued dicrete fracture modeling of gas migration experiments along with the DECOVALEX-2019 project. Validation of anisotropic, layered shale, strength and elastic properties against laboratory data from Opalinus Clay and other shales.	PS Matrix Score = H; Roadmap Score = H FY20-21 workscope:	• Primary FEP is 2.2.01.01 Evolution of EDZ (clay/shale); score = 8.00,	Abstraction suggested (fracture property response surface). A coupled version of RBSN requires dynamic input (T, p,s). Could also be used for upscaling from discrete fracture network to continuum properties for TOUGH-FLAC.
16	Diffusion of actinides through bentonite (including speciation)	• Speciation, sorption, diffusion input data	C. Joseph, M. Zavarin LLNL	T	N/A	ISC= M (clay/shale)	SAL=3			• Primary FEP is 2.1.09.13; score = 4.86	• Direct implementation in PFLOTRAN suggested (but not clear if this is a model or just a data-gathering experiment for Fick's Law). Data gathering time frame up to 6 years. (Need to review Joseph et al. 2016 for implementation suggestions.)
17	Thermodynamic and sorption database(s)	• Probably in PA. Baseline safety assessment • Thermodynamic, surface complexation/ion-exchange databases • Update of thermodynamic data for clays, zeolites, & oxy-hydroxides - Barrier degradation at high Ts • EoS for H2O (Liquid, vapor) revisiting	M. Zavarin, C. Duffin, T. Wolery LLNL Jove Colon SNL	T, M	H2OI95 --> IAPWS-95 H2O EoS Fortran code implementation	ISC = Medium (for clay/shale) SC element 3.3.1c, 3.3.2b	SAL=5 • Updates to key thermodynamic data on barrier chemical components and stable alteration phase assemblages • Sorption data analysis • Update H2O EoS - Geochemical & flow/transport codes	PS Matrix Score = M; Roadmap Score = H FY19 workscope: …	PS Matrix Score = M; Roadmap Score = H FY20-21 workscope: …	• Primary FEP is FEP 2.1.09.13; score = 4.86 • FEP 2.2.09.61 is related; • FEP 2.2.11.04 is related; score = 3.55 • FEP 2.1.05.01 is related; score = 3.50	• Thermodynamic, surface complexation/ion-exchange databases, used as input to process models • Surface complexation unlikely to be represented in PA • The current H2O EoS in PFLOTRAN (IFC-67) is considered obsolete, although it may still be adequate
17a	THC processes in EBS	• Engineered barrier (metal-clay-rock) material interactions & experimental data • Modeling (thermodynamic & reactive transport)	Caporuscio, LANL Jove-Colon, SNL	M, T	PFLOTRAN, CHNOSZ, EQ3/6	ISC = High (for clay/shale) SC element 3.3.1b, 3.3.1c	SAL=5 • Chemical processes still under development, particularly at elevated temperature conditions	PS Matrix Score = H; Roadmap Score = H FY19 workscope: …	PS Matrix Score = H; Roadmap Score = H FY20-21 workscope: …	• Primary FEPs are 2.1.04.01 (score = 3.50), 2.1.03.02, 2.1.03.04 • FEP 2.1.09.13 is related; score = 4.86 • FEP 2.2.09.61 is related; score = 3.55 • FEP 2.2.11.04 is related; score = 3.55 • FEP 2.1.05.01 is related; score = 3.50	• No model linkage to GDSA yet. • Attempting to represent in PFLOTRAN reactive transport (RT) modeling in baseline case • Modeling of phase parageneses & mechanisms (in progress)
18	Borehole-based Field Testing in Salt	• Horizontal borehole test(s) in salt to verify: geochemical, geohydraulic, and geomechanical phenomena	Kuhlman SNL Stauffer LANL Rutqvist LBNL	T	PFLOTRAN, FEHM, TOUGH-FLAC	ISC = High SC elements 3.3 & 4.2	SAL = 5 From Roadmap (for FEP 2.2.08.06): Flow regimes and pathways are important factors for long-term performance assessments.	Shakedown field test being implemented in FY18. Field test being implemented in late FY18 and FY19 for new two boreholes (120C and ambient). Will discuss in Nov 2018 meeting. 1) Instrumentation. 2) Logistics / training at WIPP. 3) Data collection 4) data interpretation 5) follow-on test design 6) troubleshooting	Additional heated temperatures, borehole configurations, and intstrumentation will be used in follow-on tests in FY19 and beyond. 1) Instrumentation. 2) Logistics / training at WIPP. 3) Data collection 4) data interpretation 5) follow-on test design 6) troubleshooting		• Modeling before and after field experiments. Test plans to be developed in FY17, execution in FY18 based on available funding. Highest priority activity in Salt R&D
18a	Laboratory Experiments to Validate Coupled Process models in Salt	coupled small-scale TH/THC/THM/THMC laboratory experiments that can be used to validate and parameterize coupled processes in salt	Kuhlman SNL Stauffer LANL Rutqvist LBNL	T, M		ISC = high	SAL = 4	As-needed laboratory tests will be scoped. Tests may be concieved to explain observations or process from field test, or from feedback in international interactions.			

Table 3-1 (cont.) SFWST R&D activities considered for potential integration into *GDSA Framework* and to support a safety case.

Task #	Task Name/ (and Work Package number -- if needed or helpful for more specificity)	Brief Task Description including Relevance (and/or input) to PA/GDSA (nPA = not direct input to PA)	Personnel/Lab	Type of Activity L = Literature review M = Modeling T = Testing or Experimental	Code (if applicable)	Importance to Safety Case (ISC) (H, M, or L -- see ISC table definitions) (Identify applicable Safety Case element from the provided figure)	Current "State of the Art" Level (SAL = 1, 2, 3, 4, or 5 -- see SAL table definitions) (Give brief update to applicable state-of-the-art "discussion(s)" shown in UFD Roadmap App. A, i.e., those discussion(s) for the highest scoring related FEPs)	Short-term (1 yr) R&D Priority Scores & Brief FY19 Work Scope Proposal (Priority Score = H, M, or L, based on combined ISC and PS -- see PS table definitions) (Also give Roadmap Score for related FEP)	Long-term (2-5 yrs) R&D Priority Scores & Brief FY20-23 Work Scope Proposal (Priority Score = H, M, or L, based on combined ISC and SAL) ("Long-term" is most applicable to SAL = 5 issues) (Also give Roadmap Score for related FEP)	Related UFD Roadmap Issue(s)/FEP(s), and associated UFD Roadmap priority scores" (Find highest scoring related FEP in App. B of UFD Roadmap)	Other Notes/Comments (e.g., type of linkage to PA-GDSA; inputs required and/or linkages to other models and experiments)
Ongoing Argillite/Crystalline/Salt/DPC/EBS Activities (WBS#s 1.08.01.03.01, 1.08.01.03.02, 1.08.01.03.03, 1.08.01.03.05, 1.08.01.03.08)											
18b	Brine Chemistry and Composition in Salt	Analysis of brine composition from other salt sites beyond WIPP. Numerical modeling of brine composition during evaporation and dry-out. Most geochemistry modeling in brine has to do with actinide chemistry	Kuhlman, Mills	L, M,T	PFLOTRAN, EQ3/6	ISC = high	SAL = 4	Part of the borehole heater test program. Samples of brine will be collected from borehole. Numerical modeling of brine (Pitzer mode) will be use to predict liquid and solid components of brine during the test, and compared against observations			
18c	Migration of capabilities to PFLOTRAN from TOUGH-FLAC & FEHM	Capabilities in TOUGH-FLAC and FEHM should be integrated into PFLOTRAN whenever possible and profitable. Could use surrogate models or lookup-tables/response surfaces	Jenn	M	PFLOTRAN, FEHM, TOUGH-FLAC	ISC = high	SAL = 5		As possible, features from FEHM and TOUGH-FLAC will be migrated to PFLOTRAN. This is the embodiment of GDSA integration.		
18d	Evolution of backfill in salt repository	Temporal, compositional, and textural evolution of 1) run-of-mine salt backfill, 2) salt with possible additives (e.g., clay, sand). Also constitutive models used to describe these processes. What are the uncertainties in using uncontrolled run-of-mine salt.	SNL	L,M,T		ISC = high	SAL = 4				
18e	Numerical modeling of dryout in multiphase	Compare, validate, and benchmark the dryout and resaturation process in PFLOTRAN (compare TOUGH, FEHM, etc.)	SNL	M	PFLOTRAN, FEHM, TOUGH	ISC = medium	SAL = 5				
19	Possibly simplified representation of drift resaturation process	• Use TH(M) to simulate development of "initial conditions" used in long-term GDSA PA model. Especially with respect to the re-saturation of the DRZ. All media (except DBH) have some amount of increased porosity and decreased saturation in the DRZ surrounding the drift. In salt and clay, the re-hydration process is likely to be coupled with mechanical drift deformation and swelling/healing. The thermal conductivity and heat capacity of the buffer/backfill are very sensitive to the distribution of moisture. If the backfill or DRZ are dry, they will be more thermally insulating.	Kuhlman(?) SNL	M	PFLOTRAN	ISC = High (for clay/shale) - same as 17a & 20 SC element 3.3.1b, 3.3.1c	SAL=5 - same as 17a & 20 • Chemical processes still under development, particularly at elevated temperature conditions		•		• Development of saturation and pressure initial conditions (or possibly start time, when a fully saturated domain is justified). • The TH (no mechanical) assessment of resaturation could be carried out with PFLOTRAN. This would be a first step to explore the dependence of the resaturation on the vadose zone parameters (i.e., van Genuchten parameters), and the sensitivity of the resaturation to these parameters, and related back to the uncertainty of these parameters. Even though these processes may never be included in the GDSA PA model, they should be explored at an appropriate scale and dimension (e.g., a 2D cross-section through a drift).
20	Possibly simplified representation of drift resaturation process with chemistry	• Use TH(M)C to simulate development of "initial conditions" used in long-term GDSA PA model. Especially with respect to the re-saturation of the DRZ. In salt and clay, the re-hydration process is likely to be coupled with mechanical drift deformation and swelling/healing. All media (except DBH) have some amount of increased porosity and decreased saturation in the DRZ surrounding the drift. In salt and clay, the re-hydration process is likely to be coupled with mechanical drift deformation and swelling/healing. • **Include critical review of clay & zeolite high temperature data that replicates resaturation**	Kuhlman(?) SNL Jove-Colon(?) SNL **Caporuscio LANL**	M	PFLOTRAN	ISC = High (for clay/shale) SC element 3.3.1c	SAL=5 • Chemical processes still under development, particularly at elevated temperature conditions	PS Matrix Score = H; Roadmap Score = H FY19 workscope: ….	PS Matrix Score = H; Roadmap Score = H FY20-21 workscope: …	• Primary FEP is probably 2.2.08.06; score = 3.65 • FEP 2.2.01.01 is related; score = 8.0	• Development of saturation and pressure initial conditions (or possibly start time, when a fully saturated domain is justified), including the effects of chemistry and two-phase flow and transport. • The THC (no mechanical, with reactive chemistry) assessment of resaturation could be carried out with PFLOTRAN. This would be a first step to explore the dependence of the full chemistry on the resaturation on the . Performing a full chemistry simulation at the drift scale (rather than the GDSA PA scale of several km), will illustrate how resaturation slows down some chemical processes and may speed up others. Dry early-time conditions in the DRZ and backfill may slow down canister corrosion.
20a	Data analysis re: Possibly simplified representation of drift resaturation process with chemistry	• Include critical review of clay high temperature clay data that replicates resaturation	Caporuscio, LANL Kuhlman(?) SNL Jove-Colon(?) SNL	T	Incorporate experimental data into PFLOTRAN	ISC = High (for clay/shale) SC element 3.3.1c	SAL=5 • Chemical processes still under development, particularly at elevated temperature conditions	PS Matrix Score = H; Roadmap Score = H FY19 workscope: ….	PS Matrix Score = H; Roadmap Score = H FY20-21 workscope: …	• Primary FEP is probably 2.2.08.06; score = 3.65 • FEP 2.2.01.01 is related; score = 8.0	• Development of saturation and pressure initial conditions (or possibly start time, when a fully saturated domain is justified), including the effects of chemistry and two-phase flow and transport. • The THC (no mechanical, with reactive chemistry) assessment of resaturation could be carried out with PFLOTRAN. This would be a first step to explore the dependence of the full chemistry on the resaturation on the . Performing a full chemistry simulation at the drift scale (rather than the GDSA PA scale of several km), will illustrate how resaturation slows down some chemical processes and may speed up others. Dry early-time conditions in the DRZ and backfill may slow down canister

Table 3-1 (cont.) SFWST R&D activities considered for potential integration into *GDSA Framework* and to support a safety case.

Task #	Task Name/ (and Work Package number – if needed or helpful for more specificity)	Brief Task Description including Relevance (and/or input) to PA/GDSA (nPA = not direct input to PA)	Personnel/Lab	Type of Activity L = Literature review M = Modeling T = Testing or Experimental	Code (if applicable)	Importance to Safety Case (ISC) (H, M, or L – see ISC table definitions) (Identify applicable Safety Case element from the provided figure)	Current "State of the Art" Level (SAL = 1, 2, 3, 4, or 5 – see SAL table definitions) (Give brief update to applicable state-of-the-art "discussion(s) shown in UFD Roadmap App. A, i.e., those discussion(s) for the highest scoring related FEPs)	Short-term (1 yr) R&D Priority Scores & Brief FY19 Work Scope Proposal (Priority Score = H, M, or L, based on combined ISC and SAL – see PS table definitions) (Also give Roadmap Score for related FEP)	Long-term (2-5 yrs) R&D Priority Scores & Brief FY20-23 Work Scope Proposal (Priority Score = H, M, or L, based on combined ISC and SAL) ("Long-term" is most applicable to SAL = 5 issues) (Also give Roadmap Score for related FEP)	Related UFD Roadmap Issue(s)/FEP(s), and associated UFD Roadmap priority scores* (Find highest scoring related FEP in App. B of UFD Roadmap)	Other Notes/Comments (e.g., type of linkage to PA-GDSA; inputs required and/or linkages to other models and experiments)
Ongoing Argillite/Crystalline/Salt/DPC/EBS Activities (WBS#s 1.08.01.03.01, 1.08.01.03.02, 1.08.01.03.03, 1.08.01.03.05, 1.08.01.03.08)											
DPC A.1	Analysis of technical and programmatic solutions for direct disposal of DPCs.	Evaluate options for DPC direct disposal. Define a set of goals for successful disposition. Address the impact of repository siting and licensing on available solutions and needed R&D. Analyze the scope and timing of needed R&D activities. Analyze uncertainty in program constraints and external inputs.	Kessler, Hardin, other SNL staff; and laboratory staff (ORNL)	L (and ongoing other activities)		NA	NA	NA	NA	NA	NA
DPC A.2	Support engagement with stakeholders	Support Federal interactions with government and private-sector stakeholders.	Kessler, Hardin, Alsaed, other SNL and laboratory staff (ORNL)	NA		NA	NA	NA	NA	NA	NA
DPC A.3	Engineering and cost analysis support	Support analysis of technical solutions by describing and ROM costing. Include "criticality control enhancements" (EPRI 2008) that could be added at loading or after cutting DPC lids off.	Sandia engineering staff	L		NA	NA	NA	NA	NA	NA
DPC A.4 (new)	Out-year support	Refine strategy and planning basis; continue stakeholder interactions	TBD	L (and ongoing other activities)		NA	NA	NA			
DPC B.1	Scoping Phase - Probabilistic post-closure DPC criticality consequence analyses	Develop technical and regulatory strategy for low consequence analyses. Identify an appropriate set of criticality FEPs. Define key parameters and metrics.	Price, Brady, Gross, Hardin, Alsaed, other SNL PA staff, other laboratory staff (ORNL)	L, M	PFLOTRAN, other codes and scripts as applicable	ISC = High	SAL = 5	PS Matrix Score = H	NA	NA	
DPC B.2	Preliminary Analysis Phase - Probabilistic post-closure DPC criticality consequence analyses	Generic probabilistic/regulatory analysis - Incorporate criticality into performance assessment using approaches to abstraction and simulation. Evaluate key parameters and metrics, and identify the most important uncertainties. Use insights from HPC calculations.	Price, Brady, Gross, Hardin, Alsaed, other SNL staff and subcontractors, other laboratory staff (ORNL)	L, M	PFLOTRAN, other codes and scripts as applicable	ISC = High	SAL = 5	PS Matrix Score = H; Roadmap Score = L	PS Matrix Score = H Add additional processes (C,R) and couplings (N,H,M,C,R) and develop site-specific PA implementation for criticality risk screening.	2.1.14.01 Criticality in Package (score based on TAD canisters in LA = 0.96)	
DPC B.3 (new)	Development Phase - Probabilistic post-closure DPC criticality consequence analysis	Continue development of analysis including process treatment, reduction of uncertainties, quantification of key parameters, and insights from multi-physics calculations.	Price, Brady, Gross, Hardin, Alsaed, other SNL staff and subcontractors, other laboratory staff (ORNL)	L, M	PFLOTRAN, other codes and scripts as applicable	ISC = High	SAL = 5	PS Matrix Score = H			
DPC B.4 (new)	Maintain and populate DPC as-loaded database	Maintain UNF-ST&DARDS database; ; analyze baseline post-closure criticality responses	ORNL staff	L,M	Database; SCALE; etc.	ISC = High	SAL = 2	PS Matrix Score = M			
DPC C.1	DPC filler and neutron absorber degradation testing	Identify potential filler compositions, and test relevant behavior (injectability, radiolysis, material interactions, leachability). Follow the FY18 workplan (SFWD-SFWST-2018-000481) with appropriate modifications to focus on promising fillers. Test Boral and other absorber materials to check boron loss, and threshold humidity/temperature corrosion for filler interaction studies.	Brady, Rigali, Basurto (SNL) Caporuscio (LANL)	L, T	NA	ISC = Medium	SAL = 3	PS Matrix Score = M	NA	NA	
DPC C.2 (new)	Fillers R&D development	Perform system-level evaluation of filler processes (gas pressure, RCRA questions, loaded canister weight, regulatory risk, etc.). Proceed with proof-of-concept testing for selected fillers, as appropriate.	TBD	L, M	NA	ISC = High	SAL = 5	PS Matrix Score = H	NA	NA	
DPC D.1	Coupled multi-physics simulation of DPC postclosure (neutronic, thermal-hydraulic & mechanical)	Analyze conditions inside and outside waste packages subjected to criticality events. Implement 2-way coupling between neutronics and thermal-hydraulics, and 1-way coupling between mechanical degradation and thermal-hydraulics and neutronics (replicate earlier studies). Incorporate conditions external to waste packages (saturated and unsaturated repositories). Evaluate how more couplings, processes (chemical, radiolysis, aqueous transport), and disruptive events (seismic) can be incorporated in future models	Hardin, Alsaed, Rodriguez, Ames, other SNL staff and subcontractors, Rutqvist (LBNL), and other laboratory staff (ORNL)	L, M	RELAP5, RELAP7, MCNP, other codes as applicable	ISC = High	SAL = 5	PS Matrix Score = M; Roadmap Score = L	PS Matrix Score = M Support risk model with additional processes and couplings, and site-specific simulations.	2.1.14.01 Criticality in Package (score based on TAD canisters in LA = 0.96)	
DPC D.2 (new)	Evaluate and develop coupled multi-physics simulation of DPC postclosure criticality	Multi-year activity to evaluate whether and how more couplings, processes (chemical, radiolysis, aqueous transport), additional cases; canister types; thermal loading; ex-container EBS performance; and disruptive events (seismic) can be incorporated in future models. Perform appropriate multi-physics calculations as needed to support probabilistic criticality consequence screening.	SNL, ORNL, others TBD	M	TBD	ISC = High	SAL = 5	PS Matrix Score = H			

Table 3-1 (cont.) SFWST R&D activities considered for potential integration into *GDSA Framework* and to support a safety case.

Task #	Task Name/ (and Work Package number -- if needed or helpful for more specificity)	Brief Task Description including Relevance (and/or input) to PA/GDSA (nPA = not direct input to PA)	Personnel/Lab	Type of Activity L = Literature review M = Modeling T = Testing or Experimental	Code (if applicable)	Importance to Safety Case (ISC) (H, M, or L -- see ISC table definitions) (Identify applicable Safety Case element from the provided figure)	Current "State of the Art" Level (SAL = 1, 2, 3, 4, or 5 -- see SAL table definitions) (Give brief update to applicable state-of-the-art "discussion(s)" shown in UFD Roadmap App. A, i.e., those discussion(s) for the highest scoring related FEPs)	Short-term (1 yr) R&D Priority Scores & Brief FY19 Work Scope Proposal (Priority Score = H, M, or L, based on combined ISC and SAL -- see PS table definitions) (Also give Roadmap Score for related FEP)	Long-term (2-5 yrs) R&D Priority Scores & Brief FY20-23 Work Scope Proposal (Priority Score = H, M, or L, based on combined ISC and SAL) ("Long-term" is most applicable to SAL = 5 issues) (Also give Roadmap Score for related FEP)	Related UFD Roadmap Issue(s)/FEP(s), and associated UFD Roadmap priority scores* (Find highest scoring related FEP in App. B of UFD Roadmap)	Other Notes/Comments (e.g., type of linkage to PA-GDSA; inputs required and/or linkages to other models and experiments)
Gap Activities for Argillite/Crystalline/Salt/DPC/EBS -- not currently scoped/funded in SFWST DR (WBS#s 1.08.01.03.01, 1.08.01.03.02, 1.08.01.03.03, 1.08.01.03.05, 1.08.01.03.08)											
50	Biosphere pathways	• Detailed biosphere pathways, processes, and FEPs	Mariner, et al SNL Others?	M	GDSA					• Biosphere FEPs score low (<1), but this is needed eventually to satisfy regulations	• This should probably wait until there are actual candidate sites • Needs to consider the various biosphere FEPs in the UFDC list (3.3.XXYY)
51	Cladding Degradation	• Cladding degradation processes (e.g., HC)	?	M, T (mainly M)	PFLOTRAN?	ISC=M - see tasks 9 & 9a	SAL=5			• FEP 2.1.02.06; score = 3.62	• Cross-reference with activity 9 & 17a
52	In-Package Flow	• Modeling of flow and transport inside waste packages/canisters • Evolution of corrosion products	GDSA team?	M, T (mainly M)	PFLOTRAN	ISC=H	SAL=5			• Primary FEP is probably 2.1.09.51; score = 3.06	• Requires development of a tractable conceptual model • Cross-reference with activity 17a, 20, & 20a
53	In-Package Chemistry	• Fully coupled in-package chemistry model, as it impacts degradation, mobilization, and transport inside the WP • Effect of canister/internal corrosion products on waste form degradation	Mariner SNL? Jove Colon SNL? Jerden ANL? Zavarin LLNL?	M	PFLOTRAN et al.	ISC=H	SAL=5 - Cross-cut EBS Int'l			• Primary FEP is probably 2.2.09.13; score = 4.86	• High fidelity electrochemistry coupled with transport • Cross-reference with activity 17a, 20, & 20a
										•	•
R&D Activities identified in Crystalline breakout session at May 2018 SFWST Annual Meeting											
88	fuel matrix degradation model	FMDM for crystalline hostrock.				H	4 or 3	M			
89	steel corrosion - incorporation of radionuclides	incorporation of radionuclides in steel corrosion products for crystalline hostrock. Dependent on waste package design.				H/M (steel/copper overpack)	4 or 5	H/M			
90	fracture-matrix diffusion	crystalline rock - see also #42 and consider relation to microstructure DFN				M	3	M			
91	Lab study EDZ	hydrologic properties of damage zone in crystalline rocks. Modeling and lab studies (LBL Seiji Nakagawa). Relevant to extent of EDZ/probability of connecting to transmissive feature.				M	4				
92	inferring field scale transmissivity from core scale fracture transmissivity	lab measurements and modeling of core scale fractures in crystalline rock (LBL Chris Doughty and Sharon Borglin). Compare to field scale measurements. Identify what is different about permeable fractures compared to nonpermeable.				H	5	H			
93	buffer erosion	in crystalline rock. Low ionic strength fluids erode engineered barrier (eg glaciation)				H	5	H			
94	radionuclide interaction w/ buffer materials	in crystalline rock. Sorption, diffusion, colloids, … smart Kds. Evolution with time?				H	3	M			
95	colloids in fractures	see also Grimsel task 35				H	4	M			
96	flow and transport in fracture	different modeling approaches - graphs, pruning, FCM, other ECPM, particle tracking v. reactive transport. Validation of simpler models against more mechanistic.				H	4	M			
97	waste package degradation	waste package failure model in crystalline rock, including identifying potential waste package materials in conceptual model.				H	4	M			
98	in-package radionuclide solubility model	for crystalline rock.				H	5	M			
99	chemical gradient at interface of buffer/crystalline rock	chemical interactions, effect on buffer stability, related to buffer erosion, colloid generation and transport, buffer materials by design				M	5	M			
100	natural/unnatural (anthropogenic) analogs for radionuclide transport in fractured rock	site-dependent				L	3	L			
101	buffer material by design	development of new generation buffer materials (thermal management, resistance to erosion, limitation of chemical gradients/interactions)				H	5	H			
Completed Argillite/Crystalline/Salt/DPC/EBS Activities (WBS#s 1.08.01.03.01, 1.08.01.03.02, 1.08.01.03.03, 1.08.01.03.05, 1.08.01.03.08)											
26	Salinity gradient / Density stratification (originally DBD)	• Salinity-dependent density	SNL	M	PFLOTRAN					• 2.2.09.01; score = 5.86 • 2.2.09.03; score = 5.40	•
28	High-Temperature Behavior	• Ability to apply PA model at temperatures up to 200C. (incorporate Hi temp experimental data)	SNL	M	PFLOTRAN, CHNOSZ et al.	ISC = Medium (for clay/shale) SC element 3.3.1b	SAL=5 • Chemical processes still under development, particularly at elevated temperature conditions	PS Matrix Score = M; Roadmap Score = H FY19 workscope: ….	PS Matrix Score = M; Roadmap Score = H FY20-21 workscope: ….	• 2.2.01.01(EDZ); score=6.13 • 2.2.08.01(H); score=3.65	• "Cross-cutting" issue with barrier degradation at high T's
28a	High-temperature experimental data	• Test PA model against available high temperature experimental data	GDSA team, SNL Caporuscio, LANL	T	Incorporate experimental/ literature data into PFLOTRAN, CHNOSZ et al.	ISC = Medium (for clay/shale) SC element 3.3.1b	SAL=5 • Chemical processes still under development, particularly at elevated temperature conditions	PS Matrix Score = M; Roadmap Score = H FY19 workscope: ….	PS Matrix Score = M; Roadmap Score = H FY20-21 workscope: ….	• 2.2.01.01(EDZ); score=6.13 • 2.2.08.01(H); score=3.65	• "Cross-cutting" issue with barrier degradation at high T's
29	Cement plug/liner degradation	• Physical and chemical effects	SNL	M	PFLOTRAN	ISC = High (for clay/shale) SC element 3.3.1b	SAL=5 • Important to seals / barrier chemical alteration	PS Matrix Score = H; Roadmap Score = H FY19 workscope: ….	PS Matrix Score = H; Roadmap Score = H FY20-21 workscope: …	• 2.2.08.06(EDZ); score=3.65 • 2.2.09.03; score = 5.40 • FEP 2.1.09.13 is related; score = 4.86 • FEP 2.2.09.61 is related; score = 3.55 • FEP 2.2.11.04 is related; score = 3.55 • FEP 2.1.05.01 is related; score = 3.50	• "Cross-cutting" issue with barrier degradation at high T's

Table 3-1 (cont.) SFWST R&D activities considered for potential integration into *GDSA Framework* and to support a safety case.

Task #	Task Name/ (and Work Package number -- if needed or helpful for more specificity)	Brief Task Description including Relevance (and/or input) to PA/GDSA (nPA = not direct input to PA)	Personnel/Lab	Type of Activity L = Literature review M = Modeling T = Testing or Experimental	Code (if applicable)	Importance to Safety Case (ISC) (H, M, or L -- see ISC table definitions) (Identify applicable Safety Case element from the provided figure)	Current "State of the Art" Level (SAL = 1, 2, 3, 4, or 5 – see SAL table definitions) (Give brief update to applicable state-of-the-art "discussion(s)" shown in UFD Roadmap App. A, i.e., those discussion(s) for the highest scoring related FEPs)	Short-term (1 yr) R&D Priority Scores & Brief FY19 Work Scope Proposal (Priority Score = H, M, or L, based on combined ISC and SAL -- see PS table definitions) (Also give Roadmap Score for related FEP)	Long-term (2-5 yrs) R&D Priority Scores & Brief FY20-23 Work Scope Proposal (Priority Score = H, M, or L, based on combined ISC and SAL) ("Long-term" is most applicable to SAL = 5 issues) (Also give Roadmap Score for related FEP)	Related UFD Roadmap Issue(s)/FEP(s), and associated UFD Roadmap priority scores" (Find highest scoring related FEP in App. B of UFD Roadmap)	Other Notes/Comments (e.g., type of linkage to PA-GDSA; inputs required and/or linkages to other models and experiments)
	International Activities (WBS# 1.08.01.03.07, et al.)										
35	Radionuclide transport as pseudocolloids, Grimsel	• Rates of radionuclide desorption from mineral colloids; input to PA, depending on type of model used in PA	J. Begg, P. Zhao, C. Joseph, M. Zavarin (LLNL)	T, M	N/A	ISC = High SC elements 3.3 (Post-Closure Basis) & 4.2 (Post-Closure Safety Assessment)	SAL = 4 Significant work has been don at GTS. But the puzzle is yet to be put together, in particular for bentonite colloids..	M-H Geosphere FEPS (crystalline rock) 2.2.05: Flow and Transport Pathways >> Medium (Crystalline) 2.2.08: Hydrologic Processes >>Low (Crystalline) 2.2.09: Chemical Processes - Transport >> Medium (Crystalline)	M-H;	• Primary FEP is 2.2.09.64 (crystalline or clay/shale/salt); score = 3.55	• Basic model has been developed in the last couple of years and will be improved upon (redox effect) in the next 3 years. • Response surface suggested (permeability, porosity, cation exchange capacity, swelling stress). • Chemical processes still under development
36	FEBEX-DP Modeling: Dismantling phase of the long-term FEBEX heater test - Modeling	• Thermal, hydrological, mechanical and chemical alteration of bentonite backfilled EBS • Validation of coupled THMC model and PA model • Supply GDSA with the porosity, permeability, swelling pressure evolution and clay mineral alteration over the course of hydration • Input from high temperature experimental data, including lack of illitisation - dependent on bulk chemistry	L. Zheng H. Xu J. Rutqvist, LBNL Caporuscio, LANL	T, M	TOUGHREACT-FLAC3D	(Jens = in blue text) ISC = High SC elements 3.3 (Post-Closure Basis) & 4.2 (Post-Closure Safety Assessment) (Carlos = red text) ISC = Medium SC element 3.3.1c	SAL = 4 SAL = 5	M-H PS Matrix Score = M; Roadmap Score = H Engineered System FEPS: Buffer/Backfill materials 2.1.04.01: Buffer/Backfill >> High 2.1.07.02, .03., .04., .09: Mechanical Processes >> Medium 2.1.08.03, .07, .08: Hydrological Processes >> Medium 2.1.11.04: Thermal Processes >> Medium	M-H PS Matrix Score = M; Roadmap Score = H	• Primary FEP is 2.1.04.01; score = 3.50	• The THMC model was developed and tested against THM data, model validation with chemical data is ongoing • Response surface suggested (permeability, porosity, cation exchange capacity, swelling stress). • Chemical processes still under development • Linked to Tasks 10, 13, 19, 20 of GDSA.
36a	FEBEX-DP Experimental Work: Dismantling phase of the long-term FEBEX heater test	• Evaluate post-test state of FEBEX barrier clay and interactions at EBS interfaces • Effects of dryout and mineral dehydration on backfill/buffer • Characterization (compositional, mineralogical) of FEBEX-DP (heated) bentonite and interactions with cement barrier	C. Jove-Colon, SNL L. Zheng, LBNL Caporuscio, LANL	T, M	N/A	ISC = High SC elements 3.3 (Post-Closure Basis) & 4.2 (Post-Closure Safety Assessment) • Post-mortem characterization of barrier alteration in response to heating (Carlos = red text) ISC = Medium SC element 3.3.1c	SAL = 4 SAL = 5	PS Matrix Score = M; Roadmap Score = H M-H PS Matrix Score = M; Roadmap Score = H Engineered System FEPS: Buffer/Backfill materials 2.1.04.01: Buffer/Backfill >> High 2.1.07.02, .03., .04., .09: Mechanical Processes >> Medium 2.1.08.03, .07, .08: Hydrological Processes >> Medium 2.1.11.04: Thermal Processes >> Medium	M-H PS Matrix Score = M; Roadmap Score = H	• Primary FEPs 2.1.04.01, 2.1.05.01 score = 3.5; 2.2.08.07 score = 2.82; 2.1.07.09 score = 2.56	• Analysis of FEBEX-DP samples will provide insights on clay buffer degradation and interactions at EBS interfaces to inform modeling approaches. • Linked to Task 12,13 of GDSA.
37	Experiment of bentonite EBS under high temperature, HotBENT	• Thermal limit of crystalline and argillite repository with bentonite EBS. • Hydrological, mechanical and chemical alteration of bentonite backfilled EBS under high temperature (200 °C) • Validation of coupled THMC model and PA model • Supply GDSA with the porosity, permeability, swelling pressure, vapor pressure evolution and clay mineral alteration under high temperature • LANL should have input from experimental work • Cross-fertilize with THC processes in EBS and thermodynamic DB development	L. Zheng (LBNL) H. Xu (LBNL) J. Rutqvist (LBNL) Caporuscio (LANL) Jove Colon (SNL)	T, M	TOUGHREACT-FLAC3D	ISC = High; SC elements 3.3 (Post-Closure Basis) & 4.2 (Post-Closure Safety Assessment)	SAL=5	Engineered System FEPS: Buffer/Backfill materials 2.1.04.01: Buffer/Backfill >> High 2.1.07.02, .03., .04., .09: Mechanical Processes >> Medium 2.1.08.03, .07, .08: Hydrological Processes >> Medium 2.1.11.04: Thermal Processes >> Medium	H	• Primary FEP is 2.1.04.01; score = 3.50	• The test was proposed in FY15, is planned to start in FY17 and will last for 5 years. • Linked to Task 12, 13 of GDSA
38	Mont Terri FE (Full-scale Emplacement) Experiment	• Thermally driven THM evolution in both the EBS components and the host-rock behavior in argillaceous formations • Resaturation and swelling of the protective buffer around the waste package • Validation of coupled THM model of bentonite and clay host rocks • Supply GDSA with flow properties (e.g. porosity and permeability) evolution in the buffer, excavation disturbed zone and host rock • Inform GDSA related to local flow created by coupled THM processes	J. Rutqvist, H. Xu, LBNL	T,M	TOUGH-FLAC	ISC = High SC elements 3.3 (Post-Closure Basis) & 4.2 (Post-Closure Safety Assessment)	SAL = 3 (Demonstration experiment)	Geosphere FEPS (for shale): 2.2.01: Excavation Disturbed Zone (EDZ) >> High (Shale) 2.2.07: Mechanical Processes >> Medium (Shale) 2.2.08: Hydrologic Processes >> Medium (Shale)	M	• Primary FEP is 2.1.04.01; score = 3.50 • Other related FEP is 2.2.01.01 Score = 8.0,	• The Mont Terri FE Experiment will be one of the largest and longest running heater tests worldwide. Heating started in 2015 and will go on for at least 15 years • Linked to Tasks 13-15 of GDSA.
38a	Mont Terri FS Fault Slip Experiment	• Pressure-induced potentail for fault reactivation and development of pathways for RN transport • Driving force for pressure buildup could be thermal pressurization, long-term hydrogen generation, or distant earthquakes • Validation of coupled THM models for fault slip and permeability evolution • Could supply GDSA with transient flow properties for faults	Y. Guglielmi	T,M	TOUGH-FLAC, 3DEC	ISC = High SC elements 3.3 (Post-Closure Basis) & 4.2 (Post-Closure Safety Assessment) Group discussion as to why this is "High"--repository will not be sited on a fault; not transferable to other host rock environments	SAL = 5		M-H	• Primary FEP is 2.2.05.01 (fractures, host rock) - Score is 3.65 Also, FEP 2.2.05.03; Score is 2.46	• Related to concerns about thermal pressurization, early on and gas pressure buildup at later stages. Aims at understanding (i) the conditions for slip activation and stability of clay faults, and (ii) the evolution of the coupling between fault slip, pore pressure and fluids migration. Results obtained by the experiment are crucial in defining mechanisms of natural and induced earthquakes, their precursors and risk assessment, and the loss of integrity of natural low permeability barriers. Fault slip can lead to radionuclide pathways. • Linked to Task 79 of GDSA.

Table 3-1 (cont.) SFWST R&D activities considered for potential integration into *GDSA Framework* and to support a safety case.

Task #	Task Name/ (and Work Package number -- if needed or helpful for more specificity)	Brief Task Description including Relevance (and/or input) to PA/GDSA (nPA = not direct input to PA)	Personnel/Lab	Type of Activity L = Literature review M = Modeling T = Testing or Experimental	Code (if applicable)	Importance to Safety Case (ISC) (H, M, or L -- see ISC table definitions) (Identify applicable Safety Case element from the provided figure)	Current "State of the Art" Level (SAL = 1, 2, 3, 4, or 5 – see SAL table definitions) (Give brief update to applicable state-of-the-art "discussion(s)" shown in UFD Roadmap App. A, i.e., those discussion(s) for the highest scoring related FEPs)	Short-term (1 yr) R&D Priority Scores & Brief FY19 Work Scope Proposal (Priority Score = H, M, or L, based on combined ISC and SAL -- see PS table definitions) (Also give Roadmap Score for related FEP)	Long-term (2-5 yrs) R&D Priority Scores & Brief FY20-23 Work Scope Proposal (Priority Score = H, M, or L, based on combined ISC and SAL) ("Long-term" is most applicable to SAL = 5 issues) (Also give Roadmap Score for related FEP)	Related UFD Roadmap Issue(s)/FEP(s), and associated UFD Roadmap priority scores" (Find highest scoring related FEP in App. B of UFD Roadmap)	Other Notes/Comments (e.g., type of linkage to PA-GDSA; inputs required and/or linkages to other models and experiments)
International Activities (WBS# 1.08.01.03.07, et al.)											
39	DECOVALEX-2019 Task E: Upscaling of modeling results from small scale to one-to-one scale based in heater test data in MHM underground research laboratory in France.	• Thermally driven THM evolution in both the EBS components and the host-rock behavior in argillaceous formations • Resaturation and swelling of the protective buffer around the waste package • Validation of coupled THM model of bentonite and clay host rocks • Supply GDSA with flow properties (e.g. porosity and permeability) evolution in the buffer, excavation disturbed zone and host rock • Inform GDSA related to local flow created by coupled THM processes	J. Rutqvist, H. Xu, LBNL	T,M	TOUGH-FLAC	ISC = High 4.3 Confidence	SAL = 4	Engineered System FEPS: Seal/liner materials 2.1.05.01: Buffer/Backfill >> Medium 2.1.07.02, .08., .09: Mechanical Processes >> Medium 2.1.08.04, .05, .07, .08, .09: Hydrological Processes, Flow Through Seals >> Medium 2.1.09.01, .03, .09, .13: Chemical Processes - Chemistry >> Medium	M	• Primary FEP is 2.1.04.01; score = 3.50 • Other related FEP is 2.2.01.01; Score = 8.0,	• The purpose of Task E is upscaling THM modeling from small size experiments (some cubic meters) to real scale emplacement cells (some ten cubic meters) all the way to scale of a waste repository (cubic kilometers). The task is aligned with the French repository program, which focuses its R&D on the Callovo-Oxfordian claystone (COx) formation near Bure in the east of France. • Linked to Tasks 13, 14, 15.
40	DECOVALEX-2019 Task A: Advective gas flow in bentonite	• Pressure buildup and gas migration in bentonite (important topic for bentonite backfill)	J. Rutqvist, K. Kim, LBNL	T, M	TOUGH-FLAC TOUGH-RBSN	ISC = High for Crystalline, Medium for Argillite? SC elements 3.3 (Post-Closure Basis) & 4.2 (Post-Closure Safety Assessment)	SAL = 5	Engineered System FEPS: Buffer/Backfill materials 2.1.04.01: Buffer/Backfill >> High 2.1.08.03, .07, .08: Hydrological Processes >> Medium 2.1.12.01, .02, .03: Gas sources and effects >> Medium	H	• Primary FEP is 2.2.08.06 ; Score 3.65 • 2.2.12.02 - Score 2.18 • 2.2.09.64 - Score 3.55	• The DECOVALEX-2019 project will provide extensive experimental and field test results on the behavior of gas generation and pressurization in bentonite and clay stone, including dilation and fracture formation. • Linked to Tasks 73, 86 of GDSA
41	DECOVALEX-2019 Task C: GREET (Groundwater REcovery Experiment in Tunnel) at Mizunami URL, Japan	• Geochemistry: Evaluate groundwater chemistry in a crystalline repository and the effect of repository construction • Utilize fracture data for validation of fracture models in crystalline rock • Evaluate reactive transport processes at the filled CTD & cement interactions	Y. Wang Jove-Colon T. Hadgu, SNL	T, M	PFLOTRAN, EQ3/6, DFN, FCM	ISC = High 4.3 Confidence	SAL = 4	Geosphere (for shale): 2.2.01: Excavation Disturbed Zone (EDZ) >> High (Shale) 2.2.07: Mechanical Processes >> Medium (Shale) 2.2.08: Hydrologic Processes >> Medium (Shale) 2.2.11: Thermal Processes >> Medium (Shale)	M	• Primary FEP is 2.2.05.01 (crystalline) score = 3.74; applicable FEP 2.2.09.51 (crystalline); 2.2.08.04 (crystalline) score = 3.23; 2.2.09.02 (crystalline) score = 5.86;	• The DECOVALEX-2019 project Task C will provide comprehensive geochemical and fracture characterization of host-rock at various locations and times. • Experimental and field test results (groundwater recovery, monitoring) will provide key information about groundwater chemical evolution. • Modeling hydro-mechanical-chemical-biological processes during groundwater recovery in crystalline rock. • Linked to Tasks 7, 13 of GDSA
42	SKB GWFTS Task Force: Longterm Diffusion Experiment LTDE-SD at the Äspö HRL	• RN Transport: Examine diffusion and sorption processes in both matrix rock and a typical conductive fracture identified in a pilot borehole • Conduct discrete fracture modeling to assess impact of micro-fractures on transport	Viswanathan, LANL	T, M	LAGRIT, PFLOTRAN	ISC = High SC elements 3.3 (Post-Closure Basis) & 4.2 (Post-Closure Safety Assessment)	SAL = 4	Geosphere FEPS (for crystalline rock) 2.2.05: Flow and Transport Pathways >> Medium (Crystalline) 2.2.08: Hydrologic Processes >>Low (Crystalline) 2.2.09: Chemical Processes - Transport >> Medium (Crystalline)	M	• Primary FEP is 2.2.09.51- Score is 3.74 and 2.2.09.53 - Score is 3.55	• Obtain data on sorption properties and processes of individual radionuclides, and their effect on natural fracture surfaces and internal surfaces in the rock matrix. • Investigate the magnitude and extent of diffusion into matrix rock from a natural fracture in situ under natural rock stress conditions and hydraulic pressure and groundwater chemical conditions.
43	Microbial Processes Affecting Hydrogen Generation and Uptake: FEBEX-DP and Mont Terri Studies	• Gas Transport: Hydrogen generation can result in long-term damage to bentonite and clay host rock • Microbial activity can lead to hydrogen uptake and reduced risk of damage; however, the transient activity of microbes in heated and pressurized bentonite/rock is not well understood	P. Nico	T, M	TBD	ISC = Medium 4.3 Confidence	SAL = 5		M	• Primary FEP is 2.2.11.04, with score of 3.74 for clay/shale; 2.2.11.04 - Score 2.4 for granite and salt; 2.2.11.04 - Score 3.55;	• The fate of repository gases generated over long periods from corrosion of metallic materials under anoxic conditions and related formation of hydrogen can result in long-term damage to bentonite and clay host rock.
44	TH and THM Processs in Salt: German-US Collaborations (WEIMOS, BENVASIM)	Model Comparison studies with Germany on TM Benchmarking (WEIMOS) and on THM Model Comparison (BENVASIM)				ISC = High	SAL = 4 (TM), SAL = 5 (THM)		M or H		
45	NEA Thermodynamic Database	• International activity to develop and maintin a commonly agreed upon set of thermodynamic data for RN studies	P. Nico	T, M	TBD	ISC = High	SAL = 4		M		
								•			•
Other DR Activities (WBS# 1.08.01.03.09)											
93	Complete and Populate Online Waste Library (OWL) SF-17SN01050101	• Develop/update a listing and inventory of DOE-managed HLW and SNF radioactive wastes which were assessed in the disposal options evaluation work and identify any additional wastes and/or waste forms to be added/updated • The On-Line Waste Library will be constructed for information on DOE-managed HLW, SNF, and other wastes that are potential candidates for deep geologic disposal, with links to supporting documents	Sassani, Price, Rogers, Walkow, et al., SNL Carter, SRNL	L, M	Web Develop		• Inventory for source term			• FEP2.1.01.01; score = 2.05	•

Table 3-1 (cont.) SFWST R&D activities considered for potential integration into *GDSA Framework* and to support a safety case.

Task #	Task Name/ (and Work Package number -- if needed or helpful for more specificity)	Brief Task Description including Relevance (and/or input) to PA/GDSA (nPA = not direct input to PA)	Personnel/Lab	Type of Activity L = Literature review M = Modeling T = Testing or Experimental	Code (if applicable)	Importance to Safety Case (ISC) (H, M, or L -- see ISC table definitions) (Identify applicable Safety Case element from the provided figure)	Current "State of the Art" Level (SAL = 1, 2, 3, 4, or 5 -- see SAL table definitions) (Give brief update to applicable state-of-the-art "discussion(s)" shown in UFD Roadmap App. A, i.e., those discussion(s) for the highest scoring related FEPs)	Short-term (1 yr) R&D Priority Scores & Brief FY19 Work Scope Proposal (Priority Score = H, M, or L, based on combined ISC and SAL -- see PS table definitions) (Also give Roadmap Score for related FEP)	Long-term (2-5 yrs) R&D Priority Scores & Brief FY20-23 Work Scope Proposal (Priority Score = H, M, or L, based on combined ISC and SAL) ("Long-term" is most applicable to SAL = 5 issues) (Also give Roadmap Score for related FEP)	Related UFD Roadmap Issue(s)/FEP(s), and associated UFD Roadmap priority scores* (Find highest scoring related FEP in App. B of UFD Roadmap)	Other Notes/Comments (e.g., type of linkage to PA-GDSA; inputs required and/or linkages to other models and experiments)
	Ongoing Argillite/Crystalline/Salt/DPC/EBS Activities (WBS#s 1.08.01.03.01, 1.08.01.03.02, 1.08.01.03.03, 1.08.01.03.05, 1.08.01.03.08)										
	GDSA Activities (WBS# 1.08.01.03.04)										
58	**GDSA Geologic Modeling**	• geologic and hydrologic conceptual framework for GDSA reference cases • data feeds to GDSA models (hydrologic parameters, stratigraphy, fractures) • Confidence in demonstrating understanding of the geologic environment • GIS analysis of site selection options	Perry, LANL	L, M	Rockworks, JewelSuite, ArcGIS	ISC = High SC element 3.3.2	SAL= 4			Primary FEP is 2.2.02.01. Score = 3.74. Other FEP 2.2.05.01 Fractures; Score = 3.65	
59	**Web Visualization of Geologic Conceptual Framework for GDSA Geologic Modeling**	• Web visualization and user interaction with geologic data and modeling to support GDSA reference cases and the Regional Geology GIS Database. • Development of 2D and 3D spatial data and web applications. • Addition of Global Survey of Deep Underground Facilities web application.	Russell, INL Perry, LANL	L, M	ArcGIS, Javascript	ISC = High SC element 3.3.2	SAL= 4			Primary FEP is 2.2.02.01. Score = 3.74. Other FEP 2.2.05.01 Fractures; Score = 3.65	
60	Commercial waste repository reference cases SF-17SN01030401	• Modification of any models or code capabilities to accommodate a repository for commercial HLW/SNF	SNL	L, M	GDSA					• FEP not explicitly scored, but "disposal system modeling" rated as a "high" priority as a "cross-cutting" issue.	•
62	QA, V&V (documentation and tests)	• V&V, benchmarking, and documentation of codes, including pre- and post-processors	Frederick, Stein, Mariner, etc. SNL	L, M	GDSA					• FEP not explicitly scored, but "disposal system modeling" rated as "high" priority as a "cross-cutting" issue.	PFLOTRAN wiki already has significant regression testing, but documentation could be improved.
63	Basic biosphere model	• Aquifer; overlying sediments; infiltration; withdrawal well(s); IAEA ERB-1A dose calculation (GDSA)	Mariner SNL	L, M	GDSA					• Biosphere FEPs score low (<1), but this is needed to portray a dose metric	• Instead use drinking water standards from YMP, i.e., a concentration metric instead of a dose metric?
64	Grid refinement	• Octree-grid adaptive mesh refinement using p4est • Block grid refinement	Hammond, SNL	M	PFLOTRAN; p4est					• FEP not explicitly scored, but "disposal system modeling" rated as "high" priority as a "cross-cutting" issue.	• Octree capability is still being developed by the originators
65	Nested EBS, near-field, far-field models	• Nesting of domains with process models of varying sophistication	G. Hammond, P. Mariner, E. Stein, J. Frederick SNL	M	PFLOTRAN					• FEP not explicitly scored, but "disposal system modeling" rated as "high" priority as a "cross-cutting" issue.	• e.g., embedding 3D domains with increasing numbers of processes, unknowns, complexity
66	Operator splitting for reactive transport	• Add operator-splitting numerical method for reactive transport	Hammond SNL	M	PFLOTRAN					• FEP not explicitly scored, but "disposal system modeling" rated as "high" priority as a "cross-cutting" issue.	• Enables larger simulations as the system of equations is smaller
67	Numerical solution methods	• Improve GENERAL multiphase convergence (analytical derivatives) • Solver convergence	Hammond SNL	M	PFLOTRAN					• FEP not explicitly scored, but "disposal system modeling" rated as "high" priority as a "cross-cutting" issue.	•
68	Simplified Representation of Mechanical processes in PA	• ROMs for creep closure • General representation of "M" in PFLOTRAN? • Simplest representation in PA is a set of initial conditions from a process model	Hammond SNL Kara LANL	M	PFLOTRAN					• Highest scoring mechanical FEP is 2.2.07.01; score = 3.83 • But FEP 2.2.01.01 (clay/shale) could be argued to apply; score = 8.0	• Important for salt at early times, but how important for directly including this process in a long-term PA?
69	Full Representation of Chemical processes in PA	• Effect of chemistry on near-field degradation and transport • Possibly a separate, "nested" model	Hammond, Jove-Colon, Mariner et al. SNL	M	PFLOTRAN	ISC = High (for clay/shale) SC element 3.3.1b	SAL=5	PS Matrix Score = H; Roadmap Score = H FY19 workscope: ….	PS Matrix Score = H; Roadmap Score = H FY20-21 workscope: …	• Highest scoring chemical FEP is 2.2.09.03 (deep borehole); score = 5.40 • But FEP 2.2.01.01 could be argued to apply (clay/shale); score = 8.0	•A separate nested model from Task #83 •Different equations in different domains •HeeHo dissertation? •Loose coupling using different processes in different domains •Compare loose coupling with tight coupling

Table 3-1 (cont.) SFWST R&D activities considered for potential integration into *GDSA Framework* and to support a safety case.

Task #	Task Name/ (and Work Package number -- if needed or helpful for more specificity)	Brief Task Description including Relevance (and/or input) to PA/GDSA (nPA = not direct input to PA)	Personnel/Lab	Type of Activity L = Literature review M = Modeling T = Testing or Experimental	Code (if applicable)	Importance to Safety Case (ISC) (H, M, or L -- see ISC table definitions) (Identify applicable Safety Case element from the provided figure)	Current "State of the Art" Level (SAL = 1, 2, 3, 4, or 5 -- see SAL table definitions) (Give brief update to applicable state-of-the-art "discussion(s)" shown in UFD Roadmap App. A, i.e., those discussion(s) for the highest scoring related FEPs)	Short-term (1 yr) R&D Priority Scores & Brief FY19 Work Scope Proposal (Priority Score = H, M, or L, based on combined ISC and SAL -- see PS table definitions) (Also give Roadmap Score for related FEP)	Long-term (2-5 yrs) R&D Priority Scores & Brief FY20-23 Work Scope Proposal (Priority Score = H, M, or L, based on combined ISC and SAL) ("Long-term" is most applicable to SAL = 5 issues) (Also give Roadmap Score for related FEP)	Related UFD Roadmap Issue(s)/FEP(s), and associated UFD Roadmap priority scores* (Find highest scoring related FEP in App. B of UFD Roadmap)	Other Notes/Comments (e.g., type of linkage to PA-GDSA; inputs required and/or linkages to other models and experiments)
GDSA Activities (WBS# 1.08.01.03.04)											
69	Full Representation of Chemical processes in PA	• Effect of chemistry on near-field degradation and transport • Possibly a separate, "nested" model	Hammond, Jove-Colon, Mariner et al. SNL	M	PFLOTRAN	ISC = High (for clay/shale) SC element 3.3.1b	SAL=5	PS Matrix Score = H; Roadmap Score = H FY19 workscope: ….	PS Matrix Score = H; Roadmap Score = H FY20-21 workscope: …	• Highest scoring chemical FEP is 2.2.09.03 (deep borehole); score = 5.40 • But FEP 2.2.01.01 could be argued to apply (clay/shale); score = 8.0	•A separate nested model from Task #83 •Different equations in different domains •HeeHo dissertation? •Loose coupling using different processes in different domains •Compare loose coupling with tight coupling
70	Pitzer model	• Implement Pitzer activity coefficients (Wolery EQ3/6 version)	Hammond, Jove-Colon SNL	M	PFLOTRAN	ISC = High SC element 3.3.2	SAL = 5 From roadmap (for FEP 2.1.09.01) Expected to be of high direct importance to long-term performance - effects potential degradation processes of engineered barriers and geochemistry inside the EBS, and solubility controls/limits. Expected to be of low importance to repository design and construction. Estimated at medium importance for overall confidence - demonstration of understanding of geochemical conditions. If we ever want to do full chemistry in a salt repository, or consider the effects of mixing brines (e.g., in a human intrusion scenario), this is required. This would also allow PFLOTRAN to take over chemistry simulations currently done by EQ3/6 (consolidation of codes)	A short-term priority, but not enough personel to implement this in short term. Requires new people (post-doc or staff) to impement.		• Highest scoring speciation FEP is 2.2.09.05 (deep borehole); score = 5.86 • FEP 2.1.09.13 is also relevant (EBS); score = 4.86	• We prefer the Wolery, rather than the Felmy, implementation • Important for repositories in salt and for deep borehole
71	Performance metrics SF-17SN01050405 SF-17SN01050408	• Develop a "standardized" set of performance metrics for each reference case (e.g., a grid of wells for granite)	Sevougian, Stein, Mariner SNL	L, M	GDSA					• FEP not explicitly scored, but "disposal system modeling" rated as "high" priority as a "cross-cutting" issue.	• This issue arose for the granite repository where the granite and fractures were effectively outcropping
72	Surface processes and features	• Develop model parameters for infiltration & surface discharge	Mariner, et al SNL	L, M	GDSA					• Surface FEPs score low (<2)	• Consider processes such as precipitation, evapotranspiration, surface runoff, streams, lakes, etc
73	Other missing FEPs (processes) SF-17SN01030401 SF-17SN01050402	• Gas generation and movement • Ongoing climatic effects • Neutron activation	Mariner, et al. SNL	M	GDSA					• Highest scoring gas FEP is 2.2.12.02 (salt); score = 3.23 • Highest scoring climate FEP is 1.3.01.01; score = 1.85	• Gas generation/ movement might be important with regard to corrosion processes and buffer stability
74	Implicit solution for decay and ingrowth	• Use global implicit solution instead of operator splitting for PFLOTRAN "sandbox" capability	Hammond SNL	M	PFLOTRAN					•	
75	Implicit solution for decay and ingrowth	• Use implicit solution instead of operator splitting for PFLOTRAN reactive transport equations	Hammond SNL	M	PFLOTRAN					•	
76	Solution density	• Liquid density dependence on salinity	Hammond SNL	M	PFLOTRAN					•	• Need to implement salinity dependence in PFLOTRAN TH mode
77	UA/SA	• Standardized set of UA/SA, including rank regression • Stability of mean, including control variates	Stein, MacKinnon, Kuhlman SNL	L, M	Dakota, etc.					•	• We already have the Dakota capability (e.g., PRCCs) • Not clear that we have a stepwise linear regression capability
78	PFLOTRAN improvements	• Checkpoint/restart capability for new process models • Gridded dataset support for initial solute concentrations	Hammond SNL	M	PFLOTRAN					•	
79	Disruptive events SF-17SN01030401 SF-17SN01050402	• PA processes initiated or dependent upon external events, such as human intrusion, glaciation, and seismicity. Also, include early WP failures.	Mariner, Sevougian, Hammond, et al. SNL et al.	L, M	GDSA					• Highest scoring disruptive event FEP is 1.2.03.01 (seismic); score = 4.94	• Requires stylized scenarios and regulations for generic repositories and for site-screening activities • Should remain on hold until there are candidate sites
80	Species and element properties	• Solute-specific diffusivities • Temperature-dependent solubilities	Hammond, Mariner SNL	M	PFLOTRAN					•	• Probably only a second order effect.
81	Solid solution model	• Precipitation and dissolution of solid solutions	Lichtner, Hammond SNL	M	PFLOTRAN					•	• A simpler version (ignoring molar volumes) may be implemented sooner
82	Isotope partitioning in presence of colloids	• The isotope partitioning and solubility model will need to account for isotopes in colloid phase when colloid model is added	Mariner, Hammond SNL	M	PFLOTRAN					• FEP 2.1.09.13, 2.2.09.05, and 2.2.09.06 are related; highest score = 5.86	• Implementation of LANL/LLNL/SNL colloid model takes precedence; adjustment to isotope partitioning model depends on colloid model
83	Waste Form-Canister-Buffer Discretization (1D -> 3D)	• 1-D transport WF-WP-Buffer transport model connected into 3-D grid	Hammond, Stein SNL	M	PFLOTRAN					• FEP not explicitly scored, but "disposal system modeling" rated as "high" priority as a "cross-cutting" issue.	
84	HLW WF degradation (simplified)	• Glass waste degradation	Frederick, Mariner SNL	M	PFLOTRAN					• Primary FEP is 2.1.02.02; score = 0.00	•
85	WP Degradation Model Framework	• Degradation of WP outer barrier over time	Mariner, Frederick SNL	M	PFLOTRAN					• FEPs 2.1.03.02, 2.1.03.03, 2.1.03.04, 2.1.03.05; scores = 4.34	
86	Multi-Component Gas Transport	• Ability to model chemical species in the gas and liquid phases.	SNL et al.	M	PFLOTRAN					• Primary FEP 2.2.09.64; score = 3.55	• We assume equilibrium between the gas and liquid phases; so the number of reactive transport degrees of freedom does not increase
87	Multi-Species Diffusion										

*FEP scores are from the UFD R&D Roadmap (DOE 2012). Higher scores indicate higher importance. Scale = 0 to 8 (see App. B. of UFD Roadmap).

3.1.1   Relationship to the Safety Case

As a geologic repository project evolves from a generic stage to a site-specific stage (see Figure 3-1), the corresponding knowledge and engineering design also mature, as documented in an evolving Safety Case or Licensing Case—see Figure 3-2. Since confidence in the safety arguments and safety evaluations of the Safety Case (vis-à-vis regulatory criteria) is the main technical decision criterion for siting a repository, the necessity of R&D activities should be judged relative to how they bolster this safety-case confidence. Thus "importance to the safety case" (ISC) is a key evaluation metric used in the ranking and prioritization of R&D (Table 3-2).

Figure 3-2 is a typical illustration of the key components of a repository safety case, each of which should be accompanied by R&D that improves confidence in its performance or knowledge. The amount of R&D still needed to enhance this confidence is a value judgment by experts and stakeholders and may be qualitatively defined by the current "state-of-the-art" of the associated scientific and/or engineering knowledge for the given component. Figure 3-3 is a schematic illustration of how to prioritize this confidence-building R&D based on two complementary criteria: the "value of the information" gained by the R&D activity and the cost of the R&D activity. The former criterion, the value of the information gained, includes both (1) the importance of the information (or R&D) to building confidence in the Safety Case and (2) the potential reduction of uncertainty (or advancement of the "state-of-the-art") provided by the R&D activity. [The cost of an R&D Activity is not considered in assigning priorities in either the 2012 Roadmap or in the present re-prioritization effort but will likely become important when the repository project moves beyond the generic stage.]
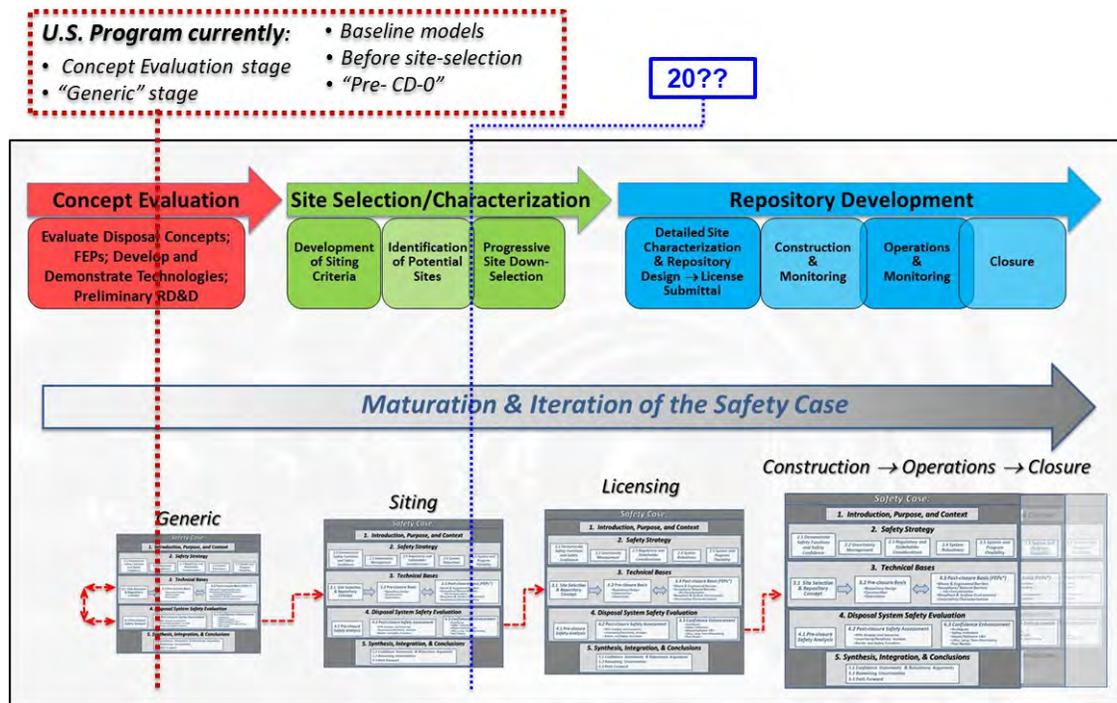
Figure 3-1   Schematic repository timeline and maturation of the safety case
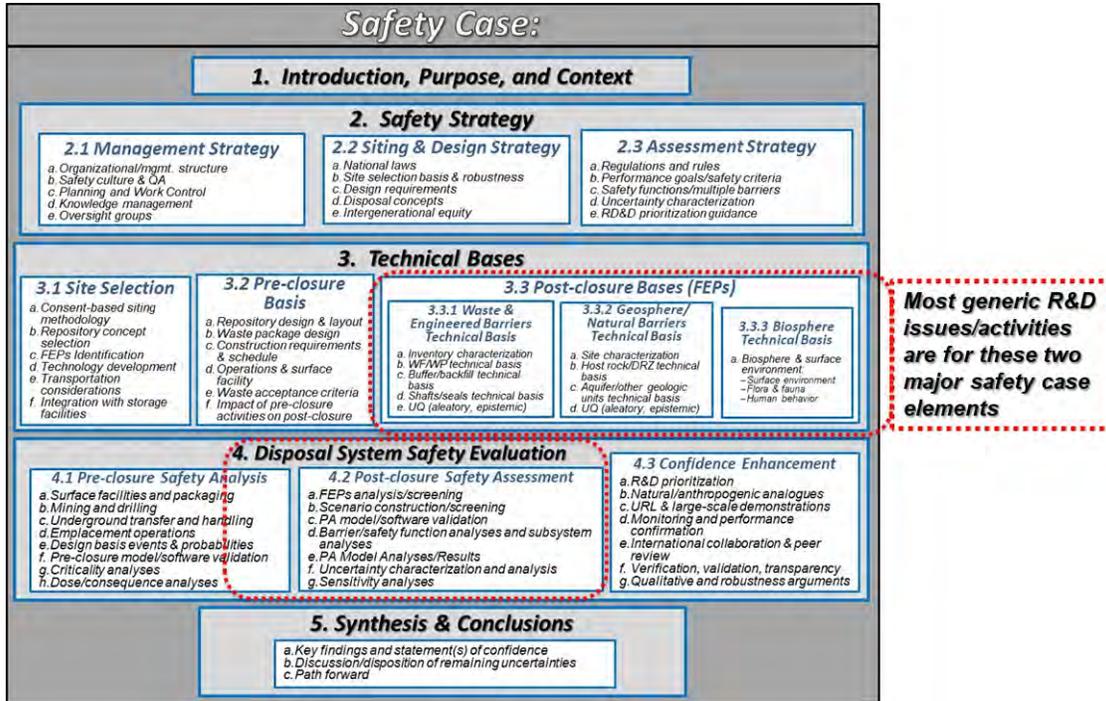
Figure 3-2   Typical elements of a deep geologic repository safety case

- **Prioritization process can be formalized (as in 2012 UFD Roadmap)**
  1. Identify a set of objectives and associated metrics, including
     - *Importance* to components of the safety case: safety assessment, technical bases, confidence-building
     - Potential to reduce key *uncertainties*, i.e., increase the TRL (or KRL, or SAL)
     - Other factors, e.g., *cost*, redundancies, synergies
  2. Evaluate each R&D activity using the metrics
  3. Define a "utility function" to combine the metric scores, to give an overall numerical score
  4. Compare utilities ("rankings") of the activities
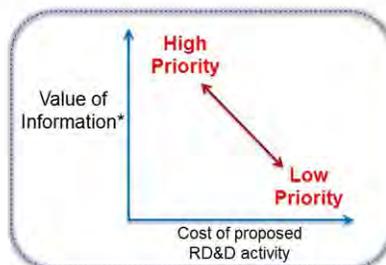
Figure 3-3   Major steps in a decision analysis

3.1.2   Prioritization Methodology

Table 3-1 shows the major model, testing, and international-collaboration R&D activities currently being conducted within the SFWST Campaign. These major R&D activities do not necessarily have a one-to-one mapping to the R&D Issues (or FEPs) in the 2012 UFD Roadmap. But it is necessary to understand and delineate this mapping or correspondence between the R&D Issues of the 2012 UFD Roadmap and the R&D Activities in Table 3-1, in order to achieve an update of the 2012 Roadmap, since it is the R&D Issues (or FEPs) that were assigned numerical priority scores in the 2012 Roadmap. The SFWST R&D activities in Table 3-1 were often designed to address more than one of the R&D Issues of the 2012 Roadmap, which is why there is not a strict one-to-one mapping.

Prior to this year's Annual Working Group Meeting (see Appendix A), project PIs and work package managers were asked to complete a preliminary re-prioritization of R&D Activities in light of project R&D conducted since 2012, as well as the current state-of-the-art for the given issue. These re-prioritization scores may be compared with the corresponding 2012 priority scores in a simple fashion— Figure 3-4 helps explain this:

1. By inspection, each current R&D Activity (i.e., each row in Table 3-1) may be linked to one or more related FEPs (i.e., R&D Issues) in Appendices A and B of DOE (2012);

2. Each current R&D Activity may be given a unique Roadmap numerical score by assigning it the old priority score of the highest-scoring related FEP (or R&D Issue) presented in Appendix B of the 2012 Roadmap;

3. This 2012 Roadmap numerical score may be converted to a qualitative "high," "medium," or "low" "Roadmap Score" by using the quantitative-to-qualitative conversion graph from the 2012 UFD Roadmap (DOE 2012, Fig. B-1). (This is illustrated here in Figure 3-4, which shows an excerpt of numerical priority scores from Appendix B of the 2012 Roadmap, as well as the graph, Figure B-1, that converts these numerical scores to qualitative scores.)
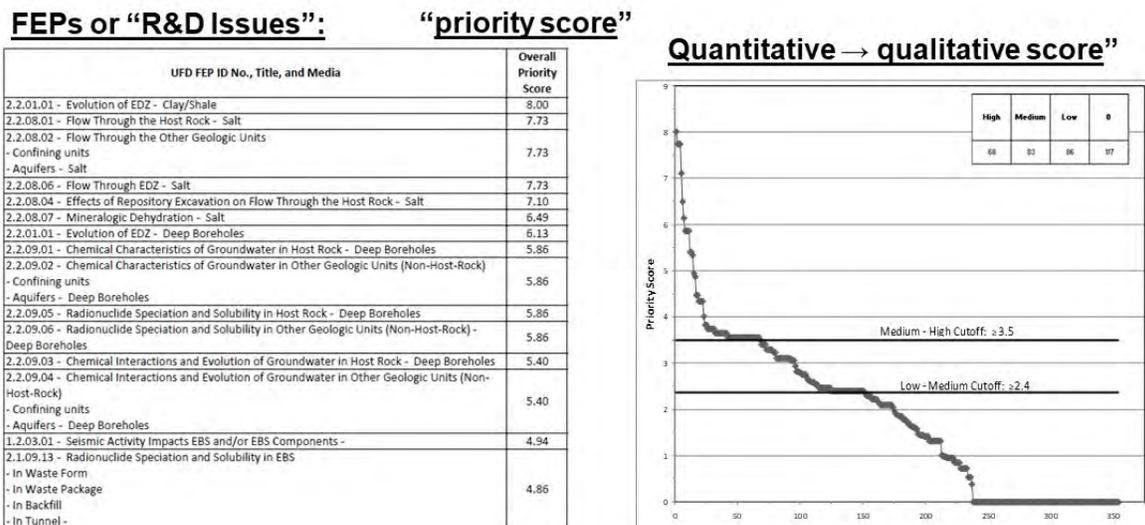
Figure 3-4   Excerpt from Appendix B of the 2012 UFD Roadmap, showing the highest scoring FEPs and the conversion of their quantitative scores to qualitative scores

The current or new R&D priority score assigned this year was by a simpler method than that of 2012. For example, it does not include "decision points" (i.e., site-screening, site-selection, etc.) in the scoring methodology because this is felt to be premature for a generic repository program. The new scoring

method (which may yet be modified for the January 2019 Roadmap Update Workshop) is documented in Table 3-2 through Table 3-4. It uses two metrics to generate a combined priority score: (1) ISC (Importance to Safety Case), shown in Table 3-2, and (2) SAL (State-of-the-Art) Level, shown in Table 3-3. The ISC and the SAL scores are then entered into the Priority Score Matrix of Table 3-4 to generate a new Priority Score for each R&D Activity in Table 3-1. It should be pointed out that the SAL metric in Table 3-3 is based on the definitions in Section 2.2.3 of the 2012 UFD Roadmap, in order to help maintain consistency with the 2012 Roadmap.

As mentioned above, new Priority Scores were developed prior to the May 2018 Annual Working Group Meeting, but were then reviewed and revised in a series of four breakout sessions (salt, argillite, crystalline, and DPC) during the Annual Meeting. Table 3-1 is a compendium of the scores and results from these breakout sessions and will be the starting point for the preparations for the January 2019 Roadmap Update Workshop.

Table 3-2   ISC (Importance to Safety Case)

ISC score	ISC Definition	Alternative Description (see safety case elements shown in Figure 3-2)
High	*High Importance to SC*	Knowledge gained by proposed R&D strongly affects one of the three elements of "Disposal System Safety Evaluation" in the Safety Case (pre-closure safety analysis, post-closure safety assessment, confidence enhancement)
Medium	*Medium Importance to SC*	Knowledge gained strongly affects one of the Technical Bases elements of the Safety Case but the Technical Basis element itself only weakly or moderately influences a safety assessment metric
Low	*Low Importance to SC*	Knowledge gained is only of a supporting nature and does not strongly affect the associated process model or model inputs

Table 3-3   SAL (State of the Art Level) (after Sec. 2.2.3 and App. A of 2012 UFD Roadmap)

State of the Art Level (SAL)	SAL Definition (use highest scoring <u>related</u> <u>FEP</u> in UFD Roadmap)	Description
5	*Fundamental Gaps in Method or Fundamental Data Needs, or Both*	The representation of an issue (conceptual and/or mathematical, experimental) is lacking, or the data or parameters in the representation of an issue (process) is lacking
4	*Improved Representation*	The representation of an issue may be technically defensible, but improved representation would be beneficial (i.e., lead to more realistic representation).
3	*Improved Confidence*	Methods and data exist, and the representation is technically defensible but there is not widely-agreed upon confidence in the representation (scientific community and other stakeholders).
2	*Improved Defensibility*	Related to confidence, but focuses on improving the technical basis, and defensibility, of how an issue (process) is represented
1	*Well Understood*	The representation of an issue (process) is well developed, has a strong technical basis, and is defensible. Additional R&D would add little to the current understanding

Table 3-4   2018 Priority Score (PS) Matrix (combination of SAL and ISC) for R&D Activities:

ISC: \ SAL:	1	2	3	4	5
High	L	M	M	M	H
Medium	L	M	M	M	M
Low	L	L	L	L	L

3.1.3   Model Integration Timeline

Tables 3-2 and 3-3 in Mariner et al. (2017), which indicate a timeline (or schedule) for maturation of the *GDSA Framework* software, as well as the coupling of process models to *GDSA Framework*, have not been revised this fiscal year but are expected to be re-evaluated prior to and following the January 2019 Roadmap Update meeting. The key point relative to these two "schedule" tables is to ensure that certain safety/performance assessment capabilities are available at certain times during the evolution of the generic R&D knowledge and the engineering design. In particular, two "capability points" are currently being used to assess the maturity of the generic performance assessment software and models (i.e., of *GDSA Framework*):

1. Near-term (~2021) "baseline" capability: process models and their implementation in *GDSA Framework* will have a certain "fidelity" that allows for a <u>complete</u> PA calculation.

2. Farther-term (~2025) "enhanced" capability: process models and their implementation in *GDSA Framework* will have a higher fidelity that brings higher confidence to the generic safety case.

Year-by-year work scopes for the R&D Activities in Table 3-1 should be designed, and integrated with each other, to support either or both of the PA capability points listed above (as well as the generic Safety Case). In fact, this has been a high priority since the time of the 2012 UFD Roadmap, which considered "Disposal System Modeling" (i.e., PA) to be a high-ranking R&D Issue (DOE 2012, Table 6 and Sec. 4.2.2).

Of course, as clearly outlined here, the importance of various FEPs to repository performance or to the Safety Case (e.g., see Table 3-2), i.e., how much R&D is warranted for a particular FEP, is most often assessed with the system performance assessment (PA) model (in this case, *GDSA Framework*). This concept is illustrated in Figure 3-5, which shows the information flow during a single stage of a repository program and how the system PA model is intended to fill a key role in guiding the directed R&D program at all stages of the project.[1] This use of *GDSA Framework* is also one of the key drivers for an ongoing model integration timeline, such as the timeline indicated in Table 3-3 of Mariner et al. (2017), which will result in certain PA model capabilities at certain time points during repository development. Those capabilities, i.e., the undefined "fidelity" of the PA model, mentioned above, are a subjective determination by experts and stakeholders, dependent on many considerations. These considerations include both technical readiness and political feasibility, where the former is not only a function of the scientific and engineering processes, but also on the financial resources applied to the problem (which is in turn a function of the "political will" associated with the project).

Finally, although the current SFWST Campaign is effectively host-rock and concept "neutral," given that there is no specific site (i.e., given the current generic stage—see Figure 3-1), R&D Activity prioritization is not necessarily host-rock neutral. In particular, if the current state-of-the-art for various FEPs is more advanced for certain host rocks, less R&D funding and work effort may be needed for those FEPs in that

---

[1] It has been argued (NWTRB 2015) that a safety assessment model cannot be used for site down-selection at the earliest stages because it is "technically complex" and "the data needed to employ sensibly such an approach simply are not available at the earliest stages of any siting effort." This report does not prejudge the amount of data available at different project stages but merely assumes a safety assessment model, as well as underlying process models, are as good as the data and assumptions they are based upon, as well as the verification and validation testing they have undergone. Modern and complex computer programs are relied upon to assure safety and reliability of nuclear weapons, to predict weather patterns and climate change, and to safely operate modern transportation systems. It is quite likely that a safety assessment model of some appropriate level of complexity will be employed during all stages of site selection and repository development, subject to the judgment of major stakeholders involved.

given host rock. An example might be certain FEPs for a salt host rock, given the long history of R&D for the WIPP bedded-salt TRU repository (DOE 1996; DOE 2014).
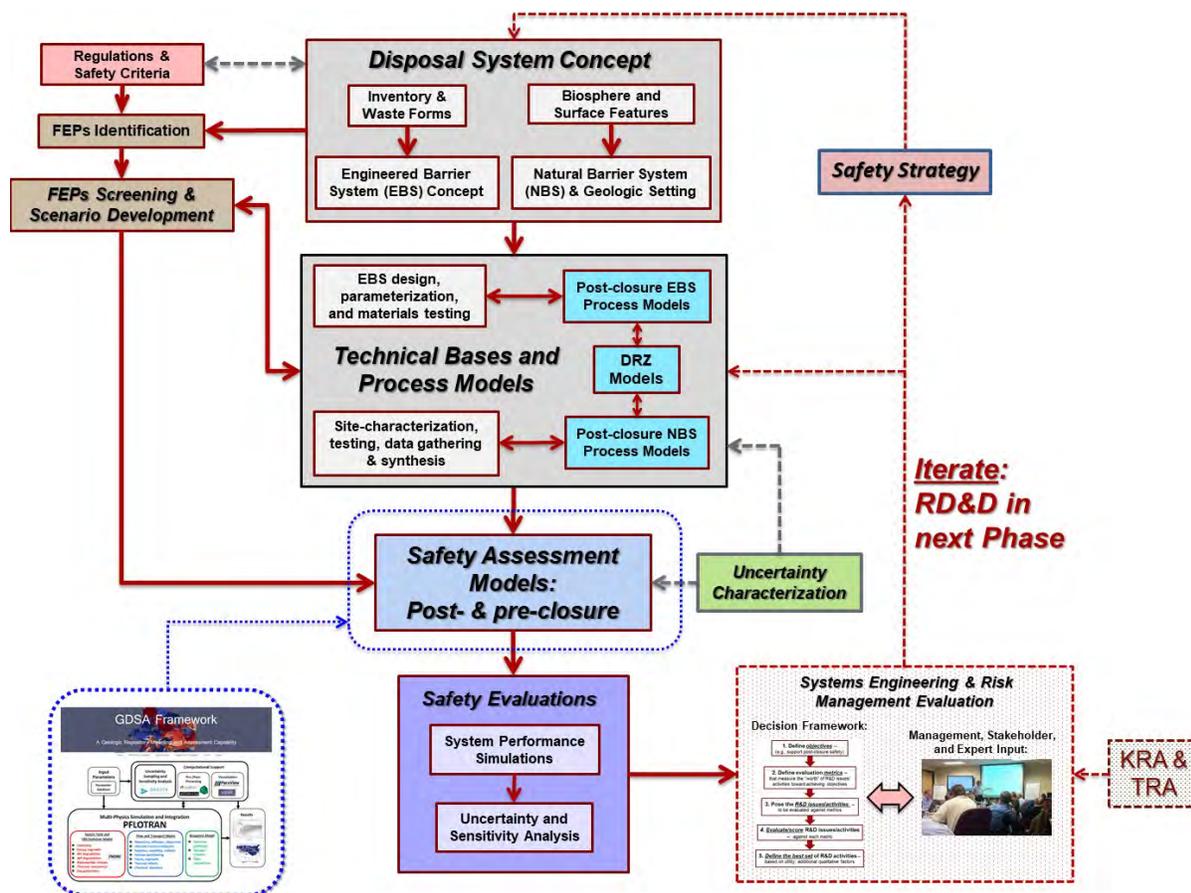
Figure 3-5   Information flow and the role of performance assessment modeling for R&D prioritization during a single stage of repository development (after Sevougian and MacKinnon 2017)

3.1.4   Considerations for the FY 2019 Roadmap Update Workshop

During the course of the May 2018 SFWST Annual Working Group Meeting, several observations were noted that will be important for the 2019 SFWST Roadmap Update Workshop:

1. Regarding "gap activities," i.e., those R&D areas that are not presently being looked at in the SFWST Campaign based on the prioritization in the 2012 Roadmap, but which may warrant further examination given current knowledge, there may be opportunities internationally to answer some of the questions – based on various underground research laboratory (URL) projects or other existing international collaborations.

2. Rankings for International R&D Activities in Table 3-1 should be consistent with the rankings for host-rock-specific or EBS-specific activities in Table 3-1, and some reconciliation is still necessary in the table. However, although consistency is a good idea, there could be real technical reasons for not having consistency – e.g., the U.S. usually considers much larger waste packages than the international community, so some current international activities (testing) may be less relevant to the U.S. program.

3. Almost all SFWST work in argillite R&D activities is related to EBS FEPs, even though some host-rock FEPs are highly scored for argillite, e.g., see "Evolution of EDZ – Clay/Shale" in Figure 3-4.

4. The EBS has different importance to argillite and crystalline host rocks (more important for crystalline), and this difference may affect the ranking of many of the International R&D Activities; or, equivalently, a separate scoring/ranking may be necessary for each host rock type for some of the International R&D Activities listed in Table 3-1, and likewise for their applicability to DPC disposal.

In moving forward with *GDSA Framework* development, the outcome of the January 2019 SFWST Roadmap Update Workshop will help prioritize future GDSA/process-model integration efforts, as well as self-contained development efforts within GDSA (e.g., Tasks #58 to #86 in Table 3-1). Some of the key related questions expected to be addressed during the January 2019 Update Workshop are:

- How does the FEP(s) associated with proposed R&D affect repository performance or confidence in the safety case, e.g., what is the ISC rating (see Table 3-2) of the FEP(s) and/or the proposed R&D Activity?

- How far advanced is the current "state of the art" knowledge regarding the associated FEP(s) and how/why does this particular R&D activity best advance the state of the art?

- What are the time scales of associated transient processes within a performance assessment (10 years, 100 years, etc.), and are these time scales important at regulatory time frames, such as 10,000 or 1,000,000 years?

- What are the key environmental inputs required for the proposed R&D activity, as well as the key outputs, parameters, and models supported or developed by the activity; in other words, can this R&D activity be easily integrated with process models and/or *GDSA Framework*?

- What is the real-time integration horizon, i.e., how long before the output of the proposed R&D activity is ready for integration with *GDSA Framework* and/or the Safety Case, and will it be ready at one of the capability points discussed above?

- What are possible "gap" activities, i.e., those important R&D issues not currently being investigated but which should be investigated based on their importance to the safety case and their current state-of-the-art?

As mentioned earlier, the results of the FY2019 SFWST Roadmap Update Workshop, and its guidance for *GDSA Framework* development and model integration, will be fully documented in a level 2 milestone, due on April 30, 2019 (M2SF-18SN010304065), entitled *GDSA Framework Development and Process Model Integration*.

3.2   Code Development

In addition to prioritizing and planning future *GDSA Framework* development (Section 3.1), the GDSA group developed the code in FY 2018. Developments are summarized in the following subsections:

- Section 3.2.1 – Stepwise linear regression

- Section 3.2.2 – Boundary condition mapping for multiphase conditions

- Section 3.2.3 – Localized corrosion framework

- Section 3.2.4 – Surrogate modeling

- Section 3.2.5 – Quality assurance test cases

3.2.1 Stepwise Linear Regression

GDSA Framework uses the software package Dakota (Adams et al. 2018) for sampling uncertain inputs and applying various methods of sensitivity analysis to the results. However, stepwise linear regression, a mainstay of traditional performance assessment sensitivity analyses, is not implemented in Dakota. In FY 2018, the GDSA team implemented a stepwise linear regression routine that takes as input the tabulated input and output parameter values returned by Dakota. The routine will be included as a post-processor in the release of Dakota version 6.9 due out in November 2019.

The stepwise linear regression routine, stepwise.py, is implemented in Python. It relies upon several freely available libraries for statistical analysis and array manipulation. These are pandas (https://pandas.pydata.org), statsmodels (http://www.statsmodels.org), patsy (https://pypi.org/project/patsy/), and numpy (http://www.numpy.org). It can be run with either Python 2 or Python 3.

3.2.1.1 Theory

Stepwise.py uses the stepwise linear regression method described by Helton and Davis (2000), resulting in a model of the form

$$\hat{y} = b_0 + \sum_{j=1}^{n_x} b_j x_j \qquad \text{Eq. 1}$$

where $\hat{y}$ is the estimated value of the output variable y, the x_j are the sampled input variables, and the coefficients b_j are used to calculate standardized regression coefficients (SRC), which indicate the relative importance of the sampled inputs to the uncertainty in y. Instead of including all sampled inputs in the regression model, stepwise regression sequentially identifies and includes only those input parameters upon which y has the greatest dependence.

Stepwise regression is useful when considering a large number of uncertain inputs, because it (1) identifies the few parameters with a strong influence and reduces (in comparison to a regression model containing all sampled input parameters) the number of coefficients that must be viewed and/or displayed by the analyst; (2) identifies unstable regression coefficients (those that are sensitive to which input variables are included in the regression); and (3) avoids overfitting the model. (See Helton and Davis (2000) for further discussion.)

Because the value of each b_j depends on the units of x_j, the b_j must be standardized before they can be compared to each other. The result is a standardized regression coefficient (SRC)

$$SRC_j = \frac{\hat{s}_j}{\hat{s}} b_j \qquad \text{Eq. 2}$$

in which b_j is normalized by the ratio of the standard deviation of the input variable x_j ($\hat{s}_j$) to the standard deviation of the output variable y ($\hat{s}$). When the x_j are independent, the absolute values of the SRCs indicate the relative importance of the x_j to y.

The value R^2 (the coefficient of multiple determination)

$$R^2 = \sum_{k=1}^{m} (\hat{y}_k - \bar{y})^2 \Big/ \sum_{k=1}^{m} (y_k - \bar{y})^2 \qquad \text{Eq. 3}$$

indicates the fraction of the variance in y accounted for by the regression model, where $\bar{y}$ is the mean of y and the sum is over m samples (Helton and Davis 2000). At each step of the regression, R^2 is returned. The difference between R^2 at the current step and the previous step is taken to be the fraction of the variance in the output accounted for by the latest addition to the regression model. If all variance in y is accounted for $R^2 = 1$.

Helton and Davis (2000) suggest three checks on whether the correct terms have been added to the regression model. The first is a comparison of the value of R^2 at the current step of the regression to the value at the previous step. R^2 will increase in size with the addition of an input variable, if the addition improves the agreement between the $\hat{y}$ estimated by the regression model and the observed values of y. A small increase in R^2 with the addition of a variable may indicate a chance effect on the output variable. If R^2 decreases or increases only a small amount with the addition of any remaining variable, the stepwise regression should be stopped.

The second check is a comparison of the predicted error sum of squares (PRESS) at the current step of the regression to that at the previous step. For a regression equation containing q input variables, $PRESS_q$ is calculated by comparing y_k to the estimated values ($\hat{y}_q(k)$) obtained from m regression equations, each one constructed with q input variables and by dropping a single observation k:

$$PRESS_q = \sum_{k=1}^{m}\left[y_k - \hat{y}_q(k)\right]^2 \qquad\qquad \text{Eq. 4}$$

PRESS will decrease in size with the addition of an input variable to the model if the addition improves the agreement between the vector of y_k and the vector of $\hat{y}_q(k)$. An increase in PRESS between step $q - 1$ and step q indicates overfitting of the data.

The third check is a statistical check that each b_j in the regression model differs from zero given that b_0 and all other $b_{\neq j}$ are in the model. The check can be performed using either an F-test or a t-test (Helton and Davis 2000), and results in a p-value for each b_j, where the p-value is the probability that b_j is equal to zero. A small p-value indicates that $b_j = 0$ is unlikely and increases confidence that the calculated non-zero b_j is correct. Typically, p-values are compared to a threshold value (α) of 0.05, 0.02, or 0.01 – in other words, the probability that $b_j = 0$ is less than 5%, 2%, or 1% is assessed.

Calculation of p-values assumes a normal distribution of error in observed values relative to the regression model and that all input variables are independent of each other. The former assumption is not true in a sampling-based sensitivity analysis, because given values of the x_j will always result in the same value of y. However, p-values still provide an "indication of how viable the relationships between input and output variables would appear to be in a study in which the underlying distributional assumptions were satisfied" (Helton and Davis 2000). Stepwise regression can take advantage of the latter assumption to identify unintentional correlations between input variables resulting from sampling – the p-value associated with a previously entered input variable will fluctuate if the input variable is correlated with the latest addition. If the p-value associated with a previously entered input variable increases above a threshold value (often chosen as 0.05), then that input variable should be removed from the regression and another step taken without it.

3.2.1.2   Implementation

To sequentially construct the linear regression model for an output variable, stepwise.py does the following:

1. Find the input variable with which the output variable has the strongest correlation (i.e., the largest correlation coefficient). Using the ordinary least squares method construct a linear regression model containing only that input variable.

2. Calculate the residual – the vector of differences between the observed values y and the estimated values $\hat{y}$. From the remaining input variables, find the one with which the residual has the strongest correlation, and recalculate the linear regression model with the addition of this input variable.

3. Compare values of R^2 and PRESS at the current step (q) to values at the previous step ($q-1$), and compare p-values to a threshold value (α).

4. If $R_q^2 > R_{q-1}^2$ and $PRESS_q < PRESS_{q-1}$, then continue the stepwise regression by repeating Step 2.

5. If $R_q^2 < R_{q-1}^2$ or $PRESS_q > PRESS_{q-1}$ then remove the last variable added to the regression and return the SRCs for the previous step.

6. If any p-value $> \alpha$, then remove the variable associated with the large p-value from the regression and take another step (repeat Step 2) without the problem variable. If the large p-value is associated with the last variable added to the regression, then remove the last variable added and return the SRCs for the previous step.

Future development of stepwise.py will increase the sophistication and flexibility of the checks on R^2, PRESS, and p-values. User-specified tolerances could be added to the checks on R^2 and PRESS to stop the stepwise regression when changes in these values become small. For the check on p-value, two thresholds (α) could be implemented, one for adding a variable to the regression and a larger one for removing a variable from the regression. Both of these could be user-specified. The check on p-values could also be improved in the case where the last variable added is associated with a p-value $> \alpha$ by taking another step while excluding that variable from the regression. These changes would make stepwise.py more similar to the stepwise code used in the WIPP PA (Gilkey 1995).

In Section 4, stepwise linear regression is applied to the FY 2017 shale reference case (Mariner et al. 2017), and the results are compared to other methods of sensitivity analysis.

3.2.2   Boundary Condition Mapping for Multiphase Conditions

When setting up a PFLOTRAN simulation, the user must define initial conditions and boundary conditions that specify the values of certain primary dependent variables (called a Dirichlet condition) or gradients of these variables (called a Neumann condition). Initial conditions typical of previous reference cases defined the pressure as hydrostatic, or the temperature field according to a simple geothermal gradient. Common boundary conditions included no fluid flow or no heat flow or applied a specific regional pressure gradient across the domain, for example. These previous references cases also assumed the subsurface was saturated. New this year, we explore an unsaturated reference case, which requires more complex initial and boundary conditions in order to set up the PFLOTRAN simulation.

For an unsaturated reference case scenario, the initial condition must define the initial saturation field, initial liquid and gas pressure, and initial temperature. The set of initial variable values at each grid cell cannot simply be guessed. Rather, a spin-up simulation is required to create and define a physically consistent set of initial variable values. If the combination of initial variable values are not physically consistent, the problem becomes numerically difficult or even impossible to solve. This year, the work flow required to set up the spin-up simulation was established, and the ability for PFLOTRAN to read in a gridded dataset of physically self-consistent variable values for the initial and boundary conditions was generalized.

When a user defines an initial or boundary condition, the user must first define a region (a set of grid cells or coordinates delineating a region in the domain) or a face, and then apply Dirichlet or Neumann conditions to the defined region(s). The Dirichlet or Neumann conditions can be steady (no variation in time), homogeneous (no spatial variation in the region), or unsteady and/or spatially variable. If the Dirichlet or Neumann conditions are spatially variable, then a gridded dataset is used to prescribe the initial or boundary conditions within the defined region or on the defined face.

Previous to this fiscal year, PFLOTRAN was limited in its ability to read in a gridded dataset to define an initial or boundary condition; PFLOTRAN assumed that all grid cells within the defined region or on the face where an initial or boundary condition was being applied were in a single thermodynamic state. In other words, all cells in the region had to be either (a) single phase liquid, (b) single phase gas, or (c) two phase liquid and gas. It was not possible to define a condition that described, say, a change in liquid saturation from fully saturated to partially saturated within one region. However, this is exactly what is required when setting up the initial conditions for an unsaturated reference case.

PFLOTRAN's limitation in its ability to read in a gridded dataset to define an initial or boundary condition that described a "multi-phase condition" stems from the governing equations and the combination of primary dependent variables that are required to mathematically define an initial or boundary value problem. If a grid cell is in a single-phase liquid state, the user must define the temperature, liquid pressure, and mole fraction of gas dissolved within the liquid. If a grid cell is instead in a single-phase gas state, the user must define the temperature, the gas pressure, and the relative humidity. Finally, if a grid cell is in a two-phase state, the user must define the temperature, the gas saturation (conversely, unity minus the liquid saturation), and the gas pressure. Given the specific combination of primary dependent variables that the user defined, PFLOTRAN would determine the thermodynamic state. However, if the user desires to define a multi-phase condition, he or she must provide values for several of the primary dependent variables, and it is no longer possible to determine the state of a grid cell based on the specific combination of the given variables.

To fix PFLOTRAN's limitation required a substantial refactoring of how the initial thermodynamic state of a grid cell was determined when assigning initial or boundary conditions. Due to the possibility of a multi-phase state within a region, the gas saturation is now used to determine the initial thermodynamic state of a grid cell in a multi-phase condition. For example, if the user wants to define a multi-phase condition, he or she must provide the temperature, liquid pressure, gas pressure, gas saturation, and gas mole fraction or relative humidity at each grid cell. Keep in mind that these values must be physically consistent at each grid cell. Also note that for each grid cell, providing all five values over-defines the thermodynamic state (e.g., more information is provided than is mathematically needed). Internally, PFLOTRAN now recognizes when a condition is over-defined and keys off this detail to advance to a new procedure where the gas saturation is checked to tag each grid cell within the multi-phase condition with a thermodynamic state. If the gas saturation is zero, then the thermodynamic state is single phase liquid. If the gas saturation is unity, then the thermodynamic state is single phase gas. And finally, if the gas saturation is above zero but less than unity, the thermodynamic state is two-phase liquid and gas. Once the correct thermodynamic state is tagged, only the required set of three primary dependent variable values is taken from the over-defined set of variables to define the initial or boundary condition.

Moreover, in order to allow for multi-phase thermodynamic states within a defined region where the user is prescribing an initial or boundary condition, the region has to be interrogated grid cell-by-grid cell. Previous to the generalization, when it was assumed that the entire region where a condition was being defined was in a single thermodynamic state, PFLOTRAN could tag all grid cells in the domain with the single thermodynamic state in one fell swoop. Because this is no longer the case, the algorithms that tagged grid cells with a thermodynamic state had to be modified with the addition of a loop. PFLOTRAN will now loop over each grid cell in a region when tagging grid cells with a thermodynamic state. While this is required for generality, it becomes unnecessary if all grid cells within a region truly are intended to

be in a single thermodynamic state. Future improvements to the new generalization routine will include a more intelligent loop, which will only loop through grid cells if required to for a multi-phase condition but condense or skip the loop if not required. Further testing will be required to ensure the improved, intelligently looping algorithms remain as robust as the current generalized implementation.

3.2.3   Localized Corrosion Framework

Waste packages degrade by multiple processes. Mechanisms include general corrosion, stress corrosion cracking (SCC), pitting corrosion, microbiologically-influenced corrosion (MIC), rock fall, initial mechanical defect, etc. Which process is important at a given time in a simulation depends on relative degradation rates and initial and local conditions. An overall waste package degradation model must account for how the various individual degradation processes affect the timing of waste package breach, performance after breach, local groundwater conditions, and precipitation of secondary minerals.

Currently, *GDSA Framework* only simulates general corrosion. It does this in one of two ways. It can use an Arrhenius equation to determine the rate of corrosion for each waste package as a function of the local temperature, or it can predetermine a waste package breach time for each waste package. In either case, the waste package is currently assumed to disappear when breached and to provide no barrier capability thereafter. No chemical corrosion reactions are simulated and no corrosion products accumulate. Corrosion rate coefficients or breach times are sampled from uncertainty distributions for each waste package so that there is spatial heterogeneity in failure times. When the rate model is used, the rate is calculated at each time step and is fully coupled to the local thermal conditions of the waste package.

This year an advanced framework was conceptualized to accommodate multiple degradation mechanisms occurring simultaneously on each waste package. In this advanced design, the *GDSA Framework* waste package degradation model tracks each mechanism independently. Degradation rates for each mechanism are calculated at each time step and are used to calculate the cumulative degradation lengths for each mechanism. When the cumulative degradation length exceeds the wall thickness, the waste package breaches.

In the new design, breaches affect the waste package's fractional area breached, i.e., the fractional area of the waste package that no longer provides an impermeable barrier. This is similar to the approach of He et al. (2011) For general corrosion, the fractional area breached changes from zero to one upon breach. For localized corrosion, it changes from zero to a positive value much less than one. For a local breach, the rate of increase in the breached fractional area is designed to be calculated by the mechanistic model and used by *GDSA Framework* to update the cumulative fractional area breached.

Fractional area breached is designed to be tracked and used by *GDSA Framework* to help simulate the effects of partial waste package performance. Modeling partial waste package performance may be important to performance assessment because small area breaches inhibit radionuclide release and may prevent the chemical conditions inside the waste package from being controlled by the chemical environment outside the waste package. Initially, it is expected that *GDSA Framework* will simulate these effects by simply adjusting fluxes through the waste package as a function of fractional area breached. Over time, more robust approaches will be developed. For example, coupled mechanistic degradation models could be used to calculate the properties of corrosion layers and crack-filling precipitates. Properties such as these would help improve calculations of fluxes across the breaches.

Figure 3-6 shows the general conceptual work flow. At the beginning of each time step, relevant local conditions and parameters that track degradation lengths and fractional breach areas for each waste package are fed to the coupled mechanistic models. The mechanistic models return rates of change in the degradation lengths, fractional breach areas, and other degradation properties as needed (e.g., permeability, porosity, and tortuosity of crack-filling corrosion products). *GDSA Framework* then adjusts

flow through the waste package cells for the time step according to the effects of the degradation processes and tracks the information that will be needed for the following time step.

Corrosion of the waste package not only affects release of radionuclides, it alters the local chemical and physical environment surrounding the waste package by consuming reactants and generating products. Corrosion produces secondary mineral precipitation and, if rapid relative to the migration of nearby aqueous and gas species, affects local aqueous and gas composition. Many of these effects provide important feedbacks that may alter degradation rates. In addition, the accumulation of precipitated secondary phases may affect radionuclide transport by providing a substrate for sorption. Corrosion could also release radionuclides generated by neutron activation. These effects may be added to *GDSA Framework* as waste package degradation models develop.
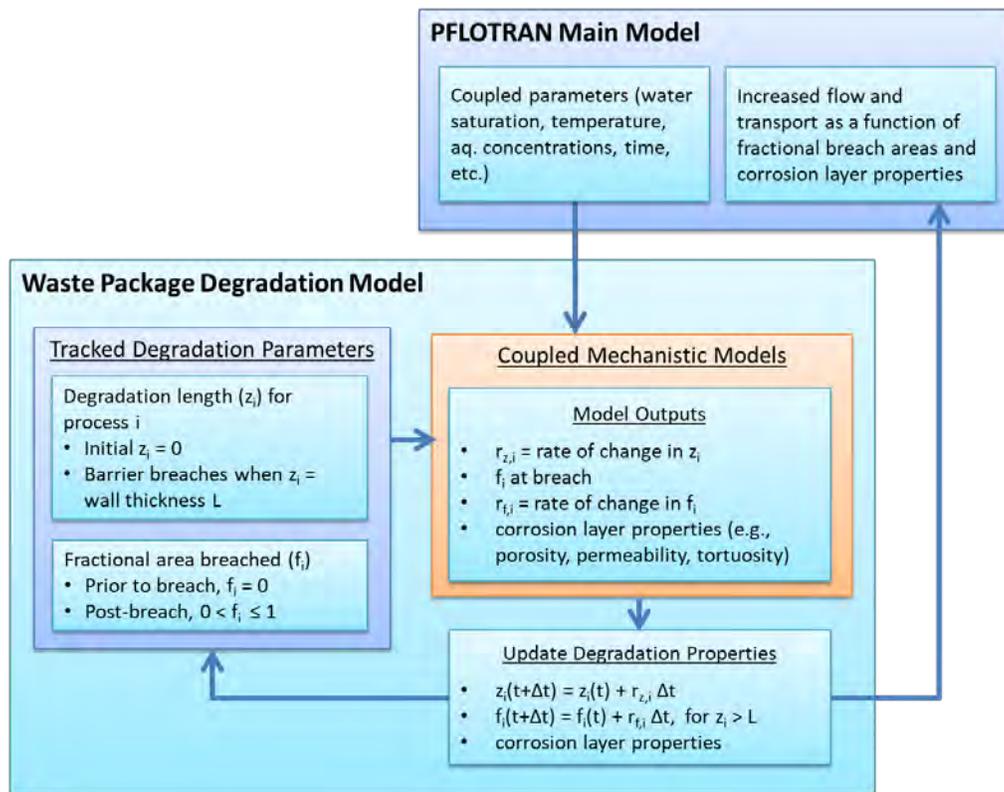
Figure 3-6   Workflow conceptualized for the waste package degradation model of the *GDSA Framework* waste package process model

3.2.4   Surrogate Modeling

A primary goal of *GDSA Framework* development is to make repository performance modeling more comprehensive and mechanistic by including as many potentially important process models as possible in total system simulations. Many of these process models are complex and too computationally expensive to include in total system simulations using today's available computer resources. However, years from now, when new repository sites are identified, available computer resources could very well be able to couple all the necessary mechanistic models. Direct coupling of mechanistic process models is preferred for total system performance assessment when it is not too expensive to do so.

Another major goal of *GDSA Framework* development is to probabilistically simulate repository concepts to help identify sources of uncertainty and prioritize future R&D. To achieve this goal in a timely manner,

developers need to consider ways to inexpensively include the effects of expensive process models in total system simulations.

Particularly demanding of mechanistic process models are repository concepts that rely heavily on the performance of waste packages and waste forms. With thousands of waste packages in a repository, thousands of time steps in a realization, and hundreds of realizations in a simulation, process models affecting the waste package and waste forms would need to be called on the order of a billion times per simulation. Because the mechanistic models of processes affecting waste packages and waste forms (e.g., general corrosion, pitting corrosion, fuel matrix degradation) often run slowly due to their complexity (i.e., often employing reactive transport, growth of alteration layers, and internal iterative solutions), such a repository simulation would be expensive.

One way to reduce the computational expense of this type of simulation is to divide the waste packages into groups based on the assumption that each waste package in a group will behave like all the others in the group. In this approach, the computational model performs the mechanistic calculations on one waste package in each group and assigns the outcomes to the rest of the group's waste packages. To reduce the computational time of the mechanistic process models by a factor of N, the average number of waste packages per group would be N. Though this approach can significantly reduce computational time, it has some associated challenges, such as:

- How would groups of waste packages be determined? A good discriminator, after waste package type, is the temperature history at the emplacement location. Other potentially important factors to consider include local groundwater fluxes, local buffer erosion, and local chemistry. For waste form dissolution, the local radionuclide concentrations can also be affected by up-gradient waste package failures. Several of these factors are affected by location and coupled processes, so they would be difficult to predict ahead of time for each waste package.

- Would all waste packages in a group rupture the same way?

- Would all waste packages in a group rupture at the same time? This is unlikely in a real repository because each waste package will be exposed to different temperature and chemical conditions, though these differences may be small within a group. A Gaussian deviation could be imposed on the waste packages to make them rupture at different times, perhaps based on local temperature history; however, this would amount to a reduced-order model and would require development and justification.

- What effect does the grouping approach have on the interactions between adjacent waste packages?

- A procedure would need to be developed to address the questions above, and modelers would need to reassess the groupings each time that relevant inputs change.

- A computational framework would need to be developed to execute the groupings, run the mechanistic models for the representative waste package of each group, and distribute results to the appropriate waste packages.

Aspects of this modeling approach were used successfully in the 1990s when analyzing numerous DSNF waste types (~250) (Rechard 1993; Rechard 1995; Rechard 1998). The numerous DSNF and CSNF waste types were grouped into less than 10 groups with similar characteristics (e.g., cladding, fuel matrix type, U enrichment). A repository grid block (or element) could have each waste type, based on the spatial distribution in the repository. The computational expense was reduced by modeling the repository with a very course grid, but the repository mesh could be changed in areas where gas or fluid flow into the

repository was highly varying such that concerns about, for example, having the same breach times of packages over a large area, could be addressed.

A more direct way to reduce the computational expense of simulating the evolution of thousands of waste packages is to develop response surface surrogate models that can rapidly emulate the mechanistic models. An ideal response surface surrogate model runs orders of magnitude faster than its parent mechanistic model and provides outputs identical to those of the mechanistic model. In practice, the speed increase is easy to achieve. The challenge is achieving acceptable accuracy.

In FY 2018, a team of GDSA modelers and mathematicians began to explore the potential value of developing a response surface surrogate model for the Fuel Matrix Degradation (FMD) model. The team includes Jim Jerden, lead developer of the FMD model. The FMD model is a mechanistic spent fuel dissolution model coded in Matlab and developed at Argonne National Laboratory and Pacific Northwest National Laboratory (Jerden et al. 2017). The model calculates used fuel dissolution rates as a function of radiolysis, alteration layer growth, diffusion of reactants through the alteration layer, temperature, and interfacial corrosion potential. During execution it employs a one-dimensional reactive transport model to simulate a set of aqueous and heterogeneous chemical reactions and to simulate diffusion of chemical species over time. The 1D model domain is typically 0.05 m in length and discretized into 30 to 100 cells.

Though a FORTRAN version of the FMD model was developed and coupled to *GDSA Framework* (Mariner et al. 2015), it runs too slowly to be included in repository simulations having hundreds to thousands of spent fuel waste packages. More efficient coding and faster solvers have been proposed for the FORTRAN FMD code, but there is no assurance that such modifications would provide the speed needed. The code would still need to execute a large number mechanistic calculations, iterate to a converged solution, and provide outputs for each cell in the 1D domain. Alternatively, a surrogate model, by comparison, would provide practically instantaneous solutions. It would use much less information (i.e., only the inputs identified by sensitivity analysis to be important), and it would use direct expressions to calculate each output.

Response surface surrogate models are trained using data generated by the mechanistic models. Response surfaces are typically nonlinear hyperplanes. Surrogate models employed to represent the response surfaces may be parametric, as in polynomial chaos surrogates, or nonparametric, as in Gaussian process surrogates or spline-based approximations. Development and use of response surface surrogate models and surrogate modeling techniques has been extensive over the past decades and has experienced widespread use in water resource modeling (Razavi et al. 2012; Hussain et al. 2015). A response surface has been successfully applied in the performance assessment for the Waste Isolation Pilot Plant. The model was the response of creeping salt to pressure changes from generation of gas as waste packages anoxically corroded (DOE 2014). Response surface surrogate models were also extensively used in performance assessments on the proposed Yucca Mountain repository (DOE 2008).

A simple form of a response surface surrogate model is a response surface lookup table. A response surface lookup table is generated by running the mechanistic model over the relevant sample space and tabulating the outputs as a function of input parameter values. This type of surrogate model inherently provides a high degree of accuracy and is fairly easily generated. However, there are important drawbacks to lookup tables:

- Lookup table interpolations introduce error.

- Error introduced by interpolations is not quantified and tracked.

- A high number of independent variables for a response surface is often not supported.

- Independent variables of lesser importance might be excluded, introducing error.

- High-resolution lookup tables require significant memory.

A response surface surrogate model in the form of a continuous function is more involved than a response surface lookup table. This type of surrogate model has its own set of advantages and disadvantages. Advantages compared to lookup tables include:

- There are no interpolations for continuous response surfaces.

- Error in a continuous surrogate model can be estimated and tracked.

- Actual data points can be added to the set of training data and weighted heavily if desired.

- Development includes sensitivity analyses that identify the important input parameters.

- A high number of independent variables can be easily accommodated.

- The response surface is represented in the code by a small set of rapidly calculated expressions.

A disadvantage of a continuous surrogate model over a lookup table is that the response surface must be fairly smooth for a good fit. Also, it may be difficult to achieve acceptable accuracy for important regions of the response surface. Acceptability, if possible, should consider both experimental uncertainty and uncertainty due to assumptions made in the development of the mechanistic model.

In FY 2019, a continuous surrogate FMD model and a FMD lookup table surrogate are planned for development and comparison. Based on this work, advantages and disadvantages of each approach will be identified. Regardless of which approach fares better, having a FMD surrogate model to use in repository simulations will be a significant advance for *GDSA Framework*. With a FMD surrogate model, *GDSA Framework* will be able to simulate spent fuel dissolution for each breached spent fuel waste package in a repository simulation. In addition, this capability will allow uncertainties in spent fuel dissolution to be propagated and sensitivities in FMD inputs to be quantified and ranked against other inputs.

A third option for the FMD model, not being pursued at this time, is to improve the efficiency of the FORTRAN FMD code. Though significant enhancements in speed can be achieved, the code must still perform a very large number of calculations at each time step. In addition, there are questions as to who will be responsible for improving, updating, and maintaining the FORTRAN FMD model, especially as the parent Matlab version evolves over time. Perhaps we will discover that for the FMD model it is better to have a modeler develop a surrogate model for *GDSA Framework* than to have a coder convert new Matlab versions to FORTRAN. By going the surrogate modeling route, FMD process modelers would be able to stay focused on their Matlab version while surrogate modelers would separately build, improve, and maintain a surrogate model. With code developers in high demand, a clean division of labor like this could be especially appealing, provided surrogate models are well-vetted and their calculations are easily spot-checked against process model calculations. Which approach is best for the FMD model may become clearer as surrogate FMD models take shape in the coming year.

3.2.5   Quality Assurance Test Cases

Several new test cases have been added this year, focusing on transport, and radionuclide decay and ingrowth. These tests expand PFLOTRAN's growing QA test suite (see Mariner et al. 2017, for additional details on PFLOTRAN's QA test suite). Additionally, automatic spatial convergence testing has been added to each existing test, which measures the relative error between the PFLOTRAN solution and the analytical solution as the grid resolution increases.

3.2.5.1   New Transport Test Cases

Diffusion-only test cases have been added which verify PFLOTRAN's transport capability when there is no flow (advection). Cases have been developed for 1D, 2D, and 3D domains, with steady-state and transient solutions. To date, the problems are limited to testing Dirichlet (scalar) boundary conditions because PFLOTRAN currently does not have the capability to handle Neumann boundary conditions for solute flux without fluid flow. The Dirichlet boundary conditions range from simple to complex as the problem dimensions grow.

The steady-state problems were developed from the existing thermal QA test problems for heat conduction only, which were originally based on Kolditz et al. (2015). Values for temperature were swapped with solute concentration, and the thermal diffusivity was replaced with a molecular diffusion coefficient. Simulation times were modified to ensure a steady state was reached in the solution. The PFLOTRAN input deck representing each test was integrated into the existing Python framework so that each test could be automatically run. Finally, documentation was written for each new test and added to the online documentation site:

https://www.pflotran.org/documentation/qa_tests/intro_transport.html#steady-transport

The following three figures (Figure 3-7, Figure 3-8, and Figure 3-9) represent the work completed during a summer internship that was supported by the GDSA project.
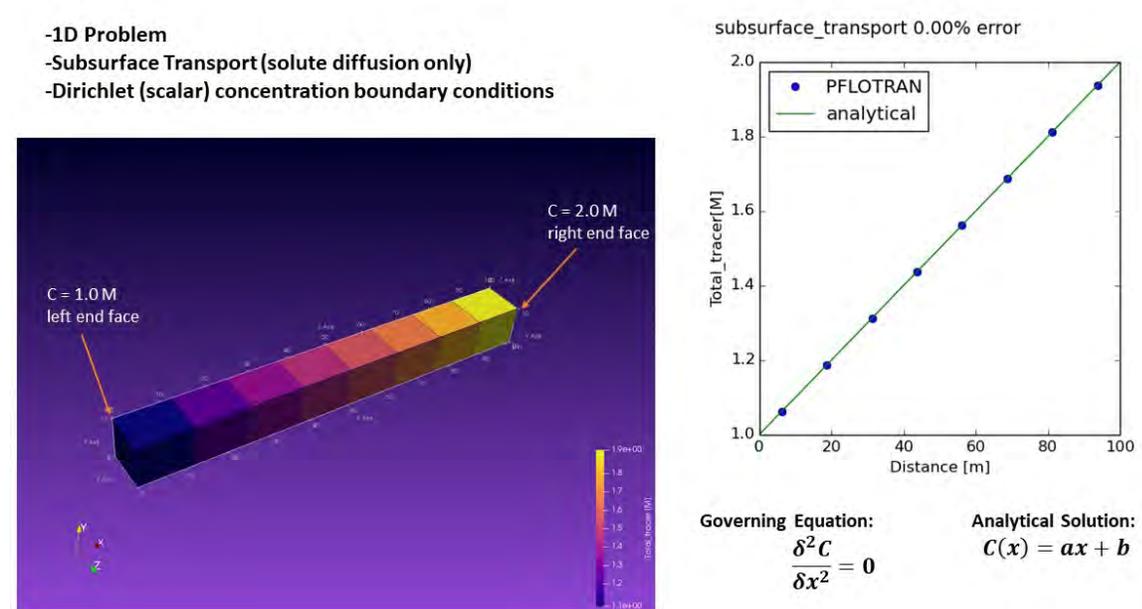
Figure 3-7   Visual summary of the 1D steady-state diffusion problem newly added to the PFLOTRAN QA Test Suite

-2D Problem
-Subsurface Transport (solute diffusion only)
-Dirichlet (scalar) concentration boundary conditions
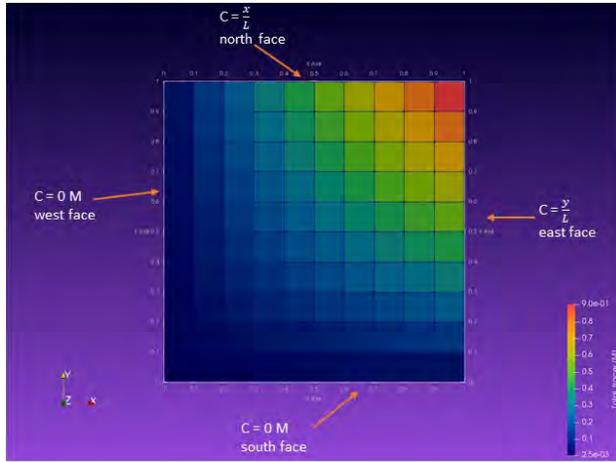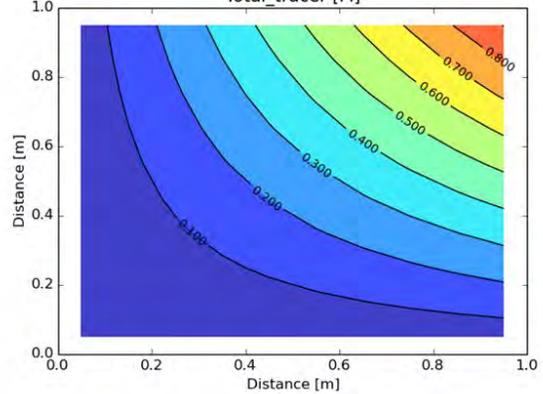
Governing Equation:

$$\frac{\delta^2 C}{\delta x^2} + \frac{\delta^2 C}{\delta y^2} = 0$$

Analytical Solution:

$$C(x,y) = C_0 \frac{x}{L}\frac{y}{L}$$

Figure 3-8   Visual summary of the 2D steady-state diffusion problem newly added to the PFLOTRAN QA Test Suite

-3D Problem
-Subsurface Transport (solute diffusion only)
-Dirichlet (scalar) concentration boundary conditions
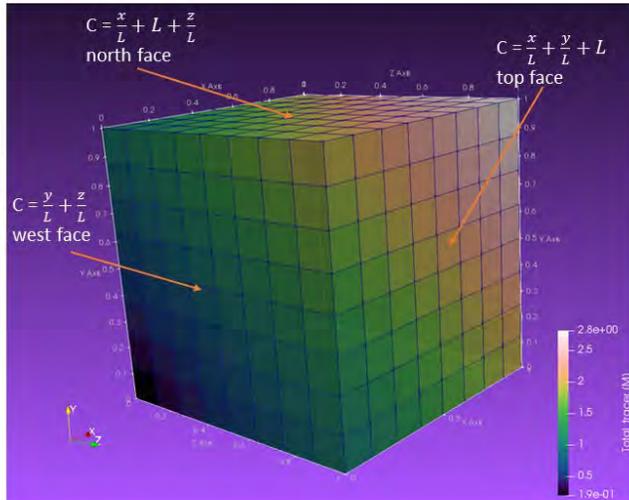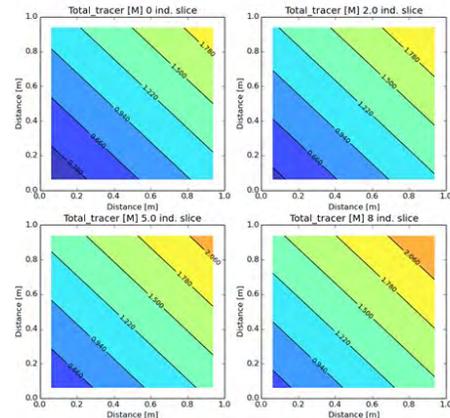
Governing Equation:

$$\frac{\delta^2 C}{\delta x^2} + \frac{\delta^2 C}{\delta y^2} + \frac{\delta^2 C}{\delta z^2} = 0$$

Analytical Solution:

$$C(x,y,z) = C_0 (\frac{x}{L} + \frac{y}{L} + \frac{z}{L})$$

Figure 3-9   Visual summary of the 3D steady-state diffusion problem newly added to the PFLOTRAN QA Test Suite

A single 1D transient diffusion-only test was also added to the PFLOTRAN QA test suite that verifies the diffusion of an initial pulse of a tracer over time. The initial pulse is represented in PFLOTRAN as an initial condition of tracer concentration in the central grid cell. The concentration profile in the discretized domain has a finite width and finite value for the concentration. However, the analytical solution that describes the transient solution represents the initial condition as a Dirac Delta function, which is infinite in concentration by infinitesimally narrow. While the same amount of mass is placed within the domain, it is distributed differently between the numerical initial condition and the analytical solution because the numerical initial condition must be discretized on a grid. Therefore, the solutions do not match at early times in the simulation, nor are they expected to, unless the grid resolution was infinitely fine. The results shown in Figure 3-10 show the two solutions after 10 years into the simulation, when it was found that the two solutions began to show agreement. While they visually look similar, the relative error at 10 years is still substantial, approximately 5%. This error can be reduced by increasing the resolution of the PFLOTRAN grid.
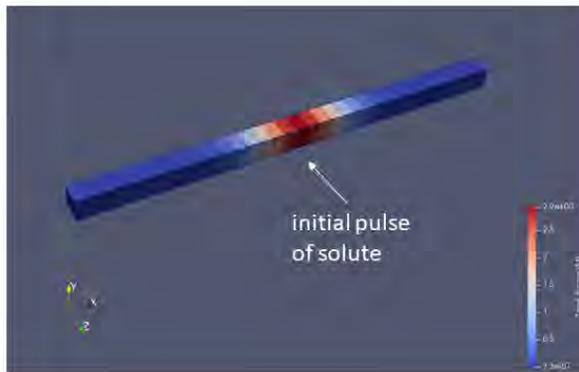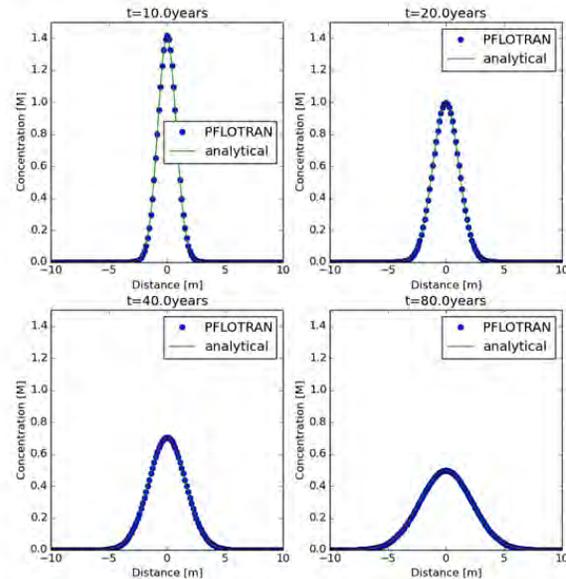
Figure 3-10 Visual summary of the 1D transient diffusion with initial tracer pulse problem newly added to the PFLOTRAN QA Test Suite

Test cases that include fluid flow (advection) in addition to diffusion are still under development. These tests are based on the 1D transient test with an initial pulse of tracer, as shown in Figure 3-10, but include a steady flow field in the positive x-direction that advects the tracer pulse as it diffuses away. The Péclet Number is the ratio between the advective transport rate, and the diffusive transport rate. The tests that include both advection and diffusion will be designed to span a range of Péclet Numbers, so that test cases where advective transport is much faster than diffusive transport, and vice versa, are verified. An example of one test, where advective transport is 32 faster than diffusive transport (e.g. Pe = 32), is shown in Figure 3-11. In this example, the high relative error is due to the mismatch between the PFLOTRAN solution and analytical solution at early simulation times due to the Dirac Delta definition for the analytical solution and the finite discretized numerical initial condition.
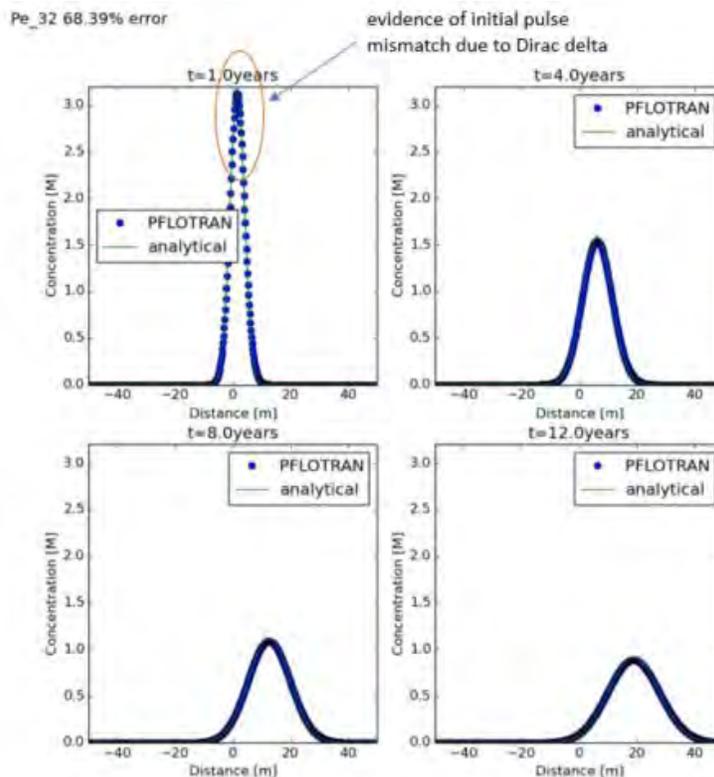
Figure 3-11 A partially developed 1D transient advection/diffusion test with an initial tracer pulse

3.2.5.2   New Radionuclide Decay and Ingrowth Test Cases

Over the history of the GDSA project, several reference cases have been developed, exploring a range of repository layouts and host rocks. However, common to all geologic repository performance assessment simulations developed under the GDSA project is that each simulation must include nuclear waste containing radionuclides which undergo decay and ingrowth. Given the importance of radionuclides in these simulations, several new QA tests are being developed which verify PFLOTRAN's calculations for radionuclide decay and ingrowth. The tests have not yet been included in the automated QA Test Suite, but are described here in their current state of progress. It is planned to integrate the radionuclide decay and ingrowth tests into the automated QA Test Suite in FY 2019 as they are individually completed.

Radionuclide decay and ingrowth is described by the Bateman equation(s). For a single species (i.e. parent) radionuclide concentration, N_p, the governing equation that describes the evolution of N_p is,

$$\frac{dN_p}{dt} = -\lambda N_p \qquad\qquad \text{Eq. 5}$$

where λ is the decay rate constant [1/T]. The analytical solution for a single species parent radionuclide, N_p, takes the form,

$$N_p = N_p^0 e^{-\lambda t} \qquad \text{(Sln.1)} \qquad\qquad \text{Eq. 6}$$

where N_p^0 is the initial value of N_p. For a daughter radionuclide, the governing equation that describes the evolution of N_d is,

$$\frac{dN_d}{dt} = \lambda_p N_p - \lambda_d N_d \qquad \text{Eq. 7}$$

where λ_p is the parent radionuclide decay rate [1/T], and λ_d is the daughter radionuclide decay rate [1/T]. The analytical solution for the concentration of a daughter radionuclide, N_d, takes the form,

$$N_d = \frac{\lambda_p}{\lambda_d - \lambda_p} N_p^o \left(e^{-\lambda_p t} - e^{-\lambda_d t} \right) + N_d^0 e^{-\lambda_d t} \qquad \text{(Sln.2a)} \qquad \text{Eq. 8}$$

where N_p^0 is the initial value of N_p and N_d^0 is the initial value of N_d. For the special case when $\lambda_p = \lambda_d$, the analytical solution for the concentration of a daughter radionuclide, N_d, becomes,

$$N_d = \left(\lambda N_p^o t + N_d^o \right) e^{-\lambda t} \qquad \text{(Sln.2b)} \qquad \text{Eq. 9}$$

PFLOTRAN has the capability to model radionuclide decay and ingrowth using two methods. The first and original method uses the traditional reactive transport capability in PFLOTRAN, using the keyword RADIOACTIVE_DECAY_REACTION. If one were to use the traditional capability, some initial mass (or concentration) of a parent radionuclide is placed within a region of the computational domain at the beginning of the simulation or via a boundary condition. There may also be specified an initial mass of a daughter radionuclide as well. The reactive transport capability calculates radionuclide transport, as well as the decay and ingrowth of the radionuclides (according to the Bateman equations), as specified by the details of the decay chain from the input deck (e.g., half-life, parent-daughter relationships) as the simulation proceeds. The Bateman equations are solved using Newton's method.

The second method, which uses PFLOTRAN's Waste Form Process Model (WFPM) and UFD Decay Process Model (UFDDPM), was designed to specifically model waste package breach and waste form dissolution, to calculate a more realistic radionuclide source term for a performance assessment simulation. The second method also uses the reactive transport capability, but only to perform transport. The radionuclide decay and ingrowth is instead calculated by the Waste Form Process Model and UFD Decay Process Model. Online documentation for more details on these two process models is located here:

https://www.pflotran.org/documentation/theory_guide/pm_ufd_decay.html

https://www.pflotran.org/documentation/theory_guide/pm_waste_form.html

The Bateman equations describing decay and ingrowth can be solved using Newton's method, or a 3-generation analytical solution derived for multiple parents and grandparents with non-zero initial daughter concentrations, as previously documented in Section 3.2.3 of Mariner et al. (2016), SAND2016-9610R.

Because it is possible for PFLOTRAN to calculate radionuclide decay and ingrowth with two possible capabilities (using the traditional reactive transport capability, or using the two specialized process models developed under the GDSA project), and it is possible to solve the Bateman equations with two possible methods (using Newton's method, or using the 3-generation analytical solution), the number or verification tests needed to provide adequate code coverage is large. In FY 2018, we've begun designing and executing the suite of tests that will eventually cover all of PFLOTRAN's radionuclide decay and ingrowth capability, and the preliminary results of these tests are presented here.

The current set of developed QA tests are organized as follows. The parent radionuclide was modeled after [241]Am, while the daughter was generic.

1. Parent-only radioactive decay, no-daughter
   a. Analytical solution is Sln.1

      b.   Tests using RADIOACTIVE_DECAY_REACTION and WFPM/UFDDPM (3-generation approach only)

2.   Parent and daughter radioactive decay/ingrowth, no initial daughter

      a.   Analytical solution is Sln.2a

      b.   Tests using RADIOACTIVE_DECAY_REACTION and WFPM/UFDDPM (3-generation approach only)

      c.   Tests for:

            i.   half-life of daughter (2.14E6 yr) >> half-life of parent (432.7 yr)

           ii.   half-life of daughter = half-life of parent (432.7 yr) [2]

         iii.   half-life of daughter (500y) < half-life of parent (432.7 yr)

3.   Parent and daughter radioactive decay/ingrowth, with an initial daughter concentration

      a.   Analytical solution is Sln.2a

      b.   Tests using RADIOACTIVE_DECAY_REACTION and WFPM/UFDDPM (3-generation approach only)

      c.   Tests for:

            i.   half-life of daughter (2.14E6 yr) >> half-life of parent (432.7 yr)

           ii.   half-life of daughter = half-life of parent (432.7 yr) [2]

         iii.   half-life of daughter (500 yr) < half-life of parent (432.7 yr)

All test case results presented are run with a constant, maximum simulation time step of 1.0 years, and results are output every 100 years. As seen in the following results, there is excellent agreement between the PFLOTRAN solution and the analytical solution with the traditional reactive transport capability (RADIOACTIVE_DECAY_REACTION) and with the WFPM/UFDDPM. It is noted that when using the WFPM/UFDDPM approach, the radionuclide inventory is released after the first day, and thus there is a sudden jump in the concentration from zero to a non-zero value after the first day of the simulation. This differs from the analytical solution because the analytical solution assumes a non-zero initial radionuclide concentration that is dissolved immediately at time zero, but when using the WFPM approach, radionuclide inventory is still sequestered inside the waste form object at time zero, which is only released after one day of simulation time.

The test cases were set up with a 100 [M] initial concentration of parent radionuclide for the RADIOACTIVE_DECAY_REACTION simulations. For the WFPM/UFDDPM simulations, the equivalent mass of radionuclide was placed into the waste form, so that if it were to dissolve into the total volume of the single grid cell (1E3 m^3) instantaneously, it would be equivalent to 100 Molar.

---

[2] Because the 3-generation approach of solving the Bateman equations that is used for the WFPM/UFDDPM is based on a 3-generation version of Sln.2a, in the case when the half-life of the daughter is exactly equal to the half-life of the parent, a division by zero occurs, and the PFLOTRAN simulation crashes. Therefore, the cases where the half-life of the daughter is exactly equal to the half-life of the parent were only run for the RADIOACTIVE_DECAY_REACTION approach, and the analytical solution is described by Sln.2b. For the WFPM/UFDDPM approach, the half-lives were made slightly different, by adding 0.00001 to the half-life of the parent.
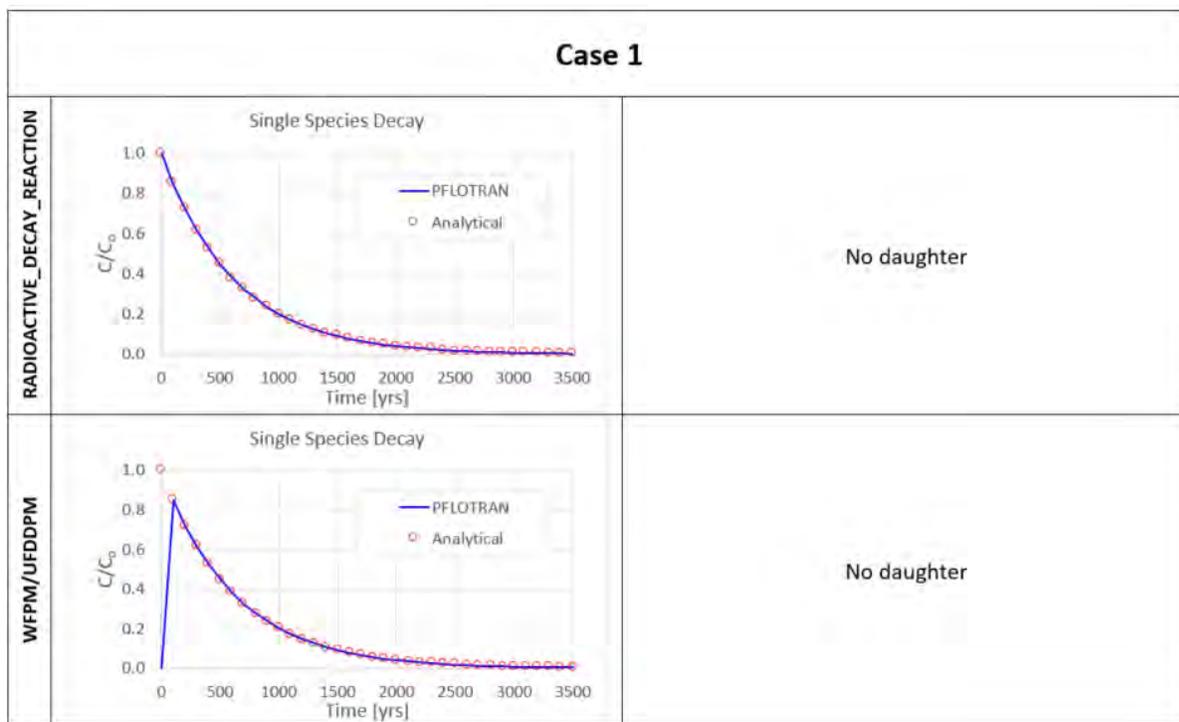
Figure 3-12 Case 1 (Parent-only radionuclide decay)
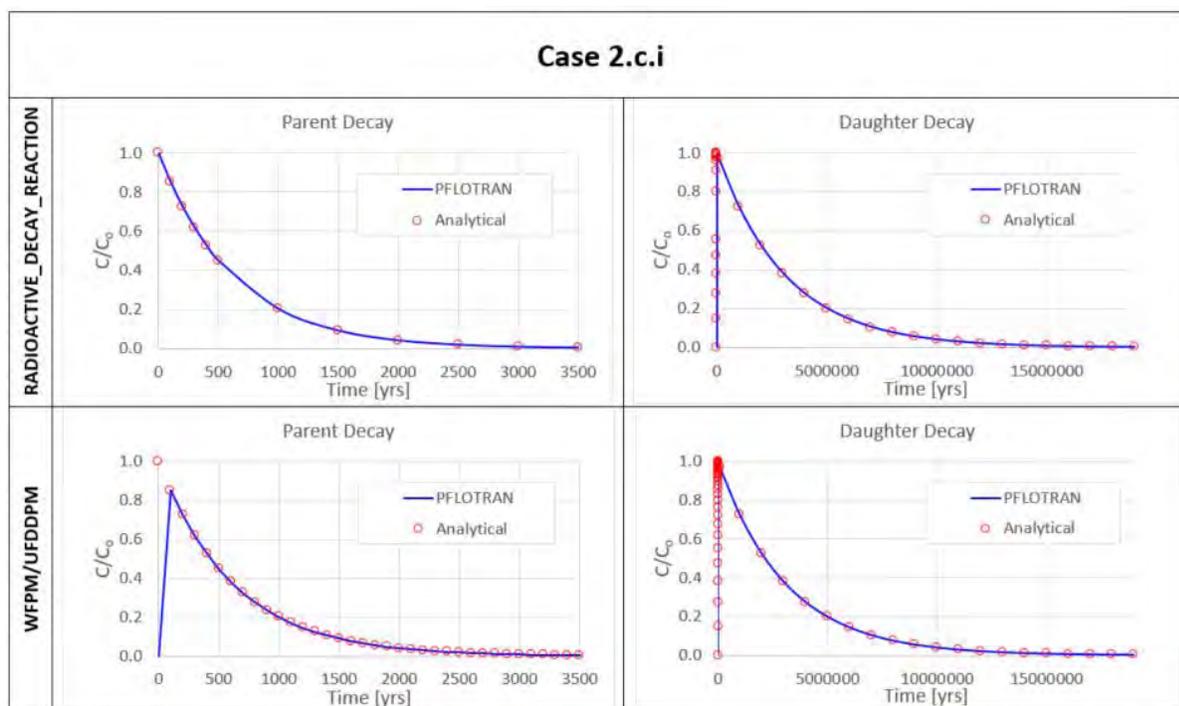
Figure 3-13 Case 2.c.i (Parent-Daughter radionuclide decay and ingrowth with no initial daughter mass where the half-life of the daughter >> the half-life of the parent)
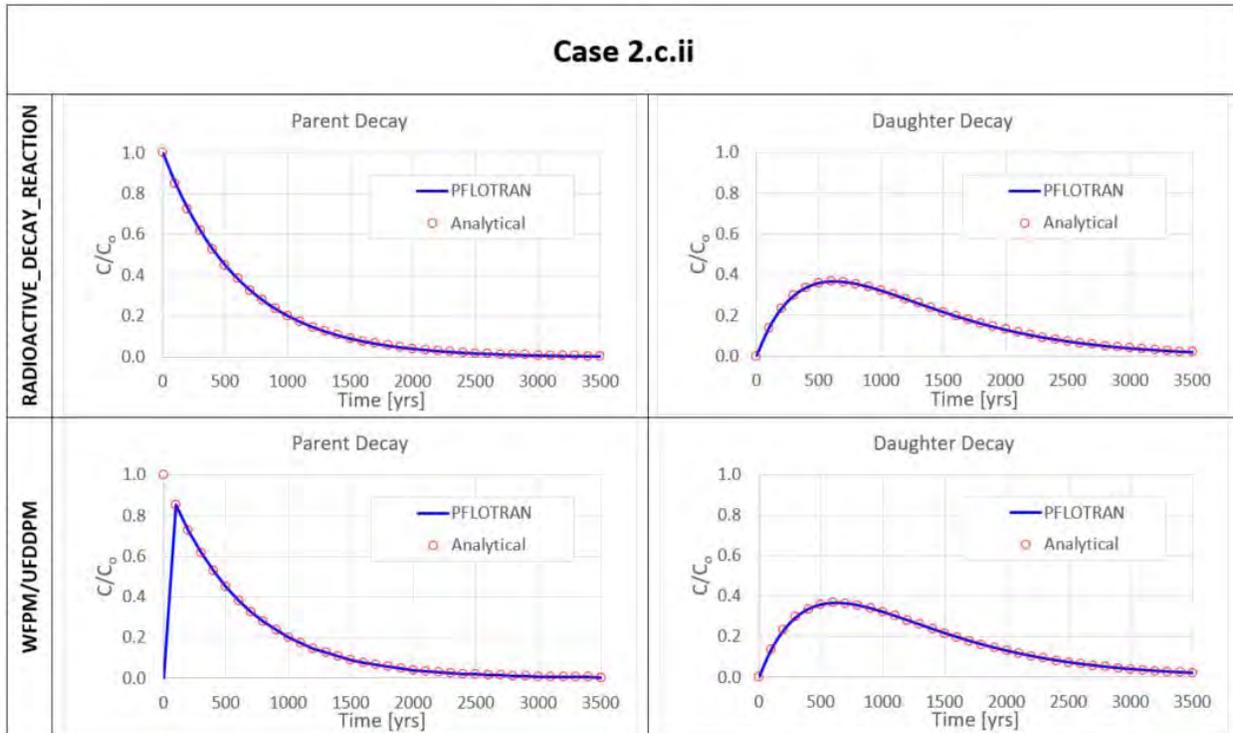
Figure 3-14 Case 2.c.i (Parent-Daughter radionuclide decay and ingrowth with no initial daughter mass where the half-life of the parent = the half-life of the daughter)
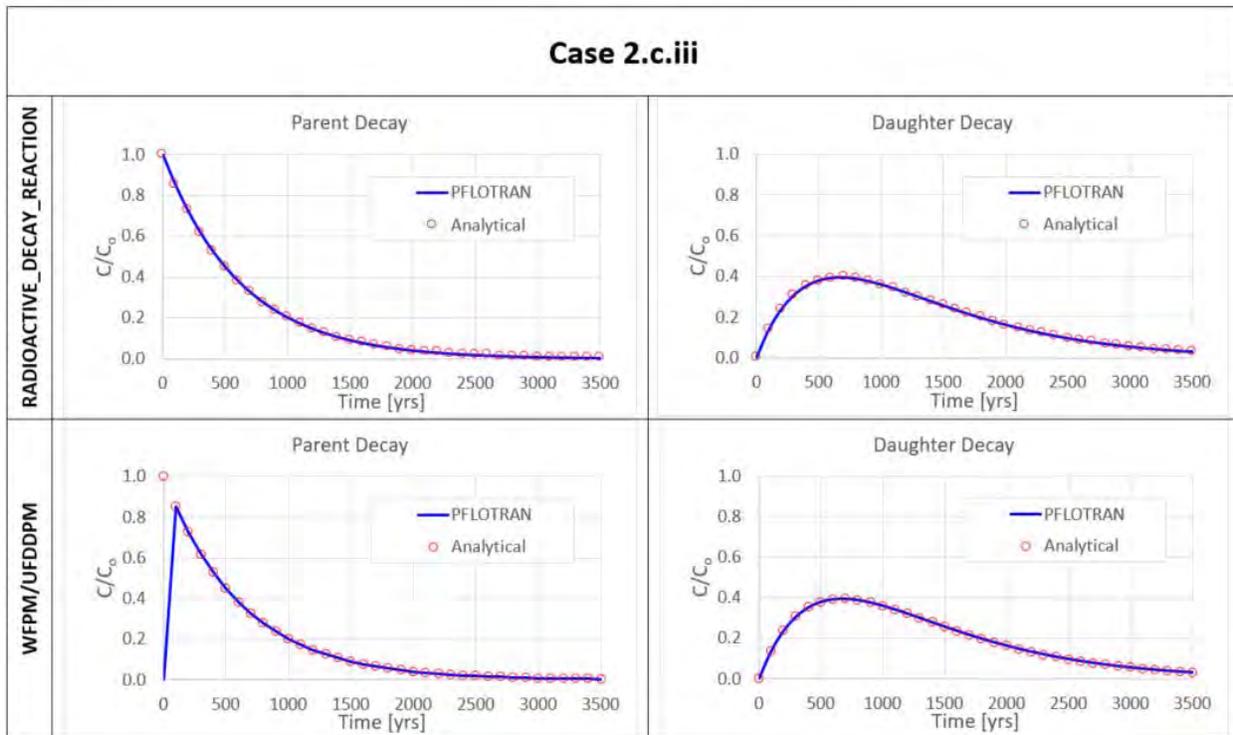
Figure 3-15 Case 2.c.iii (Parent-Daughter radionuclide decay and ingrowth with no initial daughter mass where the half-life of the parent > the half-life of the daughter)
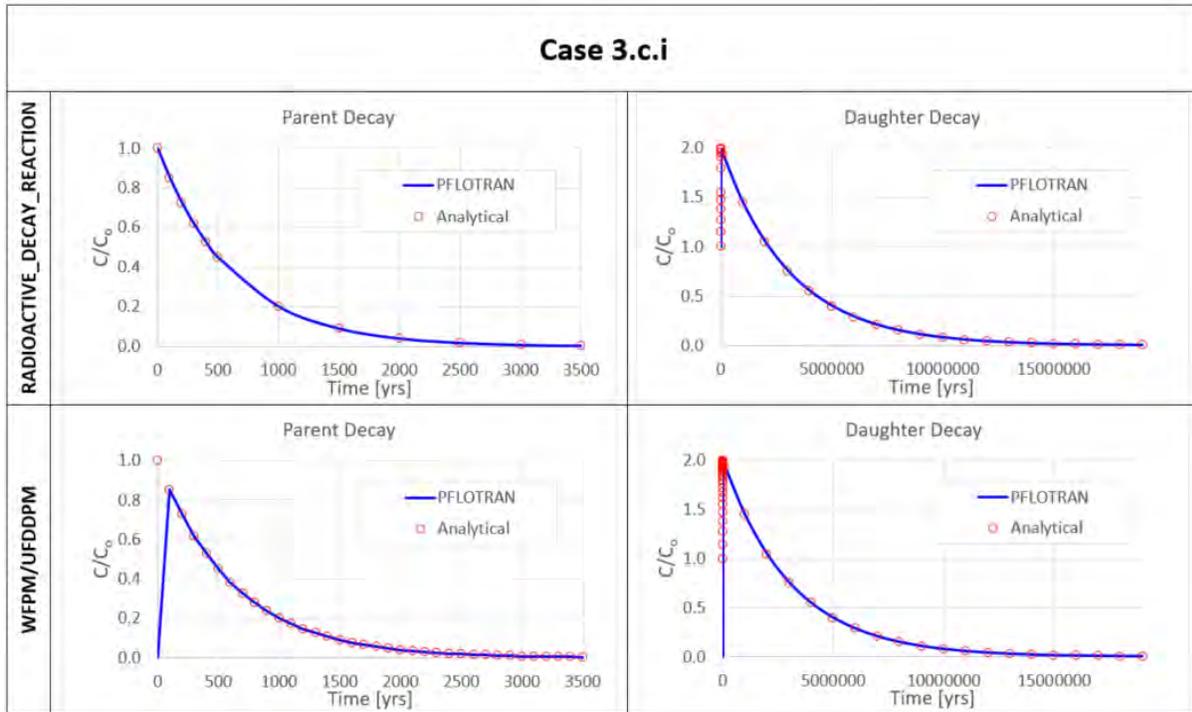
Figure 3-16 Case 3.c.i (Parent-Daughter radionuclide decay and ingrowth with non-zero initial daughter mass where the half-life of the parent << the half-life of the daughter)
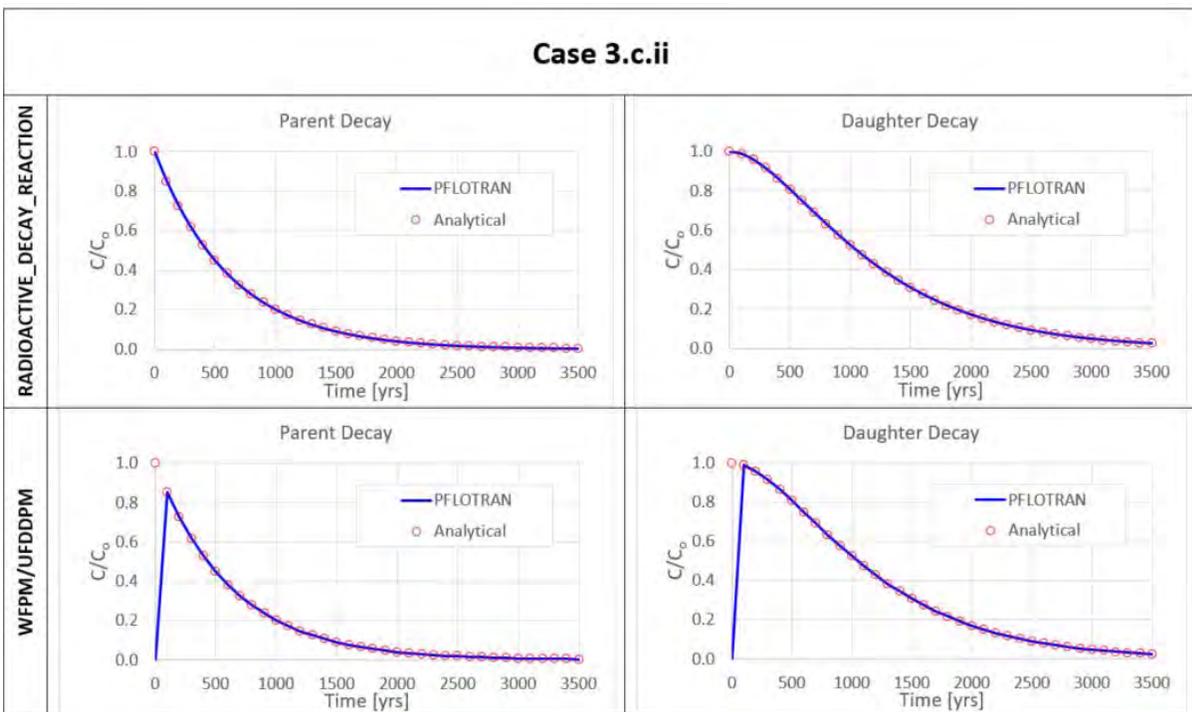
Figure 3-17 Case 3.c.ii (Parent-Daughter radionuclide decay and ingrowth with non-zero initial daughter mass where the half-life of the parent = the half-life of the daughter)
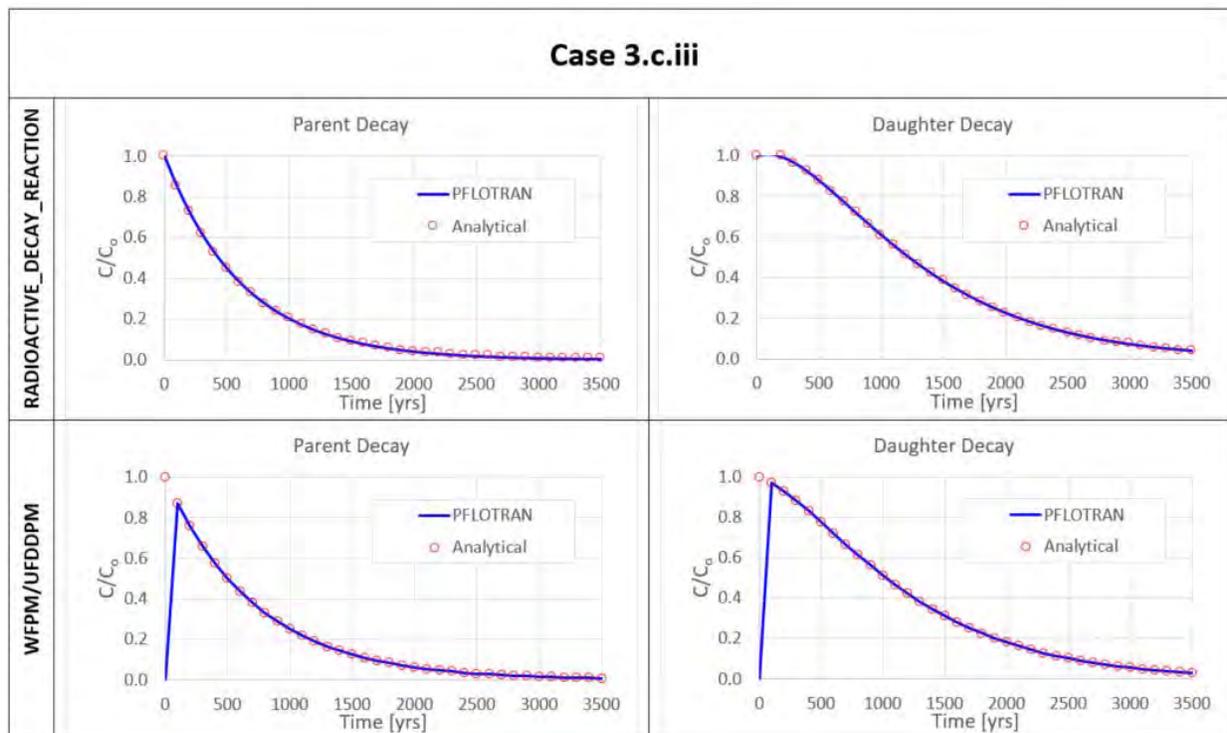
Figure 3-18 Case 3.c.iii (Parent-Daughter radionuclide decay and ingrowth with non-zero initial daughter mass where the half-life of the parent > the half-life of the daughter)

More QA tests for radionuclide decay and ingrowth will be added next FY that include testing the Newton's method of solution in addition to the 3-generation analytical solution when using the WFPM/UFDDPM approach. When using the Newton's method of solution, it is possible for significant time truncation error to plague the solution if timesteps are not chosen correctly to minimize this error. Initial analysis into quantifying this error has begun, and will be completed next FY.

3.2.5.3   Automatic Spatial Convergence Testing

Simulators, such as PFLOTRAN, solve a set of partial differential equations with initial and boundary conditions, by discretizing the mathematical equations so that they can be solved on a grid using any number of numerical methods. Because the equations are discretized, numerical error exists. The source of this error can be illustrated through the limited example of how one discretizes a simple spatial derivative. Mathematically, the true derivative is defined as,

$$\frac{df}{dj} = \lim_{\Delta j \to 0} \frac{f(j + \Delta j) - f(j)}{\Delta j}$$

Eq. 10

Numerically, the spatial derivative can be discretized in one of many possible ways, using a forward difference, backwards difference, or central difference. For example, a forward difference would be defined as,

$$f_j' = \frac{f_{j+1} - f_j}{\Delta}$$

Eq. 11

where Δ represents the grid spacing in dimension j, and f is the value of the function at point j, or $j+1$. The error associated by discretizing the derivative using a forward difference can be calculated by defining a Taylor expansion, or sum of Taylor expansions, that includes the points on the grid that appear in the discretized equation (the forward difference) for the derivative. The Taylor expansion looks like,

$$f_{j+1} = f_j + \Delta f_j' + \frac{\Delta^2}{2!} f_j'' + \frac{\Delta^3}{3!} f_j''' + \cdots \qquad \text{Eq. 12}$$

and can be rearranged to solve for the derivative as,

$$f_j' = \frac{f_{j+1} - f_j}{\Delta} - \frac{\Delta}{2!} f_j'' - \frac{\Delta}{3!} f_j''' + \cdots \qquad \text{Eq. 13}$$

The leading term in the rearranged series is the numerical forward difference, while the rest of the terms represent error terms. They are called error terms because they are addition terms that are added to the derivative which cannot be eliminated, only reduced. Because the leading term of the error terms is of order Δ, the forward difference is 1st order accurate. This means that if you increase your grid resolution by a factor of two, you can at most reduce your numerical error by a factor of two. The backward difference is also 1st order accurate; it uses points at j and $j-1$ rather than j and $j+1$. Higher order schemes can be constructed by using more points on the grid (called a stencil) to define the discretized derivative, and include the central difference as the simplest example (which uses points at j, $j-1$, and $j+1$). The central difference is second order accurate, because the leading error term is of order Δ^2, allowing the error to be reduced by a factor of four if the grid resolution is increased by a factor of two. While higher order schemes may seem the obvious way to go to reduce numerical error, they are more difficult to handle near boundaries, since stencils are often large, and require more values to be stored in memory. They may also be numerically more difficult to solve.

The automatic spatial converge process newly built into the QA Test Suite verifies the order of the algorithm used to solve the governing equations in PFLOTRAN. It works by running each test in the QA multiple times. Each time a test is run, the maximum relative error between the PFLOTRAN solution and the analytical solution is stored, before increasing the grid resolution by a factor of two for the next test run of the same test. This process is repeated at least two times, so that a graph can be constructed which shows how the relative error decreases as grid resolution was increased. When plotted on a log-log scale, the slope of the resulting line indicates the order of the algorithm. In other words, if the slope is 1, then the algorithm is 1st order accurate. If the slope is 2, then the algorithm is 2nd order accurate.

In practice, the discretized equation at the boundaries becomes less accurate than in the interior of the domain because the stencil size must be reduced at the boundaries in most cases. For example, a forward or backward difference is often used for derivatives at the boundaries while a central difference can be used for grid cells in the interior of the domain. This often leads to the order of accuracy being reduced near the boundaries. This effect is seen in the following figures, which show the results for automatic spatial convergence for 1D transient flow simulations. The largest relative error in the domain is chosen when calculating the slope of error vs. grid spacing on the log-log plot, which most likely occurs near the boundaries. While a central difference algorithm is used for the derivatives (which is 2nd order accurate), the algorithm at the boundaries is only 1st order accurate. Therefore, the worst effective order of the algorithm is actually near 1.5, as seen by the slope in Figure 3-19, Figure 3-20, and Figure 3-21.
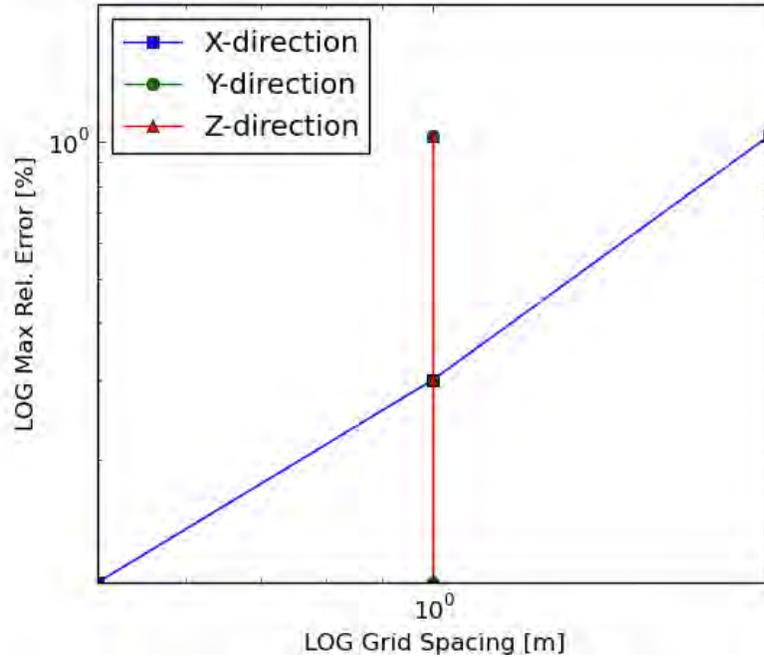
Figure 3-19 A minimum spatial convergence rate of 1.62 is observed for RICHARDS MODE simulating 1D transient flow with a Dirichlet boundary condition
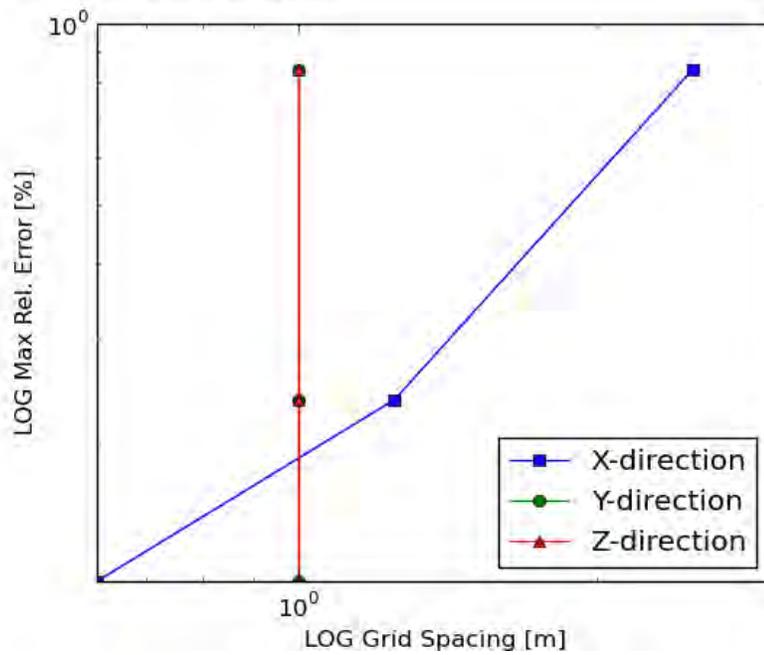
Figure 3-20 A minimum spatial convergence rate of 1.41 is observed for TH MODE simulating 1D transient flow with a Neumann boundary condition
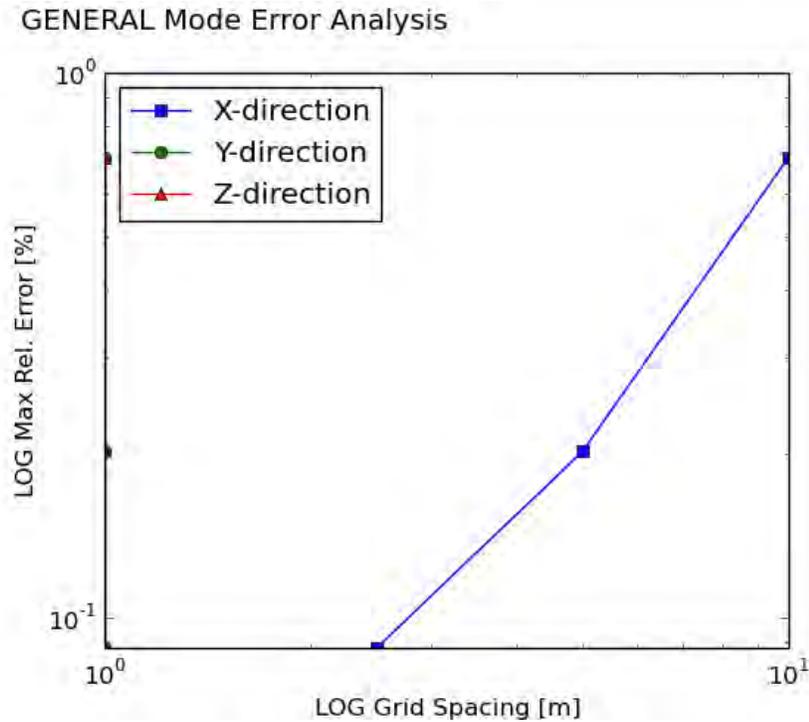
Figure 3-21 A minimum spatial convergence rate of 1.49 is observed for GENERAL MODE simulating 1D transient flow with a Dirichlet and Neumann boundary condition

3.3   Establishing *GDSA Framework*

A primary objective of the GDSA work package is to develop a disposal system modeling and analysis capability to evaluate repository performance for a range of disposal options. This capability, *GDSA Framework*, must be well-tested and accepted by peers. To this end, in addition to the verification testing discussed in Section 3.2.5, a significant effort is made each year to involve scientists and engineers outside the SFWST Campaign. This is done by publishing related work, giving presentations at international conferences, offering short courses, and promoting wider use and development of *GDSA Framework*.

The development of *GDSA Framework* benefits greatly from use in the broader scientific community. Users provide valuable feedback for developers and can contribute directly to code development by improving parts of the code or coupling new process models. Collaboration with outside users is made possible by online version control systems (e.g., Bitbucket.org) and open source access. By encouraging and facilitating use in the outside community, we expect to accelerate code development and enhance code acceptance.

The following subsections discuss several outreach efforts this year intended to facilitate the development of *GDSA Framework* and to establish *GDSA Framework* as a sound, leading-edge, and accessible repository safety assessment tool.

3.3.1   Collaborative Websites

The website pa.sandia.gov, officially launched in the fall of 2016, was developed to showcase *GDSA Framework* capability. At this website, viewers may peruse demonstrative examples of the GDSA capability found in presentations and reports generated over the past several years. The website provides

links to software employed within GDSA (i.e. Cubit, Dakota and PFLOTRAN) and cites collaborating organizations and laboratories external to the Sandia lead organization (i.e. ANL, LANL, pflotran.org, PNNL) that have contributed to the development of *GDSA Framework*.

Figure 3-22 shows the distribution of hits by city on pa.sandia.gov over the last year, measured by Google Analytics. Previously, the largest number of hits came from Albuquerque, likely due to website developers and the addition of content last year. This year the distribution of hits is more spread out across the country. Internationally, there is noticeable new activity in China, Japan, South Korea, and Taiwan.
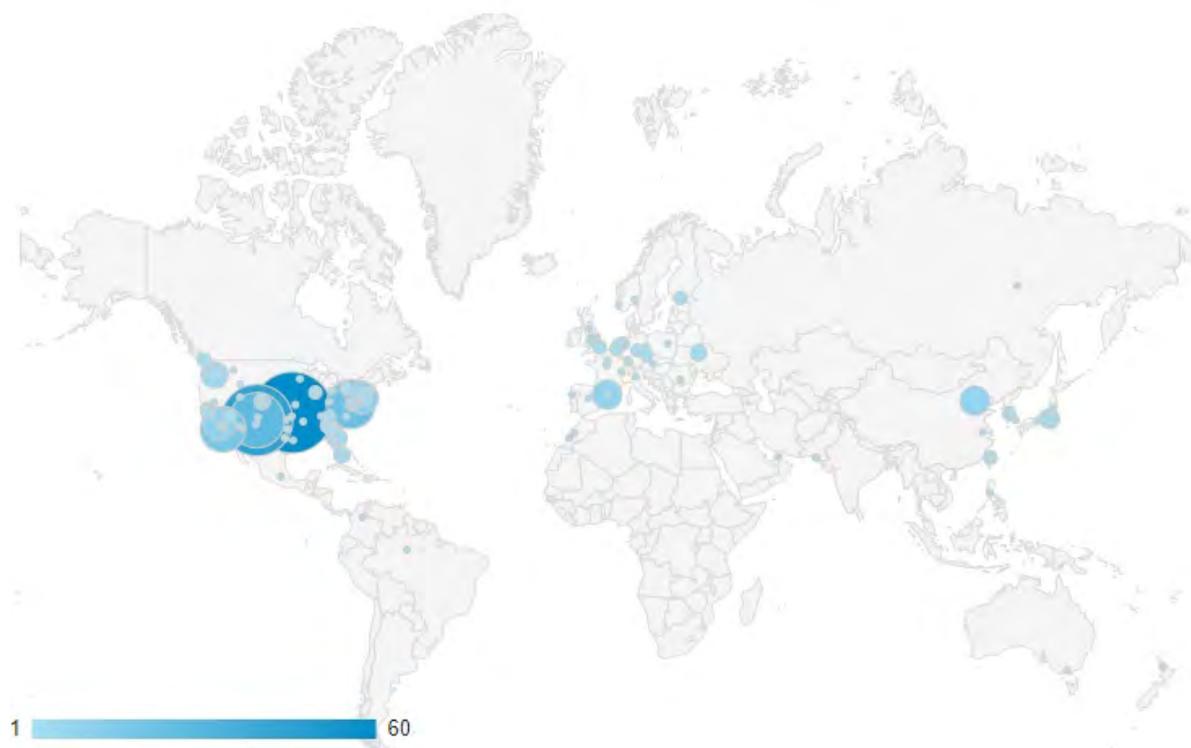
Figure 3-22 Hits on pa.sandia.gov over the past year

3.3.2   Publications

Table 3-5 lists presentations and publications featuring *GDSA Framework* delivered in FY 2018. They include presentations at public conferences (Waste Management 2018 and 2017 American Geophysical Union Fall Meeting) and closed meetings (NEA Crystalline Club and the Nuclear Waste Management Organization (NUMO) of Japan).

Table 3-5   FY 2018 Publications and Presentations Featuring *GDSA Framework*

Title	Source	Citation
US DOE Work in Nuclear Waste Disposal: Status and Crystalline Rock R&D	NEA Crystalline Club Meeting, Prague	Mariner (2017)
Performance Assessments of Generic Nuclear Waste Repositories in Shale	American Geophysical Union Fall Meeting 2017	Stein et al. (2017)
Maintaining Quality and Confidence in Open-Source, Evolving Software: Lessons learned with PFLOTRAN	American Geophysical Union Fall Meeting 2017	Frederick and Hammond (2017)
Simulating the Effect of Fracture Connectivity on Repository Performance with *GDSA Framework*	Waste Management 2018	Sevougian et al. (2018)
Performance Assessment of a Generic Nuclear Waste Repository in Shale	Waste Management 2018	Stein et al. (2018)
PFLOTRAN and Geologic Disposal Safety Assessment	Meeting at NUMO, Tokyo, Japan	Mariner and Hammond (2018)

3.3.3   Short Courses

The GDSA group attempts to conduct regular hands-on short courses as community outreach. During these short courses, the GDSA development team teaches the underlying theory behind process models implemented within PFLOTRAN, including GDSA capabilities, and the execution of PFLOTRAN on numerous computing platforms including supercomputers. The attendees install a Linux virtual machine preconfigured with PFLOTRAN and supporting software (e.g. python, Matplotlib, ParaView) onto their laptop and execute select demonstration problems, plotting the results as a post processing step. The demonstration problems become progressively more complex, incorporating larger numbers of processes on larger and more complicated domains. Attendees are also given the opportunity to pose their own problem scenarios, and the approach to implementation within PFLOTRAN is discussed. For the longer, three-day short courses, a challenge problem that is representative of the basic processes required to simulate geologic disposal of nuclear waste is posed. Attendees work in teams to designed and implemented the conceptual model within PFLOTRAN and compare results at the end of the day.

The GDSA group conducted two short courses in FY 2018. The first short course was conducted at Sandia National Laboratories on the first day of the Interagency Steering Committee on Performance and Risk Assessment Community of Practice (P&RA CoP) Annual Technical Meeting held on October 17-19, 2017. This one-day short course was a compact version of short courses held in the past.

3.3.3.1   *P&RA CoP short course*

There were approximately 14 attendees at the P&RA CoP short course. Attendees were from research and consulting institutions including DOE Office of Legacy Management, Drummond Carpenter, INTERA, Neptune and Company, New Mexico Tech, Sandia National Laboratories, Savannah River National Laboratory, and the University of California, Berkeley,

The P&RA CoP short course agenda follows:

PFLOTRAN short course schedule (one day)

Tuesday Oct. 17

8:30-12:00 Morning Session

- Setup
  - Transfer of Virtual Box to ALL machines

        o Unzipping the Virtual Box file on ALL machines
        o Installing the Virtual Box software on ALL machines
- Presentation (Intro/Overview) with questions

10:15 - 10:30 Break

- Discussion of input deck, boundary conditions, etc.
- Linux primer
- Demo: 1D Calcite
- Presentation (open source development)

12:00-1:30 Lunch

1:30 - 5:00 Afternoon Session

- Demo: Regional Doublet (incl. SOURCE_SINK, OUTPUT block)
- Paraview (opening files, basic plotting)

2:30 - 2:45 Break

- Presentation (process model coupling)
- GDSA example problem - 2D
- Presentations (support infrastructure, testing, or SIAM talk)
- QA test presentation and documentation.pflotran.org
- Open Discussion

Figure 3-23 Group photo of P&RA CoP short course attendees

3.3.3.2   Taiwan Short Course

The second short course was conducted at the headquarters of the Taiwan Power Company in Taipei, Taiwan on April 18-20, 2018. This short course had 40 attendees from numerous institutions in Taiwan including TaiPower, ITRI (Industrial Technology Research Institute), INER (Institute for Nuclear Energy Research), NCU (National Central University), CCU (National Chung Cheng University) and Sinotech Consultants. Researchers in Taiwan are primarily concerned with simulating a potential repository in a crystalline rock setting, and thus, there was much discussion regarding the balance of continuum and discrete fracture approaches to simulating flow and transport in crystalline formations.

The Taiwan short course agenda follows:

PFLOTRAN Short Course Schedule

Wednesday

9:00-11:45 Morning Session

- Setup
    - Transfer of Virtual Box to ALL machines
    - Unzipping the Virtual Box file on ALL machines
    - Installing the Virtual Box software on ALL machines
    - PFLOTRAN Primer
- Presentation (Intro/Overview) with questions

11:45-12:50 Lunch

12:50-5:00 Afternoon Session

- Presentation: Very high level input deck overview
- Demo: 1D Variably Saturated Flow
- Discussion of boundary conditions

2:30 - 2:45 Break

- Demo: 1D Calcite
- Paraview (opening files, basic plotting)
- Presentations (support infrastructure, testing)
- Demo: Copper Leaching
- Open Discussion

Thursday

9:00-11:45 Morning Session

- QA test presentation and documentation.pflotran.org
- Review: Input deck components
- Demo: Regional Doublet (incl. SOURCE_SINK, OUTPUT block)
- Paraview (more advanced 3D capability)
- Demo: Error messaging (including practice)

11:45-12:50 Lunch

12:50-5:00 Afternoon Session

- Presentation (Process Model Coupling) + Salinity
- Open source development presentation
- Presentation on advanced initial and boundary conditions
    - Presentation on Using a Gridded Dataset for a BC

2:30 - 2:45 Break

- Presentation: Multiphase flow equations
- Demo: Multiphase flow gas injection
- Demo: Multiphase repository re-saturation (implicit unstructured grid)

Friday

9:00-11:45 Morning Session

- Presentation: *GDSA Framework*
- GDSA example problem - 2D
- Intro to Challenge Problem
- Challenge Problem
    - Working individually or in small groups on the problem

11:45-12:50 Lunch

12:50-5:00 Afternoon Session

- Challenge Problem
    - Working individually or in small groups on the problem (continued)
    - Wrap up and problem solution presentation
- Closing Discussions
- Feedback

Figure 3-24 Group photo of Taiwan short course attendees

4. UNCERTAINTY QUANTIFICATION AND SENSITIVITY ANALYSIS

Sensitivity analysis (SA) is useful in modeling studies for a variety of purposes. Saltelli et al. (2008) (Section 4.1) identify four primary uses:

1. Factor prioritization: SA can be used to identify the model inputs (factors) in which a reduction of uncertainty would most reduce the uncertainty in the model output, and thus to prioritize research.

2. Factor Fixing: SA can be used to identify model inputs that could be fixed or simplified without affecting model output, and thus to create a parsimonious, less computationally expensive, and possibly more defensible model.

3. Variance Cutting: SA can be used to reduce the variance (a measure of uncertainty) in simulation output to below a specified tolerance by identifying the smallest possible set of factors to fix.

4. Factor Mapping: SA can be used to identify regions of the input parameter space that lead to extreme or interesting results.

Previous milestones related to *GDSA Framework* and the generic clay, salt, and crystalline reference cases have relied upon scatter plots and a single quantitative measure of sensitivity – simple rank (Spearman) correlation coefficients (e.g., Mariner et al. 2015; Mariner et al. 2016; Sevougian et al. 2016; Mariner et al. 2017), a measure that works well for factor prioritization when model behavior is monotonic and additive, but is otherwise limited.

In FY 2018 initial steps were taken to ensure that *GDSA Framework* has a comprehensive sensitivity analysis capability that has the potential to benefit repository performance assessment (PA) and the R&D activities that feed it in a variety of ways. This report addresses both traditional repository PA methods (stepwise linear regression, simple and partial correlation coefficients) and more computationally expensive variance-based methods recently made feasible by advances in theory and in computer hardware and software. The former work well when the system can be approximated with a linear (or monotonic), additive model, but may fail to adequately capture nonlinearities and parameter interactions. The latter can be applied to highly coupled nonlinear models to capture nonlinear (nonmonotonic) dependencies and parameter interactions.

For this report, we expanded the sensitivity analysis of the 2017 GDSA clay 12-PWR reference case, increasing the number of realizations from 50 to 200, and applying a variety of sensitivity analysis methods. These include scatter plots, simple and partial correlation coefficients (and rank transformed equivalents), stepwise linear regression (Section 3.2.1), and main and total sensitivity indices calculated via polynomial chaos expansion and Gaussian process metamodels. As in previous years, the output variable of interest is maximum ^{129}I concentration (independent of time) at predetermined locations in the model domain (observation points), and epistemic uncertain inputs include properties of the engineered and natural systems.

The application of various SA methods to the case study in this report represents a step toward developing a comprehensive sensitivity analysis capability in *GDSA Framework* and demonstrating that capability on varied reference cases with different characteristics and behaviors. The current and future work will establish a robust infrastructure of tools for performing sensitivity analyses, create understanding of which methods are useful for which problems and which purposes, and ensure that the methods in *GDSA Framework* are applicable to a wide range of potential repository problems.

4.1   Theory

4.1.1   Correlation Coefficients and Standardized Regression Coefficients

Correlation coefficients and standardized regression coefficients (obtained by stepwise linear regression) are model-dependent measures of sensitivity that assume linear correlation between one (in the case of correlation coefficients) or more (in the case of stepwise linear regression) input variables and the output variable of interest. These measures will fail to identify inputs that influence the output in a nonlinear way. and cannot be used to identify parameter interactions (multiplicative models) (Saltelli et al. 2008, Section 1.2.5). Additionally, both methods assume that uncertain inputs are uncorrelated with each other.

4.1.1.1   Simple Correlation Coefficient

A simple (or Pearson) correlation coefficient (SCC) is a measure of the linear correlation between two variables (x and y) and is defined as the covariance of the two divided by the product of their standard deviations

$$SCC = \frac{\sum_{k=1}^{m}(x_k - \bar{x})(y_k - \bar{y})}{\sqrt{\sum_{k=1}^{m}(x_k - \bar{x})^2}\sqrt{\sum_{k=1}^{m}(y_k - \bar{y})^2}} \qquad \text{Eq. 14}$$

where m is the number of observations, $\bar{x}$ and $\bar{y}$ are the mean values of x and y, and x_k and y_k denote individual values (samples) of the two variables. The simple correlation coefficient is equivalent to the standardized regression coefficient (Section 3.2.1) that results from linear regression of y on x (Helton and Davis 2000).

4.1.1.2   Partial Correlation Coefficient

A partial correlation coefficient (PCC) is a measure of the linear relationship between two variables (x and y) after the effects of other variables have been removed. It is defined as the correlation between the residuals resulting from the linear regression of x_j with $x_{\sim j}$ and y with $x_{\sim j}$, respectively, where the notation $x_{\sim j}$ means all x except x_j. For our case, in which x_j is one of n input variables, y is the output variable of interest, and b and c represent real number coefficients, the regression equations are

$$\hat{x}_j = c_0 + \sum_{p=1, p \neq j}^{n} c_p x_p \qquad \text{Eq. 15}$$

$$\hat{y} = b_0 + \sum_{p=1, p \neq j}^{n} b_p x_p \qquad \text{Eq. 16}$$

The correlation is calculated as above (for SCC), substituting $\varepsilon_x = x_j - \hat{x}_j$ and $\varepsilon_y = y - \hat{y}$ for x and y, respectively (Helton and Davis 2000).

4.1.1.3   Stepwise Linear Regression

Stepwise linear regression (explained more fully in Section 3.2.1) results in standardized regression coefficients (SRCs), the absolute magnitudes of which provide an indication of variable importance. Stepwise linear regression is, like the sensitivity indices described below, a method of variance decomposition, i.e., the fraction of variance in the output variable due to each input variable can be determined. When the input variables are uncorrelated, the difference between R^2 at the current step and

the previous step of the regression is the fraction of the variance in the output accounted for by the latest addition to the regression model (Helton and Davis 2000).

4.1.1.4   Rank Transformation

Rank transformation improves regression and correlation analyses when the relationship between variables is nonlinear but monotonic or when there are differences in scale between variables (Helton and Davis 2000). In rank transformation, the raw values of x and y are replaced with rank values. The smallest value of each variable is assigned a rank of 1, the next largest value is assigned a rank of 2, etc. up to the largest value. If equal values of the variable occur, they are assigned an average rank. This method lessens the effect of outliers and differences in scale. Simple correlation coefficients, partial correlation coefficients, and standardized regression coefficients resulting from stepwise linear regression can all be calculated substituting rank transformed values for the raw values of x and y. Correlations and coefficients calculated using this approach are interpreted as describing the relationships between ranks of variables rather than values of variables.

The analysis of the clay reference case in this report includes calculation of simple and partial rank correlation coefficients. Stepwise regression was not performed on rank transformed data.

4.1.2   Variance Decomposition with Sensitivity Indices

Like SRCs, sensitivity indices are a measure of the fraction of the variance in the output due to the variance in particular inputs. As with correlation coefficients and SRCs, the calculation depends on the assumption of uncorrelated input variables. Unlike correlation coefficients and SRCs, sensitivity indices do not depend on the assumption of any particular model (they are model-independent), and can be used to identify nonlinear influences and parameter interactions. Sensitivity indices measuring the first-order (main), higher-order, and total effects of input variables are calculated from conditional variances, variances conditional on fixed inputs.

4.1.2.1   First-order Sensitivity Index

A first-order (main) sensitivity index (S) is a number between 0 and 1 that measures the fraction of the variance in the output variable (y) due to a single input variable (x_j) without including possible parameter interactions

$$S_j = \frac{V_{x_j}\left(E_{x_{\sim j}}\left(y|x_j = x_j^*\right)\right)}{V(y)}$$

Eq. 17

In this equation, the numerator is the conditional variance of the mean (the expectation E) of y given $x_j = x_j^*$ over the range of possible points x_j^*. The notation $x_{\sim j}$ indicates that each value of the mean is calculated by varying the values of all x except x_j. The denominator is the variance of y (Saltelli et al. 2008 Section 1.2.6). A large value of S_j indicates an important variable. A small value of S_j does not necessarily indicate an unimportant variable, because a variable can have a small first-order effect, but interact with another input variable to create an important higher-order effect.

4.1.2.2   Higher-order Sensitivity Index

A higher-order sensitivity index (S_{ij}, for instance) is a measure of the effect of the interactions between two or more input variables on the variance in the output variable (y). For two input variables (x_i and x_j)

$$S_{ij} = \frac{V_{x_i,x_j}\left(E_{x_{\sim i}x_{\sim j}}(y|x_i,x_j)\right)}{V(y)} - S_i - S_j \qquad \text{Eq. 18}$$

In the first term on the righthand side, the numerator is the conditional variance of the mean of y given fixed values of both x_i and x_j (Saltelli et al. 2008, Section 1.2.11.). For a modeling study (in which no random error occurs), the sum of all possible first-order and higher-order sensitivity indices equals 1, and taken together these terms explain 100% of the variance in y. (The case study presented in Section 3.2.1 does not include analysis of higher-order sensitivity indices.)

4.1.2.3   Total Sensitivity Index

A total sensitivity index (S_T) is a measure of the total effect (alone and through interactions with other variables) of an input variable on the variance in the output variable y. It is the sum of the first-order and all higher-order sensitivity indices that include that input variable. For example, for a generic model with three sampled inputs

$$S_{T_1} = S_1 + S_{12} + S_{13} + S_{123}$$
$$S_{T_2} = S_2 + S_{12} + S_{23} + S_{123}$$
$$S_{T_3} = S_3 + S_{13} + S_{23} + S_{123}$$

<div align="right">Eq. 19</div>

The total sensitivity index is equal to

$$S_{Tj} = 1 - \frac{V_{x_{\sim j}}\left(E_{x_j}(y|x_{\sim j})\right)}{V(y)} \qquad \text{Eq. 20}$$

In the second term on the righthand side, the numerator is the conditional variance of the mean of y given fixed values of all input variables except x_j, in which each value of the mean is calculated by varying the value of x_j (Saltelli et al. 2008, Section 1.2.12). Each S_{Tj} is a number between 0 and 1, and the sum $\sum S_{Tj}$ will be greater than or equal to 1, because each higher-order effects term (e.g., S_{12}, S_{123}, etc.) appears in more than one total sensitivity index. The sum is equal to one only if all of the higher-order effects are zero, as is the case in an additive model. A non-influential input variable will have a total sensitivity index equal to zero. Finding that $S_{Tj} \approx 0$ indicates that the value of the input variable could be fixed (thus simplifying the statistical analysis) without affecting the variance in the output variable.

4.1.3   Calculating Sensitivity Indices

Calculating sensitivity indices is computationally expensive. They can be calculated exactly from the equations above, in which case the number of simulations required will be m^d, where d is the number of sampled inputs and m is the number of times each input is sampled (Weirs et al. 2012). For the clay reference case with 10 inputs sampled 50 times, the resulting number of simulations is prohibitive (50^{10}), as it will be for any computationally demanding model with even a very few sampled inputs.

Main and total sensitivity indices can instead be estimated using two sample matrices, each of dimension $m \times d$, by swapping columns of one into the other (Saltelli et al. 2010). This method requires $m(d + 2)$ model evaluations, and is the method implemented in Dakota (Weirs et al. 2012; Adams et al. 2018). For a computationally demanding model, the number of evaluations required may still be prohibitive. For the

clay reference case with a sample size of 50 this method requires $50(10 + 2) = 600$ evaluations. With a sample size of 200, 2400 evaluations are required.

Due to the large number of simulations required, surrogate models (also known as meta-models or response surfaces) are often employed to calculate sensitivity indices. Two approaches are possible. In either case, some number of realizations must be run with the original simulation code in order to derive a surrogate model describing the response of the output variable of interest to the sampled input variables. In the first approach, the surrogate model is then evaluated at least $m(d + 2)$ times to estimate the main and total sensitivity indices. In the second approach, a surrogate model is chosen from which sensitivity indices can be analytically calculated, eliminating the need for multiple evaluations of the surrogate. For the clay reference case, we demonstrate the first approach using Gaussian process surrogate models, and the second approach using polynomial chaos expansion. (Use of a surrogate model introduces model-dependence into the calculation of sensitivity indices.)

4.1.3.1   *Gaussian process surrogate model*

The use of Gaussian processes for interpolation is a technique (also known as Kriging) first developed for predicting the distribution of spatially heterogeneous properties in the geosciences. A Gaussian process surrogate model predicts the most likely value of the response (output variable y) at points on the response surface assuming that possible values for y at any point are part of a normal (Gaussian) distribution, and that the variance of that distribution is smaller close to the training points (zero at the training points) and larger further away. This is accomplished using a trend function and a correction to the trend function that accounts for the covariance of error (as a function of distance) between points on the surface (Figure 4-1). As implemented in Dakota and used on the clay reference case, the trend function is a quadratic polynomial fit to the data (training points) using least squares regression, and the covariance function is parameterized using the squared exponential function (Adams et al. 2018).
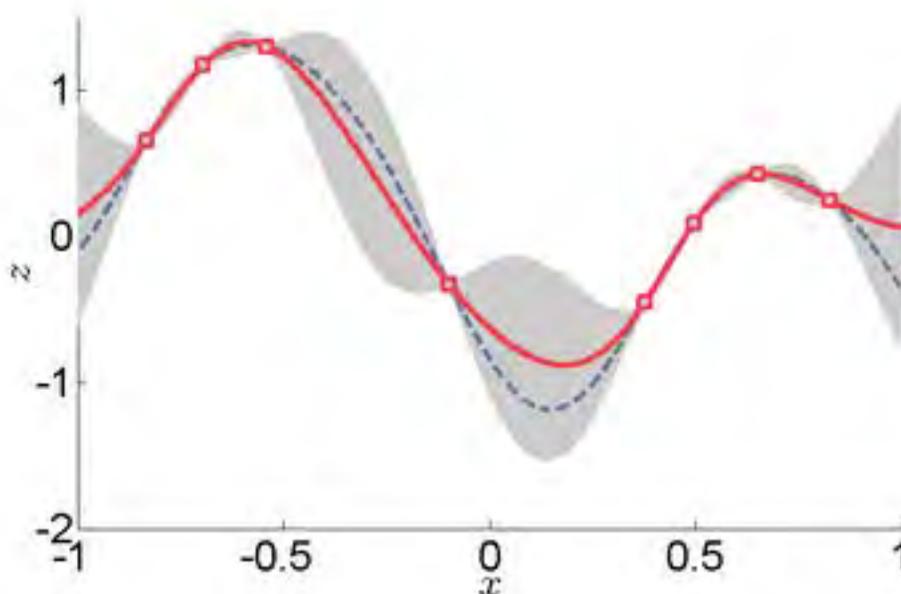
Figure 4-1   One-dimensional interpolation by Kriging, showing the data (red squares), the interpolatation (red line), confidence intervals (grey). A polynomial fit to the data is shown for comparison (dashed blue line); it does not pass through the center of the confidence intervals. (https://en.wikipedia.org/wiki/Kriging)

4.1.3.2   *Polynomial Chaos Expansion*

Polynomial chaos expansion (PCE) approximates values of the output variable y using a series expansion comprised of orthogonal polynomials from which sensitivity indices (main, total, and higher-order effects) can be obtained as analytic functions of the coefficients. The coefficients can be fit to the data using either spectral projection or linear regression (Sudret 2008; Adams et al. 2018); the latter is used in this report.

The analyst chooses an order for the polynomial expansion (see for example Figure 4-2). The number of terms in the expansion (P) depends on the number of sampled inputs (d) and the order of the polynomial (p) (Adams et al. 2018; Sudret 2008)

$$P = \frac{(d+p)!}{d!\,p!}$$

Eq. 21

Sudret (2008) determined empirically that the optimal number of training points (samples) is $m = (d-1)P$, but that iterative construction of the PCE allows it to be calculated with smaller sample size (see also Adams et al. 2018, Section 3.7). The ability to construct the PCE from small samples and the ability to obtain sensitivity indices analytically are beneficial when dealing with computationally expensive models.
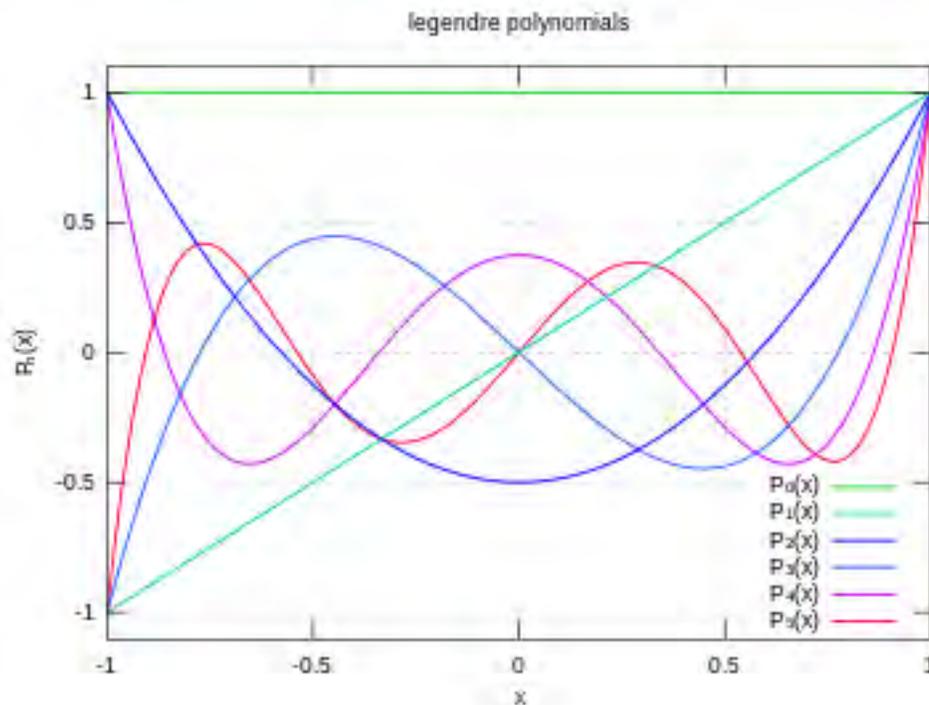
Figure 4-2   First six orders of Legendre polynomials, orthogonal polynomials that are used in polynomial chaos expansion when the distributions of the input variables are uniform, (https://en.wikipedia.org/wiki/Legendre_polynomials)

4.2   Sensitivity Analysis of the Clay Reference Case

Performance assessment simulations for the clay reference case (described in full by Mariner et al. (2017)) assume a mined repository in a thick unit of low-permeability shale. A thin limestone aquifer lies below the shale and a sandstone aquifer lies above the shale. A second sandstone aquifer lies at depth. A pressure gradient drives regional flow from west to east (left to right). Figure 4-3 shows a 2-dimensional

vertical cross section of the 3-dimensional model domain, in which the repository is visible as a series of drift faces toward the left side of the model domain. The model domain contains 6,925,936 cells.
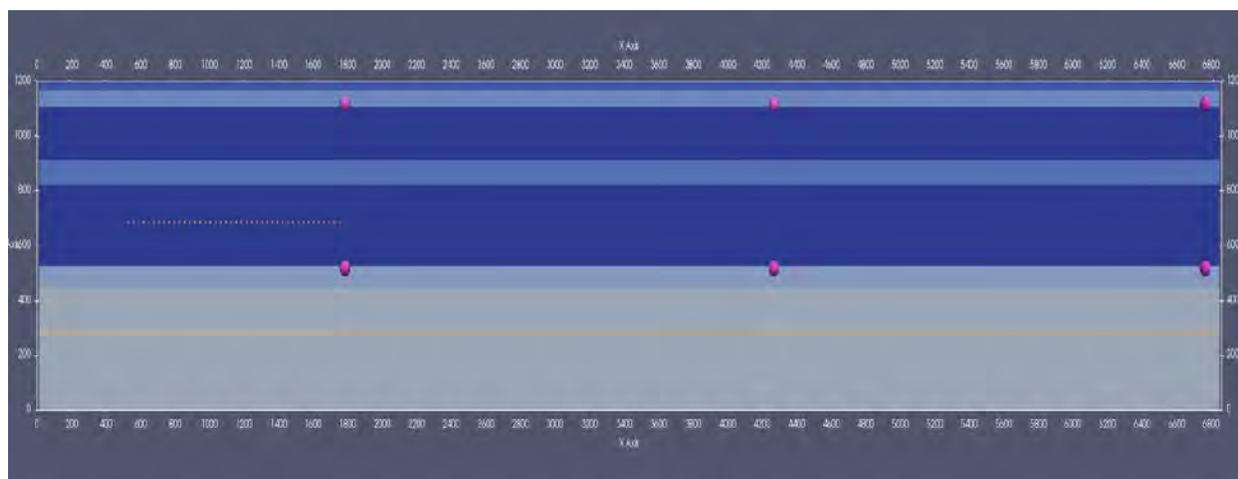
Figure 4-3   Locations of observation points in the 12-PWR model domain. From left in upper sandstone aquifer: "sand_obs1," "sand_obs2," and "sand_obs3." From left in limestone aquifer: "lime_obs1," "lime_obs2," and "lime_obs3." The deeper sandstone aquifer is the pale peach unit. A silty interval (medium blue) interrupts the shale (dark blue).

Simulations were run in a high-performance computing environment. Using 512 processes per simulation, each 1 million-year simulation took approximately three hours to complete. Processes accounted for in the simulations include waste package degradation, waste form dissolution, equilibrium-controlled radionuclide sorption and precipitation/dissolution, radioactive decay and ingrowth in all phases (aqueous, adsorbed, precipitate), coupled heat and fluid flow, and radionuclide transport via advection and diffusion. Simulations included 18 radionuclides.

Two replicates, one of 50 samples and one of 200 samples were created using Dakota's Latin Hypercube Sampling capability. Ten input parameters were sampled (Table 4-1), and concentration of ^{129}I was monitored at three locations in the limestone and three locations in the sandstone (Figure 4-3). The maximum ^{129}I concentrations (regardless of time) at each of these six observation points are the output variables for the sensitivity analysis. Dakota returns a table containing the values of all sampled input variables and all output variables (otherwise known as response functions) for every sample vector. This table becomes the input for SA methods available in Dakota and for calculation of SRCs using stepwise.py (Section 3.2.1).

Two of the sampled parameters are linear distribution coefficients (K_ds) for neptunium sorption. Discussion of neptunium concentration has been dropped from the current SA because concentrations at the observation points remain very close to background concentrations in all simulations. Correlation coefficients and sensitivity indices relating the K_ds to ^{129}I concentration provide a reference for the values returned when no correlation is expected.

Table 4-1   Sampled parameters and their distributions.

Parameter	Description	Range	Units	Distribution
rateSNF	SNF Dissolution Rate	$10^{-8} - 10^{-6}$	yr^{-1}	log uniform
rateWP	Mean Waste Package Degradation Rate	$10^{-5.5} - 10^{-4.5}$	yr^{-1}	log uniform
kSand	Upper Sandstone Permeability	$10^{-15} - 10^{-13}$	m^2	log uniform
kLime	Limestone Permeability	$10^{-17} - 10^{-14}$	m^2	log uniform
kLSand	Lower Sandstone Permeability	$10^{-14} - 10^{-12}$	m^2	log uniform
kBuffer	Buffer Permeability	$10^{-20} - 10^{-16}$	m^2	log uniform
kDRZ	DRZ Permeability	$10^{-18} - 10^{-16}$	m^2	log uniform
pShale	Host Rock (Shale) Porosity	$0.1 - 0.25$	-	uniform
bNpKd	Np K_d Buffer	$0.1 - 702$	m^{3}kg^{-1}	log uniform
sNpKd	Np K_d Shale	$0.047 - 20$	m^{3}kg^{-1}	log uniform

4.2.1   Scatter Plots

Scatter plots are a means of qualitatively assessing the influence of sampled inputs on model outputs. They contribute to an understanding of the behavior of the model and to interpretation of quantitative SA measures including correlation coefficients and sensitivity indices. Because they are likely to identify the most influential input variables, they can be useful in planning a more quantitative SA (Helton and Davis 2000), although circumstances may arise in which they fail to identify an influential parameter (Saltelli et al. 2008).

Scatter plots showing the relationships between maximum ^{129}I concentration at each of the six observation points and each of the 10 sampled input parameters are show in Figure 4-4 (50 samples) and Figure 4-5 (200 samples). In these and subsequent figures throughout this chapter Response Functions (response_fn) 1, 2, and 3 refer to maximum ^{129}I concentration at the observation points in the sandstone aquifer (sand_obs1, sand_obs2, and sand_obs3, respectively, in Figure 4-3), and Response Functions 4, 5, and 6 refer to maximum ^{129}I concentrations at the observation points in the limestone unit (lime_obs1, lime_obs2, and lime_obs3, respectively).

In both figures, a positive correlation between pShale (shale porosity) and Response Functions 1, 2, 3, and 4 is evident. From the scatter plots, a positive correlation between pShale and response functions 5 and 6 may also be inferred. Response Functions 2 and 3 are positively correlated with kSand (sandstone permeability), and Response Functions 5 and 6 are positively correlated with kLime (limestone permeability). The plots of Response Functions 2 and 3 versus kSand indicate that the permeability of the sandstone must exceed a threshold value before it can influence maximum ^{129}I concentration at down-gradient observation points in the sandstone aquifer. A similar conclusion can be drawn for the relationship between maximum ^{129}I and limestone permeability from the plots of Response Functions 5 and 6 versus kLime. By comparing, for instance, the plots of Response Function 3 versus pShale and kSand, the analyst may also infer that unless aquifer permeability is sufficiently high, shale porosity has no effect on maximum ^{129}I concentration at down-gradient locations, because ^{129}I does not reach these locations (it remains at background concentration throughout the simulation).

The nature of the relationships between sampled inputs and model outputs can be more confidently inferred from the scatter plots generated with 200 samples. For instance, from Figure 4-4 (50 samples), the analyst might infer a fairly strong monotonic relationship between Response Function 6 and pShale (given sufficiently high limestone permeability). However, in Figure 4-5 (200 realizations) more scatter is evident in this relationship.
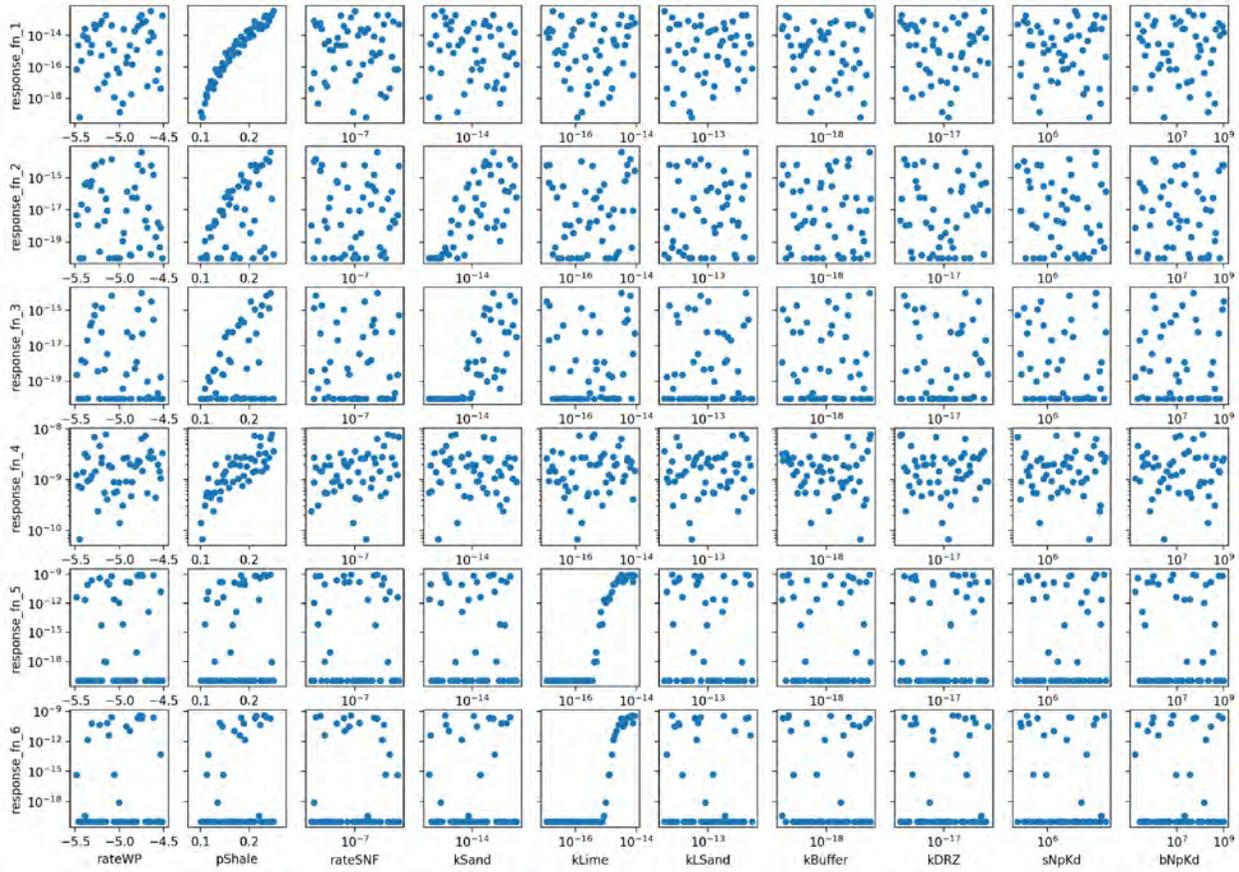
Figure 4-4   Maximum ^{129}I concentration (response functions 1 through 6) as a function of sampled inputs for replicate of 50 samples
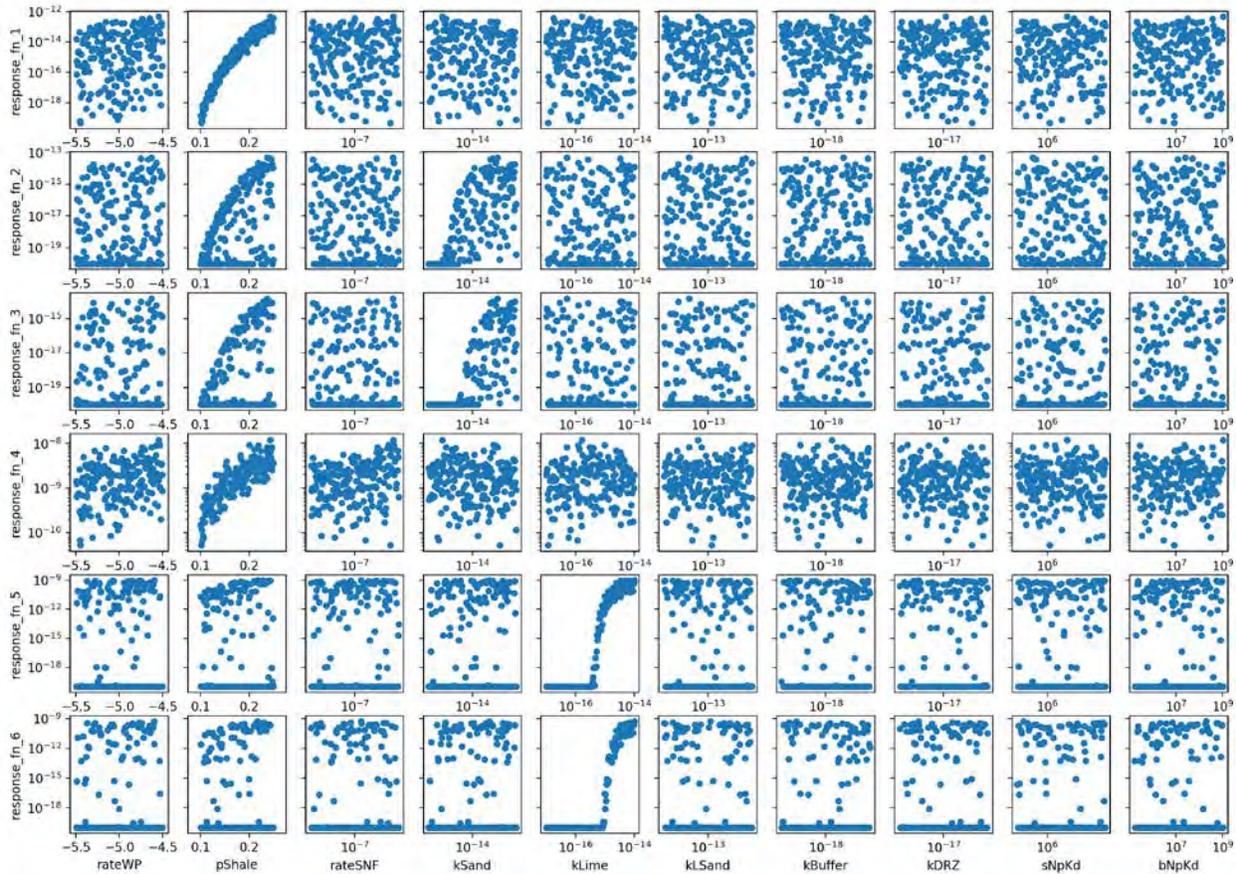
Figure 4-5   Maximum ^{129}I concentration (response functions 1 through 6) as a function of sampled inputs for the replicate of 200 samples

4.2.2   Quantification of Sensitivity

In this section, correlation coefficients, standardized regression coefficients, and sensitivity indices are presented in bar plots and in tables. Recall that correlation coefficients and SRCs are numbers between -1 and 1, and that a positive value indicates that the value of the output variable increases as the value of the input variable increases, while a negative value indicates the opposite. Sensitivity indices are always positive and are numbers between 0 and 1.

Simple and partial correlation coefficients (SCC and PCC) together with simple and partial rank correlation coefficients (SRCC and PRCC) are returned by Dakota's "postrun" analysis. Standardized regression coefficients (SRC) were calculated using stepwise.py (Section 3.2.1). Main and total sensitivity indices were calculated from evaluations of Gaussian process surrogate models fit to the data using global optimization and the "surfpack" option in Dakota. These are denoted S_{GP} and T_{GP}, respectively. Polynomial chaos expansion was performed with Dakota using "orthogonal matching pursuit" (iterative calculation of the coefficients), a 3rd order expansion for the replicate of 50 samples, and a 4th order expansion for the replicate of 200 samples. The resulting main and total sensitivity indices are denoted S_{PCE} and T_{PCE}. Because maximum ^{129}I concentrations are consistently very small ($< 10^{-13}$ mol/L) at some observation points, the PCE method failed to return sensitivity indices for some response functions due to "negligible variance." To overcome this problem, response functions were multiplied by a factor of 10^{13}, which enabled the PCE method to return sensitivity indices. Increasing the scaling factor to 10^{20}

(1/[background concentration]), resulted in sensitivity indices within approximately 1% of those calculated using the smaller scaling factor.

Measures of sensitivity for Response Functions 1, 2, and 3 (maximum [^{129}I] at sand_obs1, sand_obs2, and sand_obs3) are plotted in Figure 4-6 through Figure 4-8 and tabulated in Table 4-2 through Table 4-4. In each figure, results for the replicate of 50 samples are on the left, and results for the replicate of 200 samples are on the right. Model behavior and dependencies in the limestone aquifer are similar to behavior and dependencies in the sandstone aquifer. For completeness, bar plots of SA results are included at the end of this section for Response Functions 4, 5, and 6, but discussion focusses on Response Functions 1, 2, and 3.

In some instances, Dakota returned NaNs (Not-a-Number) when PCCs (but not PRCCs). Differences in scale among variables may have prevented the calculation, which in Dakota is accomplished through inversion of the correlation matrix (L. Swiler, personal communication) rather than through the recursive calculation described in Section 4.1.1.2. The PCCs reported below were calculated using a Python implementation of the recursive calculation.
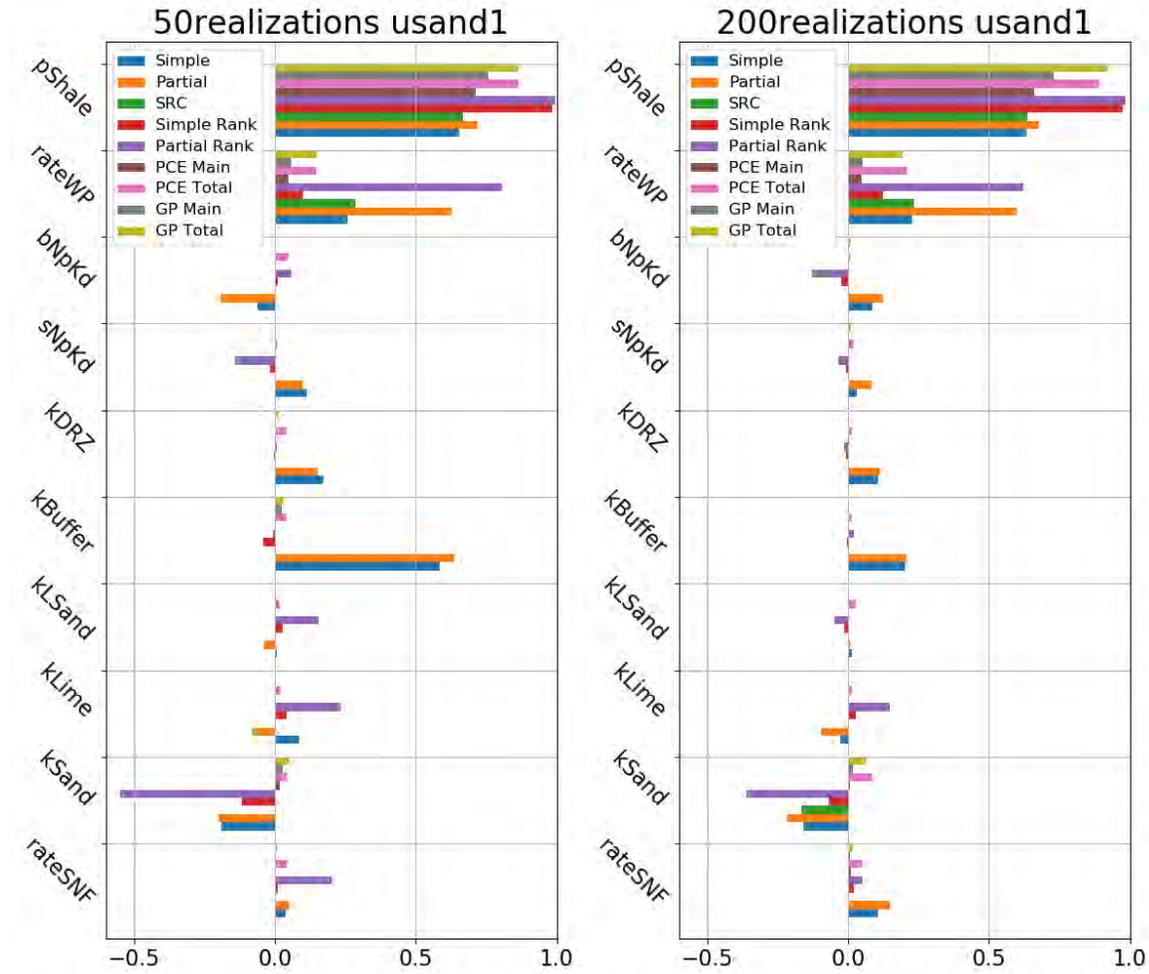
Figure 4-6   SA of Response Function 1 (max [^{129}I] at sand_obs1), 50 samples (left) and 200 samples (right)

Table 4-2   SA of Response Function 1 (max [^{129}I] at sand_obs1).

	rateSNF	kSand	kLime	kLSand	kBuffer	kDRZ	sNpKd	bNpKd	rateWP	pShale
					50 Realizations					
SCC	0.036	-0.190	0.088	0.008	0.583	0.171	0.113	-0.060	0.257	0.655
PCC	0.052	-0.199	-0.084	-0.039	0.638	0.152	0.101	-0.194	0.626	0.717
SRC					0.000				0.287	0.668
SRCC	0.009	-0.116	0.041	0.027	-0.042	-0.003	-0.018	0.011	0.099	0.983
PRCC	0.203	-0.549	0.235	0.154	-0.008	0.008	-0.141	0.057	0.806	0.995
PCEMain	0.000	0.018	0.000	0.000	0.000	0.000	0.000	0.000	0.048	0.711
PCETotal	0.045	0.045	0.020	0.017	0.042	0.041	0.009	0.049	0.149	0.862
GP Main	0.002	0.027	0.001	0.001	0.024	0.004	0.002	-0.000	0.057	0.757
GP Total	0.008	0.050	0.001	0.000	0.030	0.014	0.002	0.000	0.148	0.859
					200 Realizations					
SCC	0.107	-0.158	-0.026	0.014	0.203	0.105	0.033	0.085	0.227	0.632
PCC	0.147	-0.217	-0.097	0.008	0.205	0.115	0.081	0.125	0.598	0.677
SRC		-0.166							0.236	0.638
SRCC	0.019	-0.068	0.029	-0.015	-0.003	-0.006	-0.008	-0.023	0.124	0.973
PRCC	0.051	-0.361	0.147	-0.049	0.020	-0.015	-0.035	-0.127	0.623	0.985
PCEMain	0.010	0.005	0.000	0.001	0.000	0.001	0.000	0.001	0.049	0.661
PCETotal	0.052	0.086	0.015	0.026	0.015	0.015	0.019	0.007	0.211	0.891
GP Main	0.006	0.018	0.001	-0.000	0.001	0.000	0.001	-0.001	0.052	0.729
GP Total	0.017	0.063	0.001	0.000	0.001	0.005	0.009	0.010	0.192	0.921
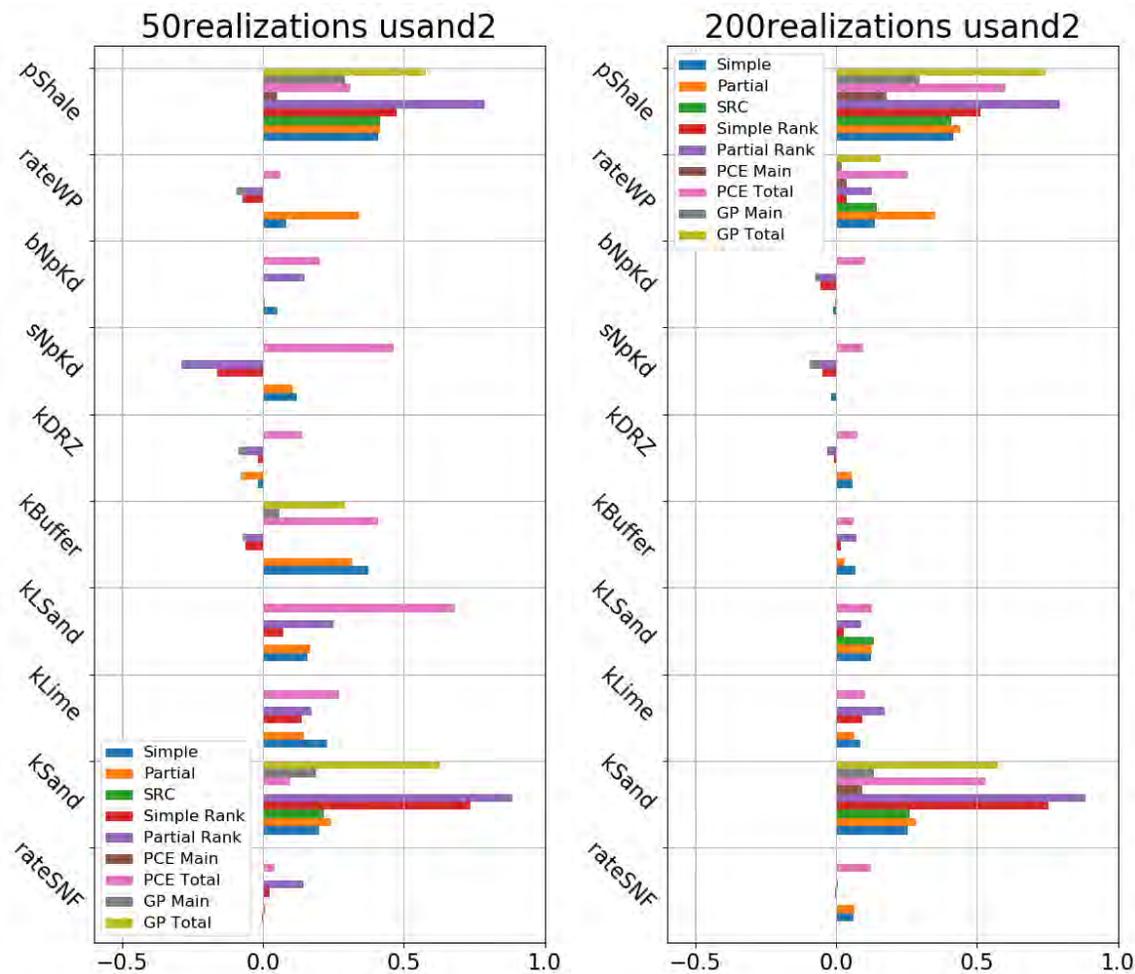
Figure 4-7   SA of Response Function 2 (max [^{129}I] at sand_obs2), 50 samples (left) and 200 samples (right)

Table 4-3   SA of Response Function 2 (max [^{129}I] at sand_obs2).

	rateSNF	kSand	kLime	kLSand	kBuffer	kDRZ	sNpKd	bNpKd	rateWP	pShale
					50 Realizations					
SCC	-0.003	0.200	0.227	0.158	0.376	-0.017	0.119	0.052	0.083	0.408
PCC	0.009	0.239	0.144	0.167	0.316	-0.078	0.108	0.005	0.341	0.415
SRC		0.218								0.417
SRCC	0.024	0.738	0.138	0.073	-0.063	-0.018	-0.163	0.001	-0.072	0.473
PRCC	0.143	0.884	0.173	0.251	-0.071	-0.086	-0.290	0.148	-0.093	0.786
PCEMain	0.000	0.000	0.000	0.001	0.000	0.001	0.000	0.000	0.001	0.051
PCETotal	0.040	0.096	0.270	0.683	0.409	0.140	0.465	0.201	0.062	0.311
GP Main	0.001	0.188	0.000	0.000	0.057	0.004	0.002	0.003	0.000	0.291
GP Total	0.002	0.628	0.001	0.001	0.291	0.005	0.004	0.003	0.002	0.579
					200 Realizations					
SCC	0.062	0.255	0.086	0.122	0.069	0.059	-0.018	-0.009	0.139	0.416
PCC	0.067	0.284	0.066	0.126	0.032	0.054	-0.001	-0.005	0.349	0.440
SRC		0.262		0.135					0.145	0.411
SRCC	-0.003	0.753	0.093	0.028	0.016	-0.008	-0.047	-0.056	0.038	0.514
PRCC	0.005	0.886	0.171	0.088	0.074	-0.033	-0.093	-0.074	0.127	0.795
PCEMain	0.003	0.094	0.000	0.002	0.003	0.001	0.000	0.000	0.038	0.179
PCETotal	0.122	0.531	0.103	0.128	0.060	0.077	0.096	0.103	0.253	0.601
GP Main	0.002	0.133	-0.000	0.000	0.001	0.000	0.001	0.001	0.020	0.295
GP Total	0.004	0.575	0.001	0.000	0.002	0.005	0.000	0.001	0.159	0.744
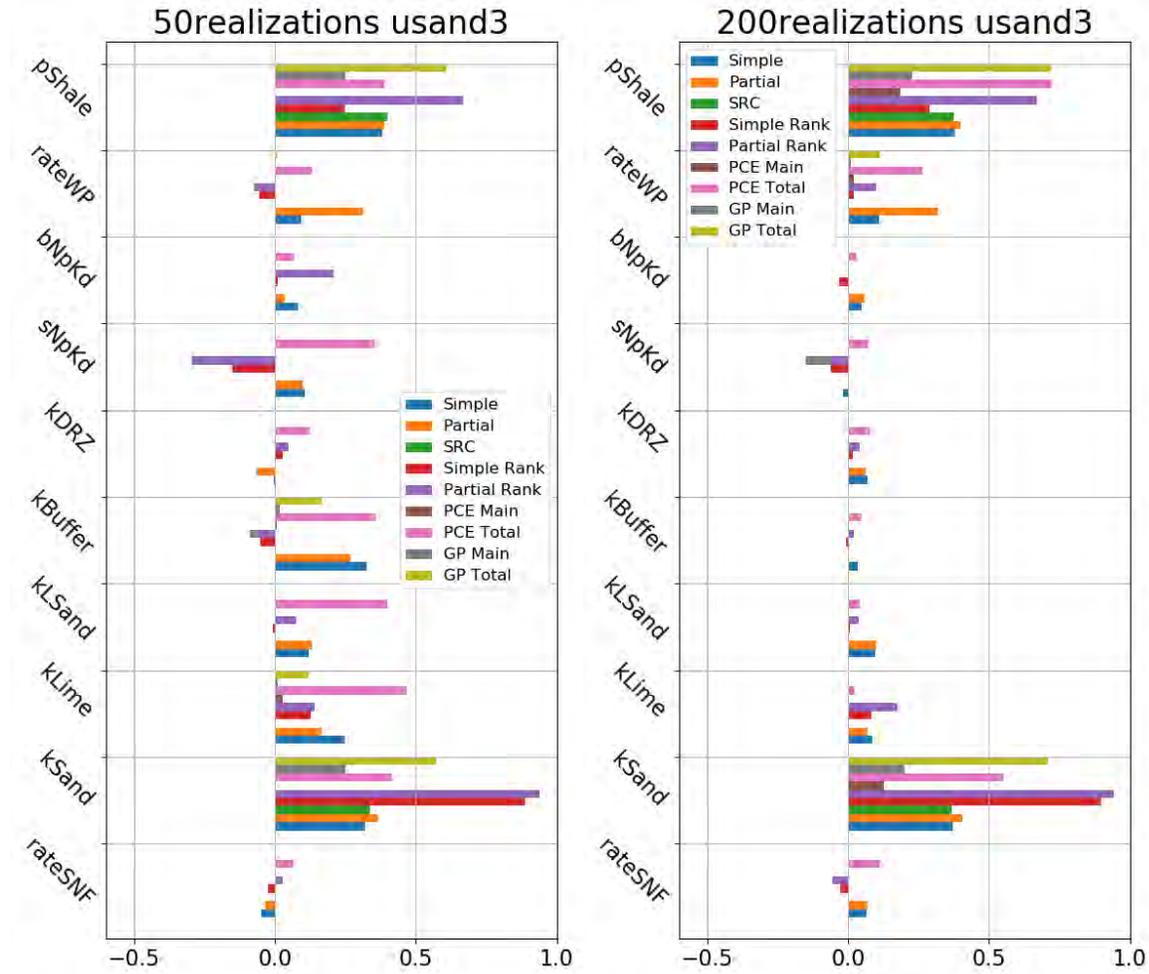
Figure 4-8   SA of Response Function 3 (max [^{129}I] at sand_obs3), 50 samples (left) and 200 samples (right)

Table 4-4   SA of Response Function 3 (max [^{129}I] at sand_obs3)

	rateSNF	kSand	kLime	kLSand	kBuffer	kDRZ	sNpKd	bNpKd	rateWP	pShale
					50 Realizations					
SCC	-0.048	0.321	0.249	0.122	0.328	-0.003	0.108	0.084	0.091	0.383
PCC	-0.035	0.366	0.165	0.130	0.267	-0.065	0.101	0.035	0.312	0.389
SRC		0.339								0.398
SRCC	-0.023	0.888	0.127	-0.008	-0.052	0.026	-0.153	0.010	-0.056	0.249
PRCC	0.028	0.940	0.140	0.077	-0.089	0.046	-0.298	0.209	-0.075	0.667
PCEMain	0.003	0.000	0.026	0.000	0.005	0.003	0.000	0.000	0.004	0.000
PCETotal	0.066	0.416	0.469	0.399	0.359	0.129	0.354	0.068	0.131	0.388
GP Main	0.000	0.252	0.011	0.002	0.016	-0.000	0.001	0.003	0.004	0.252
GP Total	0.001	0.570	0.120	0.004	0.165	0.001	0.003	0.004	0.009	0.610
					200 Realizations					
SCC	0.064	0.373	0.087	0.095	0.035	0.069	-0.016	0.049	0.110	0.379
PCC	0.069	0.404	0.069	0.099	0.003	0.062	-0.002	0.058	0.319	0.398
SRC		0.368								0.375
SRCC	-0.027	0.897	0.083	0.006	-0.007	0.018	-0.064	-0.032	0.021	0.288
PRCC	-0.055	0.941	0.175	0.037	0.020	0.041	-0.152	-0.001	0.098	0.671
PCEMain	0.000	0.127	0.000	0.001	0.000	0.000	0.000	0.000	0.021	0.184
PCETotal	0.115	0.551	0.025	0.040	0.048	0.080	0.072	0.030	0.265	0.722
GP Main	0.001	0.198	-0.000	-0.000	0.001	-0.000	0.000	-0.000	0.011	0.227
GP Total	0.002	0.710	0.000	0.000	0.000	0.003	0.000	0.000	0.112	0.718

4.2.2.1 *Comparison by method*

At observation points in the sandstone aquifer, all methods identify pShale (shale porosity), rateWP (mean waste package degradation rate), and kSand (sandstone permeability) as the input parameters with the greatest influence on maximum ^{129}I concentration. Sensitivity to pShale decreases with distance from the repository, while sensitivity to kSand increases. At sand_obs1 (closest to the repository), maximum ^{129}I concentration is negatively correlated with kSand; at sand_obs 2 and sand_obs 3, it is positively correlated. Substituting kLime for kSand, behavior at the limestone observation points is very similar to behavior at the sandstone observation points.

Different SA methods estimate the magnitude of the influence of each input variable differently. Rank correlations (SRCCs and PRCCs) that are larger than correlations on raw values (SCCs and PCCs), as for kSand at sand_obs2 and sand_obs3, suggest a monotonic but nonlinear correlation between input and output. A partial correlation coefficient (PCC or PRCC) larger than a simple correlation coefficient (SCC or SRCC), as for rateWP at sand_obs1 and for pShale at sand_obs2 and sand_obs3, reveals a correlation that was partially masked by the influence of other inputs in the calculation of the simple correlation coefficient.

Stepwise linear regression and sensitivity indices provide a measure of the fraction of the variance in the output due to the variance in an input. Table 2 compares the fraction of the variance accounted for by stepwise linear regression with the fraction of the variance accounted for by main sensitivity indices (S_{PCE} and S_{GP}) at sand_obs2. Input variables identified as improving the regression model are listed in the order they were entered into the stepwise regression. Incremental R^2 values and main sensitivity indices are summed to find the total fraction of the variance in the output accounted for by the listed inputs. Resulting values are similar in magnitude (total $R^2 = 0.275$ compared to $\sum S_{PCE} = 0.312$), and account for less than half of the variance in maximum ^{129}I concentration at sand_obs2.

Total sensitivity indices are also included in Table 2. For pShale, kSand, and rateWP, the total sensitivity index (T_{PCE} or T_{GP}) is several times larger than the main sensitivity index (S_{PCE} or S_{GP}), indicating the importance of parameter interactions. When the effects of parameter interactions are included, variance in the sampled input pShale accounts for 0.601 (T_{PCE}) or 0.744 (T_{GP}) of the total variance in maximum ^{129}I concentration at sand_obs2, almost twice that accounted for by main effects (of all input parameters) alone. In the future, analysis of higher-order sensitivity indices (which are returned by the PCE method) will quantify the effect of specific parameter interactions.

Because total sensitivity indices include the effect of parameter interactions, near zero values serve to identify sampled input variables that do not contribute to variance in the output variable of interest. Given the constraints of the simulations considered here, kDRZ (permeability of the disturbed rock zone), kBuffer (permeability of the buffer), and (as measured by T_{GP}) kLSand (permeability of the lower sandstone aquifer) could all be fixed without affecting the variance (a measure of uncertainty) in maximum ^{129}I concentration in either the upper sandstone aquifer or the limestone aquifer.

Table 4-5   **Fraction of variance accounted for by stepwise linear regression and by sensitivity indices at sand_obs2.**

Input Variable	Incremental R^2	S_{PCE}	S_{GP}	T_{PCE}	T_{GP}
pShale	0.173	0.179	0.295	0.601	0.744
kSand	0.062	0.094	0.133	0.531	0.575
rateWP	0.021	0.038	0.020	0.253	0.159
kLSand	0.018	0.002	0.000	0.128	0.000
Fraction of variance accounted for	0.275	0.312	0.449	NA	NA

4.2.2.2   *Comparison by sample size*

The difference between the results of the 50-sample replicate and the 200-sample replicate are most apparent in (1) inflated measures of influence for the less influential input variables, and (2) large values of total sensitivity index calculated from the 3rd order PCE. Inflated measures are readily apparent in Response Function 1 (Figure 4-6), for which the 50-sample replicate results in a SCC for kBuffer of nearly 0.6, compared to 0.2 in the 200-sample replicate. At sand_obs1, the 50-sample replicate results in PRCC > 0.1 for sNpKd, kLime, kLSand, and rateSNF, while the 200-sample replicate results in PRCC > 0.1 for only one of these, rateSNF.

Large total sensitivity indices from the 3rd order PCE occur for Response Functions 2 and 3 (Figure 4-7 and Figure 4-8). For example, at sand_obs2, T_{PCE} for kLSand drops from 0.68 to 0.11 when the sample size (and PCE order) is increased, and T_{PCE} for sNpKd drops from 0.46 to 0.07. The T_{PCE} values obtained from the 200-sample realization are consistent with the model implementation (neptunium K_d cannot affect ^{129}I concentration, and the permeability of the deep aquifer is unlikely to influence concentration in the uppermost aquifer), while those obtained from the 50-sample realization are not.

4.2.2.3   *Conclusion*

All SA methods identify pShale and kSand (or kLime) as the input variables having the greatest effect on the output variable of interest – maximum ^{129}I concentration at downgradient points in the sandstone (or limestone) aquifer. This result suggests that, given the constraints of the simulations performed for the clay reference case PA, reduction of uncertainty in these input variables would most reduce the uncertainty in the output variable. The finding of near zero total sensitivity indices for kDRZ, kBuffer, and kLSand at all observation points indicates that values of these input variables could be fixed without affecting uncertainty in the output variables.

The GDSA clay reference case PA is simple in comparison to expected future repository PAs, but already computationally expensive. As PA grows in size and complexity, the computational expense of each simulation as well as the number of sampled parameters may grow. Effective and efficient SA can help manage the number of parameters that need to be sampled (reducing the necessary number of model evaluations), identify opportunities to simplify the model (reducing the run time of each simulation), and maximize the return of information from the simulations that are run. The sensitivity analysis of the clay reference case demonstrated some of the SA methods available to GDSA, and provides a starting point for future exploration of SA methods in *GDSA Framework*.
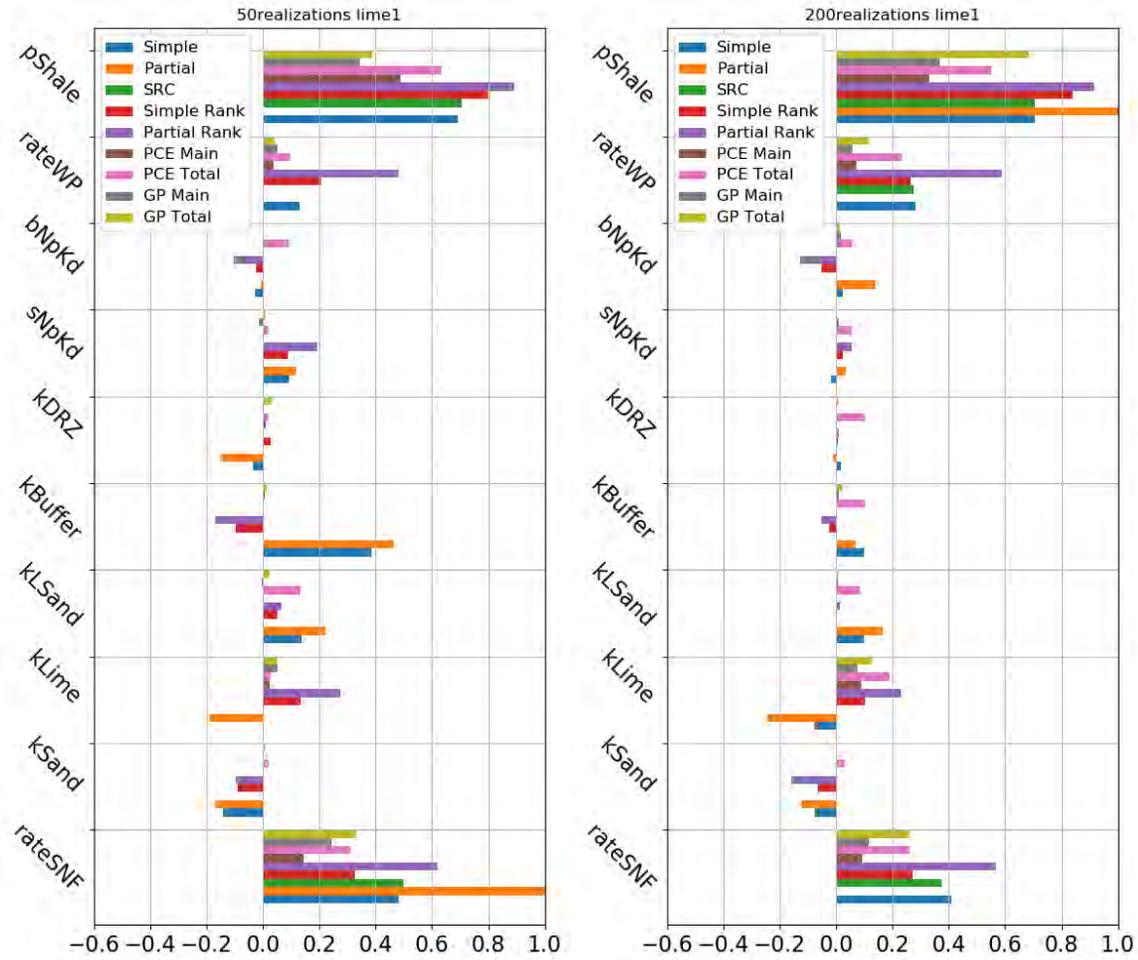
Figure 4-9   Sensitivity of Response Function 4 (max [^{129}I] at lime_obs1) to sampled inputs calculated for 50 samples (left) and 200 samples (right)
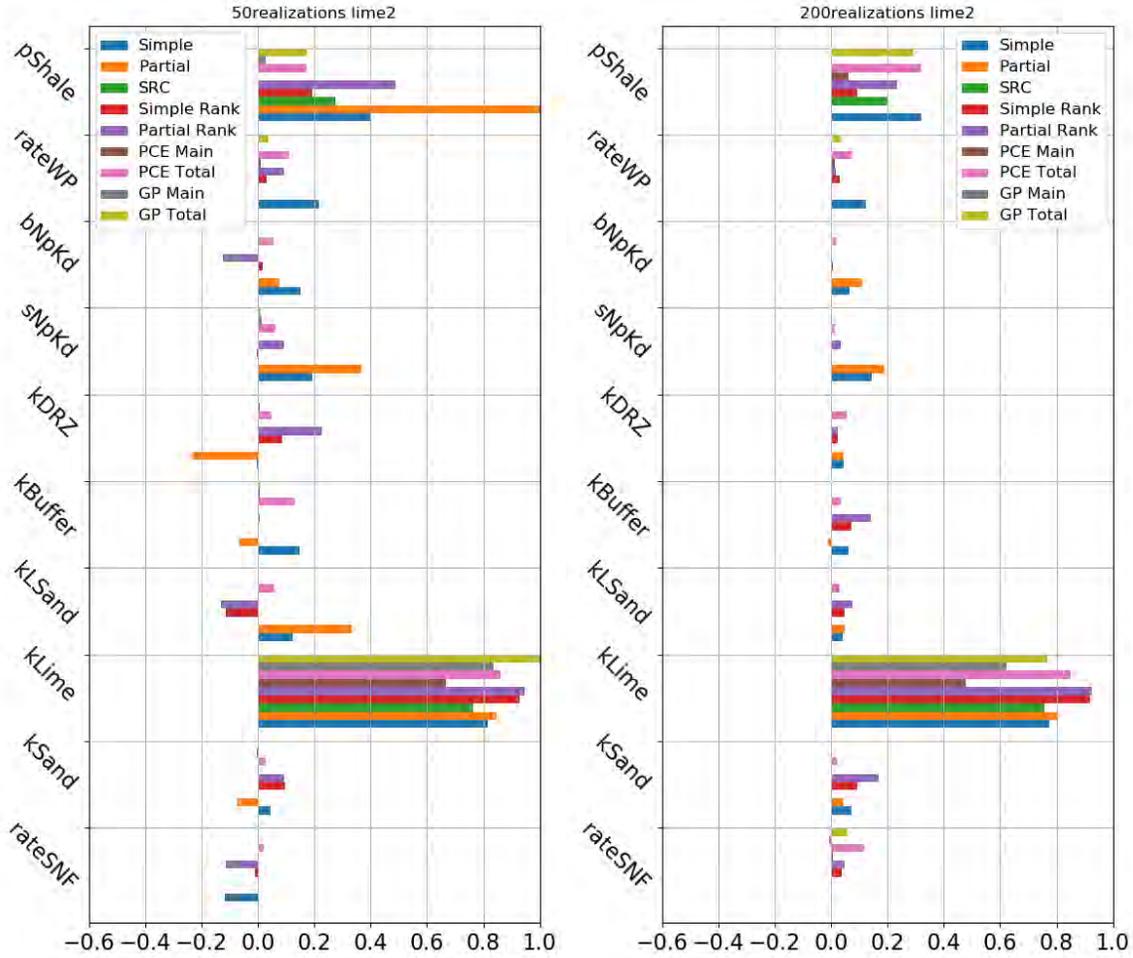
Figure 4-10 Sensitivity of Response Function 5 (max [^{129}I] at lime_obs2) to sampled inputs calculated for 50 samples (left) and 200 samples (right)
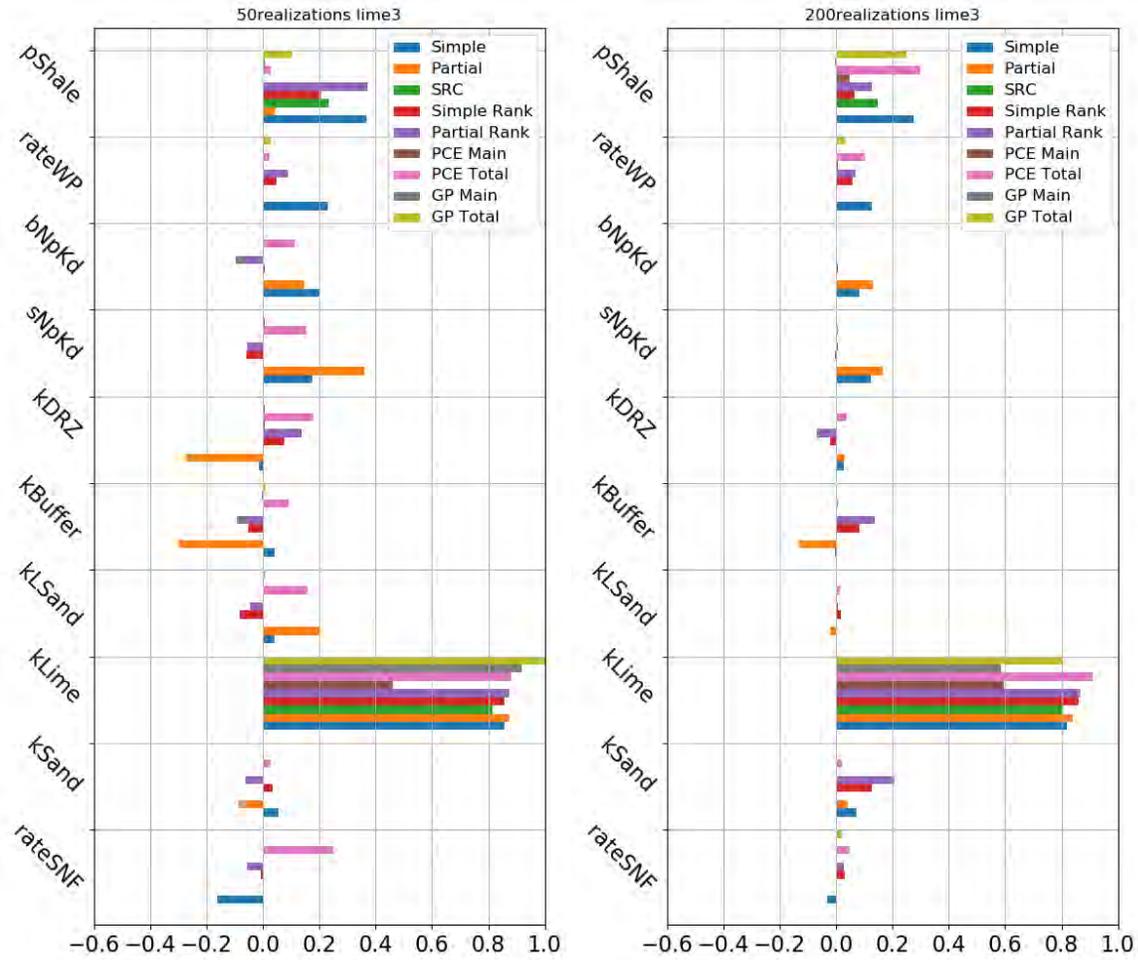
Figure 4-11 Sensitivity of Response Function 6 (max [^{129}I] at lime_obs3) to sampled inputs calculated for 50 samples (left) and 200 samples (right)

5.   UNSATURATED ALLUVIUM REPOSITORY REFERENCE CASE

Regulations typically require demonstration that multiple barriers contribute to the safety functions of waste isolation and delaying / limiting radionuclide releases and transport. There are several features of the unsaturated zone that are favorable for radionuclide delay and limited release that are the motivation for the evaluation that follows. The safety of an unsaturated zone natural barrier concept relies primarily on the delay and isolation provided by very low recharge rates, low permeability, and distance between a repository and the accessible environment. There is also a reliance on engineered barriers. Siting features in the unsaturated zone generic case that contribute to isolation of waste and delay and (or) limit radionuclide releases include location:

- **Low groundwater flux and great depth to water table** – Alluvial basins of the western United States are located in arid climates having low to relatively low (under wetter, 'ice box' climatic conditions documented in the past) recharge rates and volumes and high evapotranspiration. These factors result in less potential for groundwater to come into contact with and transport radionuclides within the natural barrier system and helps ensure waste remains isolated from the assessable environment by creating longer transport paths to an aquifer.

- **Formation thickness** – Alluvial fill in basins in the western United States can reach thicknesses on the order of 100s of meters, up to around 1,000 m. Siting a repository in a thick unit isolates waste from and provides longer transport paths to the assessable environment. This feature is also conducive to dual purpose canister disposal.

- **Lower permeability barrier** – Alluvial basins tend to have stacked playa and lacustrine sediment deposits located along or near their axes. These units serve to impede migration of radionuclides due to sorption and low permeability, thus providing another mechanism for isolating waste from the assessable environment

A schematic of the hydrology and geology of an unsaturated alluvium repository is presented in Figure 5-1. Figure 5-2 depicts the thicknesses of basin fill sediment divided into upper and lower basin fill units in Nevada, Utah, and California over the extent of the Great Basin carbonate and alluviual aquifer system study area. Greater thicknesses of alluvial fill are also feasible in NW Arizona. Perry et al. (2018) report that the large majority of basins over this southwest region have shallow alluvial aquifers. They point out that when the region was initially being developed, often by individual ranchers and farmers, water wells could not be drilled deeper than a couple of hundred meters, were often found to be dry, and were subsequently abandoned. Where a large number of deep wells have been drilled, such as at the Nevada National Security Site, a picture has emerged of a water table on the order of 500-600 meters deep. Form this observation, they speculate that there may be more basins with deep water than those currently recognized in the region.
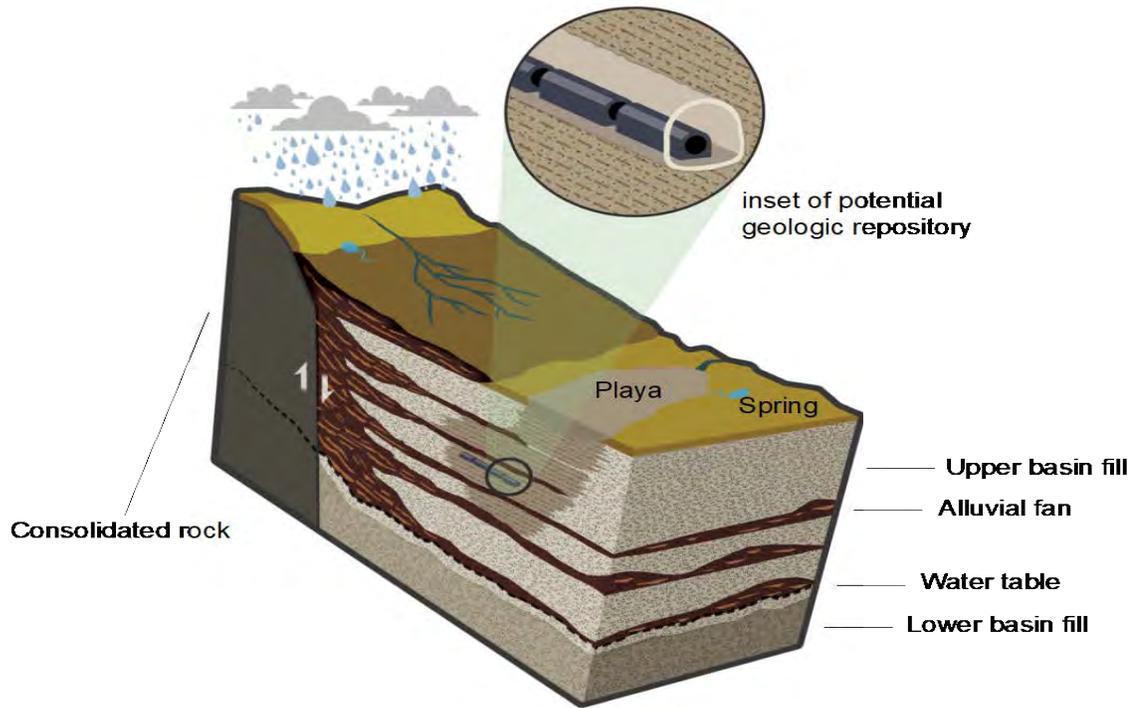
Figure 5-1   Schematic of potential unsaturated zone geologic repository. Note that impermeable fine-grained sediments, such as those found in playa deposits, may serve as a viable location for siting a repository. The schematic also depicts the lithologic heterogeneity that is expected in basin-fill valleys where alluvial fans, fluvial systems, spring discharge areas, and playas are common features.
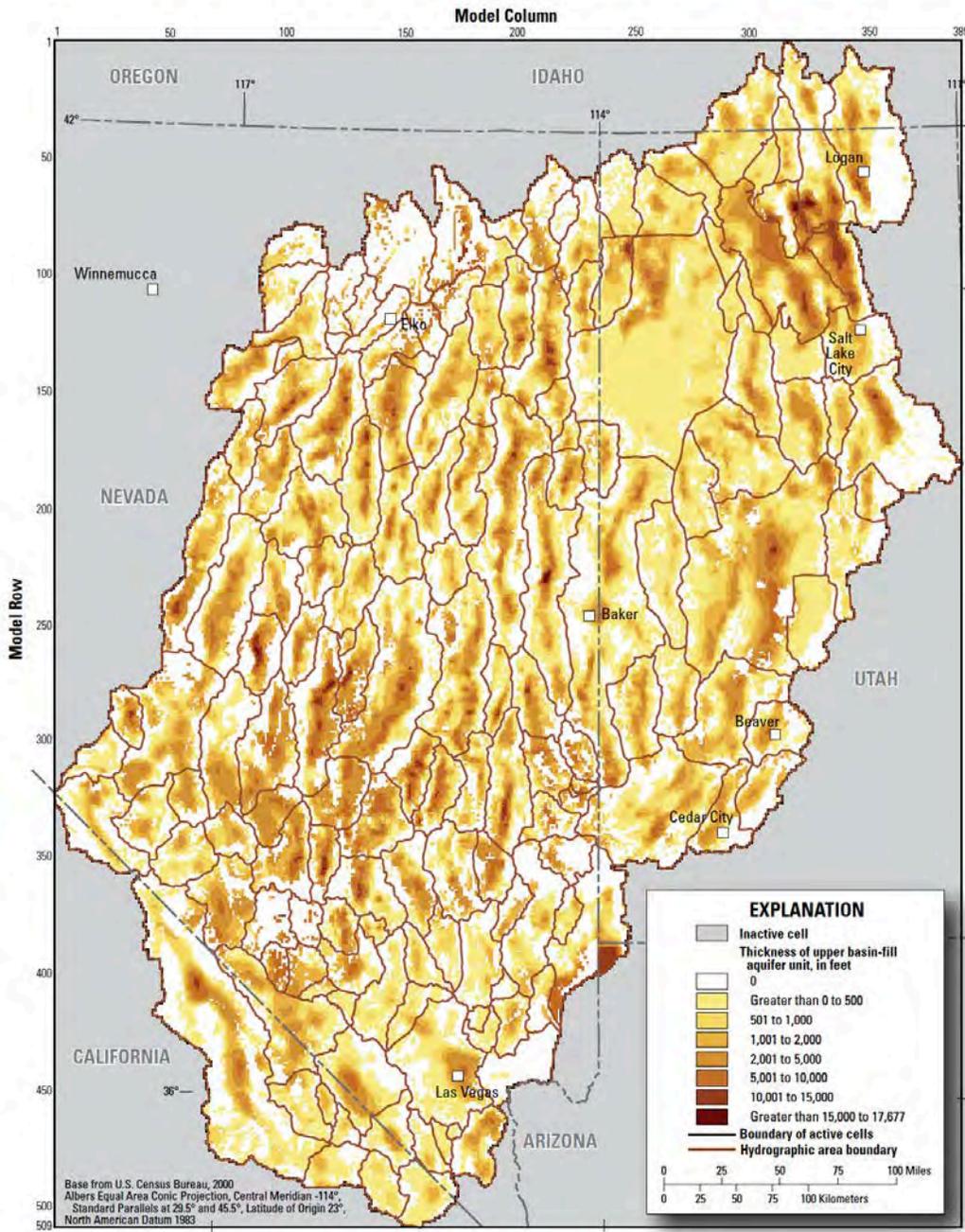
Figure 5-2   Map showing thickness, in meters, of upper basin fill of the Great Basin carbonate and alluvial aquifer system study area. Figure 12 of Brooks et al. (2014). Darker brown colors indicate valleys having thicker upper basin fill, which could serve to isolate waste from and provide longer transport paths to the assessable environment.

5.1   Natural Barrier System

The purpose of this section is to present a conceptual model for evaluating radionuclide movement through a generic unsaturated zone natural barrier system. This conceptual model includes the delineation

of hydrogeologic units within the alluvial fill of a basin with a description of generalized lithology and hydraulic and chemical properties. The unsaturated zone model, depicted in Figure 5-3, takes as its inspiration the thick alluvial valleys of the Great Basin in the western United States that formed from extensional and trans tensional tectonic processes (Perry et al., 2018). The model presented here does not include consolidated lithologies in the unsaturated zone, such as volcanics and volcaniclastics as a robust body of work has been summarized (e.g., Sandia National Laboratories, 2008; Simmons and Stuckless, 2012).
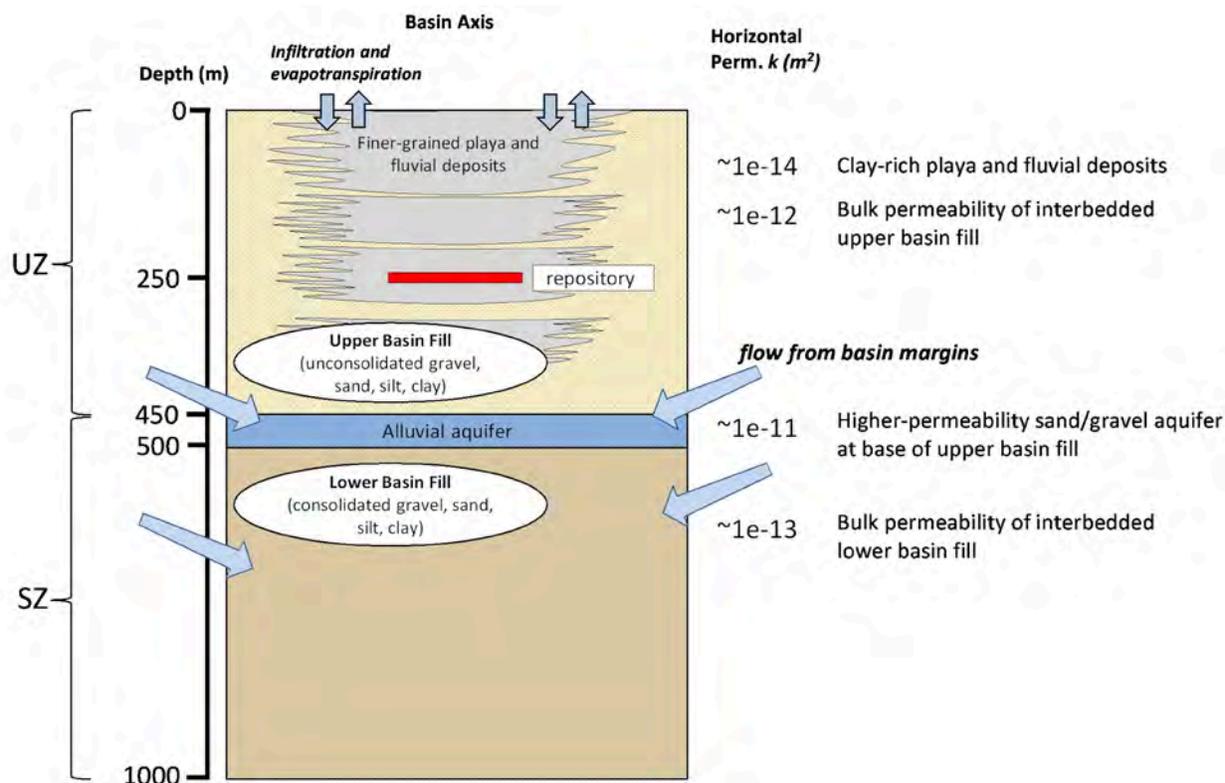
Figure 5-3   Schematic cross section of the unsaturated zone model (Perry et al., 2018) considered in this chapter. UZ = unsaturated zone; SZ = saturated zone

The Great Basin has been the subject of several programs of study (Figure 5-4) as well as smaller-scope projects that are too numerous to capture in this report. The most notable programs are the Regional Aquifer-System Analysis (RASA) conceptual model (Prudic et al., 1995), the Death Valley Regional Flow System study (Belcher, 2004), the Basin and Range Carbonate Aquifer System study (Welch et al., 2007), the Great Basin Carbonate and Alluvial Aquifer System study (Heilweil and Brooks, 2010), and characterization work completed at the Nevada National Security Site and for the Yucca Mountain Project (including the Greater Confinement Disposal Boreholes, Science Trench Boreholes, and Beatty Low Level Waste Disposal Site). Each effort is defined by different spatial extents that are summarized in Heilweil and Brooks (2010) and reproduced below for reference. Other alluvial basins exist in the western US (e.g., San Pedro Valley, AZ – Pool and Coes, 1999), however, a rich body of work exists for the Great Basin that is useful in describing generic unsaturated zone natural barrier systems.
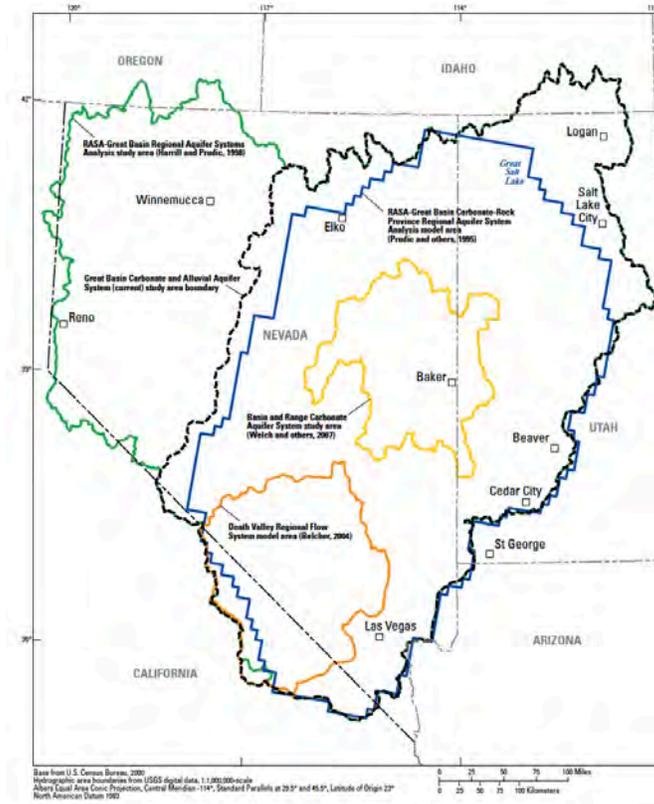
Figure 5-4   Map showing extent of the large-scale characterization and simulation projects completed on the Great Basin, US. Figure reproduced from Heilweil and Brooks (2010)

5.1.1   Hydrogeologic Framework for Generic Unsaturated Zone Natural Barrier

A hydrogeologic framework defines the physical geometry and rock types in the subsurface. The complex stratigraphy and structure of an alluvial basin can significantly influence the location and direction of groundwater flow and radionuclide movement. The occurrence and juxtaposition of permeable and impermeable units in three dimensions is important in determining the potential for radionuclide migration within and between hydrographic areas. Thus, the development of a three-dimensional hydrogeologic framework will be a necessary step in conceptualizing radionuclide movement in an unsaturated zone natural barrier.

The physical geography of the Great Basin is characterized by north or northeast trending mountain ranges separated by broad valleys. Valleys are typically 8–16 km wide and 56–113 km long. Where mountain ranges are bounded by large normal faults, the mountain fronts abruptly transition to alluvial fans that extend into the valleys. Topographic relief between mountain crests and valley floors typically ranges from 300 to 1,800 m. Valley floor altitudes vary between 900 and 1,800 m above sea level while mountain altitudes commonly range between 2,400 and 3,400 m (Heilweil and Brooks, 2010)

The Great Basin's climate varies considerably with altitude and latitude; ranging from Great Basin Woodland and Desert to Mohave Desert to Transition Desert (Belcher, 2004). The Great Basin Woodland and Desert has an average daily temperature around 25°C (Strahler, 1989). Between 1940 and 2006 average annual precipitation ranged from 3.8 to 178 cm. (Daly and others, 2004; 2008). Most of the precipitation falls as snow in the mountains at higher latitudes. Less precipitation, in the form of rain, falls in valleys and at lower latitudes. Most precipitation occurs in winter and early spring from the Pacific

Ocean and, secondarily, during the late summer and early fall Gulf of Mexico monsoon (Brenner, 1974; Weng and Jackson, 1999).

Surface-water is relatively uncommon and tends to originate in mountains on the western and eastern edges and in the northern part of the Great Basin. All surface water drains internally to the Great Basin as terminal lake or playa systems where evapotranspiration is the dominant process. Playas are dry or ephemeral lakebeds that form in closed evaporative basins and either receive surface-water flow and are non-saline or receive groundwater discharge and are saline. These terminal lake and playa systems are often pluvial lake remnants from cooler and wetter conditions during the Pleistocene. Terminal lakes and playas tend to develop along the axes of valley bottoms. Surface water generally does not flow between basins, except for a few larger river systems.

The geologic evolution of the Great Basin is characterized by Late Proterozoic to Devonian marine sedimentation along a passive continental margin; Late Devonian to Eocene compressional deformation and sedimentation patterns related to the subduction of ocean crust along the western continental margin in western Nevada; and mid- to late- Cenozoic extension, high-angle faulting, volcanism, and continental sedimentation (Levy and Christie-Blick, 1989; Dickinson, 2006). Modern Basin and Range topography began forming in Neogene time and unconsolidated sediments began filling broad, intermountain valleys. Sedimentation was largely postvolcanic, though some basalt was erupted, and modern drainages were established. In Pleistocene time, pluvial climate conditions led to the creation of numerous shallow lakes throughout the region (Reheis, 1999). A drier Holocene climate led to the drying of these lakes and the abandonment or reduction in flow of a number of springs.

The definition of hydrogeologic units is important in conceptualizing and numerically evaluating various natural barrier system scenarios. The alluvial fill of a generic unsaturated zone natural barrier system may be subdivided into two hydrogeologic units: an upper basin-fill aquifer unit representing the upper two-thirds of alluvial fill; and a lower basin fill aquifer unit representing the lower one-third of alluvial fill. These units are consistent with those used by Brooks et al. (2017) in their groundwater flow study in the Great Basin and by the body of work conducted as part of the US Geological Survey RASA program on the Great Basin (e.g., Harrill et al., 1998). The hydrogeologic units in a generic alluvial basin may form two adjoining aquifer systems with confining intervals contained within in the upper aquifer. Generally, aquifer materials are higher permeability sand and gravel alluvial fill. Each alluvial aquifer unit may include multiple sheet-shaped water-bearing zones and pod- to tabular- shaped perched water features on the order of 10s to 100s of meters in lateral extent. Unconsolidated alluvium can have secondary hydraulic conductivity that can enhance or impede fluid flow. The aquifer units are likely stratigraphically and structurally heterogeneous, resulting in a highly variable ability to store and transmit water across the basin. Playa/lacustrine sediment that is part of the upper basin fill aquifer unit is characterized by low permeability, clay-rich, fine-grained sediment and likely has fairly uniform hydraulic properties. The playa and lacustrine deposits tend to be distributed along basin axes as stacked tabular- to pod-shaped features on the order of 10 to 100s of meters in lateral extent. There is considerable uncertainty on how deep these units extend in the subsurface (Sweetkind et al., 2010a).

5.1.1.1   *Lower basin-fill aquifer unit*

The lower basin-fill aquifer unit may contain a variety of rock and sediment types including fluvial and lacustrine limestone, sandstone, siltstone, and conglomerate. Lake-bed and other fine-grained deposits may include sandy or coarse-grained material (Sweetkind et al., 2010a). The lacustrine-dominated package is expected to have moderate relative permeability due to thin bedding and fine grain size (Best et al., 1989; Sweetkind and du Bray, 2008; Raines et al., 2003; Glen et al., 2004). Coarse-grained basin fill composed of sand and gravel may be intercalated with volcanic rock or contain volcanic material. The coarse package is expected to have moderate relative permeability due to deep burial and cementation (Fouch, 1979; Fouch et al., 1979; Hintze, 1988; Ludington et al., 1996). Volcanic rocks such as ash-flow

and welded ash-flow tuffs or intermediate to felsic composition lava-flow deposits could also be buried within the basin fill. Welded tuffs are expected to have high relative permeability due to well-developed fracture networks while the other volcanic rocks are expected to have moderate relative permeability due to lithologic diversity, lack of well- developed or organized fracture networks, and potential to be hydrothermally altered (Best et al., 1989; Sweetkind and du Bray, 2008; Raines et al., 2003, Glenn et al., 2004). In the context of the Great Basin, the processes leading to deposition of lower basin fill materials occurred from early to mid-Cenozoic time. The lower basin-fill aquifer unit is taken to be under saturated conditions in this generic assessment.

5.1.1.2   *Upper basin-fill aquifer unit*

The upper basin-fill aquifer unit may contain a variety of sediment types that were deposited in lacustrine, fluvial, and alluvial environments and includes unconsolidated to semi-consolidated alluvium and colluvium and local deposits of fresh water limestone, tuffaceous sandstone and siltstone, laminated clays, and water-deposited tuffs and ash (Harrill et al., 1998; Sweetkind et al., 2010a). The upper basin fill aquifer may be composed of gravel, sand, silt, clay, and fresh-water limestone and is expected to have a large range of permeability. Prevolcanic fine-grained lake bed deposits and synvolcanic zeolitized ash deposits are expected to be less permeable. Post volcanic coarse-grained and well sorted alluvial fan and stream channel deposits are expected to be permeable and could form local aquifers. Overall, upper basin fill is expected to have moderate to low relative permeability (Fouch, 1979; Fouch et al., 1979; Hintze, 1988; Ludington et al., 1996). Upper basin fill sediment would not generally be cemented but would be semiconsolidated deeper in the basin. Thin and laterally extensive basalt flows may be present either overlying or within coarse-grained basin fill. Basalts can have high fracture permeability and permeable zones at contacts between flows, but local alteration may reduce permeability leading to moderate to low expected relative permeability overall (Hintze, 1988; Ludington et al., 1996). Pleistocene lake and modern playa sediments are found at the surface and are fine-grained. They are expected to have moderate to low relative permeability (Hintze, 1988; Ludington et al., 1996; Reheis, 1999). In the context of the Great Basin, processes leading to deposition of prevolcanic and post-volcanic upper basin fill materials are early Cenozoic- and Late Cenozoic -aged, respectively. The upper basin-fill aquifer unit is generally taken to be unsaturated and locally saturated under perched conditions. The subsurface extent of the younger basin fill is uncertain because the distinction between lower and upper basin fill has not always been emphasized in geologic studies and the relations of the units are not always easy to understand (Stewart, 1980).

5.1.2   Groundwater Movement

Within an alluvial basin, groundwater typically originates in higher altitude bedrock of mountains and moves toward lower altitude discharge areas, as illustrated in Figure 5-5. Groundwater movement can occur at local, intermediate, and interbasin scales (Toth, 1963). At a local scale, groundwater moves along shallow and short flow paths, such as from a high altitude mountainous recharge area to a nearby mountain stream or spring, or from a losing alluvial fan stream to a lower altitude evapotranspiration area. At an intermediate scale, some groundwater recharge originating in the mountains flows along paths of intermediate length and depth to discharge and evapotranspiration areas in the adjacent valley. Underflow may occur along deeper and longer flow paths through relatively high permeability rock and sediment and possibly through intervening mountains where mountain recharge does not cause a substantial groundwater mound directly beneath the mountain block (Tiedeman et al., 1998; Thyne et al., 1999).
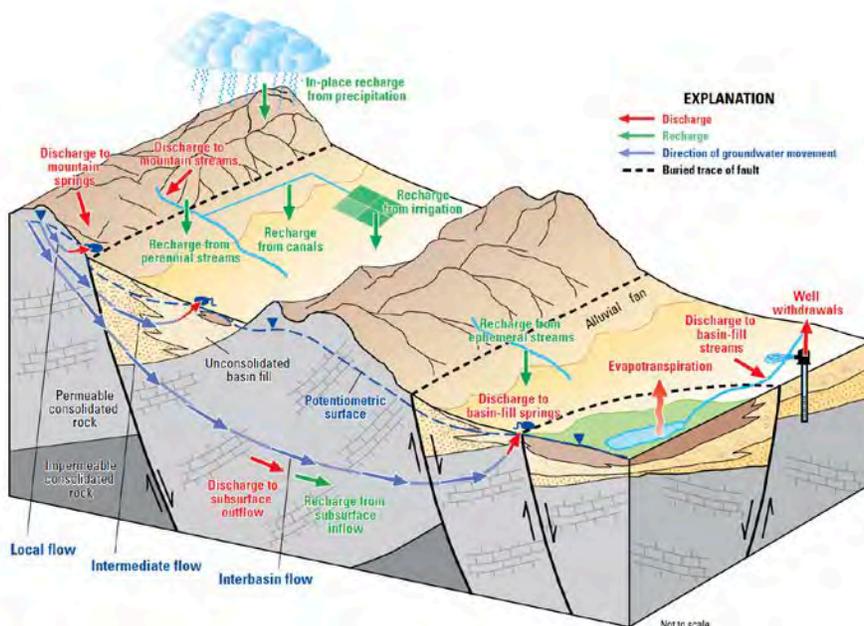
Figure 5-5   Schematic diagram of flowpaths found within the Great Basin, US, and water budget. Figure reproduced from Heilweil and Brooks (2010)

5.1.2.1   *Generic unsaturated zone conceptual model*

Within the Great Basin, groundwater generally flows from mountainous areas to the Great Salt Lake Desert, the Humboldt River, the Colorado River, and Death Valley through intergranular and (or) fracture flow mechanisms. Consolidated rock and basin-fill aquifers tend to be well connected hydraulically with upper basin fill experiencing some of the highest groundwater flow in the Great Basin (Sweetkind et al., 2010b). Other sediment or volcanic packages within alluvial basins may host local, perched aquifers, but typically have lower permeability and more heterogeneous properties and do not transmit significant regional groundwater flow. Downward vertical gradients typically exist beneath recharge areas in the mountain block or along the valley margins. Groundwater mounding in high-precipitation and (or) less permeable mountain-block areas has been observed in the generalized potentiometric surface of the Great Basin (Sweetkind et al., 2010b).

In the unsaturated parts of a groundwater flow path, vapor and liquid phases can be present. Under arid climate conditions, there is a component of upward water motion in the interval between the uppermost active layer and the deeper parts of the unsaturated zone. The active layer experiences cycles of evapotranspiration (upward water movement) and sporadic infiltration (downward water movement). The deeper parts of the unsaturated zone, roughly on the order of 80 m depth and deeper, may receive very slow-moving water from perched or relict groundwater systems from previous climatic conditions. A transition zone with zero potential is located between the deeper downward flow and shallower upward flow where no moisture movement occurs (~60 to 70 m below land surface in Area 3 at the Nevada Test ite; which is a deep arid system, Kwicklis et al., 2006).

The main controls on the evolution of saturated zone water chemistry along flow paths are surface-water compositions and recharge rates, soil-zone processes, rock-water-gas interactions in the unsaturated zone and recharge zones, quantity and composition of precipitated secondary minerals, rock-water interactions and temperature-pressure conditions in the saturated zone along flow paths, and mixing or water from different flow systems. Precipitation tends to have low salinity and organic content, is oxidizing, and is slightly acidic. The saturated zone tends to be a reducing environment and water flowing through it

generally has progressively higher salinity with increased travel time and (or) distance. pH will largely be determined by the degree to which unsaturated zone CO_2 is available and the rate at which hydrogen ions are consumed by earth material in the saturated zone. If organic carbon is present, it will tend to be preserved as long as anoxic conditions persist. In organic-rich and saturated reducing zones such as wetlands, precipitation of reduced state chemical species can also occur. With influx of oxic recharge water, the redox boundary can be pushed deeper into the saturated zone. With more oxic conditions, nitrate, sulfate, and ferric iron can be present.

The composition of unsaturated zone water, including pore water and perched water, are influenced by the composition of infiltrating precipitation and surface water, soil zone and unsaturated zone water-rock and water-air interactions, microbial processes, infiltration paths and rates, temperature, and pressure. The unsaturated zone is an oxic environment that contains water and vapor phases from the atmosphere and soil zone and includes methane (Yang, 2002). CO_2 partial pressures are particularly sensitive to soil zone processes. While variation in total gas pressure can influence the composition of unsaturated zone water, it has a more significant effect on gas flow patterns including water-vapor transport. Generally, pore water will have significantly higher concentrations of total dissolved solids than perched water or saturated zone water (Benson and McKinley, 1985). The unsaturated zone tends to contain higher salinity pore water with increasing depth, especially if recharge rates have been slow and (or) flow paths have been longer, and evaporative concentration has occurred. Lower salinity zones may be found in the vicinity of surface water. If organic carbon is present, it will tend to be degraded. The chemistry of perched water across the Great Basin is relatively poorly documented. Detailed chemistry work at the Nevada National Security Site, NV, indicates that perched water at that location has a different composition than unsaturated or saturated zone pore water. Chemical analysis seems to indicate that perched water moved through the groundwater system more rapidly, possibly through fractures in unsaturated zone tuff, and isn't the result of upwelling from the saturated zone (Simmons and Neymark, 2012).

Thomas et al. (1996) described the geochemical evolution of the basin-fill aquifer in Smith Creek Valley, NV, as part of the RASA Great Basin program. In Smith Creek Valley, recharge originates as precipitation in the surrounding mountains and solutes in the precipitation are concentrated by evapotranspiration. The water then infiltrates the soil zone and obtains additional ions by dissolving carbon dioxide gas and volcanic rock (ground- mass and phenocrysts, dominantly plagioclase feldspar) to produce a sodium-calcium bicarbonate water. Small amounts of alkali feldspar, gypsum, biotite, and possibly pyrite, illite, and chlorite are also dissolved, each adding ions to the water. Chalcedony precipitates and thus removes ions from the water, and kaolinite (or some other clay mineral) forms as the result of incongruent dissolution of the feldspars. Calcium and magnesium in the water exchange for sodium in clays in the playa area. This ion exchange results in the sodium-calcium bicarbonate water evolving into sodium bicarbonate water. Calcium may also be removed from the water by the weathering of plagioclase to Ca/Na-montmorillonite and the precipitation of a zeolite mineral. Evapotranspiration, dissolution of chloride-containing evaporative salts, and precipitation of calcite and zeolite minerals are the main processes affecting ground-water chemistry in the discharge area. These processes result in the evolution of sodium bicarbonate water into sodium chloride water. Constituents are also added by dissolution of plagioclase and alkali feldspars, gypsum (or other sulfate-containing evaporative salts), and chlorite, and kaolinite is formed by incongruent dissolution. These overall processes are supported by the work of Hershey et al. (2007) for the Basin and Range Carbonate Aquifer System study, located in the eastern part of the Great Basin.

5.1.2.2   *Impacts to radionuclide movement*

For the purposes of long-term geologic storage of spent nuclear fuel, understanding the transport of long-lived transuranic elements are most important. The chief sources of radioactivity from 1,000-10,000 yr are americium and plutonium isotopes. From about 10,000 yr to 10 m.yr. neptunium-237 is the greatest

contributor to the radioactivity of the waste (Langmuir, 1997). Isotopes such as uranium-233, uranium-234, technetium-99, carbon-14, iodine-129, and radium-226 have also been included in total system performance assessments because they are soluble and weakly sorb onto geologic media (Sandia National Laboratories, Chapter 2.4, 2008; Simmons and Neymark, 2012).

Spatial complexity and heterogeneity of alluvial material

Alluvial basins can contain a range of depositional features including: alluvial fans, rivers, streams, and playas. If volcanism occurs in the area as the basin is filling, an additional range of volcaniclastic features can also be deposited. Each of these features contain varying degrees of complexity at a range of scales in diversity of sediment size, grain arrangement, extent and geometry of sedimentary feature, and distribution and density of sedimentary features relative to one another laterally and vertically within a basin. As a primary hydrogeologic parameter, hydraulic conductivity is highly heterogeneous in most alluvial aquifers due to the complex depositional and diagenetic processes of a long-term alluvial fan evolution (Zhu et al., 2017).

Studies on flow and transport in alluvial systems highlight the importance of realistically depicting sedimentary architectures when modeling flow in heterogeneous media (Ronayne et al.; 2008). There is a large body of literature on heterogeneous alluvial-fluvial systems that shows that groundwater flow rate depends not only on connected pathways between high permeability materials but also on the geometry of the more permeable features (Andrade et al. 2000; Hunt 2001; Hunt and Idriss 2009; Ronayne and Gorelick 2006). The percolation threshold may occur at a much lower sand proportion when, for example, elongated connected features are considered (Dell'Arciprete et al. 2014). Preferential flow paths may form through stacked features in different strata (Guin et al. 2010; Ramanathan et al. 2010). Sanjeev (2016) noted that the hydraulic nature of stacked features may change with the number of strata considered.

Based on sensitivity analysis of a simulated heterogeneous alluvial system, Sanjeev et al. (2016) reported that flow in stacked channelized alluvial formations is driven by the contrast between the feature and surrounding material, the number of features, and their shape (width/depth ratio). In their analysis, effective hydraulic conductivity in the vertical direction tended to decrease with increasing channel aspect ratio because laterally extensive and thin features increase horizontal connectedness of low permeability materials which act like barriers to vertical flow.

Solubility, sorption, microbe, and colloid effects

Radionuclide migration would be impeded in the natural barrier system by interactions among water, radionuclides, and immobile mineral phases in rock and sediment. In general, the reduced form of a radionuclide is immobile and the oxidized form is more mobile. As radionuclides migrate from low oxidation potential conditions in the engineered barrier system to the higher oxidation potential condition in the natural barrier system, some may precipitate (or co-precipitate), effectively reducing the mobility of those radionuclides. Furthermore, increased solubility under more oxidizing conditions will not necessarily result in increased mobility because radionuclide availability in the natural barrier system is limited by the conditions in the waste-dominated environment.

In the unsaturated zone, plutonium does not appear to be highly affected by redox condition whereas the solubility of neptunium has been shown to vary several orders of magnitude in oxidizing environments (Efurd et al., 1996). Plutonium and neptunium solubility is expected to decrease with increasing pH and temperature, with plutonium being less soluble (Efurd et al., 1996). Americium solubility is expected to decrease toward neutral pH (Nitsche et al., 1993). Uranium is expected to have relatively low solubility based on estimates from Pena Blanca uranium deposit in Mexico (Langmuir, 1997; Simmons and Neymark, 2012). However, due to the presence of pyrite, redox conditions at Pena Blanca are reducing, and is not analogous to generally oxic conditions expected in upper alluvial fill under evaluation in this

report. Overall, uranium is expected to be slightly more soluble than americium and plutonium (Triay et al., 1997). Uranium solubility depends on the solid phase that will precipitate. It is expected that technetium will be highly soluble and weakly sorptive (Simmons and Neymark, 2012).

Plutonium appears to have a high affinity for ferric oxyhydroxides, manganese oxide, and carbonate mineral surfaces and lower affinity for clays and zeolites (Means et al., 1978; Allard, 1982; Triay et al., 1993; Brady et al., 1999). Work completed at Yucca Mountain found similar results and noted the highest degrees of sorption on samples containing carbonate or clay (Thomas, 1987). Plutonium sorption appears to be most affected by groundwater redox potential and pH, however, it was found that the presence of organic material increased sorption onto iron and aluminium oxides (Simmons and Neymark, 2012). Neptunium is expected to sorb relatively weakly under oxic conditions (Allard, 1982; Meijer et al., 1990). Neptunium appears to have the highest affinity for ferric oxides and oxyhydroxides and minerals containing ferrous iron (Simmons and Stuckless, 2010; Ding et al., 2003, 2006). Generally, neptunium sorption increases with increasing pH. Uranium is also expected to sorb relatively weakly under oxic conditions (Allard, 1982; Meijer et al., 1990). Uranium appears to have an affinity for manganese oxides (Zielinski et al., 1986; Flexser and Wollenberg, 1992). Research into uranium sorption behavior on a range of mineral types is hard to reconcile (Hsi and Langmuir, 1985; Ho and Miller, 1986; Zielinski, 1980; Tsunashima et al., 1981; Ames et al., 1983). In general, the work indicates that uranium does not have a strong affinity for clays or zeolite but has a high affinity for manganese oxides and pure iron oxides (Simmons and Neymark, 2012). Uranium sorption is on the low end and appears to be mainly controlled by pH, carbonate content, and concentrations of Ca and Mg in solution; with higher values resulting in lower sorption (Thomas, 1987).

It is increasingly recognized that subsurface environments, once thought to contain few if any microbes, have significant and diverse communities of microorganisms. In particular, shallow subsurface zones (at least 500 m below land surface) with a relatively rapid rate of water recharge and sandy sediment intervals have higher numbers of microbes. Lower microbe abundance and (or) diversity may be found in subsurface materials containing low amounts of inorganic nutrients and organic matter and with greater depth due to physical straining by small pores as microbes move downward (Maier and Pepper, 2009). Generally, microbes are distributed in the subsurface according to their aerobic and nutrient needs. The distribution of microbe communities in alluvial basins does not appear to have been reported in the literature at this time.

There are two important effects of microbial communities on radionuclide mobility: biodegradation of organic chelating agents by microbes and biotransformation of radionuclide oxidation states. Biodegradation tends to increase radionuclide mobility and has been documented for plutonium and uranium (Mahara and Kudo, 1995; 1998; Avery and Tobin, 1992; Berthelin and Munier-Lay, 1983; Francis et al., 1992; Premuzic et al., 1985; Tsezos and Volesky, 1982a, 1982b). Biotransformation works on the principal that the reduced form of a radionuclide is immobile. Microbially-induced reduction to immobile forms have been reported for uranium, technetium, and neptunium (Kauffman et al., 1986; Lovley et al., 1991; Lloyd et al., 1997; Lloyd et al., 2000).

Colloids are particles 1nm -1 µm in diameter that exist naturally in groundwater in many subsurface environments. Radionuclides can intrinsically form colloids or can adsorb onto nonradioactive colloids like clays or oxides to form psuedocolloids. New colloids can be generated or activated by perturbations in the hydrogeochemistry of subsurface systems (McCarthy and Degueldre, 1993). The more stable a colloid and tendency of a radionuclide to remain sorbed to a colloid may lead to greater transport distances in porous media. Colloids are likely to be unstable in the unsaturated zone at repository depths due to expected higher salinity. Experimental work by Triay et al. (1997) on saturated zone Yucca Mountain colloids suggests that colloidal plutonium can potentially migrate over longer distances once sorbed onto hematite or goethite colloids, and, to a lesser extent, montmorillonite colloids. Colloidal americium appears to show similar behavior (Silva et al., 1995). Documented psuedocolloid migration

distances at the Nevada Test Site range from 300 m (Buddemeister and Hunt, 1988) to 1.3 km (Kersting et al., 1999). Experimentation by McGraw (1996) concluded that hydrophyllic colloids can be rapidly transported through unsaturated media, even larger ones which typically have more limited migration in saturated systems.

O'Melia and Tiller (1993) and Degueldre et al. (1996) noted that pH, redox potential, sodium and calcium concentrations, presence of dissolved organic material, and steady state conditions aid in colloid stability. Namely, under steady state, concentration of alkali elements below 10^{-2} M and alkali-earth elements below 10^{-4} M, and large concentrations of colloidal or dissolved forms of organic carbon increase colloid stability and concentration. Changes in temperature, flow rate, pH, or redox potential can induce larger colloid concentrations (Simmons and Neymark, 2012). The distribution of colloids at a macroscale in alluvial basins does not appear to have been reported in the literature.

Structures

Mid- to late-Cenozoic differential extension in the Great Basin has led to highly extended domains alternating with less extended domains (Gans and Miller, 1983; Wernicke and others, 1984; Smith and others, 1991; Wernicke, 1992). Many of the highly extended domains appear to be separated by lateral faults which form boundaries and transfer strain between differentially extended domains. The highly extended regions also tend to contain smaller, local flow systems compared to less extended domains (Dettinger and Schaefer, 1996).

Transtensional and high-angle extensional faults associated with Great Basin extension can disrupt aquifer continuity and may alter groundwater flow paths into alluvial basins through juxtaposition of units having different hydraulic properties and (or) formation of impermeable material within fault cores. Several studies have noted the impact of faults on groundwater flow through unconsolidated sediment (Bense et al., 2003a; 2003b; Bense and Van Balen, 2004; Heynekamp et al., 1999; Rawling et al., 2001).

Brittle fault zones tend to contain a narrow core of fine-grained, relatively low-permeability gouge or clay smear that is the locus of fault displacement (Caine and others, 1996; Knott, 1993). In rock and consolidated sediment, the core zone can be flanked by faulted and fractured damage zones having enhanced secondary permeability (Caine and others, 1996; Caine and Forster, 1999). Heynekamp et al. (1999) and Rawling et al. (2001) argue that damage zones along faults in unconsolidated sediments do not contain open-fracture networks, but cataclastic deformation bands having reduced permeability. Bense et al. (2003a; 2003b) documented an additional damage zone process in 'clean' sand, called particulate flow, which can double hydraulic conductivity relative to the undisturbed sediment as deep as 1,000 m below land surface. Depths of conductivity enhancement may decrease with the presence of impurities in sand. Bense et al. (2003) also reported widths of low-permeability core zones in unconsolidated sediment on the order 10 cm and damage zone widths on the order of 2 to 5 m. Low-permeability fault cores potentially restrict fluid flow across the fault, whereas the damage zone may conduct groundwater flow to vary degrees, depending on the interplay of cataclasis and particle flow in the damage zone, parallel to the fault zone and if time-relevant regional stress field orientations are conducive to fluid flow (Beard et al., 2013; Harper and Lundin, 1997). It is also possible that core zones are irregular and discontinuous locally, resulting in discontinuous groundwater flow barriers. Chester and Logan (1986) reported considerable variations in the thickness of the core zone along a strand of the San Andreas fault that ranged from about 6 to 90 cm. The hydrologic influence of large-offset transtensional faults in the Great Basin appears to be variable as well. In some cases, transtensional faults impede lateral flow and enhance upward flow that corresponds to the locations of substantial groundwater discharge. Elsewhere, groundwater flow appears to pass directly across normal faults (Sweetkind et al., 2010b).

Secondary minerals can be volumetrically minor, but clays, zeolites, and manganese and iron oxides may be an important factor in retarding radionuclide transport through ion exchange or surface complexation reactions. Little detailed study of secondary minerals across the Great Basin has been reported. Detailed

chemistry work on unsaturated zone secondary minerals at Yucca Mountain indicates that tuff fracture fill material formed from downward percolating fracture water of meteoric origin (Paces et al., 2001; Whelan et al., 2002, 2004; Wilson et al., 2003; Wilson and Cline, 2005; Paces and Whelan, 2012). Fracture fill at Yucca Mountain is predominantly slowly formed calcite that occurs in the upper part of the unsaturated zone where larger amounts of gas flow are likely occurring due to its proximity to soil and atmospheric gases (Whelan et al., 2002).

Bense et al. (2003a, 2003b) reported diagenetic iron-oxide cementation increasing toward the core of a fault in unconsolidated sediment with a corresponding decrease in pore space. The iron-oxide distribution appeared to be concentrated along fine-grained laminae and was probably the result of repeated wetting and drying cycles due to water-table fluctuation. Other areas of increased iron-oxide concentration correspond to deformation features.

Climate

Predicting climate evolution beyond 200 ka is highly uncertain and tends to use understanding of climate variation in recent geological time to estimate the extremes within which climate and related processes may vary (McEvoy et al., 2016). Evidence from the recent geological record indicates a progressive deterioration of global climate from greenhouse conditions in early Cenozoic time (Zachos et al., 2001). Since around 2.6 Ma, multiple oscillations between glacial and interglacial intervals occurred as did longer period 'Milankovitch' cycles influenced by the shape of the Earth's orbit around the sun (Grossman, 2012; Lisiecki and Raymo, 2007; Pillans and Gibbard, 2012; Shackleton, 1987). Mid-latitude regions, including the Great Basin, appear to be sensitive to these global-scale climatic changes with marked variations occurring in prevailing climate over comparatively short periods of geological time (tens of thousands of years; Candy et al., 2011; Rose, 2009) as a result of their position relative to southward moving cold polar air masses and low latitude ocean currents. Even with consideration of anthropogenically-forced climate change, longer-term projections of climate forecast that the Northern Hemisphere will experience further cycling between relatively persistent glacial periods and shorter duration interglacial periods over the next one million years (Huybrechts, 2010; Fischer et al., 2014; Näslund and Brandefelt, 2014). The Great Basin is located far enough south of the farthest extent of ice sheets during glacial maximums in North America that effects of glacial loading, crustal rebound, and permafrost are not significant (Lindgren et al., 2015). Being inland, the effects of sea-level change are also not significant.

Climate records for the Great Basin indicate it is likely to experience hotter and drier arid and cooler, wetter pluvial internals several times over the next million years (Cochran et al., 2001). In terms of impact to radionuclide movement, less precipitation, very slow flux of pore water, and increased evapotranspiration during arid intervals is expected to lead to formation of a thicker unsaturated zone, slower radionuclide transport, and less underflow. Pluvial intervals have much greater effective moisture which leads to higher recharge and erosion rates. Even during pluvial internals, increased water in the system may have a negligible impact to the Great Basin because the rain shadow caused by the Sierra Nevada mountain range limits the number of storms capable of generating precipitation (Dewispelare et al., 1993). Furthermore, Tyler et al. (1996) report that the magnitude of most recent pluvial interval may not have been sufficient to induce recharge. Cochran et al. (2001) also report that increased erosion during wetter climate intervals in the Great Basin was on the order of 2 m is not significant for the purposes of a natural barrier system.

Heat flow

Large-magnitude extension and crustal thinning throughout the Cenozoic have caused elevated heat flow in the Great Basin (Sullivan and Snoke, 2007). Most of the geothermal systems in the Great Basin appear to be associated with Quaternary normal faulting and are non-magmatic (McKenna and Blackwell, 2004; Faulds et al., 2004). Ongoing geodetic measurements indicate continued rapid extension, suggesting that

the crust continues to thin, particularly beneath the Lake Lahontan basin which is generally located in the NW part of the Great Basin (Blewitt et al., 2003). Seismic data indicate that crustal thickness ranges between 24 and 44 km and is thinnest along the NW-SE trending Walker Lane belt (Louie, 2004). Zones of thinner crust correspond to regions of upwelling asthenosphere and higher heat flow where the Moho has moved closer to the surface. The age and origin of thermal fluids is debated but may represent Pleistocene-aged meteoric water (Lutz et al., 2002) and partially mixed magmatic fluids (Moeck et al., 2012).

The difference in density between descending cooler fluids and ascending geothermal water is the major driving force of a geothermal system. Within the Great Basin, convection of thermal fluids induced by elevated heat flow transports heat from the deep subsurface to the surface. Heat flow studies have determined mean heat flow for the Basin and Range is 105 mW-m^{-2} (standard error of mean 5 mW-m^{-2}) (Roy et al., 1968; Costain and Wright, 1973; Reiter et al., 1979; Carrier and Chapman, 1981; Chapman et al., 1981, Eggleston and Reiter, 1984; Moran, 1991; Lachenbruch et al., 1994; Powell, 1997; Henrikson and Chapman, 2002). Fluid movement tends to occur along permeable faults (Blackwell, 2002) and fluid flow velocities tend to be faster than other types of geothermal systems (Bovardsson and Pruess, 1983). Several factors and processes influence convection within the Great Basin: high geothermal gradient, high permeability ($>10^{-14}$ m^2), and high recharge rates that promote natural flow (Hochstein, 1988). Mineral alteration, dissolution, and precipitation processes like silicification, zeolitization, argillitization, and carbonate precipitation are ubiquitous in geothermal systems and may affect permeability and sorption properties of host rock and sediment.

5.2   Natural Barrier System Characteristics

The purpose of this section is to present ranges of known or estimated hydraulic and chemical values relevant for simulating radionuclide movement through a generic unsaturated zone natural barrier system. The discussion begins with an overview of flow processes relevant to the unsaturated zone.

5.2.1   Unsaturated Zone Flow Processes

There are a number of flow processes occurring within the unsaturated zone, which include (Rivett et al., 2011):

- Advection of solutes and (or) colloids and vapor through the matrix and includes any perched zones below a repository where lateral transport is likely.

- Solute dispersion caused by localized variations in flow velocity, but the distance to water table may make the process unimportant in simulation.

- Diffusion of solutes and vapor through matrix, and may be more important than dispersion if pore velocities are slow.

- Water/air phase partitioning

- Solid-aqueous partitioning

- Solid-aqueous sorption that includes colloid and mineral surfaces, adsorption, ion exchange, surface complexation, and precipitation. Where colloid movement is faster than the aqueous phase includes advection, matrix diffusion, dispersion, sorption, radioactive decay, and particle filtration of colloid.

- Adsorption air-water interface

- Vapor adsorption to solid

- Intragranular sorption

- Abiotic chemical reaction

- Microbial reaction

5.2.2   Water Budget

5.2.2.1   Recharge

Most arid soils throughout the southwest United States have experienced little to no recharge or deep infiltration in the past 10,000 yrs (Phillips 1994). Prior to groundwater development beginning largely in the 1940s, total recharge in the Great Basin Carbonate and Alluvial Aquifer System was estimated to be 15,200,000 m^3/d $\pm$ 50% over an area of approximately 177,000 km^2. The primary source of groundwater recharge is direct infiltration of precipitation. The estimated average 1940–2006 in-place recharge from precipitation is 9,800,000 m^3/d. Other forms of recharge include infiltration of surface-water runoff including irrigation return flow (1,900,000 m^3/d), recharge from mountain streams (440,000 m^3/d), recharge from imported surface water (3,300,000 m^3/d), and subsurface inflow (not estimated) (Heilweil and Brooks, 2010).

Recharge in the Death Valley Regional Flow System, which encompasses approximately 100,000 km^2, was estimated from net infiltration using a deterministic mass-balance method. The INFILv3 model simulated a mean annual potential recharge to the flow system of about 125 Mm^3 for the period 1950–99 (Faunt et al., 2010; Heveshi et al., 2003). The mean annual groundwater flow into the Death Valley Regional Flow System is estimated to be about 18.4 Mm^3 (Faunt et al., 2010). For the Death Valley area, Heveshi et al. (2003) reported a spatially averaged net-infiltration estimate of 7.8 mm/yr and a maximum net-infiltration rate of 363 mm/yr (in the Spring Mountains).

At the Nevada National Security Site, where alluvium has been studied extensively, environmental tracers indicate that in many locations recharge has not occurred for the last 100 kyr (Walvoord and Phillips 2004; Kwicklis et al. 2006; Tyler et al. 1996). Even in the event of future pluvial climate conditions, the paleohydrologic evidence at the Nevada National Security Site shows that downward liquid flux would likely be in the range of 5 to 10 mm/yr, which is much less than the saturated hydraulic conductivity (Hardin et al., 2012).

5.2.2.2   Discharge

Prior to groundwater development, total groundwater discharge in the Great Basin Carbonate and Alluvial Aquifer System was estimated to be 14,200,000 m^3/d $\pm$ 30%. The two major components of discharge are evapotranspiration and springs. Estimated groundwater discharge to evapotranspiration and springs for predevelopment conditions was 6,100,000 m^3/d and 3,300,000 m^3/d, respectively. Other forms of discharge include discharge to basin-fill streams, lakes, and reservoirs (2,200,000 m^3/d), discharge to mountain streams (5,200,000 m^3/d), and subsurface outflow (not estimated). Some previously reported estimates of discharge to evapotranspiration and springs were made while groundwater withdrawals were occurring; an additional 1,100,000 m^3/d adjustment to natural discharge for well withdrawals was estimated for the predevelopment groundwater budget (Heilweil and Brooks 2010).

Mean annual discharge from evapotranspiration for the Death Valley Regional Flow System is estimated at about 115.5 Mm^3 (San Juan et al., 2010). Annual natural discharge from springs not accounted for in evapotranspiration studies is estimated at about 16.8 Mm^3. The mean annual groundwater flow out of the flow system is estimated to be about 9.5 Mm^3 (Faunt et al., 2010).

5.2.3   Physical Properties

Among the physical parameters for alluvium, the most important for unsaturated flow simulation are: saturated porosity, residual moisture, saturated hydraulic conductivity, and parameters that describe functional relationships between moisture content and pressure head (water retention curve) and moisture content and unsaturated hydraulic conductivity (Cochran et al., 2001). A mean valley floor hydraulic gradient of 0.005 m/m was calculated from Lopes et al (2006). The smallest gradients in the flattest part of each alluvial valley were selected to minimize basin-floor topography that is desirable for repository siting.

The Greater Confinement Disposal units at the Nevada National Security Site, NV, are vertical boreholes drilled in unsaturated desert alluvium. The boreholes were used for the disposal of waste, including transuranic waste, from 1983 through 1989. Waste packages were placed in boreholes between approximately 21 to 37 m below land surface and the holes were then backfilled with native alluvium. The system has been characterized and monitored; the results of which provide useful information in understanding unsaturated alluvial systems in general (REECo, 1993 and references contained within Cochran et al., 2001). Particle size analysis at the Science Trench Boreholes, within the Greater Confinement Disposal units, indicates unsaturated alluvium contains variable assemblages of grain sizes and is considered geologically heterogeneous. UE5PW-1 displays a general fining upward sequence until approximately 40 m below land surface, where a coarsening upward sequence begins and continues to the surface. UE5PW-2 appears to have two fining upward sequences, one from 125 m to the surface, and another from 250 to 125 m. UE5PW-3 has an overall fining upward sequence interrupted by a coarse section from approximately 75 to 85 m below land surface. The profiles are predominantly coarse sand and gravel with accessory silt and clay. The alluvium composition is estimated to be 20% gravel, 70% sand, and less than 8.5% silt / clay. Volumetric water contents throughout the unsaturated zone are very small, ranging from about 5% to about 15% below about 2 m from land surface, showing an increasing trend with depth in the upper 35 m. Very near the ground surface they can be as low as 1% to 3%. The overall average moisture content at depths beneath 35 m is less than 10%. With an average porosity of about 30%, water fills less than one third of the void space. Estimating upward advection is difficult under arid conditions. An upward advective water flux of 10^{-2} to 10^{-1} mm/yr has been estimated for the Greater Confinement Disposal units that results in upward advective migration of about 1 m in 10,000 years (assuming a volumetric moisture content of 10%).

In a subsequent study at the Nevada National Security Site, Kwicklis et al. (2006) measured and simulated depth profiles in the upper 50 m of alluvial material for moisture content, saturation, and water potential, simulated vapor flux to a depth of 100 m, and simulated liquid flux to a depth of 500 m. Their work also estimated tortuosity for alluvium. The simulations report an average water content of about 8%. Liquid fluxes below a depth of approximately 63 m are downward and increase with depth, eventually reaching a maximum of about 0.13 mm/yr just above the water table (~490 m below land surface). Above a depth of 63 m, liquid fluxes are upward and increase to a maximum of 0.011 mm/yr at a depth of about 15 m. Liquid fluxes decrease between depths of 15 to 2 m probably due to the root zone at 2 m. As liquid water fluxes decrease, vapor fluxes increase and reach a maximum of about 0.02 mm/yr at depths of about 3 to 4 m. At depths below about 30 m, there is a relatively constant upward vapor flux of 0.0025 mm/yr.

Brooks et al. (2017) provide a compilation of hydraulic parameters that represents analyses completed for the Death Valley Regional Flow System (Belcher et al., 2001) and the Great Basin Carbonate and Alluvial Aquifer System (Brooks et al., 2014; Stolp et al., 2017). Bunch and Harill (1984) also reported hydraulic conductivities of RASA-Great Basin basin-fill deposits (not included in the table below) derived from aquifer tests of 17 wells that range from 0.006 to 40 m/d, that is considered applicable to basin-fill deposits that have not been reworked by perennial streams (Harrill et al., 1998). The mean and median values for all 17 wells are 24 and 25 m/d, respectively. Ranges of hydraulic conductivity were

compiled for broad physiographic settings by Plume (1996), who concluded that values of hydraulic conductivity should be larger toward basin margins and smaller, and within broader ranges, near the basin axis. Hydraulic properties from these sources are presented in Table 5-1.

Masbruch et al. (2014) also report horizontal-to-vertical anisotropy estimates from their calibrated model for Snake Valley, UT, which includes estimates for playa deposits. Tortuosity was estimated for the upper 1.55 m at Owens Dry Lake, CA, as being from 0.11 to 0.60 (Tyler et al., 1997). Values for the heat capacity of playa deposits were not found in a literature search.

Porosity values are derived from Domenico and Schwartz (1998), Smyth et al., (1979), and Kwicklis et al. (2006). Values are the result of field observations at a limited number of wells (n = 2) and simulation-derived estimates. Morris and Johnson (1967) report a range of porosities observed for playa materials from 0.26 to 0.57.

Thermal conductivity of alluvium is low with measured values on re-compacted samples ranging from 0.5 to 0.8 W/m-K, and in situ values in the range 1 to 1.2 W/m-K (summarized by Hardin et al. 2012; estimated from regional heat flow and the existing geothermal gradient by Smyth et al. 1979). Eppelbauem et al. (2014) report a range of thermal conductivities for playa material from 0.8 to 2.1 W/m-K.

Table 5-1   Summary of compiled hydraulic properties for alluvial material applicable to the western United States and that will be applied to the generic flow and transport simulation

Hydraulic parameter	Lower basin fill	Upper basin fill, non-playa	Upper basin fill, playa
Horizontal hydraulic conductivity – geometric mean (m/d)	0.06	1.5	3.0
Horizontal hydraulic conductivity – arithmetic mean (ft/d)	1.5	11	10
Horizontal hydraulic conductivity – minimum (m/d)	0.00003	0.00006	0.003
Horizontal hydraulic conductivity – maximum (m/d)	6.1	130	34
Horizontal hydraulic conductivity – 95-percent confidence interval of geometric mean (m/d)	0.00006 – 80	0.006 - 430	0.02 – 460
Vertical anisotropy – initial value (unitless)	1.00	10.00	—
Vertical anisotropy – minimum reasonable (unitless)	0.10	1.00	—
Vertical anisotropy – maximum reasonable (unitless)	10.00	5000	—
Horizontal-to-vertical anisotropy (unitless)	9.9	9.9	51
Horizontal-to-vertical anisotropy – 95-percent confidence interval (unitless)	2.0 – 49	2.0 – 49	19 – 133
Tortuosity – estimated value (unitless)	0.63		0.11 – 0.60
Tortuosity – 95-percent confidence interval (unitless)	0.41 – 0.99		—
Porosity (unitless)	0.3 – 0.5		0.26 – 0.57
Thermal conductivity of alluvium (W/m-K)	0.5 – 1.2		0.8 – 2.1
Rock heat capacity (MJ/m^3/K)	2.30 – 2.54		—

Dashed line indicates no value reported.

Brooks et al. (2016); Masbruch et al. (2014); Tyler et al. (1997); Domenico and Schwartz (1998); Smyth et al., (1979); Kwicklis et al. (2006); Hardin et al. 2012; Wildemeersch et al. (2014), Eppelbauem et al., 2014; Morris and Johnson, 1967

Heat capacity data for several mineral groups (smectite, illite, cristobalite, quartz, feldspar, muscovite, and calcite) are summarized in Bechtel (2004). Bechtel (2004) also reports calculated rock heat capacities relevant to Yucca Mountain, NV. Alluvial material is lumped with the Tiva Canyon Tuff and is not reported separately. Wildemeersch et al. (2014) modeled and measured heat capacity values for shallow alluvial material composed of clay, sand, and gravel (0 to 10 m below land surface) in Belgium that resulted in heat capacity values of 2.54 and 2.30 MJ/m^3/K, respectively.

Unsaturated zone parameter values derived from measurements and calculations from the Greater Confinement Disposal Boreholes, NV, are summarized in Table 5-2. Details on the sample wells and method used to fit the measurements into van Genuchten and Mualem functions are discussed in Appendix D of Cochran et al. (2001). The mean parameter values of the distributions developed in Shott et al. (1998) are also listed.

Table 5-2   Unsaturated alluvium hydraulic property values from the Greater Confinement Disposal Boreholes, Nevada National Security Site, NV, that will be applied to the generic flow and transport simulation

Parameter	Mean value	Value
Saturated hydraulic conductivity (m/d)	0.82	0.72
Residual moisture content (unitless)	0.06	0.065
Saturated moisture content (unitless)	0.33	0.36
van Genuchten fitting parameter (cm^{-1})	0.071	0.036
van Genuchten fitting parameter (unitless)	1.4	1.94
Reference	Cochran et al. (2001)	Shott et al. (1998)

5.2.4   Chemical Properties

Thomas et al. (1996) studied a closed alluvial basin, Smith Creek Valley, NV, as part of the US Geological Survey RASA Great Basin project. They report that playa sediments are composed of 77 to 93% silt and clay. Clay-mineral analyses (Table 5-3) indicate the playa-area sediments consist primarily of illite and mixed-layer montmorillonite and illite, with lesser amounts of montmorillonite and kaolinite. Quartz, plagioclase, potassium feldspar, and calcite are also present. X-ray diffraction analysis of bulk sediment samples indicate that the zeolite minerals natrolite, thomsonite (or a zeolite intermediate between the two), and clinoptilolite are present also. In addition, the non-clay minerals quartz, feldspar, chlorite, gypsum, and calcite were identified.

Stoller-Navarro Joint Venture (2005) reported on a range of characteristics of alluvium in and around the Nevada National Security Site, NV. A summary of the whole rock mineralogy for alluvial material is listed in Table 5-4.

Table 5-3   X-ray diffraction analyses of playa-area sediments, Smith Creek Valley, NV. Generally, it is expected that montmorillonite and kaolinite have a great ability to sorb transuranic species than illite.

Site	Sample depth (ft)	Clay content	Relative abundance*							
			Clay minerals				Non-clay minerals			
			Illite	Mont-morillonite	Mixed layer**	Kaolinite	Quartz	Plagioclase	K-feldspar	Calcite
A	2.0	Moderate	1	3	—	2	1	2	3	—
	21.5	Minor	1	2	—	—	1	2	—	—
B	5.5	Abundant	3	1	—	2	1	3	2	—
	23.0	Minor	1	—	2	—	1	—	2	—
	34.0	Moderate	1	—	2	3	1	3	2	—
C	7.5	Moderate	2	3	1	4	1	2	3	4
	22.5	Minor	1	—	2	—	1	—	2	—
	34.0	Abundant	2	—	1	3	2	3	1	—
D	5.5	Moderate	1	—	2	—	1	2	—	3
	22.5	Abundant	2	—	1	3	1	2	—	3
	27.0	Abundant	2	—	1	3	1	2	—	3
E	16.5	Moderate	2	—	1	3	1	2	3	—

Dashed line indicates no value reported.
*Mineral abundance is an arbitrary ranking of relative amounts of mineral in each sample, with 1 representing the most abundant mineral and 4 the least abundant mineral.
**Interlayered montmorillonite-illite
Thomas et al. (1996)

Table 5-4   Whole rock mineralogy of alluvium for selected locations around the Nevada National Security Site, NV

Location	Mass % smectite	Mass % mica	Mass % zeolite	Mass % hematite	Mass % calcite
Yucca Flat	30	3.4	1.3	—	18.2
Beatty Low Level Waste Disposal Site	3	1	3	—	—
Beatty Low Level Waste Disposal Site	5.5	1	3	—	—
Beatty Low Level Waste Disposal Site	3	1	3	—	—
Yucca Flat	0	2.5	3		
Frenchman Flat	11.6	3.3	19.7	0.3	2.6

Dashed line indicates no value reported.
Stoller-Navarro Joint Venture (2005)

5.2.4.1   *Pore fluid and vapor chemistry of Great Basin alluvial material*

The main processes controlling the geochemical evolution of ground water in arid basin-fill aquifers in the Great Basin are: dissolution of volcanic tuff and tuff-derived basin-fill deposits; cation exchange of calcium and magnesium in the water for sodium in clay minerals; weathering of plagioclase to montmorillonite; precipitation of zeolite minerals; concentration of dissolved constituents by evapotranspiration; dissolution of chloride and sulfate evaporative salts; and precipitation of calcite (Thomas et al., 1996).

Major and minor ion geochemical and isotope tracer data for pore and vapor chemistry from alluvial aquifers in the Great Basin has been variously reported and compiled in key geochemical studies such as

Thomas et al. (1996), Hershey et al. (2007) and Gardner and Masbruch (2015) though other sources of geochemical data also exist in the literature, US Geological Survey National Water Information System, and state information systems. Example data are presented in Table 5-5. Characterization work completed for the Greater Confinement Disposal Boreholes at the Nevada National Security Site, NV, includes geochemical measurements for unsaturated zone alluvial material (Estrella et al., 1993; Cochran et al., 2001). The Nevada National Security Site Underground Test Area GEOCHEM04 (Stoller-Navarro Joint Venture, 2004) database also contains geochemical information sometimes not available in the other sources. A summary example from Smith Creek Valley, NV and from the Greater Confinement Disposal Boreholes are listed below (Thomas et al., 1996; Estrella et al., 1993; Cochran et al., 2001). No measured values for vapor phases (such as CO_2 or CH_4 abundances) in the Great Basin was found in the literature. Thomas et al. (1996) also reported that dissolved-solids concentration increases from 90 mg/L in the recharge area to 51,000 mg/L in the discharge area in Smith Creek Valley.

Table 5-5   Chemical characteristics (mg/L) of unsaturated zone alluvial material from the Great Basin

Chemical Parameter	Precipitation	Recharge	Na-Ca-HCO₃	Na-HCO₃	Na-Cl water	Ue5ST-1 82.5–82.75	Ue5ST-1 115.0-115.25
pH*	—	7.8	6.9	6.9	7.7	7.00 – 9.00	7.00 – 9.00
Na^+	0.7	16.0	35	112	9,044	2,000	1,710
Ca^{+2}	1.1	9.8	28	14.3	251	44.1	203
K^+	0.3	2.1	6.2	7.0	102	102	104
Mg^{+2}	0.2	1.6	4.5	2.0	74	28.1	92.0
Cl^-	2.2	5.6	20.4	38.7	13,100	2,130	2,310
SO_4^{-2}	1.5	11.0	36	14.7	3,680	—	—
SO	—	—	—	—	—	373	276
SiO_4^{-4}	—	36	58	21.7	10.2	—	—
SiO	—	—	—	—	—	70.0	70.0
TIC**	—	59	115	287	872	1,386	1,306
NO	—	—	—	—	—	24.0	2.8
Location	Smith Creek Valley, NV	Smith Creek Valley, NV	Smith Creek Valley, NV	Smith Creek Valley, NV	Smith Creek Valley, NV	Frenchman Flat, NV	Frenchman Flat, NV
Reference	Thomas et al. (1996)	Thomas et al. (1996)	Thomas et al. (1996)	Thomas et al. (1996)	Thomas et al. (1996)	Estrella et al. (1993)	Estrella et al. (1993)

Dashed line indicates no value reported.
*Standard units
**TIC = total inorganic carbon

Taken together this work indicates that pore water having pH 6 to 8.5 and moderate ionic strengths might be expected in a generic unsaturated zone concept for a natural barrier system (Simmons and Neymark, 2012).

5.2.4.2   Radionuclide solubility

Generally, oxidizing conditions such as those typically observed in the unsaturated zone, lead to higher radionuclide solubility than more reducing conditions. Radionuclide solubility limits provide an upper bound on radionuclide concentrations that could go into solution and a basis for examining long-term radionuclide behavior. Solubility experiments of transuranic species are uncommon and solubility experiments involving unsaturated zone alluvium were not found in a literature search. Calculated solubility, particularly related to work at corrective action units at the Nevada National Security Site, NV, are reported in the literature (e.g., Yu, 2007; Stoller-Navarro Joint Venture., 2006). In terms of

experimental work, Erfud et al. (1996) conducted solubility experiments on low ionic strength Yucca Mountain water from well J-13 over a range of temperature and pH conditions. J-13 water represents water that has interacted with unsaturated zone tuff, but not alluvial material.

Erfud et al. (1996) report that neptunium has a molar solubility that ranges from $5.8\pm2.5 \times 10^{-6}$ to $9.4\pm1.2 \times 10^{-4}$ M and plutonium that ranges from $3.6\pm1.1 \times 10^{-9}$ to $4.7\pm1.1 \times 10^{-8}$ M over temperature ranges from 25 to 90 °C and pH from 6.0 to 8.5. Over the same temperature and pH ranges, Nitsche et al. (1993) report americium solubility that ranges from $3.1\pm1.7 \times 10^{-10}$ to $3.6\pm0.7 \times 10^{-6}$ M. Langmuir (1997) reported U solubility $\sim10^{-7}$ M. These are relatively low solubility values, indicating more insoluble behaviors. These values are all for oxidizing conditions. Cochran et al. (2001) also report calculated solubility for radionuclides in unsaturated alluvium studied at the Greater Confinement Disposal Boreholes at the Nevada National Security Site (NNSS). Ranges for oxidizing conditions are shown in Table 5-6.

Table 5-6   Molar solubility values for radionuclides for purposes of modeling radionuclide transport. These are relatively low solubility values, indicating more insoluble behaviors. These values are all for oxidizing conditions.

Species	Minimum value	Maximum value	Expected value
Pu	3×10^{-9}	10^{-6}	5.1×10^{-7}
Am	10^{-10}	10^{-6}	5×10^{-7}
Np	5×10^{-6}	10^{-3}	1.4×10^{-4}
U	10^{-8}	10^{-2}	3.2×10^{-5}

Triay et al. (1997), Langmuir (1997); Rechard (1995); Efurd et al. (1996)

NOTE: Values are from expert elicitations, except where updated by experimental data from Efurd et al. (1996)

5.2.4.3   Sorption coefficients

The solubility limits of radionuclides can act as an initial barrier to radionuclide migration from an engineered barrier system. Once radionuclides dissolve in water that is moving to the natural barrier system, sorption of radionuclides onto the surrounding alluvial material becomes a second barrier.

Sorption coefficient values are empirical and represent a very simplistic model of sorption on soil, sediment, or rock. Sorption coefficient values are highly dependent on environmental factors, including but not limited to pH, redox condition, particle size distribution, organic matter content, biological activity, and temperature. Ideally, site-specific sorption coefficients should be determined for the range of aqueous and geological conditions in the specific system to be modeled. However, literature-derived values are commonly used for screening calculations. Mechanistic models are a more robust approach because they explicitly account for sorbate concentration, charge, competing ion concentration, variable surface charge on the alluvial material, and solution species distribution. Truly mechanistic adsorption models are rarely applied mainly because natural mineral surfaces are very irregular and difficult to characterize. Zavarin (2004) developed a method to upscale mechanistic models to assign sorption coefficients that has been applied at the Nevada National Security Site.

In the past laboratory sorption data acquired for radionuclide transport were based on experiments conducted under atmospheric (oxidizing) conditions mainly because of the simplicity of the tests and when the system under evaluation was thought to be predominantly under the influence of oxic water. There is a growing body of literature evaluating sorption under reducing conditions, such as in microbially-induced anoxic environments. Hu et al. (2008) report measured radionuclide sorption coefficients under a range of oxic-anoxic conditions appropriate for tuff and alluvium in the unsaturated system at the Nevada National Security Site.

Primary sources of alluvium sorption data include Frenchman Flat specific laboratory values in Wolfsberg (1978a) and a memorandum written by Wolfsberg (1978b); however, mineralogy of the rock

samples and water chemistries used during these experiments were not included in the documentation making these values difficult to interpret. Yucca Flat alluvial experiments were reported in Wolfsberg et al. (1983) and Zavarin et al. (2002). Additional data were available from the Beatty Low-Level Waste Storage Facility (Wolfsberg et al., 1983) and the Yucca Mountain Project data discussed by Triay et al. (1997), DOE/ORD (2001), and DOE/ORD (2004) and stored in the Yucca Mountain Project Technical Data Management System.

Generally, existing sorption data suggest Pu and Am are sorbing to strongly sorbing and Np, U, and Tc are weakly sorbing to sorbing on unsaturated alluvium at the NNSS . Sorption coefficients for alluvium at the NNSS are shown in Table 5-7.

Table 5-7   Radionuclide sorption coefficients (mL/g) for alluvium at the Nevada National Security Site, NV. Reported values will be applied to the generic flow and transport simulation

Species	(Value, probability)	Best value (range)	Best value (range)	Mean value ± st dev (range)	Value
Pu	mean = 100; range = 50 to 300; standard deviation = 15	0.9 (1.4 – 0.4) ($O_2 = 10^{-5}$) 1.3 (1.8 – 0.8) ($O_2 = 10^{-10}$) 1.9 (2.3 – 1.4) ($O_2 = 10^{-15}$)	2.1 ($O_2 = 0.2$)	4,091 ± 4,448 (230 – 21,000)	
Am	Range = 1,000 to 10,000; mean = 5,500; standard deviation = 1,500	3.7 (4.1 – 3.4)	4.2 (4.7 – 3.7)	174,469 ± 214,582 (3,200 – 1,400,000)	
Np	(1.8, 0.) (4.0, 0.05) (8.7, 0.95) (13, 1.0)	0.7 (1.1 – 0.3)	1.5 (2.0 – 1.1)	8.57 ± 5.08 (1.83 – 22)	25 to 30 over pH 7.5 to 8.5
U	(0, 0.) (5.39, 0.05) (8.16, 0.95) (20, 1.0)	0.4 (0.8 – 0.03)	0.8 (1.3 – 0.3)	6.36 ± 5.04 (0.9 – 60)	
Am	Range = 1,000 to 10,000; mean = 5,500; standard deviation = 1,500	3.7 (4.1 – 3.4)	4.2 (4.7 – 3.7)	174,469 ± 214,582 (3,200 – 1,400,000)	
Tc	0			2.16 ± 3.48 (0 – 12)	
Material	Alluvium, devitrified	Alluvium	Alluvium	Alluvium*	Alluvium
Location	Yucca Mountain	Frenchman Flat	Frenchman Flat	Nevada Test Site	Fortymile Wash
		calculated	calculated	measured	measured
Reference	Sandia National Laboratories (2008)	Zavarin (2004)	Tompson et al. (2001)	Hu et al. (2008)	Bertetti and Werling (2004)

5.3   Simulation

Simulations assume (1) a mined repository at 255 m depth; (2) a head gradient of 0.005 m/m from west to east (Lopes et al., 2006); (3) a regional heat flux of 105 mW/m² (Roy et al., 1968; Costain and Wright, 1973; Reiter et al., 1979; Carrier and Chapman, 1981; Chapman et al., 1981, Eggleston and Reiter, 1984;

Moran, 1991; Lachenbruch et al., 1994; Powell, 1997; Henrikson and Chapman, 2002) and a mean annual surface temperature of 25 °C (Strahler, 1989); and (4) an unsaturated model domain.

Processes accounted for in the simulation include waste package degradation, waste form (UO2) dissolution, equilibrium-controlled radionuclide sorption and precipitation/dissolution, radioactive decay and ingrowth in all phases (aqueous, adsorbed, precipitate), coupled heat and fluid flow, and radionuclide transport via advection and diffusion. Mechanical dispersion is conservatively neglected in this iteration of the unsaturated zone reference case. Including it would result in earlier arrival of radionuclides at observation points, but lower peak concentrations.

5.3.1   Numerical Implementation

Simulations will comprise one deterministic simulation of the 12-PWR case and a suite of probabilistic simulations for the 12-PWR case using *GDSA Framework*. The unstructured mesh was gridded with Cubit (Blacker et al. 2016). Probabilistic inputs for the simulations will be prepared using Dakota's Latin Hypercube Sampling (LHS) capability. Simulations of flow and transport will be run with PFLOTRAN (Hammond et al. 2014).

5.3.2   Model Domain and Discretization

The model domain was gridded for 12-PWR simulations. The half-symmetry model domain is 3915 m in length (X), 1065 m in width (*Y*), and 1005 m in height (*Z*). Observation points were placed 30 m down-gradient of the repository, in the upper basin fill unit immediately underlying the upper basin fill confining unit that contains the repository, in the upper basin fill aquifer unit, and the lower basin fill unit. Most of each domain is discretized into cells 15 m on a side. Emplacement drifts within the domain are discretized into cells 1.67 m (5/3 m) on a side. The domain contains 2,402,205 cells.

Figure 5-6 shows an example of the configuration of the repository and natural barrier system.

5.3.3   Material Properties

Natural barrier material properties are discussed earlier in this chapter and include deterministic parameter values and sampled parameter ranges. The simulation will draw from this information.
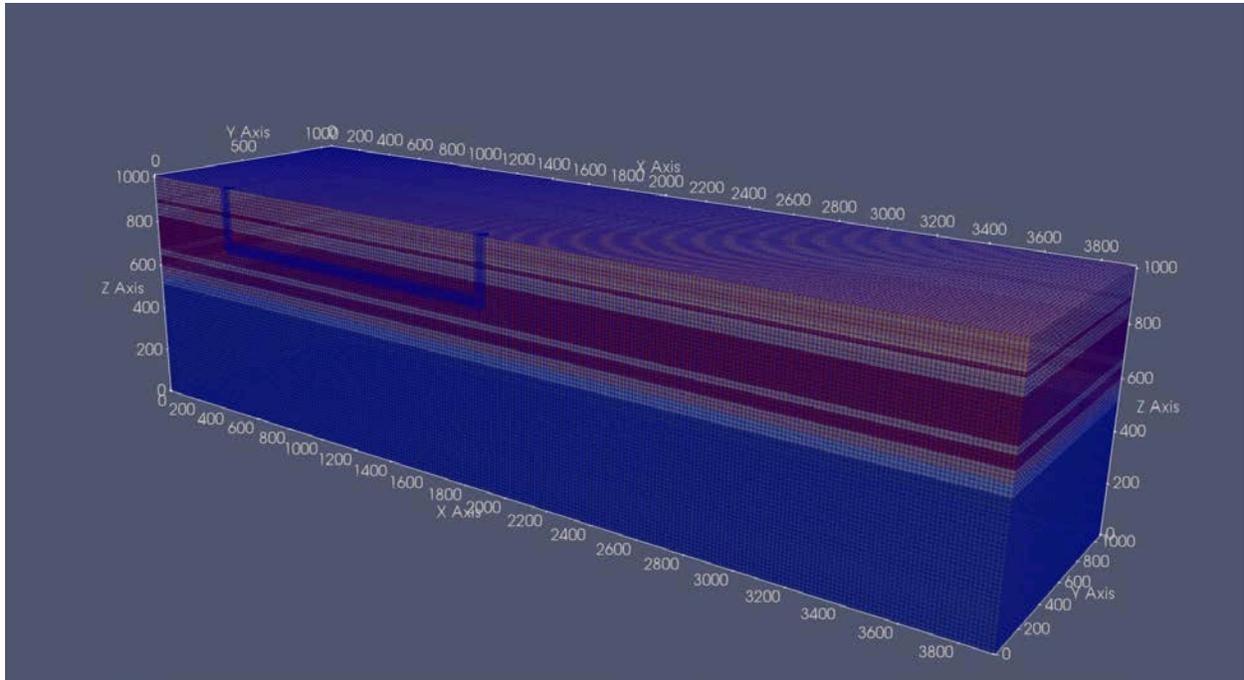
Figure 5-6   Example of the configuration of the repository and natural barrier system that will be simulated in PFLOTRAN. Light pink represents upper basin fill confining units, red represents upper basin fill, light blue represents the upper basin fill aquifer, and darker blue represents lower basin fill. The blue "U" shaped feature show a vertical slice through the repository where gridding is finer. Distances along the axes are in meters, where 1000 m is land surface and 0 m is the bottom of the model domain. The left side of the figure represents a western direction.

6.   SUMMARY AND CONCLUSIONS

This report describes the FY 2018 activities of the Geologic Disposal Safety Assessment (GDSA) group of the Spent Nuclear Fuel and Waste Science and Technology (SFWST) Campaign. The primary mission of the GDSA group is to develop a geologic disposal system modeling capability for nuclear waste that can be used to probabilistically assess the performance of disposal options and proposed sites. The GDSA capability is a framework called *GDSA Framework* that employs HPC-capable codes PFLOTRAN and Dakota. In FY 2018 the GDSA group:

- Added and improved repository modeling and analysis capabilities;

- Added multiple verification tests to quality assurance documentation;

- Expanded integration with other work packages;

- Exercised new sensitivity analysis capabilities on the shale reference case;

- Developed a new generic reference case for unsaturated alluvium;

- Conducted two PFLOTRAN/*GDSA Framework* short courses; and

- Presented *GDSA Framework* capabilities at international conferences and meetings.

Code development this year focused on adding sensitivity analysis capabilities, improving user initialization of multi-phase conditions in cells, designing a model framework for multiple waste package degradation processes, exploring possible surrogate modeling approaches, and adding new quality assurance test cases.

Sensitivity analysis capabilities of *GDSA Framework* were improved by adding stepwise linear regression, a mainstay of traditional performance assessment sensitivity analysis. Stepwise regression sequentially identifies and includes only those input parameters having the greatest dependence. This regression tool is especially useful when considering a large number of uncertain inputs because it eliminates insignificant parameters, identifies unstable regression coefficients, and avoids overfitting the model.

With the development of a new reference case for unsaturated host rock, an improved method for initializing conditions in cells in regions of unsaturated sediments was needed. A spin-up simulation is required to create and define a physically consistent set of initial values for cells of an unsaturated region. This year, the work flow for the spin-up simulation was established, and the ability for PFLOTRAN to capture the self-consistent values was generalized.

The coupling of process models to *GDSA Framework* was examined this year on two fronts: for waste package degradation and for possible development of rapid surrogate models. In the case of waste package degradation, multiple processes (e.g., general corrosion, pitting corrosion, stress corrosion cracking, etc.) act to degrade waste packages. A model framework to execute and track degradation for each coupled process model for each waste package was developed for implementation in FY 2019. In addition, an investigation began into the potential for rapid surrogate models to emulate complex process models. Simulations having thousands of waste packages cannot have waste package or waste form process models, such as the Fuel Matrix Degradation model, that perform a large number of calculations at each call. If adequate surrogate models can be developed, such process models can be effectively coupled in PA calculations.

A major effort was made this year to enhance integration of work packages across the campaign. The agenda of the 2018 SFWST Annual Working Group Meeting was largely planned by the GDSA group to facilitate integration communication. At this meeting, "evaluation" sessions were held that were aimed at assessing the current state-of-the-art of various ongoing R&D activities, the remaining R&D effort

appropriate for those activities, and the current priority of those activities for each of the major generic repository host-rock environments. Results of these sessions are documented in this report. The sessions were conducted in preparation for the SFWST Roadmap Update Workshop in FY 2019. The SFWST Roadmap Update Workshop is scheduled for January 2019.

As part of the GDSA Uncertainty and Sensitivity Analysis Methods work package, initial steps were taken in FY 2018 to ensure that *GDSA Framework* has a comprehensive sensitivity analysis capability. Traditional repository PA methods (stepwise linear regression, simple and partial correlation coefficients) and more computationally expensive variance-based methods were addressed. The former methods work well when the system can be approximated with a linear (or monotonic), additive model. The latter can be applied to highly coupled nonlinear models to capture nonlinear (nonmonotonic) dependencies and parameter interactions. The shale reference case developed in FY 2017 was used to exercise the new set of capabilities and to calculate sensitivity indices using various methods including polynomial chaos expansion and Gaussian process modeling.

In addition, as part of the GDSA Repository Systems Analysis work package, a new unsaturated alluvium reference case was conceptualized this year. This reference case considers the thick alluvial valleys of the Great Basin in the western United States and the low-permeability playa/lacustrine sediments situated therein. Several features of this type of host rock are favorable to waste isolation, including low groundwater fluxes, low permeability, and low water saturation. This type of environment is favorable to the disposal of dual purpose canisters because low water saturation greatly reduces the possibility of criticality events. This report focuses on the natural barrier system, movement of water through these sediments, and the physical and chemical characteristics of the host rock. A reference case repository layout is under development and has been meshed for *GDSA Framework* simulation in FY 2019.

As in the previous year, significant effort went into publications, presentations, short course offerings, expanding the user base, and establishing a broader user group of *GDSA Framework* collaborators. Results and developments of *GDSA Framework* were presented in several international venues. In addition, two PFLOTRAN workshops were held, one in Albuquerque and one in Taiwan. Outreach like this supports a primary objective of the GDSA work package by facilitating testing of, and feedback on, PFLOTRAN and *GDSA Framework* and by increasing the likelihood outside users will contribute directly to code development in the future. Collaboration with outside users is made possible by online version control systems (e.g., Bitbucket.org) and open source access. By encouraging and facilitating use in the outside community, we expect to accelerate development of *GDSA Framework* and to establish *GDSA Framework* as a leading geologic repository safety assessment tool.

Progress in the development of *GDSA Framework* continues to affirm that HPC-capable codes can be used to simulate important multi-physics couplings directly in a total system performance assessment of a geologic repository. The generic repository applications modeled to date indicate that the developing capability can simulate complex coupled processes in a multi-kilometer domain while simultaneously simulating the coupled behavior of sub-meter-scale features and processes within the repository.

While *GDSA Framework* has greatly advanced over the past several years, continued development is needed to ensure it is ready for application to potential sites that may be selected in the near future. The challenge is to address the remaining needs using available resources. Meeting this challenge will require close integration with technical teams across the SFWST Campaign.

7. REFERENCES

Adams, B. M., K. R. Dalbey, M. S. Eldred, L. P. Swiler, W. J. Bohnhoff, J. P. Eddy, D. M. Vigil, P. D. Hough and S. Lefantzi (2012). DAKOTA, A Multilevel Parallel Object-Oriented Framework for Design Optimization, Parameter Estimation, Uncertainty Quantification, and Sensitivity Analysis: Version 5.2+ User's Manual. SAND2010-2183. Sandia National Laboratories, Albuquerque, New Mexico.

Adams, B. M., M. S. Ebeida, M. S. Eldred, G. Geraci, J. D. Jakeman, K. A. Maupin, J. A. Monschke, J. A. Stephens, L. P. Swiler, D. M. Vigil, T. M. Wildey and e. al. (2018). Dakota, A Multilevel Parallel Object-Oriented Framework for Design Optimization, Parameter Estimation, Uncertainty Quantification, and Sensitivity Analysis: Version 6.8 User's Manual. Sandia National Laboratories. Albuquerque, NM: 384.

Adams, B. M., M. S. Ebeida, M. S. Eldred, J. D. Jakeman, L. P. Swiler, W. J. Bohnhoff, K. R. Dalbey, J. P. Eddy, K. T. Hu, D. M. Vigil, L. E. Baumann and P. D. Hough (2013). Dakota, a Multilevel Parallel Object-Oriented Framework for Design Optimization, Parameter Estimation, Uncertainty Quantification, and Sensitivity Analysis, Version 5.3.1+ Theory Manual. SAND2011-9106, Updated May 22, 2013, http://dakota.sandia.gov/. Sandia National Laboratories, Albuquerque, New Mexico.

Allard., B., 1982, Sorption of actinides in granitic rock: SKB TR-82-21, Stockholm, Sweden, Svensk Karnbransleforsorjning A.B., 61 p.

Ames, L.L., McGarrah, J.E., and Walker, B.A., 1983, Soprtion of trace constituents from aqueous solutions onto secondary minerals: 1. Uranium: Clays and Clay Minerals, v. 31, no. 5, p. 321-334.

Andrade Jr, J.S., Buldyrev, S.V., Dokholyan, N.V., Havlin, S., King, P.R., Lee, Y., Paul, G., and Stanley, H.E., 2000, Flow between two sites on a percolation cluster: Physical Review E 62, no. 6: p. 8270.

Arnold, B. W., P. V. Brady, S. J. Bauer, C. Herrick, S. Pye and J. Finger (2011). Reference Design and Operations for Deep Borehole Disposal of High-Level Radioactive Waste. SAND2011-6749. Sandia National Laboratories, Albuquerque, New Mexico.

Avery, S.V., and Tobin, I.M., 1992, Mechanism of strontium uptake by laboratory and brewing strains of Saccharomyces cereviciae: Applied Environmental Microbiology, v. 58, no. 12, p. 3883.

Balay, S., J. Brown, K. Buschelman, V. Eijkhout, W. D. Gropp, D. Kaushik, M. G. Knepley, L. Curfman McInnes, B. F. Smith and H. Zhang (2013). PETSc Users Manual. ANL-95/11 – Revision 3.4. Argonne National Laboratory, Argonne, Illinois.

Beard, L.S., Anderson, Z.W., Felger, T.J., and Seixas, G.B., 2014, Geologic Framework of thermal springs, Black Canyon, Nevada and Arizona: US Geological Survey Open-File Report 2013-1267-B, 68 p.

Bechtel SAIC, 2004, Heat Capacity Analysis Report ANL-NBS-GS000013 Rev 01, 100 p.

Belcher, W.R., ed., 2004, Death Valley regional ground-water flow system, Nevada and California—Hydrogeologic and transient ground-water flow model: U.S. Geological Survey Scientific Investigations Report 2004–5205, 408 p., 2 pls.

Belcher, W.R., Elliott, P.E., and Geldon, A.L., 2001, Hydraulic property estimates for use with a transient ground-water flow model of the Death Valley regional ground-water flow system, Nevada and California: U.S. Geological Survey Water-Resources Investigations Report 01-4210, 28 p.

Bense, V. F. and Van Balen, R.T., 2003, Hydrogeological aspects of fault zones on various scales in the Roer Valley Rift System: Journal of Geochemical Exploration, v. 78-79, p. 317–320.

Bense, V. F., Van Balen, R.T., and De Vries, J.J., 2003a, The impact of faults on the hydrogeological conditions in the Roer Valley Rift System: an overview, Netherlands: Journal of Geosciences, v. 82, p. 41–53.

Bense, V. F., Van den Berg, E.H., and, Van Balen, R.T., 2003b, Deformation mechanisms and hydraulic properties of fault zones in unconsolidated sediments; the Roer Valley Rift System, the Netherlands: Hydrogeology Journal, v. 11, p. 319–332.

Benson, L.V., and McKinley, P.W., 1985, Chemical composition of groundwater in the Yucca Mountain area, Nevada, 1971-84: US Geological Survey Open-File Report 85-484, 10 p.

Bertetti, F.P., Prikryl, J., Werling, B., 2004, Development of Updated Total-system Performance Assessment Parameter Distributions for Radionuclide Transport in the Saturated Zone. CNWRA, San Antonio, Texas.

Berthelin, L., and Munier-Lay, C., 1983, Microbial mobilization and pre-concentration of uranium from various rock materials by fungi: Environmental Biogeochemistry, v. 35, p. 395.

Best, M.G., Christiansen, E.H., Deino, A.L., Gromme, C.S., McKee, E.H., and Noble, D.C., 1989, Excursion 3A—Eocene through Miocene volcanism in the Great Basin of the Western United States, *in* Chapin, C.E., and Zidek, Jiri, eds., Field excursions to volcanic terranes in the Western United States, v. II, Cascades and Intermountain West: New Mexico Bureau of Mines and Mineral Resources Memoir 47, p. 91–133.

Blackwell, D.D., Leidig, M., Smith, R., Johnson, S., and Wisian, K.W., 2002, Exploration and development techniques for Basin and Range geothermal systems; examples from Dixie Valley, Nevada, in Geothermal energy—the baseload renewable resource: Geothermal Resources Council Transactions, v. 26, p. 513–518

Blewitt, G., Coolbaugh, M., Sawatzky, D., Holt, W., Davis, J., Bennett, R., 2003, Targeting of potential geothermal resources in the Great Basin from regional to basin- scale relationships between geodetic strain and geological structures. Geothermal Resources Council Transactions; v. 27, p. 3–7.

Bovardsson, G.S., Pruess, K., and Lippmann, M.J., 1986, Modeling of Geothermal Systems: Journal of Petroleum Technology, p. 1007-1021.

Brady, P.V., H.W. Papenguth, and J.W. Kelly, 1999. Metal sorption to dolomite surfaces. Appl. Geochem. 14(5):569.

Brenner, I.S., 1974, A surge of maritime tropical air—Gulf of California to southwestern United States: Monthly Weather Review, v. 102, p. 375–389.

Brooks, L.E., Masbruch, M.D., Sweetkind, D.S., and Buto, S.G., 2014, Steady-state numerical flow model of the Great Basin carbonate and alluvial aquifer system study area: U.S. Geological Survey Scientific Investigations Report 2014–5213, 124 p., 2 plates.

Brooks., L.E., 2017, Groundwater Model of the Great Basin Carbonate and Alluvial Aquifer System Version 3.0: Incorporating Revisions in Southwestern Utah and East Central Nevada: US Geological Survey Scientific Investigations Report 2017-5072, 92 p.

Buddemeier, R.W., and Hunt, J.R., 1988, Transport of colloidal contaminants in groundwater – radionuclide migration at the Nevada Test Site: Applied Geochemistry, v. 3, p. 535-548.

Bunch, R.L., and Harrill, J.R., 1984, Compilation of selected hydrologic data from the MX missile-siting investigation, east-central Nevada and western Utah: US Geological Survey Open-File Report 84-702, 128 p.

Caine, J. S., Evans, J.P., and Forster, C.B., 1996, Fault zone architecture and permeability structure: Geology, v. 24, p. 1025–1028.

Caine, J.S., and Forster, C.B., 1999, Fault zone architecture and fluid flow: insights from field data and numerical modeling: Geophysical Monograph Series 113, p. 101-127.

Candy, I., Silva, B., Lee, J., 2011, Climates of the early Middle Pleistocene in Britain: environments of the earliest humans in northern Europe. 11-22, in, Ashton, N., Lewis, S., Stringer, C., eds., The Ancient Human Occupation of Britain: Development in Quaternary Science, Elsevier.

Carrier, D.L., and Chapman, D.S., 1981, Gravity and thermal models for the Twin Peaks volcanic center, southeastern Utah: Journal of Geophysical Research, v. 86, p.10287-10302.

Chapman, D.S., Clement, M.D., and Mase, C.W., 1981, Thermal regime of the Escalante Desert, with analysis of the Newcastle geothermal system: Journal of Geophysical Research, v. 86, p. 11735-11746.

Chen, X., G. Hammond, C. Murray, M. Rockhold, V. Vermeul and J. Zachara (2013). "Applications of ensemble-based data assimilation techniques for aquifer characterization using tracer data at Hanford 300 area," Water Resources Research, 49:7064-7076.

Chen, X., H. Murakami, M. Hahn, G. E. Hammond, M. L. Rockhold, J. M. Zachara and Y. Rubin (2012). "Three-Dimensional Bayesian Geostatistical Aquifer Characterization at the Hanford 300 Area using Tracer Test Data," Water Resources Research, 48.

Chester, F.M., and Logan, J.M., 1986, Implications for mechanical properties of brittle faults from observations of the Punchbowl fault zone, California: Pure Applied Geophysics, v. 124, p. 79-106.

Clayton, D., G. Freeze, T. Hadgu, E. Hardin, L. Lee, J. Prouty, R. Rogers, W. M. Nutt, J. Birkholzer, H. H. Liu, L. Zheng and S. Chu (2011). Generic Disposal System Modeling - Fiscal Year 2011 Progress Report. SAND 2011-5828P, FCRD-USED-2011-000184. Sandia National Laboratories, Albuquerque, New Mexico.

Cochran, J.R, and 16 others, 2001, Compliance assessment document for the transuranic wastes in the greater confinement disposal boreholes at the Nevada Test Site, v. 2: Sandia National Laboratories, Albuquerque, New Mexico, SAND2001-2977, 811 p.

Costain, J.K. and Wright, P.M., 1973, Heat flow at Spor mountain, Jordan Valley, Bingham and La Sal, Utah: Journal of Geophysical Research, v. 78, p. 8687-8698.

Daly, C., Gibson, W.P., Doggett, M., Smith, J., and Taylor, G., 2004, Up-to-date monthly climate maps for the conterminous United States, *in* Conference on Applied Climatology, 14th, American Meteorological Society 84th Annual Meeting, January 13–16, 2004, Seattle, Paper 5.1.

Daly, C., Halbleib, M., Smith, J.I., Gibson, W.P., Doggett, M.K., Taylor, G.H., Curtis, J., and Pasteris, P.A., 2008, Physiographically-sensitive mapping of temperature and precipitation across the conterminous United States: International Journal of Climatology, v. 6, no. 15, p. 2,031–2,064.

Degueldre, C., Grauer, R., Laube, A., Oess, A., and Silby, H., 1996, Colloid properties in grantic groundwater systems, II – stability and transport study: Applied Geochemistry, v. 11, p. 697-710.

Dell'Arciprete, D., Vassena, C., Baratelli, F., Giudici, M., Bersezio, R., and Felletti, F., 2014, Connectivity and single/dual domain transport models: Tests on a pointbar/ channel aquifer analogue: Hydrogeology Journal v. 22, no. 4, p. 761–778.

Dettinger, M.D., and Schaefer, D.H., 1996, Hydrogeology of structurally extended terrain in the eastern Great Basin of Nevada, Utah, and adjacent states, from geologic and geophysical models: U.S. Geological Survey Hydrologic Investigations Atlas HA–694–D, 1 sheet, scale 1:15,000,000.

Dewispelare, A.R., Herren, L.T., Mikalas, M.P., and Clemen, R.T., 1993, Expert Elicitation of Future Climate in the Yucca Mountain Vicinity: Iterative Performance Assessment Phase 2.5: Center for Nuclear Waste Regulatory Analyses, San Antonio TX, Report CNWRA 93-016.

Dickinson, W.R., 2006, Geotectonic evolution of the Great Basin: Geosphere, v. 2, no. 7, p. 353–368.

Ding, M., Reimus, P.W., Ware, S.D., and Meijer, A., 2003, Experimental studies of radionuclide migration in Yucca Mountain alluvium, in proceedings of the 10th International High-Level Radioactive Waste Management Conference, Las Vegas, Nevada, 30 March-2 April 2003; La Grange Park, Illinois, American Nuclear Society, p. 126-135.

Ding., M., Reimus, P.W., Chipera, S., and Scism, C., 2006, Sorption characteristics of radionuclides on clays in Yucca Mountain alluvium, in proceedings of the 11th International High-Level Radioactive Waste Management Conference, Las Vegas, Nevada, 30 April -4 May 2006; La Grange Park, Illinois, American Nuclear Society, p. 385-389.

DOE (1996). Title 40 CFR Part 191 Compliance Certification Application for the Waste Isolation Pilot Plant. DOE/CAO-1994-2184. U.S. Department of Energy, Carlsbad, New Mexico.

DOE (2008). Yucca Mountain Repository License Application Safety Analysis Report. DOE/RW-0573, Revision 1, http://www.nrc.gov/waste/hlw-disposal/yucca-lic-app/yucca-lic-app-safety-report.html#1. US Department of Energy, Washington, DC.

DOE (2011). Used Fuel Disposition Campaign Disposal Research and Development Roadmap. FCRD-USED-2011-000065 REV 0. Fuel Cycle Technologies, Office of Nuclear Energy, US Department of Energy, Washington, DC.

DOE (2012). Used Fuel Disposition Campaign Disposal Research and Development Roadmap. FCR&D-USED-2011-000065, REV 1. U.S. DOE Office of Nuclear Energy, Used Fuel Disposition, Washington, D.C.

DOE (2014). Title 40 CFR Part 191 Subparts B and C Compliance Recertification Application 2014 for the Waste Isolation Pilot Plant. DOE/WIPP 15-3503. U.S. Department of Energy, Carlsbad, New Mexico.

DOE/ORD, 2001, Unsaturated Zone and Saturated Zone Transport Properties (U0100), ANL-NBS-HS-000019, Rev. 0, ICN 02, Las Vegas, NV.

DOE/ORD, 2004, Site-Scale Saturated Zone Transport, MDL-NBS-HS-000010, Rev 01, ICN 00. Las Vegas, NV.

Domenico, P.A., and Schwartz, P.A., 1998, The origin of porosity and permeability, chap. 2 *of* Physical and chemical hydrogeology (2): New York, John Wiley and Sons, Inc., p. 13–32.

Efurd, D.W., Runde, W., Banar, J.C., Roensch, F.R., Palmer, P.D., Clark, D.L., and Tait, C.D., 1996, Measured solubilities and speciation of neptunium and plutonium in J-13 groundwater: Milestone 3411: Los Alamos, New Mexico, Los Alamos National Laboratory, 67 p.

Eggleston, R.E., and Reiter, M., 1984, Terrestrial heat- flow estimates from petroleum bottom- hole temperature data in the Colorado Plateau and eastern Basin and Range province: Bulletin of the Geological Society of America, v. 95, p. 1027-1034.

Epplebaum, L., Kutasov, I., and Pilchin, A., 2014, Applied Geothermics: Springer, 183 p.

Estrella, R., S. Tyler, J. Chapman, and M. Miller. 1993. "Area 5 Site Characterization Project - Report of Hydraulic Property Analysis Through August 1993." Water Resources Center Publication #45121, Desert Research Institute, DOE/NV/10845-41.

Faulds J.E., Coolbaugh, M., Blewitt, G., Henry, C.D., 2004, Why is Nevada in hot water? Structural controls and tectonic model of geothermal systems in the northwestern Great Basin Geothermal Resources Council Transactions, v. 28, p. 649–654.

Faunt, C.C., Blainey, J.B., Hill, M.C., D'Agnese, F.A., and O'Brien, G.M., 2010, Chapter F. Transient flow model, *in* Belcher, W.R., and Sweetkind, D.S., eds., Death Valley regional groundwater flow system, Nevada and California—Hydrogeologic framework and transient groundwater flow model: U.S. Geological Survey Professional Paper 1711, p. 251–344.

Fischer, U.H., Bebiolka, A., Brandefelt, J., Follin, S., Hirschorn, S., Jensen, M., Keller, S., Kennell, L., Näslund, J.O., Normani, S., Selroos, J.O., Vidstrand., P., 2014, Radioactive wastes under conditions of future ice ages, in, Haeberli, W., Whiteman, C., eds., Snow and Ice-related Hazards, Risks and Disasters: Elsevier, Oxford, 812 p.

Flexser, S., and Wollenberg, H.A., 1992, Radioelements and their occurrence with secondary minerals in heated and unheated tuff at the Nevada Test Site, in, Proceedings of the 3rd International High-Level Radioactive Waste Management Conference, Las Vegas, Nevada, 12-16 April 1992: La Grange Park, Illinois, American Nuclear Society, v. 2, p. 1593-1598.

Fouch, T.D., 1979, Character and paleogeographic distribution of upper Cretaceous(?) and Paleogene non-marine sedimentary rocks in east-central Nevada, *I,n* Armentrout, J.M., Cole, M.R., and TerBest, H., Jr., eds., Cenozoic paleogeography of the western United States: Society of Economic Paleontologists and Mineralogists, Pacific Section, Pacific Coast Paleogeography Symposium 3, p. 97–111.

Fouch, T.D., Hanley, J.H., and Forester, R.M., 1979, Preliminary correlation of Cretaceous and Paleogene lacustrine and related non-marine sedimentary and volcanic rocks in parts of the Great Basin of Nevada and Utah, *in,* Newman, G.W., and Goode, H.D., eds., Basin and Range symposium and Great Basin field conference: Rocky Mountain Association of Petroleum Geologists and Utah Geological Association, p. 305–312.

Francis, A.L., Dodge, C.L., and Gillow, I.B., 1992, Biodegradation of metal citrate complexes and implications for toxic-metal mobility: Nature, v. 356, p. 140.

Frederick, J. M. and G. E. Hammond (2017). "Maintaining quality assurance within software evolution: Lessons learned with PFLOTRAN," 2017 SIAM Conference on Mathematical and Computational Issues in the Geosciences, Erlangen, Germany, Sep 11-12.

Freeze, G. and P. Vaughn (2012). Development of an Advanced Performance Assessment Modeling Capability for Geologic Disposal of Nuclear Waste: Methodology and Requirements. SAND2012-10208. Sandia National Laboratories, Albuquerque, New Mexico.

Freeze, G., P. E. Mariner, J. A. Blink, F. A. Caporuscio, J. E. Houseworth and J. C. Cunnane (2011). Disposal System Features, Events, and Processes (FEPs): FY11 Progress Report. FCRD-USED-2011-000254. SAND2011-6059P. Sandia National Laboratories, Albuquerque, New Mexico.

Freeze, G., P. Gardner, P. Vaughn, S. D. Sevougian, P. E. Mariner and V. Mousseau (2013a). Evaluation of Advanced Performance Assessment Modeling Frameworks: Annotated Outline. FCRD-UFD-2013-000218, SAND2013-6913P. Sandia National Laboratories, Albuquerque, New Mexico.

Freeze, G., W. P. Gardner, P. Vaughn, S. D. Sevougian, P. Mariner, V. Mousseau and G. Hammond (2013b). Enhancements to the Generic Disposal System Modeling Capabilities. SAND2013-10532P, FCRD-UFD-2014-000062. Sandia National Laboratories, Albuquerque, New Mexico.

Gans, P.B., and Miller, E.L., 1983, Styles of mid-Tertiary extension in east-central Nevada, *in,* Gurgel, K.D., ed., Geologic excursions in the overthrust belt and metamorphic core complexes of the intermountain region, Nevada: Utah Geological and Mineral Survey Special Studies 59, p. 107–160.

Gardner, P.M., and Masbruch, M.D., 2015, Hydrogeologic and geochemical characterization of groundwater resources in Deep Creek Valley and adjacent areas, Juab and Toole Counties, Utah, and Elko and White Pine Counties, Nevada: US Geological Survey Scientific Investigations Report 2015-5097, 66 p.

Gilkey, A. P. (1995). User's Manual for STEPWISE, Version 2.20. Sandia National Laboratories, Carlsbad, New Mexico.

Glen, J.M.G., McKee, E.H., Ludington, S.D., Ponce, D.A., Hildenbrand, T.G., and Hopkins, M.J., 2004, Geophysical terranes of the Great Basin and parts of surrounding provinces: U.S. Geological Survey Open-File Report 2004–1008, 303 p.

Grossman, E.L., 2012. Oxygen isotope stratigraphy: The Geologic Time Scale, p. 181–206.

Guin, A., Ramanathan, R., Ritzi, Jr., R.W., Dominic, D.F., Lunt, I.A., Scheibe, T.D., and Freedman, V.L., 2010, Simulating the heterogeneity in braided channel belt deposits: 2. Examples of results and comparison to natural deposits: Water Resources Research, v. 46, p. 4516.

Hammond, G. E. and P. Lichtner (2010). "Field-scale modeling for the natural attenuation of uranium at the Hanford 300 area using high performance computing," Water Resources Research, 46.

Hammond, G. E., P. C. Lichtner and M. L. Rockhold (2011b). "Stochastic simulation of uranium migration at the Hanford 300 Area," Journal of Contaminant Hydrology, 120-121:115-128.

Hammond, G. E., P. C. Lichtner, C. Lu and R. T. Mills (2011a). "PFLOTRAN: Reactive Flow and Transport Code for Use on Laptops to Leadership-Class Supercomputers." Groundwater Reactive Transport Models. F. Zhang, G. T. Yeh and J. Parker. Bentham Science Publishers.

Hammond, G. E., P. C. Lichtner, R. T. Mills and C. Lu (2008). "Toward petascale computing in geosciences: application to the Hanford 300 Area," Journal of Physics Conference Series, 125:12051-12051.

Hammond, G., P. Lichtner and C. Lu (2007). "Subsurface multiphase flow and multicomponent reactive transport modeling using high performance computing," Journal of Physics: Conference Series 78:1-10.

Hardin, E., and 10 others, 2012, Repository reference disposal concepts and thermal load management analysis: Sandia National Laboratories, Albuquerque, New Mexico, SAND2012-9737P, 345 p.

Hardin, E., T. Hadgu, D. Clayton, R. Howard, H. Greenberg, J. Blink, M. Sharma, M. Sutton, J. Carter, M. Dupont and P. Rodwell (2012). Repository Reference Disposal Concepts and Thermal Load Management Analysis. FCRD-UFD-2012-000219 Rev. 2. US Department of Energy, Washington, DC.

Harper, T. R., and Lundin, E.R., 1997, Fault seal analysis: reducing our dependence on empiricism, in, Hydrocarbon Seals: Importance for Exploration and Production, Møller-Pedersen, P., and Koestler, A.G., eds.: Elsevier, NPF Special Publications, v. 7, p. 149–165.

Harrill, J.R., and Prudic, D.E., 1998, Aquifer systems in the Great Basin region of Nevada, Utah, and adjacent States—Summary report: U.S. Geological Survey Professional Paper 1409–A, 66 p.

He, X., O. Pensado, T. Ahn and P. Shukla (2011). "Model abstraction of stainless steel waste package degradation," International High-Level Radioactive Waste Management Conference, April 10-14, 2011, Albuquerque, New Mexico.

Heilweil, V.M. and Brooks, L.E., eds., 2010, Conceptual model of the Great Basin Carbonate and Alluvial Aquifer System: US Geological Survey Scientific Investigations Report 2010-5193, 192 p.

Helton, J. C. and F. J. Davis (2000). "Sampling-Based Methods." Sensitivity Analysis. A. Saltelli, K. Chan and E. M. Scott. Wiley, Chichester, U.K. 102-153.

Henrikson, A., and Chapman, D.S., 2002, Terrestrial heat flow in Utah: Utah Geological Survey Open-File Report 431, 47 p.

Hershey, R. L., Justet, L., Heilweil, V., Gardner, P., Lyles, B. F., Earman, S. B., Thomas, J. M., Lundmark, K., 2007, Water Chemistry and Ground-water Flowpath Delineation in the Basin and Range Regional Carbonate Aquifer System (BARCAS), Eastern Nevada and Western Utah: DRI Report No. 41230.

Hevesi, J.A., Flint, A.L., and Flint, L.E., 2003, Simulation of net infiltration and potential recharge using a distributed parameter watershed model of the Death Valley region, Nevada and California: U.S. Geological Survey Water-Resources Investigations Report 2003-4090, 161 p.

Heynekamp, M. R., Goodwin, L.B., Mozley, P.S., and Haneberg, W.C., 1999, Controls on fault-zone architecture in poorly lithified sediments, Rio Grande Rift, New Mexico: Implications for fault-zone permeability and fluid flow, in, Haneberg, W.C., Mozley, P.S., Casey, J., Moore, J., and Goodwin, L.B., eds., Faults and Subsurface Fluid Flow in the Shallow Crust: American Geophysical Union Monograph 113, p. 27–51.

Hintze, L.F., 1988, Geologic history of Utah: Brigham Young University Geology Studies Special Publication 7, 202 p.

Ho, C.H., and Miller, N.N., 1986, Adsorption of uranyl species from bicarbonate solution onto hematite particles: Journal of Colloid and Interface Science, v. 110, p. 165-171.

Hochstein, M.P., 1988, Assessment and modeling of geothermal reservoirs (small utilization schemes): Geothermics, v. 17, no. 1, p. 15-49.

Hsi, C.K.D., and Langmuir, D., 1985, Adsorption of uranyl onto ferric oxyhydroxides – application to the surface complexation site-binding model: Geochmica et Cosmochimica Acta, v. 49, p. 1931-1941.

Hu, Q.H., Zavarin, M., and Rose, T.P., 2008, Effect of reducing groundwater on the retardation of redox-sensitive radionuclides: Geochemical Transactions, v. 9, np. 12, 1-24.

Hunt, A. 2001. Applications of percolation theory to porous media with distributed local conductances: Advances in Water Resources, v. 24, no. 3: p. 279–307.

Hunt, A., and Idriss. B., 2009. Percolation-based effective conductivity calculations for bimodal distributions of local conductances: Philosophical Magazine, v. 89, no. 22–24: p. 1989–2007.

Hussain, M. S., A. A. Javadi, A. Ahangar-Asr and R. Farmani (2015). "A surrogate model for simulation-optimization of aquifer systems subjected to seawater intrusion," Journal of Hydrology, 523:542-554.

Huybrechts, P., 2010, Vulnerability of an underground radioactive waste repository in northern Belgium to glaciotectonic and glaciofluvial activity during the next 1 million years: Departement Geografie VUB, Report. 10, p. 01–26.

Jerden, J., V. K. Gattu and W. Ebert (2017). Progress Report on Development of the Spent Fuel Degradation and Waste Package Degradation Models and Model Integration. SFWD-SFWST-2017-000091, SFWD-SFWST-2017-000095. Argonne National Laboratory, Lemont, Illinois.

Kauffman, J.W., Laughlin, W.C., and Baldwin, R.A., 1986, Microbiological treatment of uranium mine waters: Environmental Science and Technology, v. 20, p. 243.

Kersting, A.B., Efurd., D.W., Finnegan, D.L., Rokop, D.J., Smith, D.K., and Thompson, J.L., 1999, Migration of plutonium in groundwater at the Nevada Test Site: Nature, v. 397, no. 6714, p. 56-59.

Knott, S. D., 1993, Fault seal analysis in the North Sea: American Association of Petroleum Geologists Bulletin, v. 77, p. 778–792.

Kolditz, O., H. Shao, W. Wang and S. Baur, Eds. (2015). Thermo-Hydro-Mechanical-Chemical Processes in Fractured Porous Media: Modelling and Benchmarking: Closed-Form Solutions. Switzerland, Springer International Publishing.

Kwicklis, E.M., Wolfsberg, A.V., Stauffer, P.H., Walvoord, M.A., and Sully, M.J., 2006, Multiphase, multicomponent parameter estimation for liquid and vapor fluxes in deep arid systems using hydrologic data and natural environmental tracers: Vadose Zone Journal, v. 5, p. 934-950.

Lachenbruch, A.H., Sass, J.H., and Morgan, Paul, 1994, Thermal regime of the southern Basin and Range province; Implications of heat flow for regional extension and metamorphic core complexes: Journal of Geophysical Research, v. 99, p. 22121-22133.

Langmuir, D., 1997, Aqueous Environmental Geochemistry: Upper Saddle River New Jersey, Prentice-Hall., 600 p.

Levy, M., and Christie-Blick, N., 1989, Pre-Mesozoic palinspastic reconstruction of the eastern Great Basin (Western United States): Science, v. 245, p. 1,454–1,462.

Lichtner, P. C. and G. E. Hammond (2012). Quick Reference Guide: PFLOTRAN 2.0 (LA-CC-09-047) Multiphase-Multicomponent-Multiscale Massively Parallel Reactive Transport Code. LA-UR-06-7048. December 8, 2012. Los Alamos National Laboratory, Los Alamos, New Mexico.

Lindgren, A., Hugelius, G., Kuhry, P., Christensen, T.R., and Vandenberghe, J., 2015, GIS-based maps and area estimates of northern hemisphere permafrost extent during the last glacial maximum: Permafrost and Preglacial Processes: v. 27, no. 1.

Lisiecki, L.E., and Raymo, M.E., 2007. Plio–Pleistocene climate evolution: trends and transitions in glacial cycle dynamics: Quaternary Science Review, v. 26, no. 1, p. 56–69.

Livermore, CA: Lawrence Livermore National Laboratory.

Lloyd, J.R., Cole, J.A., and Macaskie, L.E., 1997, Reduction and removal of heptavalent technetium from solution by Escherichia coli: Journal of Bacteriology, v. 179, p. 204.

Lloyd, J.R., Yong, P. and Macaskie, L.E., 2000, Biological reduction and removal of Np(V) by two microorganisms: Environmental Science and Technology, v. 34, p. 1297.

Louie, J.N., 2004, Crustal thickness and seismic velocity in the Great Basin, Presentation at the Great Basin Geothermal Workshop, Reno: University of Nevada.

Lovely, D.R., Phillips, E.J.P., Gorby, Y.A., and Landa, E.R., 1991, Microbial reduction of uranium: Nature, v. 350, p. 413.

Lu, C. and P. C. Lichtner (2007). "High resolution numerical investigation on the effect of convective instability on long term CO2 storage in saline aquifers," Journal of Physics Conference Series, 78:U320-U325.

Ludington, S., Cox, D.P., Leonard, K.R., and Moring, B.C., 1996, Cenozoic volcanic geology of Nevada, in, Singer, D.A., ed., An analysis of Nevada's metal-bearing mineral resources: Nevada Bureau of Mines and Geology Open-File Report 96–2, 10 p.

Lutz, S.J., Moore, J.N., Blamey, N.J.F., Norman, D.I., 2002, Fluid-inclusion gas chemistry of the Dixie Valley (NV) geothermal system, in, Proceedings of the 27th Workshop on geothermal reservoir engineering. Stanford, CA; Stanford University, January 28–30.

Mahara, Y., and Kudo, A., 1995, Plutonium released by the Nagasaki A-bomb: Mobility in the environment: Applied Radioactive Isotopes, v. 11, p. 1191.

Maier, R.M., and Pepper, I.L., 2009, Environmental Microbiology, Earth Environments, in, Methods of Enzymology: Academic Press, v. 397, 585 p.

Mariner, P. E. (2017). US DOE Work in Nuclear Waste Disposal: Status and Crystalline Rock R&D. Presented at Crystalline Rock Club Meeting, Dec. 5, 2017. SAND2017-12855 PE. Prague, Czech Republic.

Mariner, P. E. and G. E. Hammond (2018). PFLOTRAN and Geologic Disposal Safety Assessment. Presented to modelers at Nuclear Waste Management Organization of Japan (NUMO). SAND2018-5960 PE. Sandia National Laboratories, Tokyo, Japan.

Mariner, P. E., E. R. Stein, J. M. Frederick, S. D. Sevougian and G. E. Hammond (2017). Advances in Geologic Disposal System Modeling and Shale Reference Cases. SFWD-SFWST-2017-000044, SAND2017-10304 R. Sandia National Laboratories, Albuquerque, New Mexico.

Mariner, P. E., E. R. Stein, J. M. Frederick, S. D. Sevougian, G. E. Hammond and D. G. Fascitelli (2016). Advances in Geologic Disposal System Modeling and Application to Crystalline Rock. FCRD-UFD-2016-000440, SAND2016-9610 R. Sandia National Laboratories, Albuquerque, New Mexico.

Mariner, P. E., W. P. Gardner, G. E. Hammond, S. D. Sevougian and E. R. Stein (2015). Application of Generic Disposal System Models. FCRD-UFD-2015-000126, SAND2015- 10037 R. Sandia National Laboratories, Albuquerque, New Mexico.

Masbruch, M.D., Gardner, P.M., and Brooks, L.E., 2014, Hydrology and numerical simulation of groundwater movement and heat transport in Snake Valley and surrounding areas, Juab, Millard, and Beaver counties, Utah, and White Pine and Lincoln counties, Nevada: US Geological Survey Scientific Investigations Report 2014-5103, 122 p.

McCarthy, J.F., and Degueldre, C., 1993, Sampling and characterization of colloids and particles in groundwater for studying their role in contaminant transport – Environmental particles, in, Buffle, J., and

van Leeuwen, H.P., eds., Environmental Analytical and Physical Chemistry Series, v. 2: Boca Raton, Florida, Lewis Publishers, p. 247-315.

McEvoy, F.M., Schofield, D.I., Shaw, R.P., and Norris, S., 2016, Tectonic and climatic considerations for deep geological disposal of radioactive waste: A UK perspective: Science of the Total Environment, v. 571, p. 507-521.

McGraw, M.A., 1996, The effect of colloid size, colloid hydrophobicity, and volumetric water content on the transport of colloids through porous media [PhD dissertation]: Berkeley, University of California, 176 p.

McKenna, J.R., Blackwell D., 2004, Numerical modeling of transient Basin and range extensional geothermal systems. Geothermics, v. 33, no. 4, p. 57–76.

Meacham, P. G., D. R. Anderson, E. J. Bonano and M. G. Marietta (2011). Sandia National Laboratories Performance Assessment Methodology for Long-Term Environmental Programs: The History of Nuclear Waste Management. SAND2011-8270. Sandia National Laboratories, Albuquerque, New Mexico.

Means, J.L., Crerar, D.A., and Borcsik, M.P., 1978, Adsorption of Co and selected actinides by Mn and Fe oxides in soils and sediments: Geochimica et Cosmochimica Acta, v. 42, p. 1763-1773.

Meijer, A., Triay, I., Knight, S., Cisneros, M., 1990, Sorption of radionuclides on Yucca Mountain tuffs, in, Proceedings of the Topical Meeting on Nuclear Waste Isolation in the Unsaturated Zone, FOCUS '89, Las Vegas, Nevada, 17-21 September 1989: La Grange Park, Illinois, American Nuclear Society, p. 113-117.

Mills, R., C. Lu, P. C. Lichtner and G. Hammond (2007). "Simulating subsurface flow and transport on ultrascale computers using PFLOTRAN," 3rd Annual Scientific Discovery through Advanced Computing Conference (SciDAC 2007), BostonJournal of Physics Conference Series, U387-U393.

Moeck, I., Hinz, N., Faulds, J., Bell, J., Kell-Hills, A., Louie, J., 2010, 3D geological mapping as new method in geothermal exploration: a case study from Central Nevada: Geothermal Resources Council Transactions, v. 34, p. 807–12.

Moran, K.J., 1991, Shallow thermal regime at the Jordanelle dam site, central Rocky Mountains, Utah: [MS thesis] Salt Lake City, University of Utah, 141 p.

Morris, D. A. and Johnson, A. I.: Summary of Hydrologic and Physical Properties of Rock and Soil Materials, as Analyzed by the Hydrologic Laboratory of US Geological Survey 1948–60, Water Supply Paper 1839-D, US Geological Survey, Washington, 42 pp., 1967.

Näslund, J.O., Brandefelt, J., 2014. Timing of future glacial inception, in, Haeberli, W., Whiteman, C., eds., Snow and Ice-related Hazards, Risks and Disasters: Elsevier, p. 347–353.

Navarre-Sitchler, A., R. M. Maxwell, E. R. Siirila, G. E. Hammond and P. C. Lichtner (2013). "Elucidating geochemical response of shallow heterogeneous aquifers to CO2 leakage using high-performance computing: implications for monitoring CO2 sequestration," Advances in Water Resources, 53:44-55.

Nitsche, H., Gatti, R.C., Standifer, E.M., Lee, S.C., Muller, A., Prussin, T., Deinhammer, R.S., Maurer, H., Becraft, K., Leung, S., and Carpenter, S.A., 1993, Measured solubilities and speciations of neptunium, plutonium, and americium in a typical groundwater (J-13) from the Yucca Mountain Region: Los Alamos, New Mexico, Los Alamos National Laboratory Report LA-12562-MS, 118 p.

NWTRB (2015). Designing a Process for Selecting a Site for a Deep-Mined, Geologic Repository for High-Level Radioactive Waste and Spent Nuclear Fuel: Overview and Summary. Report to the United States Congress and the Secretary of Energy, November 2015. U.S. Nuclear Waste Technical Review Board, Washington, D.C.

O'Melia, C.R., and Tiller, C.L., 1993, Physiochemical aggregation and deposition in aquatic environments, in Buffle, J., and van Leeuwen, H.P., eds., Environmental Particles, Environmental Analytical and Physical Chemistry Series Volume, v. 2: Boca Raton, Florida, Lewis Publishers, p. 353-386.

Paces, J.B., and Whelan, J.F., 2012, The paleohydrology of unsaturated and saturated zones at Yucca Mountain, Nevada and vicinity, in Stuckless, J.S., ed., Hydrology and Geochemistry of Yucca Mountain and Vicinity, Southern Nevada and California: Geological Society of America Memoir 209, 86 p.

Paces, J.B., Neymark, L.A., Marshall, B.D., Whelan, J.F., and Peterman, Z.E., 2001, Ages and origins of calcite and opal in the exploratory studies facility tunnel, Yucca Mountain, Nevada: US Geological Survey Water Resources Investigations Report 01-4049, 95 p.

Perry, F.V., and others, 2018, Regional Geologic Evaluations for Disposal of HLW and SNF: Alluvial Basins of the Basin and Range Province.

Perry, F.V., Kelley, R.E., Dobson, P.F., and Houseworth, J.E., 2015. A GIS Database to Support the Application of Technical Siting Guidelines to a Deep Borehole Field Test. FCRD-UFD-2015-000603, Los Alamos Unlimited Release LA-UR-15-22397. 43p

Phillips, S.P., and Belitz, K., 1991, Calibration of a textured-based model of a ground-water flow system, western San Joaquin Valley, California: Ground Water, v. 29, p. 702–715.

Pillans, B., and Gibbard, P., 2012, The Quaternary Period: p. 979–1010.

Plume, R.W., 1996, Hydrogeologic framework of the Great Basin region of Nevada, Utah, and adjacent states: U.S. Geological Survey Professional Paper 1409-B, 64 p.

Pool, D.R., and Coes, A.L., 1999, Hydrogeologic investigations of the Sierra Vista subwatershed of the Upper San Pedro Basin, Cochise County, southeast Arizona: US Geological Survey Water Resources Investigations Report 99-4197, 47 p.

Powell, W.G., 1997, Thermal state Colorado Plateau-Basin and Range transition, [PhD dissertation] Salt Lake City, University of Utah, 232 p.

Premuzic, E.T., Francis, A.I., Lin, M., and Schubert, J., 1985, Induced formation of chelating agents by Pseudomonas aeruginosa grown in the presence of uranium and thorium: Archives of Environmental Contamination and Toxicology, v. 14, p. 759.

Prudic, D.E., Harrill, J.R., and Burbey, T.J., 1995, Conceptual evaluation of regional ground-water flow in the Carbonate-Rock Province of the Great Basin, Nevada, Utah, and adjacent states: U.S. Geological Survey Professional Paper 1409–D, 102 p.

Raines, G.L., Connors, K.A., Moyer, L.A., and Miller, R.J., 2003, Spatial digital database for the geologic map of Nevada: U.S. Geological Survey Open-File Report 03–66, 33 p.

Ramanathan, R., Guin, A., Ritzi, Jr., R.W., Dominic, D.F., Freedman, V.L., Scheibe, T.D., and Lunt, I.A., 2010, Simulating the heterogeneity in braided channel belt deposits: 1. A geometric-based methodology and code: Water Resources Research: v. 46: p. 4515.

Rawling, G. C., Goodwin, L.B., and Wilson, J.L., 2001, Internal architecture, permeability structure, and hydrologic significance of contrasting fault zone types: Geology, v. 27, p. 43–46.

Razavi, S., B. A. Tolson and D. H. Burn (2012). "Review of surrogate modeling in water resources," Water Resources Research, 48.

Rechard, R. P. (1993). Initial performance assessment of the disposal of spent nuclear fuel and high level waste stored at Idaho National Engineering Laboratory. SAND93-2330/1/2, Vols. 1-2. Sandia National Laboratories, Albuquerque, New Mexico.

Rechard, R. P. (1995). Performance Assessment of the Direct Disposal in Unsaturated Tuff of Spent Nuclear Fuel And High-Level Waste Owned by US Department of Energy. SAND94-2563/1,2,3. Sandia National Laboratories, Albuquerque, New Mexico.

Rechard, R. P. (1998). Update to assessment of direct disposal in unsaturated tuff of spent nuclear fuel and high-level waste owned by US Department of Energy. DOE/SNF/REP-015, INEEL/EXT-98-00185, SAND98-0795. US Department of Energy, Washington, D.C.

Rechard, R. P. (2002). "General approach used in the performance assessment for the Waste Isolation Pilot Plant," Scientific Basis for Nuclear Waste Management XXV, Boston, Massachussetts, November 26-29, 2001, Materials Research Society.

Rechard, R. P. and C. T. Stockman (2014). "Waste degradation and mobilization in performance assessments of the Yucca Mountain disposal system for spent nuclear fuel and high-level radioactive waste," Reliability Engineering and System Safety, 122(2):165-188.

Rechard, R. P. and M. S. Tierney (2005). "Assignment of probability distributions for parameters in the 1996 performance assessment for the Waste Isolation Pilot Plant, Part 1: Description of process," Reliability Engineering and System Safety, 88(1):1-32.

Rechard, R.P., ed., 1995, Executive Summary, Volume 1, Performance assessment of the direct disposal in unsaturated tuff of spent nuclear fuel and high-level waste owned by U.S. Department of Energy: Albuquerque, New Mexico, Sandi National Laboratories Report SAND94-2563/1, 44 p.

REECo. 1993. Hydrogeologic Data for Science Trench Boreholes at the Area 5 Radioactive Waste Management Site, Nevada Test Site, Nye County Nevada. Special Projects Section, Environmental Restoration & Technology Development Department, Environmental Management Division, Reynolds Electrical & Engineering Co., Inc., Las Vegas, Nevada.

Reheis, M., 1999, Extent of Pleistocene lakes in the western Great Basin: U.S. Geological Survey Miscellaneous Field Studies Map MF–2323, scale 1:800,000.

Reiter, M., Mansure, A.J., and Shearer, C.F., 1979, Geothermal characteristics of the Colorado Plateau: Tectonophysics, v. 61, p. 183-195.

Rivett, M.O., Wealthall, G.P., Dearden, R.A., and McAlary, T.A., 2011, Review of unsaturated-zone transport and attenuation of volatile organic compound (VOC) plumes leached from shallow source zones: Journal of Containment Hydrology, v. 123, p. 130-156.

Ronayne, M.J., and Gorelick. S.M., 2006, Effective permeability of porous media containing branching channel networks: Physical Review, v. E 73, no. 2: p. 26305.

Ronayne, M.J., Gorelick, S.M., and Caers, J., 2008, Identifying discrete geologic structures that produce anomalous hydraulic response: An inverse modeling approach: Water Resources Research, v. 44, p. 8426.

Rose, J., 2009, Early and Middle Pleistocene landscapes of eastern England: Proceedings of the Geological Association, v. 120, no. 1, p. 3–33.

Roy, R.F., Decker, E.R., Blackwell, D.D., and Birch, F.S., 1968, Heat flow in the United States: Journal of Geophysical Research, v. 73, p. 5207-5221.

Saltelli, A., M. Ratto, T. Andres, F. Campolongo, J. Cariboni, D. Gatelli, M. Saisana and S. Tarantola (2008). Global Sensitivity Analysis The Primer. Chichester, U.K., Wiley.

Saltelli, A., P. Annoni, I. Azzini, F. Campolongo, M. Ratto and S. Tarantola (2010). "Variance based sensitivity analysis of model output. Design and estimator for the total sensitivity index," Computer Physics Communications, 181(2):259-270.

Sandia National Laboratories, 2008, Yucca Mountain Repository License Application: Safety Analysis Report, DOE/RW-0573, update 1, Chapter 2 Repository Safety After Permanent Closure, 3548 p.

Sanjeev, K.J., Ariethoz, G., Mathews, G., Vial, J., and Kelly, B.F.J., 2016, Influence of alluvial morphology on upscaled hydraulic conductivity: Groundwater, v. 54, no. 3, 384-393 pp.

Sevougian, S. D., E. R. Stein, G. E. Hammond, P. E. Mariner, J. M. Frederick and E. Basurto (2018). "Simulating the Effect of Fracture Connectivity on Repository Performance with GDSA Framework," Waste Management 2018, Phoenix, Arizona.

Sevougian, S. D., E. R. Stein, M. B. Gross, G. E. Hammond, J. M. Frederick and P. E. Mariner (2016). Status of Progress Made Toward Safety Analysis and Technical Site Evaluations for DOE Managed HLW and SNF. Sandia National Laboratories. Albuquerque, NM: 188.

Sevougian, S. D., G. A. Freeze, P. Vaughn, P. Mariner and W. P. Gardner (2013). Update to the Salt R&D Reference Case. FCRD-UFD-2013-000368, SAND2013-8255P. Sandia National Laboratories, Albuquerque, New Mexico.

Sevougian, S. D., G. A. Freeze, W. P. Gardner, G. E. Hammond and P. E. Mariner (2014). Performance Assessment Modeling and Sensitivity Analyses of Generic Disposal System Concepts. SAND2014-17658. Sandia National Laboratories, Albuquerque, New Mexico.

Shackleton, N.J., 1987. Oxygen isotopes, ice volume and sea level. Quaternary Science Reviews, v. 6, no. 3, p. 183–190.

Shott, G. J., L. E. Barker, S. E. Rawlinson, M. J. Sulley, and B. A. Moore. 1998. Performance Assessment for the Area 5 RWMS at the Nevada Test Site, Nye County Nevada (Rev 2.1). DOE/NV/11718-176. Report to the U.S. Department of Energy, Nevada Operations Office, Las Vegas, Nevada.

Silva, R.J., Bidoglio, G., Rand, M.H. Robouch, P.B., Wanner, H., and Puigdomenech, I., 1995, Chemical thermodynamics of americium: Volume 2 of Chemical Thermodynamics: Amsterdam, Elsevier, 374 p.

Simmons, A.M. and Neymark, L.A., 2012, Conditions and processes affecting radionuclide transport, in, Stuckless, J.S., ed., Hydrology and Geochemistry of Yucca Mountain and Vicinity, Southern Nevada and California: Geological Society of America Memoir 209, 86 p.

Simmons, A.M., and Stuckless, J.S., 2010, Analogues to features and processes of a high-level radioactive waste repository proposed for Yucca Mountain, Nevada: US Geological Survey Professional Paper 1779, 195 p.

Smith, D.L., Gans, P.B., and Miller, E.L., 1991, Palinspastic restoration of Cenozoic extension in the central and eastern Basin and Range province at latitude 39–40 degrees N, *in* Geology and ore deposits of the Great Basin, Reno NV: Geological Society of Nevada Symposium Proceedings, p. 75–86.

Smyth, J.R., B.M. Crowe, P.M. Halleck, and A.W. Reed 1979. A preliminary evaluation of the radioactive waste isolation potential of the alluvium-filled valleys of the great basin. Informal Report LA-7962-MS, Los Alamos National Laboratory.

Stein, E. R., P. E. Mariner, J. M. Frederick, S. D. Sevougian and G. E. Hammond (2018). "Performance Assessment of a Generic Nuclear Waste Repository in Shale," Waste Management 2018, Phoenix, Arizona.

Stein, E. R., S. D. Sevougian, P. E. Mariner, G. E. Hammond and J. M. Frederick (2017). "Performance Assessments of Generic Nuclear Waste Repositories in Shale," American Geophysical Union Fall Meeting 2017, New Orleans, Louisiana.

Stewart, J.H., 1980, Geology of Nevada, a discussion to accompany the geologic map of Nevada: Nevada Bureau of Mines and Geology Special Publication 4, 136 p.

Stoller-Navarro Joint Venture, 2005, Phase II contaminant transport parameters for the groundwater flow and contaminant transport model of corrective action unit 98: Frenchman Flat, Nye County, Nevada, Rev. 0, 458 p.

Stolp, B.J., Brooks, L.E., Solder, J.E, 2017, Hydrology and numerical simulation of groundwater flow and streamflow depletion by well withdrawals in the Malad-Lower Bear River Area, Box Elder County, Utah: U.S. Geological Survey Scientific Investigation Report 2017–5011, 113 p., 6 appendixes,

Strahler, A.N., 1989, Elements of Physical Geography, 4th edition: John Wiley and Sons, New York, 565 p.

Stuckless, J.S., 2012, Hydrology and geochemisty of Yucca Mountain and vicinity, southern Nevada and California: Geological Society of America Memoir 209, 402 p.

Sudret, B. (2008). "Global sensitivity analysis using polynomial chaos expansions," Reliability Engineering & System Safety, 93(7):964-979.

Sullivan, W.A., and Snoke, A.W., 2007, Comparative anatomy of core-complex development in the northeastern Great Basin, USA. Rocky Mt: Geology, v. 42, no. 1, p. 1–29.

Sweetkind, D.S. and du Bray, E.A., 2008, Compilation of stratigraphic thicknesses caldera-related Tertiary volcanic rocks, east-central Nevada and west-central Utah: U.S. Geological Survey Digital Data Series DS–271, 40 p.

Sweetkind, D.S., Belcher, W.R., Faunt, C.C., and Potter, C.J., 2010, Chapter B. Geology and hydrology, *in* Belcher, W.R., and Sweetkind, D.S., eds., Death Valley regional groundwater flow system, Nevada and California—Hydrogeologic framework and transient groundwater flow model: U.S. Geological Survey Professional Paper 1711, p. 19–94.

Sweetkind., D.S., Cederberg, J.R., Mabbruch, M.D., and Buto, S.G., 2010, Hydrogologic Framework, in, Heilweil, V.M. and Brooks, L.E., eds., 2010, Conceptual model of the Great Basin Carbonate and Alluvial Aquifer System: US Geological Survey Scientific Investigations Report 2010-5193, 192 p.

Sweetkind., D.S., Masbruch, M.D., Heilweil, V.M., and Buto, S.G., 2010, Ch. C Groundwater Flow, in, Heilweil, V.M. and Brooks, L.E., eds., Conceptual model of the Great Basin Carbonate and Alluvial Aquifer System: US Geological Survey Scientific Investigations Report 2010-5193, 192 p.

Thomas, J.M., Welch, A.H., and Dettinger, M.D., 1996, Geochemistry of isotope hydrology of representative aquifers in the Great Basin region of Nevada, Utah, and adjacent states: US Geological Survey Professional Paper 1409-C, 110 p.

Thomas, K.W., 1987, Summary of sorption measurements performed with Yucca Mountain, Nevada, tuff samples and water from well J-13: Los Alamos, New Mexico, Los Alamos National Laboratory Report LA-10960-MS, 99 p.

Thyne, G.D., Gillespie, J.M., and Ostdick, J.R, 1999, Evidence for interbasin flow through bedrock in the southeastern Sierra Nevada: Geological Society of America Bulletin, v. 111, p. 1,600–1,616.

Tiedeman, C.R., Goode, D.J., and Hseih, P.A., 1998, Characterizing a ground water basin in a New England mountain and valley terrain: Ground Water, v. 36, no. 4, p. 611–620.

Tompson A.F.B., Zavarin M., Bruton C.J., and Pawloski G.A., 2001, Simplified Hydrologic Source Term for Frenchman Flat Sensitivity Studies: Internal Report, Lawrence Livermore National Laboratory, Livermore, California.

Toth, J., 1963, A theoretical analysis of groundwater flow in small drainage basins: Journal of Geophysical Research, v. 68, no. 8, p. 2,354–2,356.

Triay., I.R., Meiher, A., Conca, J.L., Kung, K.S., Rundberg, R.S., Streitelmeier, B.A., and Tait, C.D., 1997, Summary and synthesis report on radionuclide retardation for the Yucca Mountain site characterization project: Los Alamos, New Mexico, Los Alamos National Laboratory Report LA-13262-MS.

Tsezos, M., and Volesky, B., 1982, The mechanism of uranium biosorption by Rhizopus arrhizus: Biotechnology and Bioengineering, v. 24, p. 385.

Tsunashima, A., Brindley, G.W., and Bastovanov, M., 1981, Adsorption of uranium from solutions by montmorillonite – compositions and properties of uranyl montmorillonites: Clays and Clay Minerals, v. 29, no. 1, p. 10-16.

Tyler, S.W., Chapman, J.B., Conrad, S.H., Hammermeister, D.P., Blout, D.O., Miller, J.J., Sully, M.J., and Ginanni, J.M., 1996, Soil-water flux in the southern Great Basin, United States: Temporal and spatial variations over the last 120,000 years: Water Resources Research, v. 32, p. 1481–1499.

Tyler, S.W., Kranz, S., Parlange, M.B., Albertson, J., Katul, C.G., Cochran, G.F., Lyles, B.A., and Holder, G., 1997, Estimation of groundwater evaporation and salt flux from Owens Lake, California, USA: Journal of Hydrology, v. 200, p. 110-135.

Vaughn, P., G. Freeze, J. Lee, S. Chu, K. D. Huff, W. M. Nutt, T. Hadgu, R. Rogers, J. Prouty, E. Hardin, B. Arnold, E. Kalinina, W. P. Gardner, M. Bianchi, H. H. Liu and J. Birkholzer (2013). Generic Disposal System Model: Architecture, Implementation, and Demonstration. FCRD-UFD-2012-000430 Rev. 1, SAND2013-1539P. Sandia National Laboratories, Albuquerque, New Mexico.

Walvoord, M.A., and Phillips, F.M., 2004, Identifying areas of basin-floor recharge in the Trans-Pecos region and the link to vegetation: Journal of Hydrology, v. 292, p. 59-74.

Weirs, V. G., J. R. Kamm, L. P. Swiler, S. Tarantola, M. Ratto, B. M. Adams, W. J. Rider and M. S. Eldred (2012). "Sensitivity analysis techniques applied to a system of hyperbolic conservation laws," Reliability Engineering & System Safety, 107:157-170.

Welch, A.H., Bright, D.J., and Knochenmus, L.A., eds., 2007, Water resources of the Basin and Range carbonate-rock aquifer system, White Pine County, Nevada, and adjacent areas in Nevada and Utah: U.S. Geological Survey Scientific Investigations Report 2007–5261, 96 p.

Weng, C., and Jackson, S.T., 1999, Late glacial and Holocene vegetation history and paleoclimate of the Kaibab Plateau, Arizona: Paleogeography, Paleoclimatology, Paleoecology, v. 153, p. 179–201.

Wernicke, B.P., 1992, Cenozoic extensional tectonics of the U.S. Cordillera, *in* Burchfiel, B.C., Lipman, P.W., and Zoback, M.L., eds., The Cordilleran orogen, conterminous U.S.: Boulder, Colorado, Geological Society of America, Geology of North America, v. G–3, p. 553–581.

Wernicke, B.P., Guth, P.L., and Axen, G.J., 1984, Tertiary extensional tectonics in the Sevier thrust belt of southern Nevada, *in* Lintz, J.P., ed., Western geological excursions: Mackay School of Mines, Reno, University of Nevada, Geological Society of America, Cordilleran Section, Field Trip Guidebook, p. 473–510.

Whelan, J.F., Paces, J.B., and Peterman, Z.E., 2002, Physical and stable-isotope evidence for formation of secondary calcite and silica in the unsaturated zone, Yucca Mountain, Nevada: Applied Geochemistry, v. 17., no., 6, p. 735-750.

Whelan, J.F., Paces, J.B., Peterman, Z.E., Marshall, B.D., and Neymark, L.A., 2004, Reply to the comment on "Physical and stable isotope evidence for formation of secondary calcite and silica in the unsaturated zone, Yucca Mountain, Nevada," by Y.V. Dublyanski, S.E. Smirnov, and G.P. Palyanova: Applied Geochemistry, v. 19, p. 1879-1889.

Wildemeersch, S., Jamin, P., Orban, P., Hermans, T., Klepikova, M., Nguyen, F., Brouyere, S., Dassargues, A., 2014, Coupling heat and chemical tracer experiments for estimating heat transfer parameters in shallow alluvial aquifers: Journal of Contaminant Hydrology, v. 169, p. 90-99.

Wilson, N.S.F., and Cline, J.S., 2005, Reply to the comment on "Origin, timing, and temperature of secondary calcite-silica mineral formation at Yucca Mountain, Nevada" by Y.V. Dublyanski, S.E. Smirnov, and G.P. Palyanova: Applied Geochemistry, v. 69, p. 4391-4395.

Wilson, N.S.F., Cline, J.S., and Amelin, Y.V., 2003, Origin, timing, and temperature of secondary calcite-silica mineral formation at Yucca Mountain, Nevada: Geochmica et Cosmochimica Acta, v. 67, p. 1145-1184.

Wolfsberg, K., 1978a, Sorption-Desorption Studies of Nevada Test Site Alluvium and Leaching Studies of Nuclear Test Debris: LA-7216-MS, Los Alamos, NM: Los Alamos National Laboratory.

Wolfsberg, K., 1978b, Sorptive Properties of Alluvium, Office Memorandum dated October 24, 1978: Los Alamos, NM: Los Alamos National Laboratory.

Wolfsberg, K., Bayhurst, B.P., Levy, S.S., Lawrence, F.O., Knight, S.D., Mitchell, A.J., Ogard, A.E., and Wanek, P.L., 1983, Research and Development Related to Sorption of Radionuclides on Soils: LA-UR-83-800, Los Alamos, NM, Los Alamos National Laboratory.

Yang, I.C., 2002, Percolation flux and transport velocity in the unsaturated zones, Yucca Mountain, Nevada: Applied Geochemistry, v. 17., p. 807-817.

Yu, Z., Lin, Y., Johannesson, K., Smiecinski, A. J., Stetzenbach, K. J., 2007, Geochemical modeling of solubility and speciation of uranium, neptunium, and plutonium.

Zachos, J., Pagani, M., Sloan, L., Thomas, E., Billups, K., 2001, Trends, rhythms, and aberrations in global climate 65 Ma to present: Science, v. 292, no. 5517, p. 686–693.

Zavarin, M., Carle, S.F., and Maxwell, R.M., 2004, Upscaling Radionuclide Retardation – Linking the Surface Complexation and Ion Exchange Mechanistic Approach to a Linear Kd Approach, UCRL-TR-204713:

Zavarin, M., Roberts, S.K., Rose, T.P., Phinney, D.L., 2002, Validating Mechanistic Sorption Model Parameters and Process for Reactive Transport In Alluvium, UCRL-ID-149728: Livermore, CA: Lawrence Livermore National Laboratory.

Zhu, L., Gong, H., Dai, Z., Guo, G., and Teatini, P., 2017, Modeling 3-D permeability distribution in alluvial fans using facies architecture and geophysical acquisitions: Hydrology and Earth Systems Science: v. 21, p. 721-733.

Zielinski, R.A., Bush, C.A., Spengler, R.W., and Szabo, B.J., 1986, Rock-water interaction in ash-flow tuffs (Yucca Mountain, Nevada, USA) – The record from uranium studies: Uranium, v. 2, p. 361-386.

Zielinski., R.A., 1980, Uranium in secondary silica – a possible exploration guide: Economic Geology and the Bulletin of the Society of Economic Geologists, v. 75, p. 592-602.

APPENDIX A: 2018 SFWST ANNUAL WORKING GROUP AGENDA

FINAL SCHEDULE – May 18, 2018 (SAND2018-5435 O)
SFWST Annual Working Group Meeting
DISPOSAL RESEARCH (DR) SCHEDULE

TUESDAY, MAY 22, 2018

8:30-9:30 am	**Welcome & SFWST Campaign Updates** • DR & ST High Level Updates • Ram Murthy: QA Update	Auditorium
9:30-9:50 am	**Break**	SEB Foyer
9:50 – 10:20 am	**DR NEUP Topical Session** (Ruth Tinnacher, California State University East Bay).	Classroom #1242
10:20-12:00	**DPC Session** (Hardin, Banerjee)	Classroom #1242
Noon-1:30 pm	**Lunch** (on your own)	
1:30-2:15 pm	**International Session** (Birkholzer)	Classroom #1242
2:15-2:45 pm	**DR Integration Intro – Objectives, Goals** (MacKinnon/McMahon)	Classroom #1242
2:45-3:05 pm	**Break**	SEB Foyer
3:05-5:00 pm	**DR Integration** (Sevougian) **DR Roadmap** (Sassani) **GDSA Status** (Mariner)	Classroom #1242
5:00-5:30 pm	**Online Waste Library** (OWL) demo (Sassani)	Classroom #1242

WEDNESDAY, MAY 23, 2018

8:00-10:00 am	**Argillite Disposal R&D** (Includes EBS R&D) Jove-Colon/Matteo • Carlos F. Jove Colon – (SNL) Disposal in Argillite R&D WP Overview • Jonny Rutqvist – Summary of LBNL FY18 Coupled THM Process Model Developments and Validations • Yves Guglielmi – LBNL Argillite expanded work-scope on fault slip and in situ THM monitoring using new multi-physics borehole tool • Ed Matteo – (SNL) EBS Crosscuts and Integration in the FY18 Workscope • Florie Caporuscio – (LANL) Disposal in Argillite R&D: Accomplishments & Path Forward (Argillite & EBS) • Mavrik Zavarin – (LLNL) Update on corrosion studies • Carlos F. Jove Colon – (SNL) Disposal in Argillite International Collaborations WP Overview • Mavrik Zavarin – (LLNL) TDB Development: Surface Complexation Modeling	Classroom #1242
10:00-10:20 am	**Break**	SEB Foyer
10:20-12:20 pm	**Crystalline Disposal R&D** (includes EBS R&D) Wang/Matteo • Yifeng Wang (SNL) Disposal in crystalline – overview • Hari S. Viswanathan (LANL) Discrete fracture network modeling in crystalline rock • Teklu Hadgu (SNL) Flow & transport modeling for Mizunami site	Classroom #1242

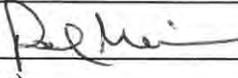|		
	• Elena Kalinina (SNL) Field data synthesis and upscaling for fractured rocks • Hakim Boukhalfa (LANL) Update on colloid-facilitated radionuclide transport • Pat Dobson (LBNL) FY18 LBNL Crystalline R&D updates • Hao Xu (LBNL) Coupled THMC models for bentonite under high temperature • Liange Zheng (LBNL) Studying bentonite: FEBEX-DP and HotBENT • Melissa M. Mills (SNL) Update on smectite-to-illite transformation • Patricia Fox (LBNL) Effect of Long-Term Bentonite Heating on U(VI) Adsorption • Cindy Atkins-Duffin (LLNL) Update on NEA-TDB activities • Yifeng Wang (SNL) Update on Decovalex 2019 Tasks A & F	
12:20-1:50 pm	**Lunch** (on your own)	
1:50-3:50 pm	**Salt Disposal R&D** (Includes EBS R&D) Kuhlman/Matteo • Kris Kuhlman (SNL): WIPP Heater Test Overview • Doug Weaver (LANL): WIPP Support and Logistics • Phil Stauffer (LANL): Update on Salt Disposal R&D • Jonny Rutqvist (LBL): Update on Salt Disposal R&D • Melissa Mills (SNL): Laboratory Brine Evap. Studies • Peter Johnson (LANL): Coupled THC Processes in Salt • Yuxin Wu (LBL): Geophysics in Heater Test • Ed Matteo (SNL): International / EBS / Sealing	Classroom #1242
3:50-4:10 pm	**Break**	SEB Foyer
4:10-5:40 pm	**Prioritize & Scope FY19 DR Activities:** • Crystalline Breakout Session (Mariner) • Salt Breakout Session (Kuhlman) • DPC Breakout Session (Hardin) • Argillite Breakout Session (Sassani)	Classroom #1242 Classroom #1245 Conf. room #2251 Classroom #1240

THURSDAY, MAY 24, 2018

8-9:15 am	**Prioritize & Scope FY19 DR Activities (cont'd):** • Crystalline Breakout Session (Mariner) • Salt Breakout Session (Kuhlman) • DPC Breakout Session (Hardin) • Argillite Breakout Session (Sassani) **Cross-cutting Activities**	Classroom #1242 Classroom #1245 Conf. room #2251 Classroom #1240
9:15-10 am	• International (Birkholzer) • EBS (Matteo)	Classroom # 1242
10-10:20 am	**Break**	SEB Foyer
10:20-11:30 am	**DR Summary Integration & Planning Session** – overall prioritization and review of cross-cutting R&D issues; review FY19 and out-year scope (Sevougian, Mariner, Sassani, Kuhlman, Hardin)	Classroom #1242
11:30-Noon	**Working Group Debrief and Closing**	Auditorium

APPENDIX E
NTRD DOCUMENT COVER SHEET[1]

Name/Title of Deliverable/Milestone/Revision No.	Advances in Geologic Disposal Safety Assessment and an Unsaturated Alluvium Reference Case
Work Package Title and Number	GDSA Framework Development (SF-18SN01030406)
Work Package WBS Number	1.08.01.03.04
Responsible Work Package Manager	Paul Mariner _(signature)_ (Name/Signature)
Date Submitted	

Quality Rigor Level for Deliverable/Milestone[2]	☐ QRL-1 ☐ Nuclear Data	☐ QRL-2	☒ QRL-3	☐ QRL-4 Lab QA Program[3]

This deliverable was prepared in accordance with   Sandia National Laboratories
                                                 (Participant/National Laboratory Name)

QA program which meets the requirements of

     ☒ DOE Order 414.1   ☐ NQA-1   ☐ Other

This Deliverable was subjected to:

☒ Technical Review	☐ Peer Review
Technical Review (TR)	**Peer Review (PR)**
Review Documentation Provided	**Review Documentation Provided**
☐ Signed TR Report or,	☐ Signed PR Report or,
☐ Signed TR Concurrence Sheet or,	☐ Signed PR Concurrence Sheet or,
☒ Signature of TR Reviewer(s) below	☐ Signature of PR Reviewer(s) below

Name and Signature of Reviewers

Robert Rechard _(signature)_

NOTE 1: *Appendix E should be filled out and submitted with the deliverable. Or, if the PICS:NE system permits, completely enter all applicable information in the PICS:NE Deliverable Form. The requirement is to ensure that all applicable information is entered either in the PICS:NE system or by using the NTRD Document Cover Sheet.*

- *In some cases there may be a milestone where an item is being fabricated, maintenance is being performed on a facility, or a document is being issued through a formal document control process where it specifically calls out a formal review of the document. In these cases, documentation (e.g., inspection report, maintenance request, work planning package documentation or the documented review of the issued document through the document control process) of the completion of the activity, along with the Document Cover Sheet, is sufficient to demonstrate achieving the milestone.*

NOTE 2: *If QRL 1, 2, or 3 is not assigned, then the QRL 4 box must be checked, and the work is understood to be performed using laboratory QA requirements. This includes any deliverable developed in conformance with the respective National Laboratory / Participant, DOE or NNSA-approved QA Program.*

NOTE 3: *If the lab has an NQA-1 program and the work to be conducted requires an NQA-1 program, then the QRL-1 box must be checked in the work Package and on the Appendix E cover sheet and the work must be performed in accordance with the Lab's NQA-1 program. The QRL-4 box should not be checked.*